

Polymer-embedded magnetic carbon-coated nanoparticles as versatile catalyst supports

Dissertation

Zur Erlangung des Doktorgrades der Naturwissenschaften

Dr. rer. nat.

der Fakultät für Chemie und Pharmazie

der Universität Regensburg



vorgelegt von

Andreas Hartl

aus Lichteneck

Regensburg 2020

Die Arbeit wurde angeleitet von: Prof. Dr. Oliver Reiser

Promotionsgesuch eingereicht am: 26.11.2020

Promotionskolloquium am: 26.01.2021

Prüfungsausschuss:	Vorsitz:	Prof. Dr. Oliver Tepner
	1. Gutachter:	Prof. Dr. Oliver Reiser
	2. Gutachterin:	Prof. Dr. Julia Rehbein
	3. Prüfer:	Prof. Dr. Robert Wolf

Der experimentelle Teil der vorliegenden Arbeit wurde im Zeitraum von November 2016 bis September 2020 unter der Anleitung von Prof. Dr. Oliver Reiser am Institut für Organische Chemie der Universität Regensburg angefertigt.

Besonders bedanken möchte ich mich bei Herrn Prof. Dr. Oliver Reiser für die Aufnahme in seinen Arbeitskreis, die Überlassung des interessanten Themas, die anregenden Diskussionen und die stete Unterstützung.

Für meine Familie

*"I would rather have questions that can't be answered
than answers that can't be questioned."*

- *Richard P. Feynman (1918 – 1988)*

Table of contents

A. Introduction	1
1. Aromatic Hydrogenations	1
1.1. Mechanism of heterogeneously catalyzed arene hydrogenations	1
1.2. Aromatic hydrogenation in fuel refinery	2
1.3. Applications in the bulk chemical synthesis	3
1.4. Menthol synthesis – Symrise process	5
1.5. Aromatic hydrogenation in liquid organic hydrogen carriers (LOHCs)	7
1.6. Aromatic hydrogenations in the valorization of biomass-derived chemicals	8
1.7. Synthesis of fine chemicals - fluorinated cyclohexanes	10
1.8. Enantioselective aromatic hydrogenation	11
2. Catalyst systems for Aromatic hydrogenations	13
2.1. Soluble metal nanoparticles as catalysts	13
2.2. Polymer-supported metal nanoparticle catalysts	15
2.3. Magnetic nanoparticles as catalyst supports	18
2.4. Magnetic nanoparticle supported metal nanoparticle catalysts	19
2.5. Magnetic Co/C nanoparticles as catalyst supports	22
2.6. Co/C nanoparticle supported hydrogenation catalysts	23
B. Main part	26
1. Magnetic Co/C nanoparticle supported Ru nanoparticle catalyst for aromatic hydrogenations 26	
1.1. Catalyst synthesis	26
1.1.1. Co/C Nanoparticle supported microporous organic polymer synthesis	26
1.1.2. Co/C nanoparticle supported poly(ethylenimine) polymer synthesis	27
1.1.3. Initial ruthenium incorporation studies	29
1.1.4. Initial hydrogenation test reactions	31
1.1.5. Further studies on high nitrogen content poly(ethylenimine) polymers	32
1.1.6. Effects of polymer variations on the hydrogenation performance	34
1.1.7. Incorporation method improvements	36
1.1.8. Storage and oxidation stability	36
1.2. Recycling and leaching studies	37
1.3. Substrate scope	39
1.4. Conclusion	42

2.	Magnetic Co/C nanoparticle supported chiral phosphoric acid catalysts	43
2.1.	Chiral phosphoric acid catalysis	43
2.2.	Immobilization methods for chiral phosphoric acids	44
2.3.	Results and discussion	48
2.3.1.	BINOL polymerization and subsequent phosphorylation	48
2.3.2.	Direct polymerization of chiral phosphoric acids	50
2.3.3.	Direct Mannich reaction	54
2.3.4.	Friedel-Crafts alkylation of indole	55
2.3.5.	Conjugate addition to <i>ortho</i> -quinone methides	56
2.3.6.	Transfer hydrogenation of 2-substituted Quinolines	59
2.4.	Conclusion	66
C.	Summary	67
D.	Zusammenfassung	69
E.	Experimental Part	72
1.	General information	72
2.	General synthesis procedures	76
3.	Co/C Nanocomposites	78
4.	Chiral phosphoric acids	89
5.	Starting materials	102
6.	Catalysis products	109
F.	References	122
G.	Appendix	127
1.	NMR Spectra	127
2.	GC chromatograms	145
3.	Chiral GC chromatogram	156
4.	HPLC Chromatograms	157
5.	Curriculum Vitae	163
H.	Acknowledgment - Danksagung	165
I.	Declaration	167

Abbreviations

)))	ultrasound	HPLC	high-performance liquid chromatography
acac	acetylacetone	ICP-OES	inductively coupled plasma-optical emission spectrometry
AIBN	2,2'-azobis(2-methylpropionitrile)	IL	ionic liquid
BINOL	1,1'-bi-2-naphthol	IR	infrared
Boc	<i>tert</i> -butyloxycarbonyl	LOHC	liquid organic hydrogen carrier
CAAC	cyclic alkyl amino carbene	LUMO	Lowest unoccupied molecular orbital
CD	cyclodextrin	MNP	magnetic nanoparticle
Co/C	Carbon-coated cobalt	MOP	microporous organic polymer
conc.	concentrated	MTHF	methyl tetrahydrofuran
CPA	chiral phosphoric acid	n.d.	not determined
d.r.	diastereomeric ratio	<i>n</i> -BuLi	<i>n</i> -butyl lithium
dba	dibenzylideneacetone	NHC	N-heterocyclic carbene
DCE	1,2-dichloroethane	NMR	nuclear magnetic resonance
DCM	dichloromethane	NP(s)	nanoparticle(s)
dist	distilled	PAA	poly(acrylic acid)
DVB	divinylbenzene	Pd/C	Palladium on charcoal
EA	ethyl acetate	PE	petroleum ether
<i>ee</i>	enantiomeric excess	PEG	poly(ethylene glycol)
emu	electromagnetic unit	PEI	poly(ethyleneimine)
equiv.	equivalent(s)	PPI	poly(propyleneimine)
FA	furfuryl alcohol	ppm	parts per million
FDA	formaldehyde dimethyl acetal	PS	polystyrene
FID	flame ionization detector	<i>p</i> -TSOH	<i>para</i> -toluenesulfonic acid
GC	gas chromatography	PVP	poly(vinylpyrrolidone)
r.t.	room temperature		

Sat.	saturated
SDS	sodium dodecyl sulfate
TEM	transmission electron microscopy
TEOS	tetraethyl orthosilicate
THF	tetrahydrofuran
THFA	tetrahydrofurfuryl alcohol
TLC	Thin-layer chromatography
TMEDA	tetramethylethylenediamine
TOF	turn over frequency
TON	turn over number
TRGO	thermally reduced graphene oxide
TRIPS	triisopropylphenyl
v/v	volume to volume ratio
wt%	weight percent

A. Introduction

1. Aromatic Hydrogenations

Hydrogenation reactions are among the most basic, but also fundamentally important organic transformations. Especially aromatic hydrogenations have gathered a large interest in industrial as well as academic research. A short insight into the most important topics of this subject will be given, including the role of aromatic hydrogenations in fuel refinery, in the production of bulk and fine chemicals as well as in new research towards other highly selective transformations. Hydrogenation reactions always require the use of a catalyst, which has made the development of new catalytic systems a key factor. While numerous different catalyst types are known, a particular focus will be laid on transition metal nanoparticles (NPs) as well as magnetically recoverable catalysts due to their combination of high catalytic activity and facile reusability. Since a full detailed overview of this subject would surpass the scope of this work, several recent reviews are referenced highlighting different areas of this field.^[1–6]

1.1. Mechanism of heterogeneously catalyzed arene hydrogenations

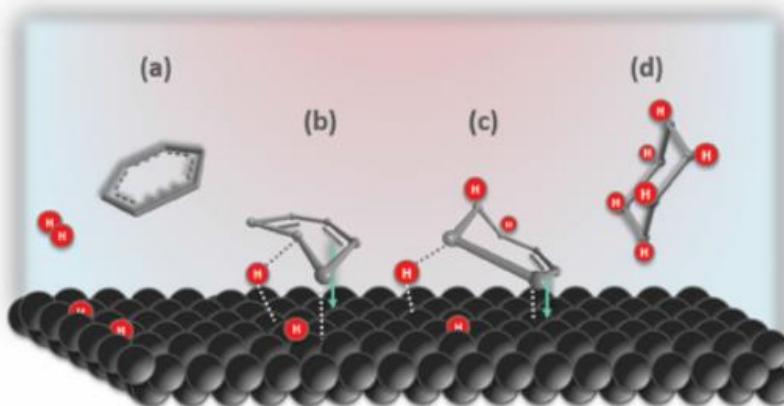


Figure 1: Mechanism of aromatic hydrogenations. Reprinted with permission from [4]. Copyright © 2019 Wiley-VCH Verlag GmbH & Co. KGaA, Weinheim

The hydrogenation of benzene with heterogeneous metal catalysts is usually explained with the Horiuti-Poyani mechanism (Figure 1).^[4] Hydrogen is first adsorbed on the surface forming active metal hydride species (a). The benzene ring is activated through coordination, which facilitates the hydrogen transfer from the surface, forming a cyclohexadiene intermediate (b). In this step, the kinetic barrier from aromatic stabilization of the substrate is overcome and the subsequent hydrogenation steps to cyclohexene (c) and finally cyclohexane (d) proceed more rapidly. Therefore, the thermodynamic (cyclohexane) product is

formed in most cases. Although the selective, partial hydrogenation of arenes usually requires special catalysts and reaction setups, the field has attracted a lot of scientific attention due to the high synthetic versatility of the resulting cycloolefines. The topic will be further discussed in greater detail in chapter 1.3.

In the case of higher substituted arenes, the mechanism also explains the usually high cis-selectivity of the reaction. While the hydrogenation of one double bond always occurs from the same (surface) side in a cis fashion, the hydrogen transfer to the other double bonds could in theory also take place from the opposite side. However, due to the coordination of the substrate to the surface, a π facial exchange through a dissociation-reassociation sequence is required for this to happen. Since the second and third hydrogenation steps are faster than the first, the all-cis isomer is predominantly observed as the main product without considering the influence of other factors, such as thermodynamic stability.

1.2. Aromatic hydrogenation in fuel refinery

Historically, the first successful hydrogenation of benzene was performed by Sabatier and Senderens in 1901.^[7] Since then, the field was majorly progressed by the fuel refining industry. Due to more and more health hazards and environmental concerns being attributed to impurities of aromatics, sulfur, and nitrogen in the combustion fuels, governmental restrictions have been steadily increased over the years with the goal of reducing those contaminations in fuels to a minimum.^[8-10] The removal of aromatics from fuels initially proved to be a major challenge for the industry as traditional hydrotreating methods used to remove sulfur and nitrogen turned out to be very inefficient for aromatic hydrogenations. The conventionally used catalysts containing sulfided CoMo and NiMo on alumina were only active at high temperatures of over 300 °C.^[10] With the hydrogenation of aromatics being an exothermic reaction, the equilibrium got heavily shifted towards the aromatics at those temperatures, requiring greater hydrogen pressures to counteract. Therefore, the need to remove aromatics at lower reaction temperatures sparked interest in the development of new catalysts for aromatic hydrogenations.

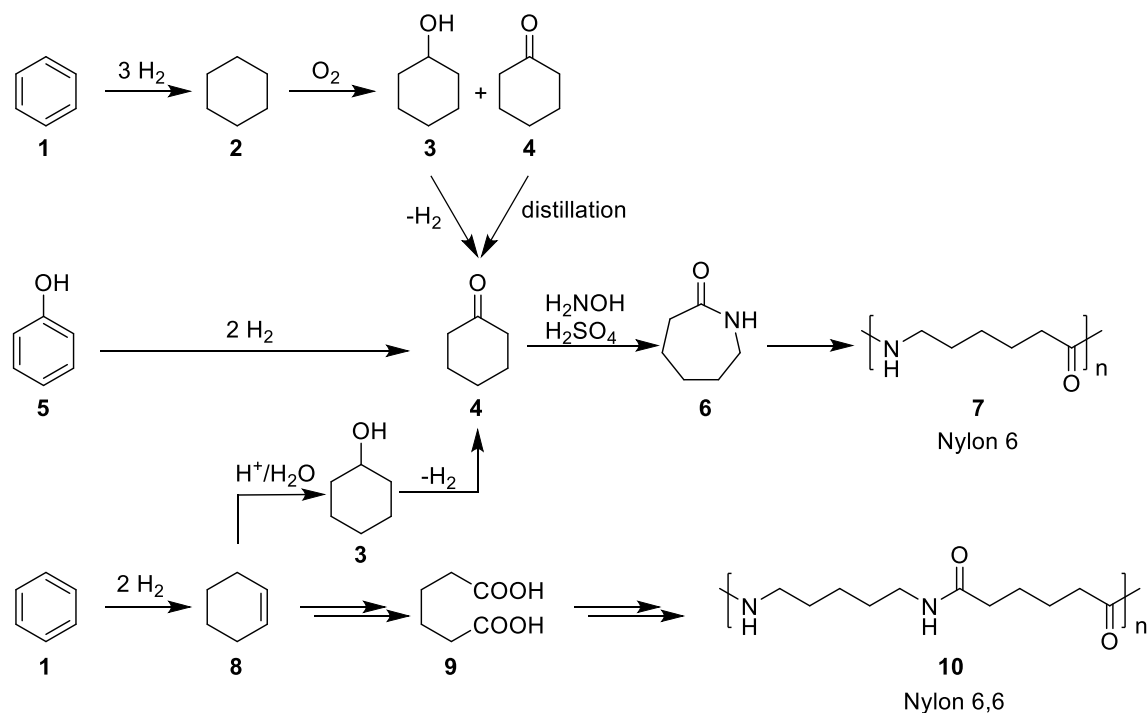
A series of supported noble metal catalysts mainly based on ruthenium, rhodium, palladium, osmium, iridium, or platinum were developed to live up to the challenge.^[11,12] While those catalysts showed great reactivity in the aromatic hydrogenation at a lower temperature (even r.t.), they adsorbed sulfur-containing species leading to rapid catalyst poisoning. As a result, new reactor designs had to be employed using multi-step processes with separate sulfur and nitrogen removal and subsequent aromatic hydrogenation. Moreover, the catalysts themselves were further improved utilizing for example Y-zeolite as support for Platinum or Palladium clusters. The support heavily influences the metal clusters making

them more electron-deficient and thus reducing the binding energy to the electron-accepting sulfur atoms, resulting in higher tolerance levels of the catalysts.^[10]

However, even with the age of fossil fuels slowly but still surely coming to an end, the field of aromatic hydrogenation has already expanded its utility beyond its petrochemical origins onto gaining significant value in the fields of organic synthesis, hydrogen storage, and even biomass conversion.

1.3. Applications in the bulk chemical synthesis

One of the largest industrial application for aromatic hydrogenations is the synthesis of the bulk chemicals cyclohexane (**2**), cyclohexene (**8**) and cyclohexanone (**4**). These are mainly used as precursors for the synthesis of adipic acid (**9**) and ϵ -caprolactam (**6**) which in turn are utilized as monomers for Nylon 6,6 (**7**) and Nylon 6 (**10**), respectively (Scheme 1).^[13,14]



Scheme 1: Aromatic hydrogenations in bulk chemical synthesis.

For cyclohexanone, mainly two synthetic pathways are industrially used. Either the total hydrogenation of benzene to cyclohexane followed by oxidation to cyclohexanone or the direct approach through the selective hydrogenation of phenol (**5**). While the oxidation pathway has no issues of selectivity during the hydrogenation, the harsh conditions required for the subsequent oxidation result in the formation of

undesired byproducts^[15] including cyclohexanol (**3**), which needs to be dehydrogenated in an additional step.^[14] The direct hydrogenation from phenol to cyclohexanone therefore is a significant improvement in terms of sustainable chemistry, especially with the potential accessibility of phenol from renewable resources such as lignin in mind.^[16,17] Earlier, the hydrogenation of phenol was performed using a Ni-catalyst resulting exclusively in the formation of cyclohexanol, but the investigation of different noble metal catalysts showed promising results when supported Pd catalysts were employed.^[18,19] Further research on support as well as promoter materials, resulted in catalysts exhibiting very good selectivities for cyclohexanone of >95%. Additionally, it was found that the use of Lewis acids (e.g. AlCl₃) in combination with commercial catalysts such as Pd/Al₂O₃ gave almost 100% selectivity for cyclohexanone even at full conversion.^[20]

The production of cyclohexene also plays a big role as it can not only be oxidized to adipic acid but can also be transformed to cyclohexanol under acidic conditions and then converted to cyclohexanone through dehydrogenation.^[14] This represents another synthetic pathway for cyclohexanone that also bypasses the unselective oxidation step of the cyclohexane route. However, the selective aromatic hydrogenation of benzene to cyclohexene also proved to be initially very challenging.^[5] Due to the loss of stabilization energy in the first hydrogenation step, the complete hydrogenation to cyclohexane is heavily favored and cyclohexene could mostly only be observed at low conversion levels of benzene. The most important development to achieve significant selectivities in this transformation was the utilization of sophisticated tetraphase reactor setups, containing an organic benzene phase, an aqueous phase with the catalyst in it, and the gaseous phase hydrogen (Figure 2).^[21] This reactor design exploits the roughly 6x higher solubility of benzene in water compared to cyclohexene.^[22] Due to the higher concentration of benzene in the aqueous phase, desorption of cyclohexene from the catalyst is promoted through competitive adsorption and the cyclohexene gets continuously extracted back into the organic phase because of its lower solubility. Especially catalysts based on Ru showed good selectivities in combination with this setup of around 60% cyclohexene, revealing the feasibility of this approach, which was then also commercialized by Asahi.^[23]

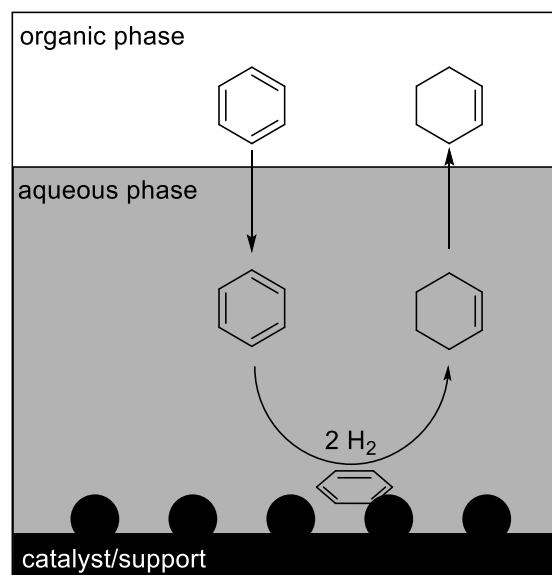
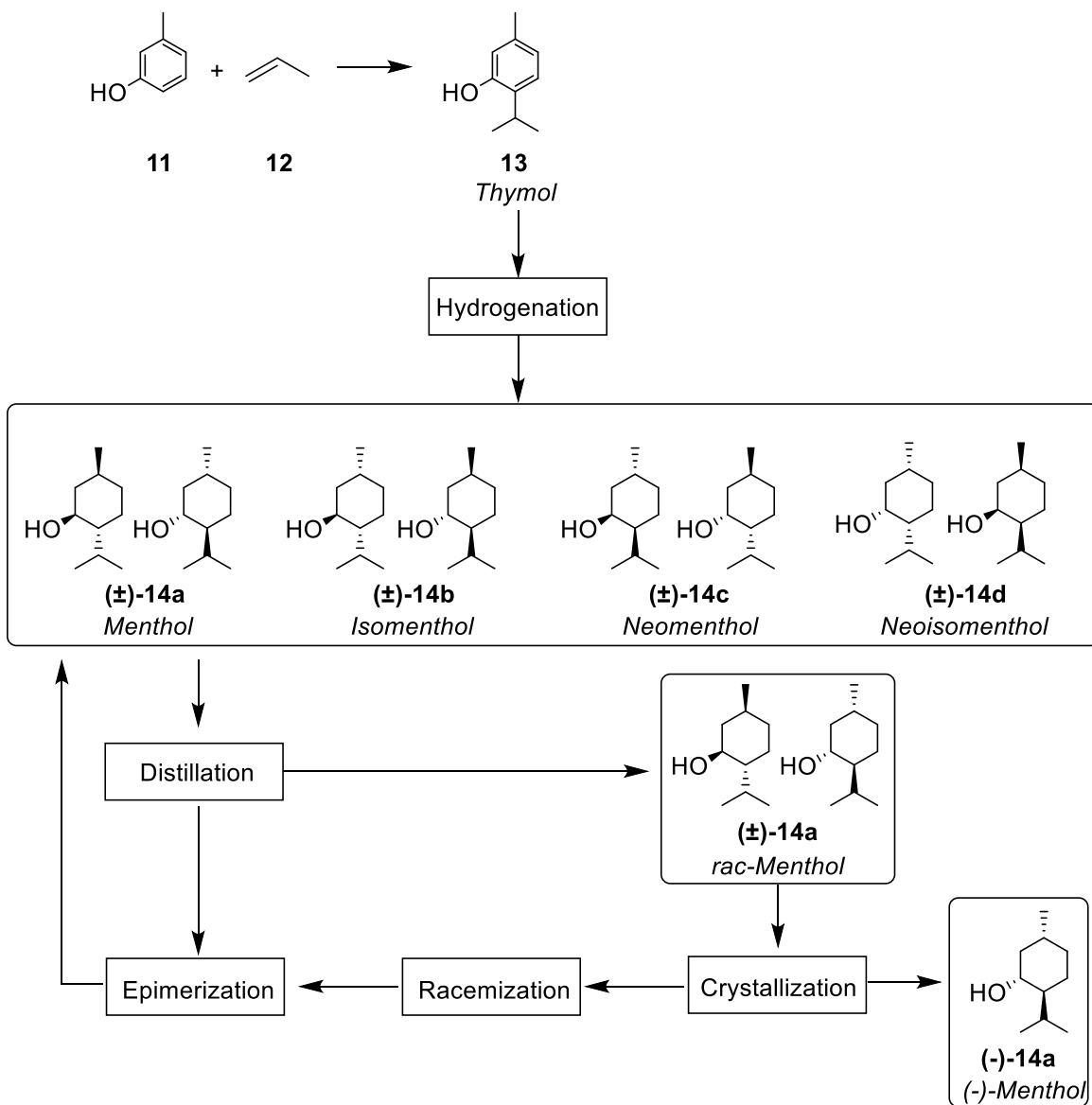


Figure 2: Simplified graphical representation of a tetrphase-reactor setup, only showing the hydrogenation to cyclohexene. Adapted with permission from [22]. Copyright © 1992 Published by Elsevier B.V.

1.4. Menthol synthesis – Symrise process

(-)-Menthol ((-)-**14a**) is one of the most important fragrance products on the market. It is used extensively in perfumery and cosmetic products such as toothpaste or lotions, but also in cigarettes due to its unique cooling effect and minty flavor. The pharmaceutical industry also uses (-)-menthol amongst other things, as a treatment for skin diseases, colds or as a local anesthetic for minor injuries.^[24] The production volume of (-)-menthol is estimated to be more than 19,000 metric tons per year.^[25] While the majority of the production is still achieved through crystallization from the oil of the field mint (*Mentha arvensis*), mainly done in India and China, the dependency on the annual crop yield and the growing demand have led to the emergence of several synthetic approaches. The largest synthetic production of (-)-menthol is using the Symrise process, with its key step being the aromatic hydrogenation of thymol (**13**) (Scheme 2).^[26]



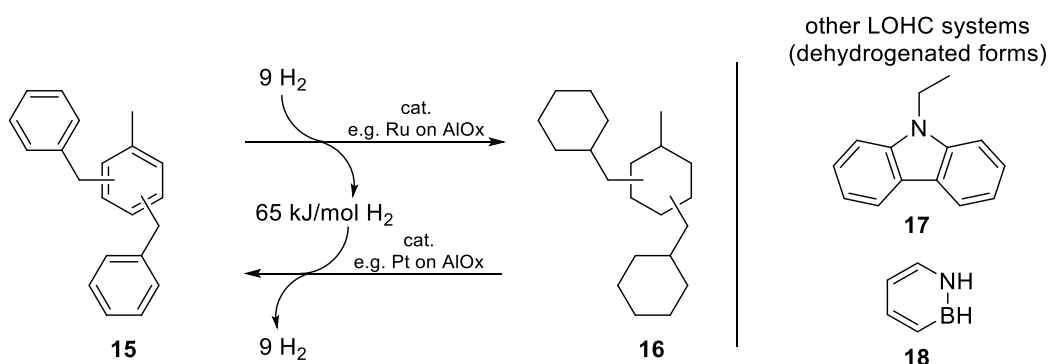
Scheme 2: Simplified representation of the Symrise process for the production of (-)-Menthol (-)-14a. Adapted with permission from [28]. Copyright © 2008 Elsevier B.V. All rights reserved.

The reaction is performed at high temperatures in such a way that the product distribution represents the thermodynamic equilibrium. So the thermodynamically more stable trans-isomers (**14a-c**) with more substituents in the equatorial positions of the cyclohexyl-chair are formed exclusively. The product mixture contains a ratio of 60:30:10 of (±)-menthol (**14a**), (±)-isomenthol (**14b**) and (±)-neomenthol (**14c**), respectively with only traces of (±)-neoisomenthol (**14d**). The (±)-menthol gets separated from the other diastereomers through distillation and the chiral resolution of the racemate is achieved by the selective crystallization of the racemic menthyl-benzoates after the introduction of optically pure seed crystals^[27]. Additionally, the unwanted diastereomers are recycled through epimerization over a Ni-catalyst at high

temperatures under hydrogen pressure to suppress the formation of the byproduct menthone.^[28] Through this highly efficient recycling process, an overall yield of >90% (-)-menthol is achieved, showcasing the success of this aromatic hydrogenation approach.

1.5. Aromatic hydrogenation in liquid organic hydrogen carriers (LOHCs)

Apart from organic synthesis, aromatic hydrogenation is also used as a key step for the operation principle of liquid organic hydrogen carriers (LOHCs) which should not be completely overlooked, and thus only a very brief introduction of the ideas, challenges and progression will be made. The idea behind LOHCs is for them to largely replace existing fossil fuels by utilizing fuel cells to produce energy from their released hydrogen.^[29] Due to the storage and safety concerns with elemental hydrogen (low ignition energy, low density, diffusion even through solids), LOHCs represent a storage option for hydrogen through chemical binding, resulting in a safer to use, long-term stable, and transportable material that can utilize the preexisting infrastructure for fossil fuel transportation and storage (e.g. pipelines, fuel tanks, etc.) with minimal adaptation requirements.



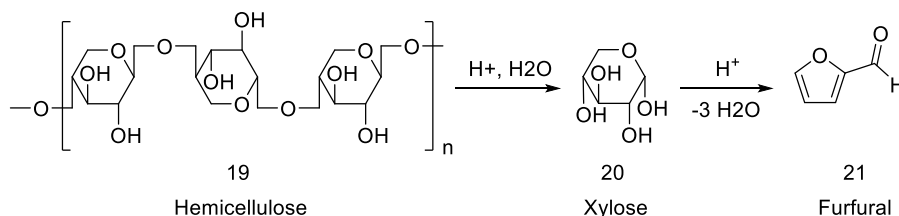
Scheme 3: Examples for LOHC systems.

One of the candidates tested as a potential LOHC system was dibenzyltoluene (**15**)/perhydrodibenzyltoluene (**16**) (scheme **3**), which showed promising results with a high storage capacity (6.2 wt% H₂) and very wide liquid range.^[30] The latter is an important feature for LOHCs since ideally the substance should be liquid not only at room temperature for easier handling and transportation but also at the higher temperatures required to perform the endothermic dehydrogenation reaction, in order to avoid complex purification steps for the released hydrogen. Unfortunately, due to the high dehydrogenation enthalpy (65 kJ/mol H₂)^[31] of the system, the catalytic dehydrogenation required temperatures of >250 °C. While the storage and reuse of “waste heat” from the exothermic hydrogenation reaction is theoretically

possible in a centralized operation, e.g. in a Solar-energy storage/release “battery” system, a decentralized utilization e.g. in a fuel production facility/fuel consumption (automobile) scenario generally requires lower dehydrogenation enthalpies to be efficient. While other LOHC systems have been developed with lower dehydrogenation enthalpies like N-ethylcarbazole (**17**)^[32] or 1,2-dihydro-1,2-azaborine (**18**)^[33], none of them was yet able to overcome different issues such as low liquid range, thermal lability and degradation, storage stability, reversibility of the hydrogenation/dehydrogenation process, and also scalability of production. Hence, the search for an ideal LOHC system is still an ongoing field of research, as well as the exploration of suitable catalysts to more efficiently overcome the kinetic barriers.

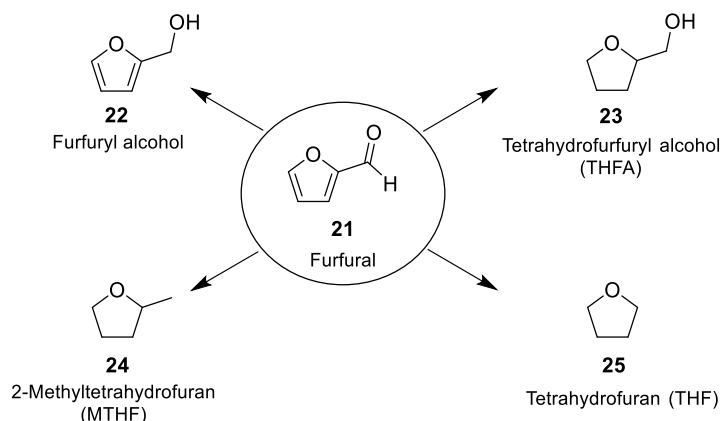
1.6. Aromatic hydrogenations in the valorization of biomass-derived chemicals

Another emerging sector of industrial applications for (hetero)aromatic hydrogenations is the biorefinery, aiming to produce and establish “new”, alternative, valuable feedstock chemicals ultimately derived from biomass, striving to replace the diminishing fossil fuel-based compounds. One of these promising chemicals gaining a lot of attention is the furan derivative furfural (**21**).^[34,35] The production of furfural is achieved with the hydrolysis of hemicellulose (**19**) into its monomeric pentoses like xylose (**20**) and arabinose, followed by an acid-catalyzed dehydration, as shown in Scheme 4.^[36]



Scheme 4: Production of furfural (**21**) from hemicellulose (**19**).

The majority (~60%) of furfural is converted to furfuryl alcohol (FA, **22**) which is mainly used as a monomer for cross-linked polymers in foundry resins^[37] or furan fiber-reinforced plastics used for piping.^[38] However, utilizing different catalyst systems and reaction conditions to hydrogenate the furan ring and/or the aldehyde moiety for selective transformations to tetrahydrofurfuryl alcohol (THFA, **23**), 2-methyltetrahydrofuran (MTHF, **24**) or even tetrahydrofuran (THF, **25**, through decarbonylation) is a subject of intense research (Scheme 5).^[39]



Scheme 5: Reductive transformations of furfural (**21**).

THFA (**23**) is the total hydrogenation product of furfural and is considered a green solvent used in printing inks or cleaning agents.^[40] It can also be employed as biofuel similar to bioethanol or as raw material for the synthesis of other valuable chemicals such as dihydropyran or 1,5-pentanediol.^[39,41,42] Industrially, THFA is synthesized in a two-step process through the reduction to furfuryl alcohol and subsequent hydrogenation of the furan ring with supported Ni catalysts.^[43] On a laboratory scale, several catalyst systems have been developed for the hydrogenation of furfural to THFA with moderate to good selectivities. Recently, Zhang *et al.* even showed 100% THFA selectivity at full furfural conversion with a hydroxyapatite-supported Pd catalyst under mild conditions (40 °C, 10 bar H₂, 3 h).^[44]

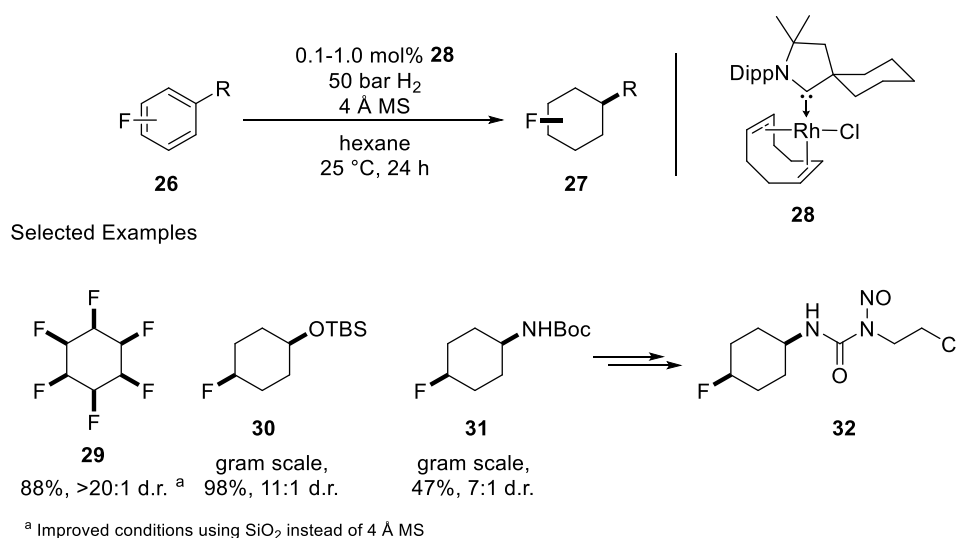
Another valuable chemical derived from furfural is MTHF (**24**). It is used as a higher boiling, more stable alternative solvent to THF and can be used as a gasoline additive due to its excellent combustion properties.^[35,39] Commonly, MTHF is either synthesized from the hydrogenation of levulinic acid^[45] or 2-methylfuran^[46] (both derived from furfural) and only recently a one-step process for the direct conversion of furfural to MTHF has been reported by Zhu *et al.*^[47] A continuous fixed-bed reactor was used with a combination of supported Cu and Pd catalysts achieving a high yield of up to 97% at ambient H₂ pressure. While high temperatures (170 °C) still are required for this process, the avoidance of intermediates and the simplified product isolation *via* extraction results in a lower overall energy consumption and might lead to economic feasibility.

Finally, the direct synthesis of THF from furfural *via* decarbonylation-hydrogenation sequence would be one of the most attractive transformations. THF is widely used as a laboratory solvent but also as a monomer for anionic polymerization. The resulting polytetramethylene glycol ether is used extensively in urethane elastomers and fibers.^[43] Different industrial syntheses of THF are known such as the hydrogenation of maleic anhydride^[48], which is produced by oxidation of *n*-butane and thus is still reliant

on the fossil fuel feedstock. While some catalyst systems have been developed for the direct synthesis from furfural, the formation of coke during the process and the resulting catalyst deactivation seem to be the main issues for the usually low yields.^[35] In contrast, good results were obtained by García-Suárez *et al.* achieving 92% yield at 95% conversion with an H₂O₂ treated Pd/C catalyst in a microwave-assisted hydrogenation in aqueous media at 100 °C.^[49] Although the scalability of these processes might be an issue due to the special conditions required, the success of the diverse catalyst systems and reaction conditions developed for the various transformations of furfural shows the importance of continuous, goal-oriented research eventually leading towards a more environmentally benign chemical industry.

1.7. Synthesis of fine chemicals - fluorinated cyclohexanes

Apart from the industrial-scale production of (-)-menthol, aromatic hydrogenations are also slowly being established as alternative synthetic pathways in other fine chemical syntheses. Recently, Glorius *et al.* utilized this strategy to gain access to all-*cis*-(multi)fluorinated cycloalkanes.^[50] Due to the high polarization of the C-F bond, these compounds are highly desired for their properties in material science.^[51] However, their synthesis is often difficult and involves multiple steps, especially to achieve the targeted all *cis*-configuration which maximizes the dipole moment of the molecules through 1,3-diaxial C-F bonds. The introduction of fluorine groups is also used in agrochemical and pharmaceutical applications to fine-tune parameters such as polarity, pK_a value or metabolic stability.^[52,53]

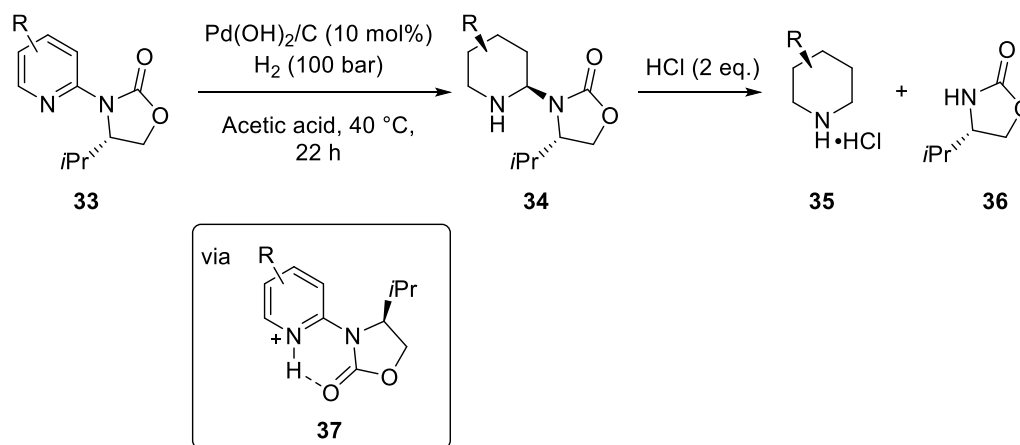


Scheme 6: Hydrogenation of fluorinated arenes by Glorius *et al.*^[50]

The main issue with accessing fluorinated compounds through aromatic hydrogenation before was the predominant hydrodefluorination reaction resulting in regular cyclohexanes usually being the main product. The authors managed to overcome this problem by using a strongly electron-donating cyclic-alkyl-amino-carbene (CAAC) ligand for their homogeneous Rh catalyst (**28**) in combination with nonpolar solvents such as hexane, resulting in the hydrogenation products being isolated in good yields of up to 98%. Different protected functional groups were also tolerated such as protected alcohols (**30**) or amines (**31**), demonstrating the versatility of this method to synthesize building blocks for further functionalization. This was also shown by the incorporation of **31** in the synthesis of a commercial anti-cancer drug giving rise to the lomustine analog (**32**). Additionally, it was possible to shorten the synthesis of one of the most polar organic molecules, *cis*-1,2,3,4,5,6-hexafluorocyclohexane (**29**), from the prior 12 steps^[54] to a single step using cheap hexafluorobenzene as a precursor. The methodology could also be further expanded, giving rise to *cis*-(multi)fluorinated piperidines^[55] and surmount the hydrogenolysis of other important substituents like silyl groups^[56] and even unprotected boronic acids.^[57]

1.8. Enantioselective aromatic hydrogenation

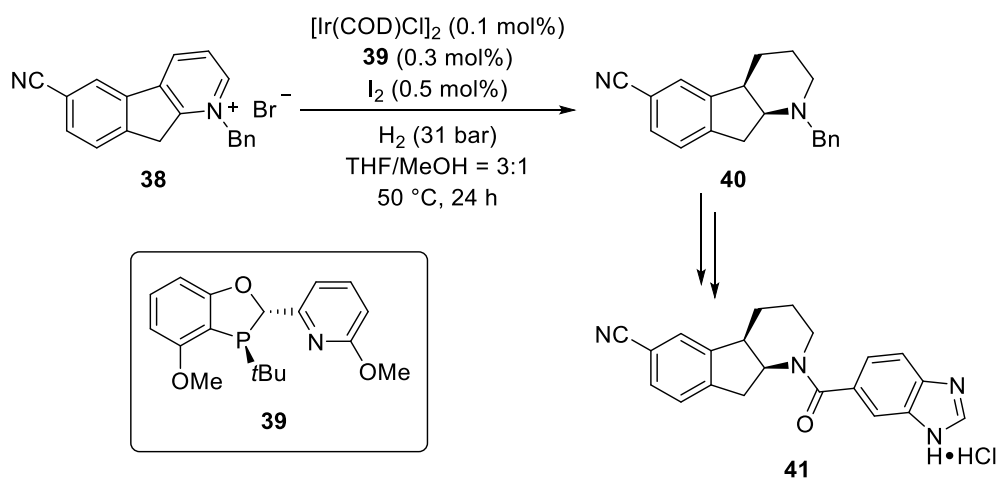
Due to the complexity of fine chemical synthesis, the development of enantioselectivity for aromatic hydrogenations was a necessary step towards their broader application. One method to accomplish this is the introduction of a chiral auxiliary to achieve a diastereoselective hydrogenation while employing a comparatively cheap, achiral catalysts. Glorius *et al.* used this approach to develop an enantioselective hydrogenation for pyridines using the Evans auxiliary and a Pd(OH)₂/C catalyst in acetic acid (Scheme 7).^[58]



Scheme 7: Enantioselective hydrogenation of N-heteroarenes using a chiral auxiliary.^[58]

According to the authors, the acidic reaction conditions played three important roles for the reaction: The hydrogenation of the pyridine ring is facilitated through the formation of the pyridinium salt, the catalyst poisoning is reduced by protonating lewis basic species and the conformation of the auxiliary (**37**) is locked through hydrogen bonding, thus allowing the *iso*-propyl group to sterically shield one side of the substrate. The auxiliary (**36**) could then be efficiently removed by HCl and quantitatively recovered, giving rise to substituted piperidines (**35**) with up to 3 new stereocenters.

A more direct approach to achieve enantioselectivity is, of course, the use of a chiral catalyst such as homogeneous transition metal complexes with a chiral ligand. An abundance of those catalyst systems has already been developed, mainly based on Ir, Rh and Ru in combination with diverse ligands such as biphosphines, N-heterocyclic carbenes (NHCs) or diamine ligands.^[1] Although homogeneous transition metal catalysts will not be discussed in further detail, one particularly interesting application is shown nevertheless below (Scheme 8), in the synthesis of a promising Type 2 diabetes inhibitor (**41**).^[59]

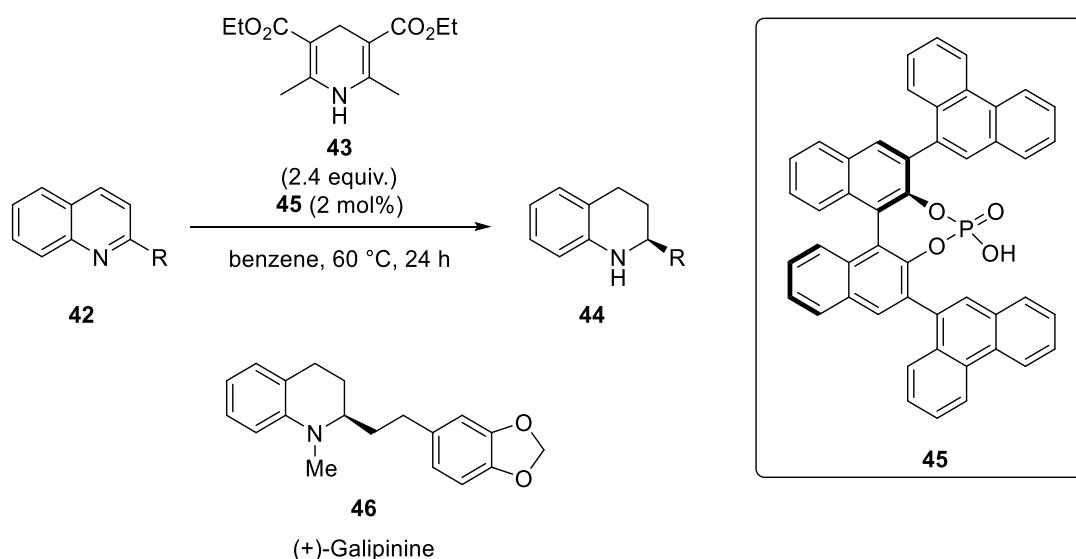


Scheme 8: Homogeneously catalyzed, enantioselective hydrogenation as key step in the total synthesis of **41**.^[59]

The Ir-based catalyst with a dihydrobenzoxaphosphole ligand (**39**) was able to chemoselectively reduce the pyridinium moiety of **38** with preservation of the nitrile group and the benzene ring in an excellent yield of 97% and good selectivity of 70% ee on a multikilogram scale. The total synthesis of compound **41** could therefore be improved from 15 steps with an overall yield of 3% to only 7 steps with an overall yield of 38% showing the power of aromatic hydrogenations as a synthetic shortcut.

Rueping *et al.* also demonstrated an organocatalytic option by using BINOL-based chiral phosphoric acids (CPAs, **45**) for an enantioselective reduction of 2-substituted quinolines (**42**).^[60] In this case, Hantzsch dihydropyridine (**43**) was used as a hydride source making this process a transfer hydrogenation. The

resulting 1,2,3,4-tetrahydroquinolines (**44**) are an important structural motive in many biologically active compounds such as (+)-galipinine (**46**) which could be potentially used as an anti-malarial drug.^[61]



Scheme 9: Enantioselective transfer hydrogenations using CPAs by Rueping *et al.*^[60]

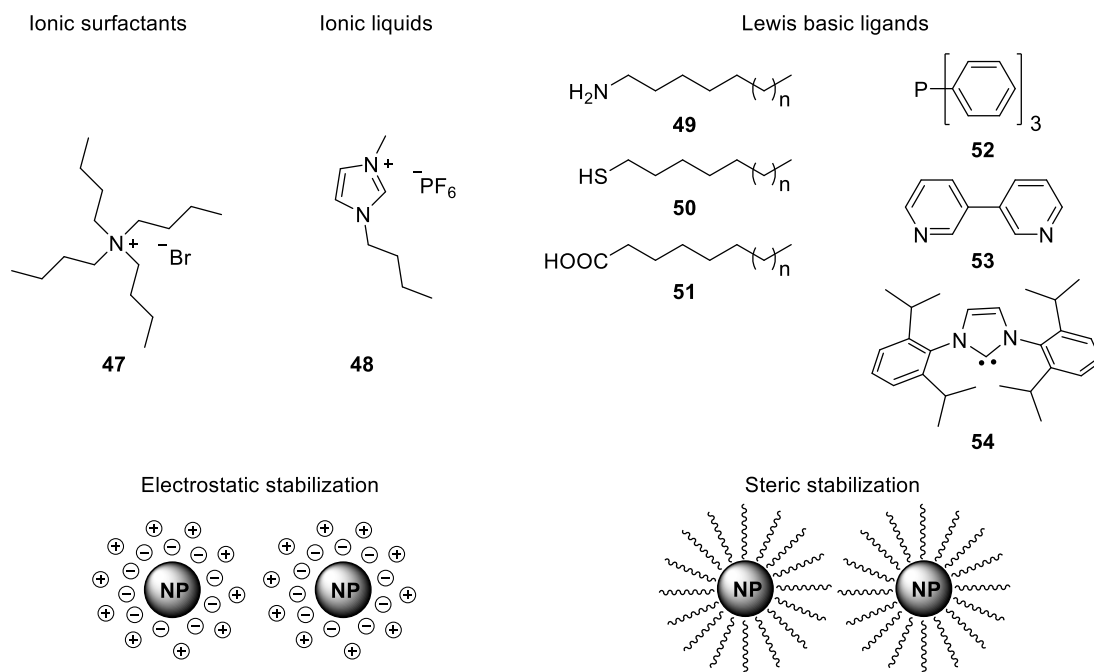
The authors found that the axial chirality of the BINOL backbone, combined with large aromatic substituents in the 3,3'-positions such as 9-phenanthrene gave excellent selectivities of >99% presumably due to efficient π -stacking with the substrate, shielding one side from the hydride transfer. The high chemical stability and robustness as well as the versatility through adaptation with different substituents also make these CPAs ideal candidates for immobilization onto solid supports to improve their recyclability. This will be further discussed in the Main Part chapter two, together with a more detailed mechanism of the reaction.

2. Catalyst systems for Aromatic hydrogenations

2.1. Soluble metal nanoparticles as catalysts

Apart from the heterogeneous catalysts mentioned earlier for most of the industrial applications and the homogeneous catalysts mainly used for more selective transformations, metal NP catalysts have also attracted a lot of attention.^[6] Not only have numerous homogeneous catalyst systems been shown to have NPs as their active species, including the previously mentioned Rh-CAAC catalyst (**28**) for fluoro-arene hydrogenations^[62], but also preformed metal NPs were studied extensively as arene hydrogenation catalysts for their unique properties. Metal NPs are often considered as “semiheterogeneous” catalysts acting at the frontier between homogeneous and heterogeneous systems.^[63] Their large surface area,

arising from their small particle size (1-10 nm in diameter), results in high catalytic activities under usually mild conditions comparable to homogenous catalysts. At the same time, due to their heterogeneous nature, they still retain the advantages of simple separation and recovery. Usually, the synthesis of metal NPs is achieved with two main methods: the reduction of metal salts or oxides and the decomposition of organometallic metal (0) complexes.^[13,64] However, due to the inherent instability of NPs owing to their size, their stabilization by various supporting agents is one of the most important factors during and after the synthesis. Depending on the supporting agents, they prevent the agglomeration of NPs either by steric or by electrostatic repulsion and have a heavy influence on the catalytic activity of the system. The most common classes of supporting agents are polymers (covered in chapter 2.2), ionic surfactants^[65-67], ionic liquids^[4,68] and lewis basic (donor) ligands (Scheme 10).



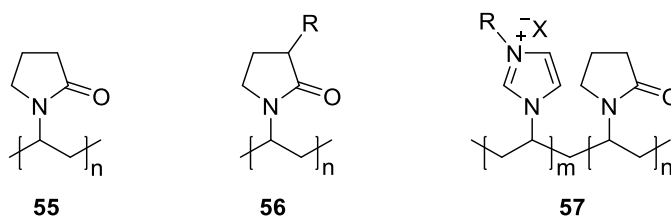
Scheme 10: Stabilizing agents for metal NP catalysts.

Ionic surfactants like tetraalkylammonium bromide (**47**)^[67] and ionic liquids (ILs) such as 1-*n*-butyl-3-methylimidazolium hexafluorophosphate (BMI•PF₆, **48**)^[69] generally exhibit only relatively weak interactions with the NPs and their stabilizing effect is derived from the formation of a protective layer around the NPs, shielding the surface mainly through electrostatic interactions. These stabilizing agents are mainly used in biphasic liquid-liquid (water or IL/substrate) systems to enable simple recovery and reusability of the NPs by phase separation.

In contrast, lewis basic ligands coordinate to the surface of the NPs with their donor atoms (e.g. O, N, S, P) and expose the (usually hydrophobic) backbone of the ligand to the solution forming protective layers around the NPs.^[70] This stabilization system not only allows the control over the growth of the NPs by varying the amount of stabilizers added but also the modification of the protective layer and the resulting reactivity through fine-tuning the electronic and steric properties of the ligands. Typical ligands used for the stabilization of NPs are long-chain alkyl amines, thiols or fatty acids (**49 - 51**) but also smaller organic molecules such as triphenylphosphine (**52**), 3,3-bipyridines (**53**), or even NHCs (**54**).^[71,72] Especially NHCs have been considered as ideal ligands for stabilization due to their excellent electron donor properties and oxidation stability, compared to phosphines, through the introduction of bulky residues.^[73]

2.2. Polymer-supported metal nanoparticle catalysts

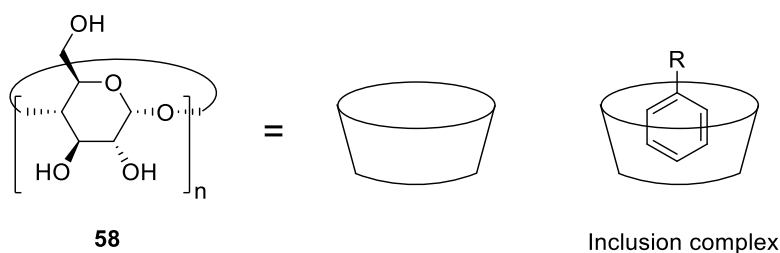
While a plethora of different polymers and macromolecular structures have been studied for the stabilization of NP catalysts^[74], poly(N-vinyl-2-pyrrolidone) (PVP, **55**) is among the most well-researched candidates due to its non-toxic nature and solubility in most polar solvents. Numerous modifications to chain length but also the introduction of alkyl side chains (**56**) on the pyrrolidone or copolymerization with other monomers (**57**) have been studied.^[75–78]



Scheme 11: Different modifications of PVP used as NP stabilizers.

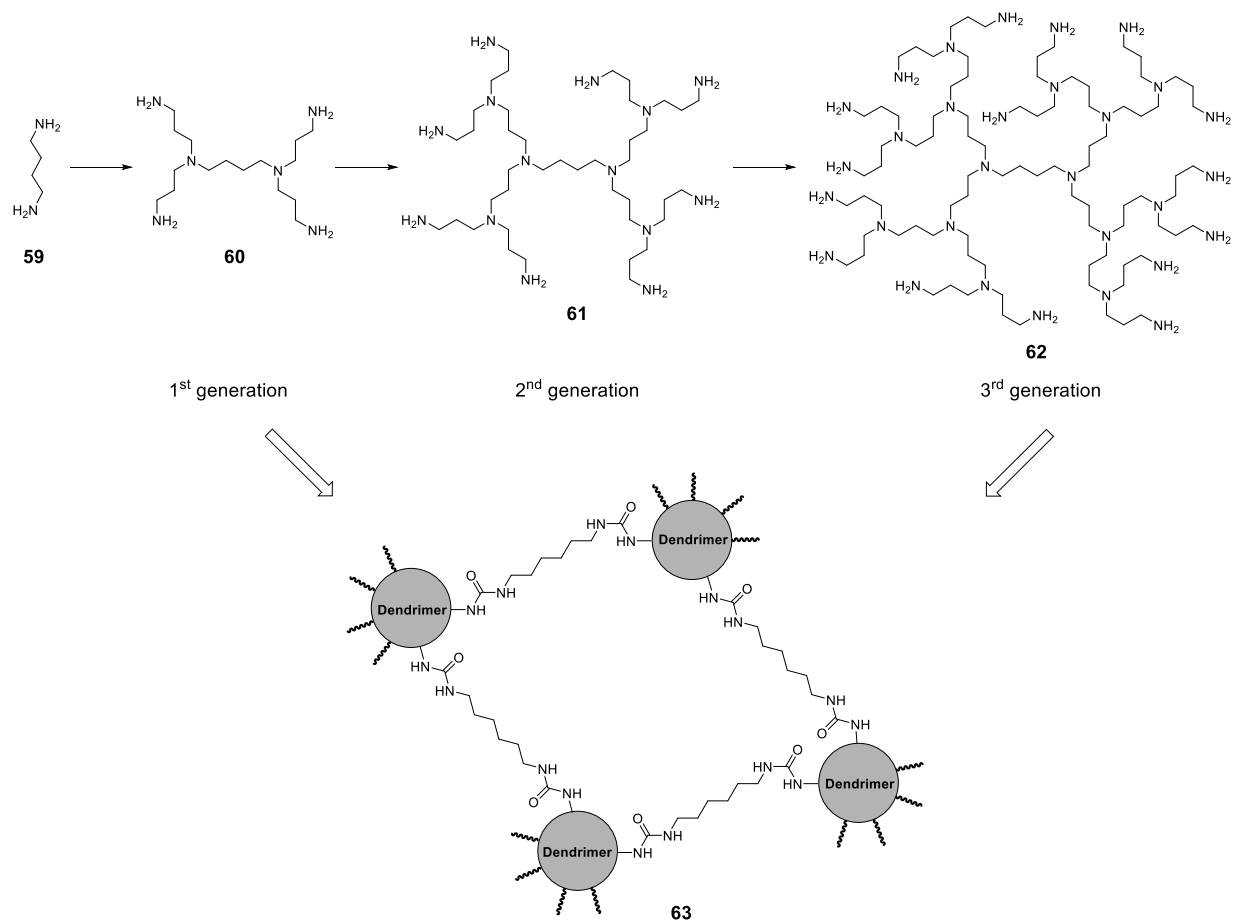
Most remarkably, Xu *et al.* in 2006 employed a long-chained, amphiphilic PVP with an average molecular weight of 1,250,000 g/mol to stabilize Ru NPs as arene hydrogenation catalyst.^[79] The catalyst was used in a two-phase water/organic system and excellent TOFs of 45,000 h⁻¹ and 29,000 h⁻¹ were achieved for the hydrogenation of benzene and toluene, respectively (80 °C, 40 bar H₂). The high reactivity was attributed to the formation of microreactors in the aqueous phase by the PVP-Ru NPs. The microreactors not only prevented agglomeration of the NPs, but they also provided a hydrophobic microenvironment for catalyst and substrate, improving the interaction between them. In addition, a significant increase in benzene solubility in the aqueous phase was observed in the presence of those microreactors due to their hydrophobic properties. Interestingly, while the electron-rich substrate anisole was still reduced with a

high TOF of 16,000 h⁻¹, the reaction was significantly slower with electron-poor substrates such as methylbenzoate (TOF 1,100 h⁻¹) due to the reduced electron density in the aromatic system.



Scheme 12: Structure of cyclodextrins and depiction of an inclusion complex.

Several studies have also been performed on the utilization of cyclodextrins (CDs, **58**) together with or without other stabilizing agents.^[80] CDs are cyclic oligosaccharides made of glucopyranose units that can stabilize the surface of NPs through steric interaction or coordination with the numerous –OH groups (Scheme **12**). However, due to their cyclic shape, they can also interact with different substrates and form inclusion complexes that can influence the selectivity of subsequent reactions. Ponchel *et al.* in 2011 also showed that CDs in combination with PVP can control the growth of Ru NPs leading to improved reactivity in the aqueous hydrogenation of furfural (30 °C, 10 bar).^[81] They also observed a slightly different product distribution of FA/THFA with a ratio of 94/6 without CDs to 90/10 when CDs were employed. Later, Hou *et al.* developed a copolymer of cyclodextrins with polyethylene glycol (PEG-CD) to stabilize Ru NPs that could selectively reduce several biomass-derived platform molecules, including the hydrogenation of furfural to THFA with 95% conversion and 99% selectivity, although at harsher reaction conditions (130 °C, 40 bar).^[82] Karakhanov *et al.* also used cyclodextrins together with polyacrylic acid (PAA) stabilized Rh NPs in a tetraalkylammonium ionic liquid to achieve a selective hydrogenation of phenol to cyclohexanone under relatively mild conditions (80 °C, 10-40 bar, 100% selectivity).^[83] The application of methylated CDs without further stabilizing agents was investigated by Roucoux *et al.*^[84] The resulting Ru NPs showed different selectivities in the hydrogenation of styrene under mild conditions (20 °C, 1 bar). Depending on the methylation degree and the ring size (6-8) of the CDs the formed product was exclusively ethylbenzene or ethylcyclohexane.



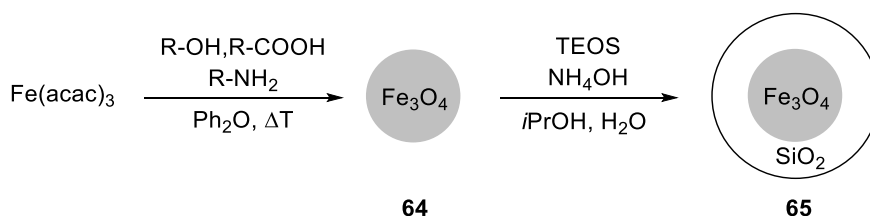
Scheme 13: Crosslinked dendrimer spheres as NP stabilizing agents developed by Karakhanov *et al.*^[85]

Crosslinked matrices of dendrimers as stabilizing agents for Ru NPs were also investigated by Karakhanov *et al.* (Scheme 13).^[85] Dendrimers are macromolecules exhibiting a regular, branched structure with a controlled size depending on the amount of branching sites from the central core (generations), usually forming three-dimensional spheres. This arrangement allows for a facile manipulation of selectivity and other properties by modification of the terminal groups covering the surface of the spheres as well as the catalyst recovery by fractional precipitation.^[86] The authors used poly(propylene imine) (PPI) dendrimers (60 - 62) with 1,4-diaminobutane (59) as a core and the crosslinking was achieved with hexamethylene diisocyanate (Scheme 13). Interestingly, it was found that third-generation dendrimers (62) favored the formation of smaller (1 nm) NPs while with first-generation (60) dendrimers larger (4 nm) NPs were formed. Surprisingly, catalyst 62 showed less activity in the hydrogenation of different phenol substrates, which was attributed to the smaller NPs being more prone to oxidation and the lower steric hindrance in dendrimer matrix 60. The use of water as a solvent also proved to increase the reactivity of the catalyst by 1.5 to 50-fold depending on the substrate, with the highest reactivity being achieved in the hydrogenation of resorcinol (TOF = 80,727 h⁻¹). Several other water-soluble substrates could also be reduced to the

corresponding cyclohexanols with good reactivities under relatively mild conditions (85 °C, 30 bar) such as phenol (TOF = 1,260 h⁻¹) or hydroquinone (TOF = 16,360). The same catalyst system was also employed in a two-phase system (water/substrate) for the hydrogenations of benzene and alkylated benzenes such as ethylbenzene or *o*-xylene with satisfactory TOFs of 4,675 h⁻¹, 1,320 h⁻¹ and 390 h⁻¹, respectively.

2.3. Magnetic nanoparticles as catalyst supports

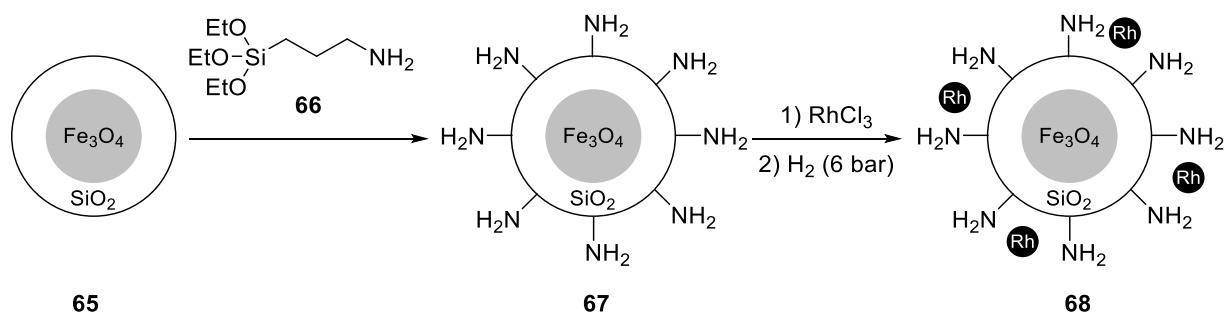
Another class of supports for NP catalysts that is gaining in popularity are magnetic NPs (MNPs).^[87–89] They exhibit the same advantageous properties of their non-magnetic counterparts, such as a larger surface area due to their high surface-to-volume ratio which can act as a catalyst itself in some transformations^[90,91] or serve as a platform for the immobilization of catalytically active species.^[92] In addition, the key attribute is of course the simple and efficient removal of those NPs from solution with an external magnet, eliminating the need for other separation techniques such as filtration or extraction. A large variety of MNPs has been developed over the years based on the metals Fe, Co or Ni as well as some of their alloys and oxides.^[88] One of the most widely used and well-studied systems are magnetite (Fe₃O₄) NPs (**64**), due to their low toxicity as well as their cheap and easy preparation. The synthesis can be readily achieved, for example through the thermal decomposition of Fe(acac)₃ in the presence of stabilizers such as oleic acid and oleyamine.^[93] The small size (3–20 nm) of the resulting NPs also renders them superparamagnetic and thus they possess no magnetization in the absence of an external magnetic field which makes them relatively stable towards agglomeration. In cases where unwanted side reactions from the magnetic core need to be suppressed or the stability of the NPs cannot be ensured under the reaction conditions, core-shell systems were found to be a very successful approach. The MNPs (core) deliver the desired magnetic properties and are surrounded by an inert protective layer (shell) that stabilizes them from degradation and allows the immobilization of other catalytically active species such as metal complexes, organocatalysts or other NPs. While numerous types of shell systems are known, such as organic ligands or polymers, inorganic materials like carbon or mainly silica are very prominent. A stable silica shell of variable thickness can be directly grafted on the surface of Fe₃O₄ NPs using the Stöber method.^[94] This sol-gel approach relies on the hydrolysis of tetraethoxysilane (TEOS) with aqueous ammonia. The thickness of the shell can be fine-tuned by varying the concentrations of TEOS and ammonia and the resulting silanol groups on the surface can be readily functionalized.



Scheme 14: Synthesis of silica-coated Fe_3O_4 NPs.

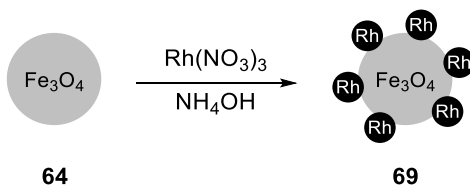
2.4. Magnetic nanoparticle supported metal nanoparticle catalysts

Even though MNPs have been extensively used as catalyst supports for a variety of different transformations, the reports on MNP supported catalysts for aromatic hydrogenations are relatively scarce. The first example was published in 2008 by Rossi *et al.* where the aforementioned silica-coated Fe_3O_4 NPs (**65**) were used, functionalized with amino groups through oligomerization with 3-(aminopropyl)-triethoxysilane (**66**).^[95] The amino groups were then utilized to immobilize RhCl_3 which was then reduced *in situ* by hydrogen to form Rh NPs. The resulting catalyst (**68**) showed excellent magnetic properties and could be efficiently recovered and reused for at least 20 times without only a negligible amount of Rh leaching into the products (<0.67 ppm). However, the achieved TOFs in the hydrogenation of benzene at 6 bar H_2 were only 825 h^{-1} and 196 h^{-1} at $75 \text{ }^\circ\text{C}$ and $25 \text{ }^\circ\text{C}$, respectively.



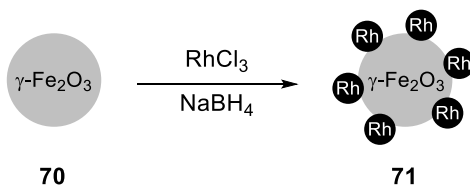
Scheme 15: Immobilization of Rh NPs on amino-functionalized $\text{SiO}_2 @ \text{Fe}_3\text{O}_4$ NPs by Rossi *et al.*^[95]

Later, the authors demonstrated that the catalyst can also be used for the hydrogenation of anthracene under similar conditions, although the required reaction times and catalyst loading were significantly higher due to the annelated polyaromatic system of the substrate.^[96]



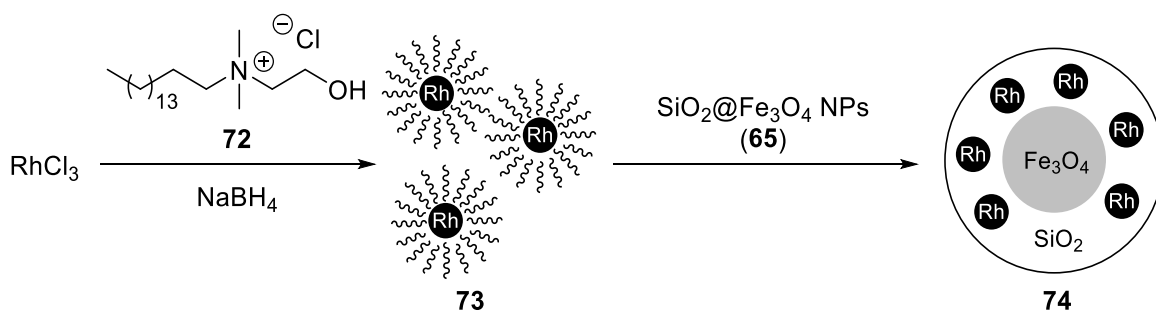
Scheme 16: Direct deposition of Rh NPs on Fe_3O_4 NPs by Shaikh *et al.*^[97]

Shaikh *et al.* reported Rh NPs directly immobilized on the surface of Fe_3O_4 NPs by a mild reduction of $\text{Rh}(\text{NO}_3)_3$ with ammonia in aqueous media, for the reduction of N-heteroarenes in water as well as neat arenes.^[97] The hydrogenation of neat benzene required relatively harsh conditions of 100 °C and 30 bar H_2 to achieve full conversion with a TOF of 297 h^{-1} while for toluene only 70% conversion was obtained even at 130 °C and 50 bar H_2 (TOF = 29 h^{-1}). N-heteroarenes such as quinoline or pyridine were hydrogenated in water to 1,2,3,4-tetrahydroquinoline and piperidine. For quinoline, a TOF of 54 h^{-1} was achieved at 50 °C with 20 bar while pyridine required 115 °C and 40 bar (TOF = 217 h^{-1}). However, the catalyst performed significantly better under transfer hydrogenation conditions employing tetrahydroxydiboron as a reductant, reaching a TOF of 1,632 h^{-1} in the reduction of quinoline.



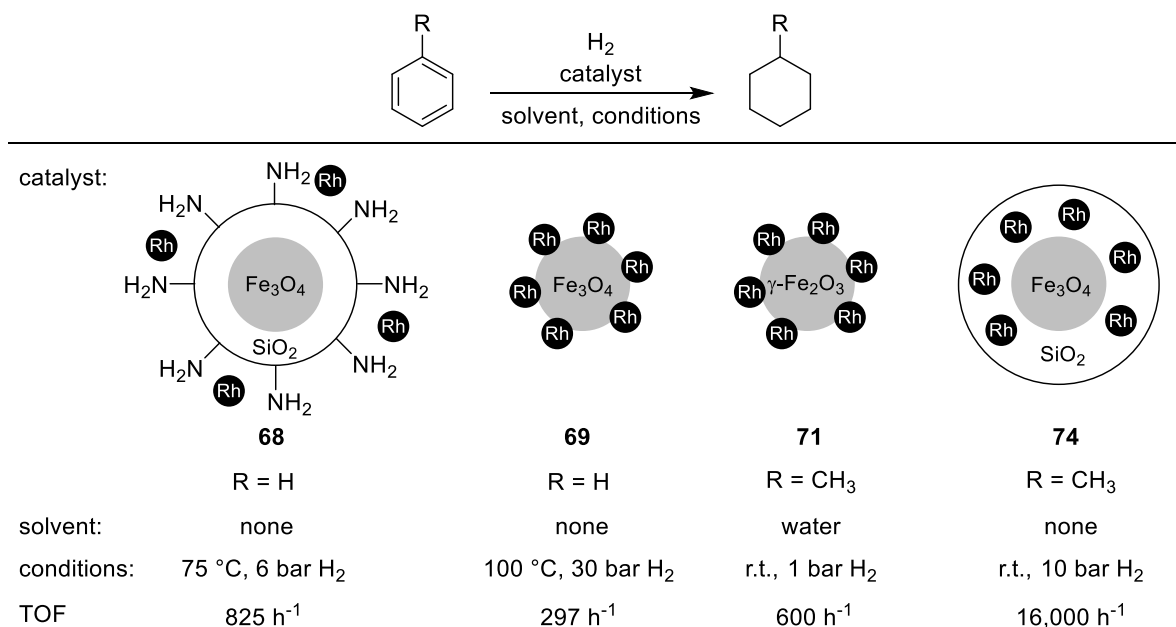
Scheme 17: Direct deposition of Rh NPs on $\gamma\text{-Fe}_2\text{O}_3$ NPs by Roucoux *et al.*^[98]

A very similar catalyst system was reported in 2016 by Roucoux *et al.*, using maghemite ($\gamma\text{-Fe}_2\text{O}_3$) NPs (**70**) as magnetic support.^[98] In this case, the Rh NPs were synthesized from RhCl_3 with NaBH_4 as a reducing agent. The catalyst (**71**) was active in the hydrogenation of arenes using a biphasic water/substrate system at r.t. with only 1 bar H_2 . Considering these mild conditions, a good TOF of 600 h^{-1} for the hydrogenation of toluene was achieved and the catalyst could be recycled for five runs without any loss in catalytic activity.



Scheme 18: Wet impregnation of $\text{SiO}_2@Fe_3O_4$ NPs with colloidal Rh NPs by Rossi and Roucoux *et al.*^[99]

Lastly, Rossi and Roucoux *et al.* developed an alternative approach for the immobilization of NPs on magnetic supports, by pre-synthesizing surfactant stabilized Rh NPs (**73**) and transferring them onto silica-coated Fe_3O_4 NPs (**65**) by wet impregnation.^[99] The resulting catalyst (**74**) was mainly tested for the hydrogenation of alkenes, but also showed a remarkable reactivity in the hydrogenation of aromatic compounds such as toluene, achieving an impressive TOF of 16.000 h^{-1} under mild conditions (neat, r.t., 10 bar H_2). Unfortunately, only low activities were observed when oxygenated arenes such as anisole or *m*-cresol were used as substrates (10% and 1.5% yield, respectively). A short overview of the so far developed catalyst systems and their hydrogenation performance is given below (Scheme 19).



Scheme 19: Overview over magnetically recoverable NP catalysts for aromatic hydrogenations.

2.5. Magnetic Co/C nanoparticles as catalyst supports

Another promising type of magnetic core-shell NPs are carbon-coated cobalt (Co/C) NPs.^[100,101] These exhibit a significantly higher saturation magnetization (158 emu/g)^[102] compared to the previously discussed Fe₃O₄ NPs (82 emu/g).^[93] This allows the attachment of larger amounts of non-magnetic material like polymers or linkers, while still being removable with an external magnet within just a few seconds. The attached groups can facilitate their use in diverse applications e.g. when high catalyst loadings or better dispersibility in different solvents are required, making the Co/C NPs attractive for potential use as a magnetic support. In 2007 Stark *et al.* also reported a reliable large scale (>30 g/h) synthesis for these Co/C NPs-based on the reducing flame spray pyrolysis of a metal-organic precursor under nitrogen atmosphere.^[102] The carbon coating is achieved by the controlled addition of acetylene to the Co NPs, which decomposes under the conditions, forming 2 – 4 graphene-like layers around the cobalt core. The resulting Co/C NPs have a diameter of 20 – 50 nm, are air-stable up to a temperature of 160 °C and pH resistant within a range of 4 – 11, proving the excellent protection capabilities of the carbon layers for otherwise pyrophoric Co NPs. The carbon surface can be used for the direct deposition of catalytically active NPs, but also non-covalent immobilization of pyrene tagged catalysts^[103] or even covalent functionalization *via* diazonium chemistry with different linkers for more sophisticated catalytic systems.^[101]

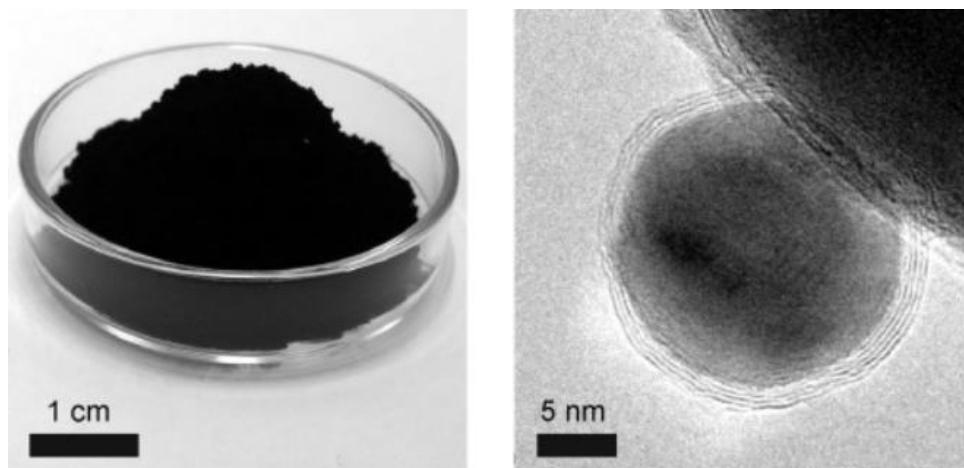
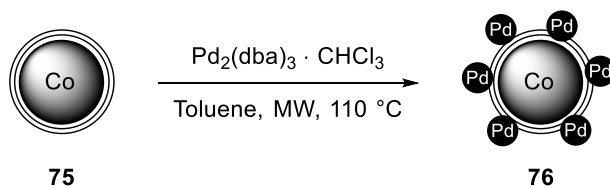


Figure 3: Photograph of about 5 g of the air-stable Co/C NPs (left), TEM image of Co/C NPs (right). Reprinted with permission from [102]. Copyright © 2007 WILEY-VCH Verlag GmbH & Co. KGaA, Weinheim

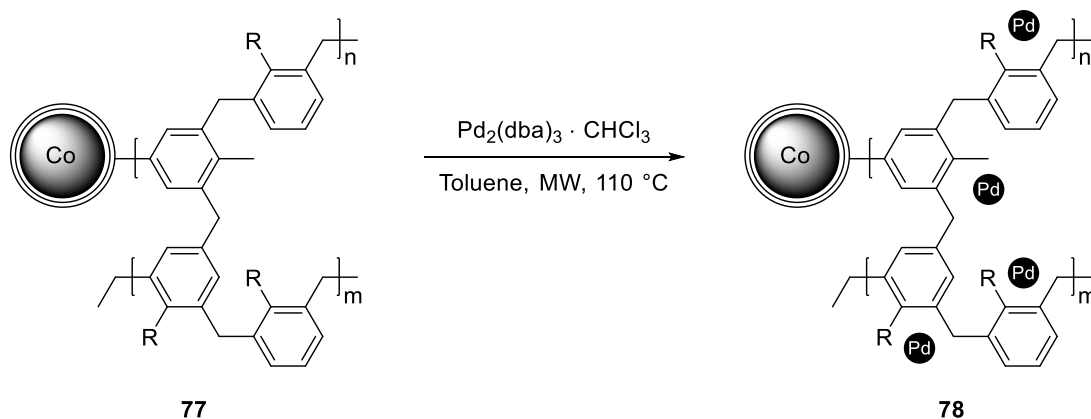
2.6. Co/C nanoparticle supported hydrogenation catalysts

Within the last decade, Reiser *et al.* have developed several catalytic systems for the hydrogenation of olefins, alkynes and nitro-groups, as well as other transformations.^[103–105] Even though, these systems proved to be highly efficient in their applications, no Co/C NP-based catalysts for the hydrogenation of arenes are known so far. Since the concepts of these catalytic systems can be effectively transferred towards the development of new aromatic hydrogenation catalysts, a selection of different Pd NP based magnetic Co/C nanocatalysts will be highlighted.



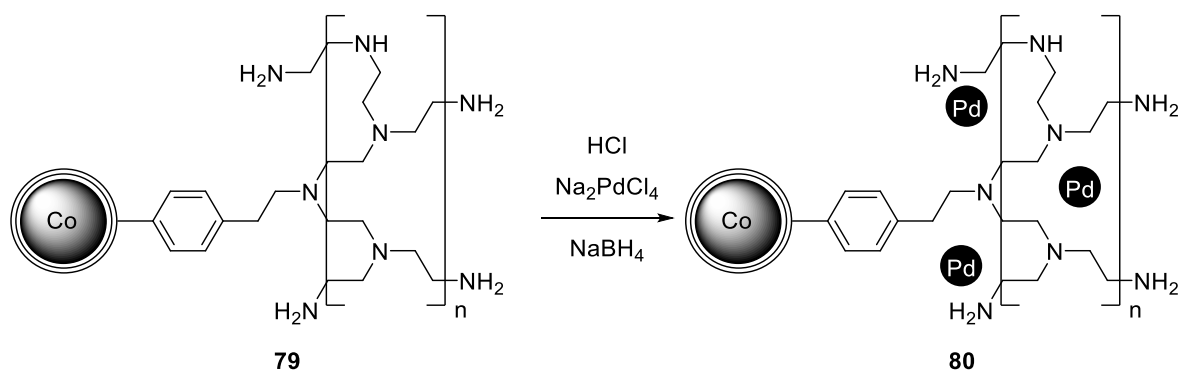
Scheme 20: Direct deposition of Pd NPs on Co/C NPs by Reiser *et al.*^[106]

In 2014, the group reported the direct deposition of Pd NPs on the carbon surface of Co/C NPs (**75**) through the microwave-assisted, thermal decomposition of $\text{Pd}_2(\text{dba})_3 \cdot \text{CHCl}_3$ with an immobilization efficiency of up to 100%.^[106] The resulting catalyst (**76**) was highly active in the hydrogenation of alkenes under mild conditions (r.t., 1 bar H_2), achieving an excellent TOF of up to $11,095 \text{ h}^{-1}$ in the reduction of *trans*-stilbene. The catalyst could be magnetically recovered and reused for six consecutive runs, even though the TOF decreased from $3,722 \text{ h}^{-1}$ to $2,203 \text{ h}^{-1}$ during the recycling procedure, corresponding to a 40% reactivity loss. While the loss of reactivity could not be attributed to a single factor, a combination of deactivation modes such as agglomeration of the Pd NPs, marginal Pd leaching ($\leq 6 \text{ ppm/cycle}$), oxidation or substrate/product inhibition of the Pd surface and loss of nanocomposites during recycling was suspected.



Scheme 21: Immobilization of Pd NPs in MOP@Co/C NPs by Reiser *et al.*^[107]

A new approach to achieve a better stabilization and protection of the Pd NPs was published in 2019.^[107] Therefore, a microporous organic polymer (MOP) was covalently grafted to the surface of the Co/C NPs through a Friedel-Crafts type polymerization of different aromatic monomers with formaldehyde dimethyl acetal (FDA) as an external crosslinker. With the Pd NPs being encapsulated into the MOP, an improved protection of the Pd NPs from agglomeration should be provided while still allowing access to the catalytically active sites due to the materials' inherent porosity.^[108] Again, the Pd NPs were synthesized and encapsulated according to the above mentioned microwave-assisted decomposition of $\text{Pd}_2(\text{dba})_3\text{-CHCl}_3$, achieving almost quantitative incorporation of Pd (Scheme 21). The best results were obtained with a toluene- or 2,2'-biphenol-based polymer giving TOFs of up to $3,000 \text{ h}^{-1}$ in the hydrogenation of styrene (r.t., 1 bar H_2). The effectiveness of the MOP to prevent NP agglomeration was demonstrated by increasing the Pd loading of the catalyst from 0.2 wt% up to 3.9 wt% without any loss in catalytic activity. In contrast, a steep decline in activity was observed with the previous catalyst (**76**) already when the loading was increased from 0.2 wt% to 0.8 wt%. The MOP catalysts (**78**) could also be successfully recovered and reused for six consecutive runs. However, the observed higher loss in reactivity (55%-57% compared to 40%) suggests that not all of the aforementioned deactivation modes could be sufficiently suppressed. Interestingly, the chosen monomers had a large effect on the detected Pd leaching of the catalyst and thus the leaching could be significantly reduced from an average 15 ppm/cycle to 2 ppm/cycle when 2,2'-biphenol was used instead of toluene.



Scheme 22: Immobilization of Pd NPs in PEI@Co/C NPs by Reiser *et al.*^[109]

Finally, Pd NPs incorporated into a poly(ethyleneimine) (PEI) polymer grafted on the Co/NPs (**80**) should be highlighted.^[109] This system is especially interesting due to its hydrophilic character, enabling the hydrogenation of alkenes in aqueous media. In this case, the incorporation of Pd NPs was carried out under slightly acidic conditions (pH 6) *via* the reduction of Na_2PdCl_4 with NaBH_4 , since the coordination of the PdCl_4^{2-} ions with the positively charged ammonium groups of the PEI polymer ensured a uniform distribution of Pd NPs across the polymer. The resulting catalyst showed high activity in the hydrogenation

of 4-hydroxy-2-cyclopentenone in aqueous media under mild conditions (r.t., 1 bar H₂) achieving TOFs of up to 2,450 h⁻¹. Additionally, excellent recycling properties were observed using this system, with only a minor decrease in reactivity (yield dropping from 98% to 92%) within seven consecutive runs and an average Pd leaching of 3 ppm/cycle.

The same catalyst was also be used for other transformations such as Heck couplings or Tsuji-Trost allylations^[109] and without the Pd NPs, the system revealed promising results as an Hg²⁺ scavenger for potential applications in wastewater treatment.^[110] Considering its application as support for aromatic hydrogenations, this approach seemed to have the highest potential. Not only because of its high water compatibility and excellent recycling performance, but also due to its structural resemblance with the aforementioned PPI dendrimers developed by Karakhanov *et al.*^[85], which also showed good catalytic activity, with incorporated Ru NPs.

With the aim of developing a novel, Co/C-based catalyst system for aromatic hydrogenations, all three of the aforementioned approaches were investigated, i.e. the direct deposition of NPs on the Co/C surface, the incorporation into a MOP (**77**) and into a PEI polymer (**79**). Even though the utilization of an arene-containing catalyst support such as the MOP (**77**) for aromatic hydrogenations seems counterintuitive due to the unpredictable changes in support properties in the case of a hydrogenation of the polymer, several such systems have demonstrated the feasibility of this approach.^[111–114] Given their numerous successful applications in this field, Ru NPs were chosen as catalytically active species.^[70] Additionally, the immobilization of CPAs with a method inspired by the grafting of the MOPs was examined, potentially giving rise to an enantioselective catalyst for aromatic hydrogenations following the previously mentioned procedure developed by Rueping *et al.* (Scheme 9).

B. Main part

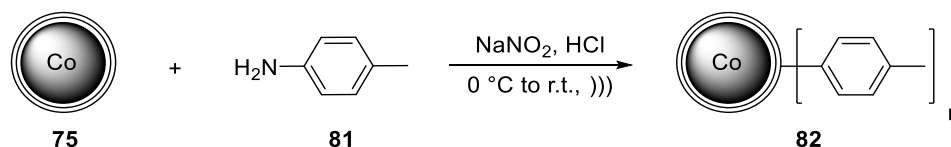
1. Magnetic Co/C nanoparticle supported Ru nanoparticle catalyst for aromatic hydrogenations

1.1. Catalyst synthesis

For the purpose of this work, the two previously introduced hybrid materials toluene-MOP@Co/C (**77**) and PEI@Co/C (**79**) were synthesized according to the literature procedures^[100,107]. In the case of **79**, several synthesis modifications were tested to study the effects of these alterations on the resulting hydrogenation performance.

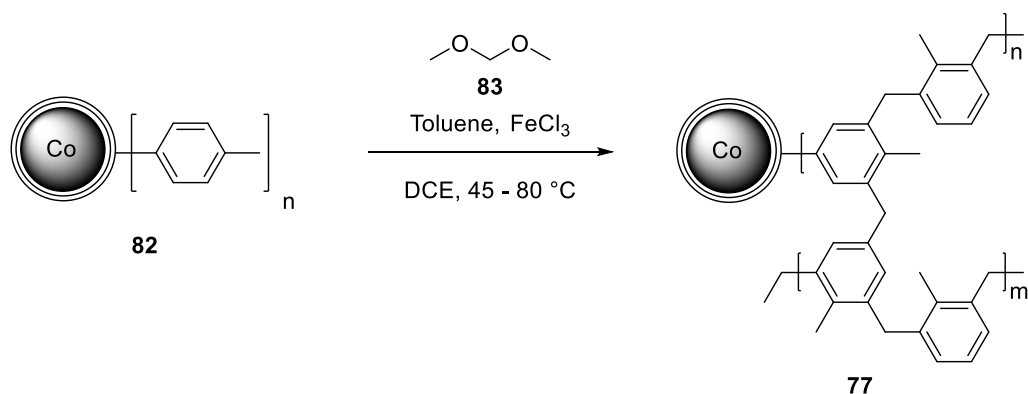
1.1.1. Co/C Nanoparticle supported microporous organic polymer synthesis

To covalently attach the toluene-based MOP to the Co/C NPs (**75**) the surface of the NPs had to be functionalized with an arene moiety (Scheme **23**). Therefore, *para*-toluidine (**81**) and NaNO₂ were used under acidic conditions to give the unstable diazonium salt of **81**. After nitrogen extrusion, the *in situ* generated aryl radical could then form a covalent bond to the carbon surface, giving rise to the toluene functionalized NPs (**82**).^[102]



Scheme 23: Synthesis of toluene functionalized Co/C NPs (**82**) *via* diazonium chemistry.^[102]))) = ultrasound.

Subsequently, the toluene-based MOP was grafted to the functionalized NPs (**82**). For this connection, Reiser *et al.*^[107] modified a polymerization method originally published by Tan *et al.*^[115] For the polymerization, toluene and the toluene functionalized NPs (**82**) were used as monomers together with FeCl₃ as catalyst and formaldehyde dimethyl acetal (FDA, **83**) as an external crosslinker, using 1,2-dichloroethane (DCE) as a solvent (Scheme **24**). Through this Friedel-Crafts type polymerization, the monomers were interconnected by the formation of CH₂ bridges, with methanol as the only byproduct.

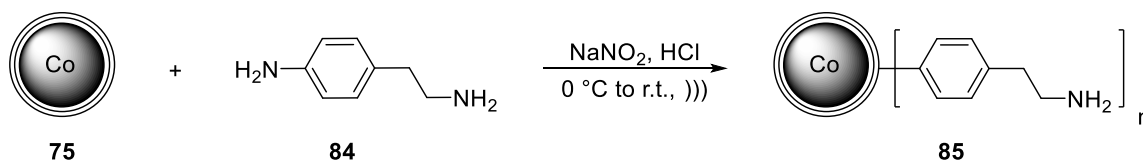


Scheme 24: Synthesis of MOP@Co/C NPs (**77**) following a modified method by Reiser *et al.*^[107]

After washing and drying, the resulting polymer (**77**) showed a carbon content of 36 wt% C. This confirmed the attachment of a significant amount of polymer when compared with the toluene-functionalized Co/C NPs (**82**) bearing a carbon content of 5 wt% C.

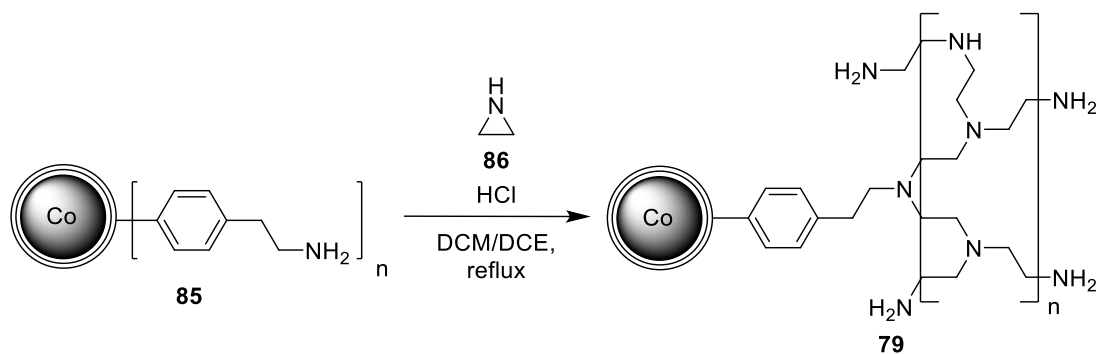
1.1.2. Co/C nanoparticle supported poly(ethylenimine) polymer synthesis

Analogous to the above-described polymerization technique, the Co/C NPs (**75**) again had to be functionalized with a suitable linker, namely amino groups, in the first step (Scheme 25). This was achieved using the established diazonium chemistry^[102] and 4-(2-aminoethyl)aniline (**84**), resulting in the amino-functionalized Co/C NPs (**85**) with a nitrogen content of 0.1 wt% N.



Scheme 25: Synthesis of amino-functionalized Co/C NPs (**85**) *via* diazonium chemistry.^[102]))) = ultrasound.

The amino-functionalized Co/C NPs (**85**) were then subjected to the acid-catalyzed ring-opening polymerization of aziridine (**86**), giving rise to a covalently bound PEI polymer around the Co/C NPs (Scheme 26).^[100]



Scheme 26: Synthesis of PEI@Co/C NPs (**79**) *via* acid-catalyzed ring-opening polymerization of aziridine (**86**).^[100]

Variations in the resulting degree of polymerization could be achieved by changing the solvent from DCM to DCE, modifying the stoichiometric ratio of aziridine (**86**) to NPs (**85**), and prolonging or shortening the reaction time. The success of the polymerization could easily be quantified by the distinct increase of the nitrogen content, comparing the amino-functionalized Co/C NPs (**85**) with only 0.1 wt% N to the PEI@Co/C NPs (**79**) with up to 14 wt% N.

Table 1: Synthesis of PEI@Co/C NPs (**79**) with diverse N-contents by variation of solvent, ratio of **85/86**, and reaction time.

Entry	Solvent ^a	Ratio 85/86 [m/m] ^b	Time [h]	N-content [wt%] ^c	Compound
1	DCM	0.38	24	0.6	79a
2	DCM	0.33	72	3.1	79b
3	DCM	0.33	24	0.5	79c
4	DCM	0.33	24	0.7	79d
5	DCM	0.33	24	0.9	79e
6	DCM	2.0	24	0.3	79f
7	DCE	0.35	24	7.8	79g
8	DCE	0.33	72	14	79h
9	DCE	10	24	0.3	79i

^a Reactions in DCM were performed at 40 °C and in DCE at 80 °C, ^b mass ratio of amino-functionalized NPs (**85**) to aziridine (**86**),

^c determined by elemental analysis.

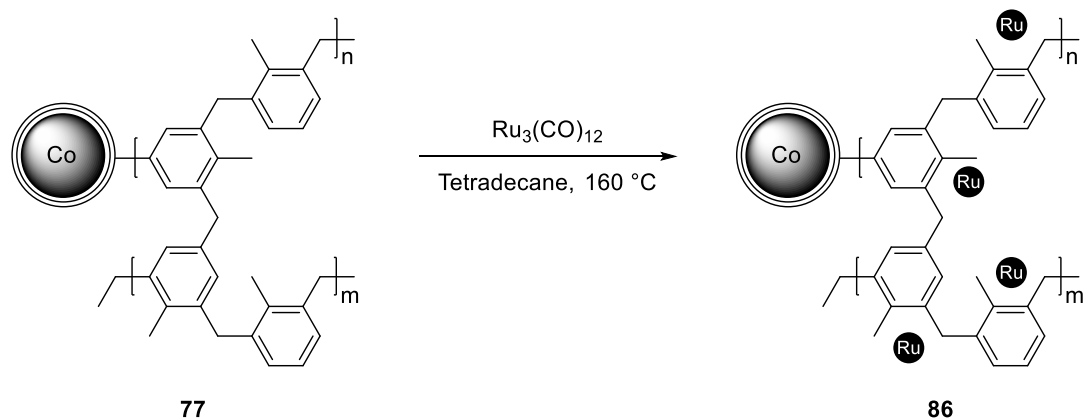
Generally, the use of DCE as solvent and prolonged reaction times resulted in higher polymerization degrees, giving PEI@Co/C NPs (**79**) with a larger nitrogen content compared to the reaction products in DCM. With DCM, a relatively low polymer content of 0.6 wt% N was achieved within 24 h which could be increased to 3.1 wt% N with a longer reaction time of 72 h (Table 1, entries 1 and 2). Repeating the

experiments also showed an inconsistency in the nitrogen content of the compounds ranging from 0.5 wt% N to 0.9 wt% N, even though no parameters were changed (Table 1, entries 3-5). This phenomenon was attributed to weak binding of the polymer to the NPs in the case of DCM as solvent, which lead to large amounts of non-magnetic material being removed during the washing steps, causing inconsistent polymer loadings. In order to reduce the amount of non-magnetic material, the stoichiometric ratio of NPs (**85**) to aziridine (**86**) was increased. Thereby, it was possible to synthesize compounds with very little polymer contents of only 0.3 wt% N (Table 1, entry 6). In contrast, when DCE was employed as solvent, an overall much higher polymer content of 7.8 wt% N (24 h) and 14 wt% N (72h) was observed (Table 1, entries 7 and 8). Changing the stoichiometric ratio, in this case, revealed that the polymerization was also more efficient in DCE and only about 1/6th of the aziridine had to be used to achieve the same loading of 0.3 wt% N as with DCM (Table 1, entry 9).

Overall, the use of DCE as solvent for the polymerization showed several advantages over the results in DCM. The more effective polymerization resulted in less formation of non-magnetic polymer and thus less waste of the employed aziridine. Additionally, a larger coating of polymer on the NPs would also allow the incorporation of more Ru NPs and therefore also increase the loading of catalytically active sites on the compound, which is often desired when higher catalyst loadings are required for reactions. A larger polymer should also allow for a more even distribution of the Ru-NPs in the polymer, leading to an even size distribution of smaller Ru-NPs that show increased reactivity.

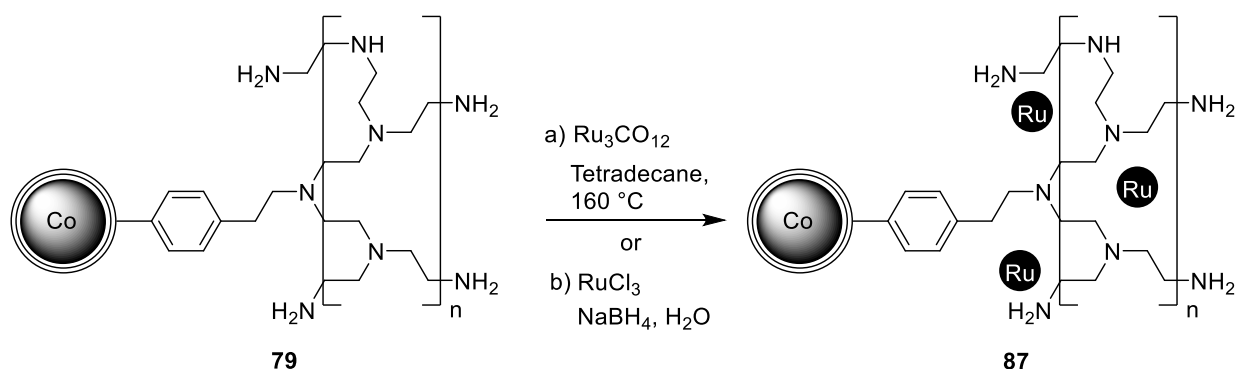
1.1.3. Initial ruthenium incorporation studies

For the incorporation of the catalytically active Ru-NPs into the MOP@Co/C NPs (**77**) the thermal decomposition of Ru₃(CO)₁₂ was chosen as the NP synthesis method. This approach has proved its efficiency for the deposition of Ru NPs onto thermally reduced graphite oxide (TRGO) as heterogeneous support by Janiak *et al.*, providing an active catalyst for the hydrogenation of benzene^[116]. Furthermore, also homogeneous stabilizers such as sodium dodecylsulfate (SDS), sodium 2-ethylhexanoate or PVP (**55**) have been employed by García *et al.* to successfully synthesize highly active colloidal Ru NPs, which were tested in the reduction of nitriles.^[117]



Scheme 27: Immobilization of Ru NPs using the thermal decomposition of $\text{Ru}_3(\text{CO})_{12}$.

Due to the hydrophobic nature of the toluene-based polymer (**77**), tetradecane was used as a high-boiling, non-stabilizing solvent. The mixture was heated to $160\text{ }^\circ\text{C}$ for 30 min, upon which the $\text{Ru}_3(\text{CO})_{12}$ decomposed, giving rise to the immobilized Ru@MOP@Co/C NPs catalyst (**86**) with a loading of 1.6 wt% Ru, corresponding to 60% immobilization of the used Ru (Scheme **27**).



Scheme 28: Immobilization of Ru NPs in PEI@Co/C NPs (**79**).

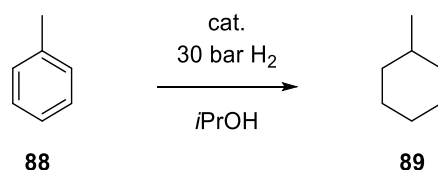
In the case of the PEI@Co/C NPs (**79**), two different Ru incorporation methods were tested. On the one hand, the thermal decomposition of $\text{Ru}_3(\text{CO})_{12}$ and on the other hand, the high water dispersibility of the PEI system was taken into account, allowing the reduction of RuCl_3 in aqueous media, using NaBH_4 as reductant (Scheme **28**). Due to the use of comparably cheap metal salts as nanoparticle precursors, this chemical reduction method is a widely applied and well-established synthesis route for NPs. Özkar *et al.* used this strategy to immobilized Ru NPs on nanozeolites, gaining access to a reusable, green catalyst for the hydrogenation of neat arenes under mild conditions ($25\text{ }^\circ\text{C}$, $<3\text{ bar H}_2$). In the case of the reduction of benzene, a high TOF of $5,430\text{ h}^{-1}$ was achieved.^[118]

With 40% incorporation and a corresponding loading of 1.3 wt% Ru, the thermal decomposition method gave slightly worse results when PEI@Co/C NPs (**79a**) were used compared to the incorporation in the MOP-system (**77**). Presumably, this could be a result of the poor dispersibility of the highly polar PEI NPs in the non-polar solvent tetradecane.

For the reduction method, initially two PEI@Co/C compounds were compared. One with a low nitrogen content of 0.6 wt% N (**79a**) derived from the polymerization in DCM and one with a higher nitrogen content of 7.8 wt% N (**79g**) from the polymerization in DCE. For compound **79g** a high incorporation of 80% was obtained, with the corresponding catalyst having a loading of 1.4 wt% Ru. In contrast, for compound **79a** the immobilization resulted in only 10% of the Ru getting incorporated in the polymer giving a loading of 1.7 wt% Ru. An overview of the aforementioned achieved incorporations and loadings is also given in Table 2 in the next chapter.

1.1.4. Initial hydrogenation test reactions

To assess the catalytic activity of the synthesized compounds, the hydrogenation of toluene (**88**) was chosen as a model reaction due to its lower toxicity compared to the commonly used benzene (Scheme 29). The reactions were carried out in a stainless-steel autoclave at 30 bar H₂ pressure, with a small amount (40 vol%) of isopropanol to ensure a better dispersion of the NPs.



Scheme 29: Hydrogenation of toluene (**88**) as a model reaction to test the catalytic activity of the Ru-catalysts.

While the MOP@Co/C derived compound (**86**) was found to be catalytically active, achieving a conversion of 46% within 24 h at 50 °C (Table 2, entry 1), the concerns towards the stability of the material under these conditions turned out to be substantiated. When a 2nd run of the reaction was performed with the recycled catalyst, the conversion already dropped to only 21%, alongside with a visible degradation of the material through the formation of non-magnetic polymer. For this reason, the research focus was changed to the PEI@Co/C NPs-based Ru-catalysts (**87**).

When the catalysts derived from the PEI@Co/C NPs (**79a**) with a low nitrogen content (0.6 wt%) were employed an improved reactivity was observed. Using the thermal decomposition method, full conversion was achieved in 24 h, although the elevated temperature of 50 °C was still required and only minimal (3%) conversion was obtained at r.t. (Table 2, entries 2 and 3). The best results were reached with the chemical reduction method, making it possible to reduce the reaction temperature to r.t. while giving full conversion after only 5 h (Table 2, entry 4).

Table 2: Comparison of different incorporation methods and the resulting performances in the hydrogenation of toluene (**88**).

Entry	Polymer	NP synthesis			Hydrogenation performance		
		Precursor	Incorporation [%]	Loading [wt%] ^a	Temp [°C]	Time [h]	Conversion [%] ^b
1	77	Ru ₃ CO ₁₂	60	1.6	50	24	46 (21 ^c)
2	79a	Ru ₃ CO ₁₂	40	1.3	50	24	100
3	79a	Ru ₃ CO ₁₂	40	1.3	r.t.	24	3
4	79a	RuCl ₃	10	1.7	r.t.	5	100
5	79g	RuCl ₃	80	1.4	r.t.	24	-

^a Determined by ICP-OES, ^b Reaction conditions: 10 mmol toluene (**88**), 0.4 mL isopropanol, 0.03 mol% (entries 1-3) or 0.015 mol% (entries 4 and 5) Ru-catalyst (**87**), 30 bar H₂ pressure, conversion determined by GC-FID, ^c 2nd run of the catalyst in entry 1.

For the catalyst derived from the PEI@Co/C NPs **79g** with a high nitrogen content (7.8 wt% N) no catalytic activity could be observed (Table 2, entry 5). However, due to the aforementioned desirable advantages of the polymer, as well as the good incorporation of 80% of the employed Ruthenium, the incorporation of Ru-NPs in these polymers was further investigated. Especially considering the overall economics of the total catalyst synthesis, the attractiveness of a highly recyclable catalyst is significantly diminished when the majority of the expensive noble metal is lost during the incorporation. Therefore, the high retention of the employed metal inside the polymer was deemed to be a good starting point for further research.

1.1.5. Further studies on high nitrogen content poly(ethylenimine) polymers

Since numerous factors during the synthesis play a role and can influence the size and topology of the resulting NPs, several different parameters and reaction conditions were investigated. One of the important aspects to take into consideration is the metal loading of the compound. As already previously

mentioned in the case of Pd@Co/C NPs (**76**), the reactivity of the catalyst can be drastically influenced by changing the metal loading on the corresponding material. For example, a higher concentration of metal precursor during the synthesis might lead to the formation of larger particles, or when more NPs of any size are incorporated in the polymer the chance for aggregation of the NPs is increased. In both cases, the available surface area is limited and thus the activity is reduced. While the previous catalysts (Table 2, entries 3-6) all had similar Ru loadings between 1.3 wt% and 1.7 wt%, more significant loading variations had to be investigated to determine the effects of this aspect. For this purpose, using the higher nitrogen content of the polymer in **79g**, three different loadings from 1.6 wt% Ru to 8.0 wt% Ru were tested. In all cases, the incorporation of the metal was good and above 75%, with the surprisingly best incorporation rate of 97% at the highest employed loading (Table 3, entries 1-3). However, no catalytic activity was observed with these catalysts, leading to the conclusion that the formation conditions of the NPs might be the reactivity determining factor rather than the proposed loading.

Table 3: Ru incorporation studies in PEI@Co/C NPs (**79c**).

Entry	Polymer	Employed Ru [wt%]	Ru-loading [wt%] ^a	Incorp. [%] ^a	Variation ^b	Conversion [%] ^c
1	79g	1.6	1.2	75	-	-
2	79g	4.1	3.2	77	-	-
3	79g	8.0	7.7	97	-	-
4	79g	4.2	3.3	78	1 equiv. HCl	-
5	79g	4.3	2.9	68	2 equiv. HCl + slow add.	-
6	79g	4.0	1.9	48	9 equiv. HCl + slow add.	-
7	79g	4.1	3.1	75	2 equiv. KOH	-
8	79g	4.1	3.7	89	slow add.	-

^a determined by ICP-OES, ^b equivalents given relative to NaBH₄, slow add. = addition in 5 portions over 10 min, ^c Reaction conditions: 10 mmol toluene (**88**), 0.4 mL isopropanol, 0.015 mol% Ru-catalyst (**87**), r.t., 30 bar H₂ pressure, 24 h reaction time, conversion determined by GC-FID.

Another important factor is the hydrolysis of NaBH₄ in aqueous media, which acts as a competing reaction to the reduction of RuCl₃. When the hydrolysis exceeds the NP formation, insufficient reduction of RuCl₃ can occur, leading to either poor incorporation or the incorporation of inactive metal species. The hydrolysis of NaBH₄ is mainly influenced by the pH of the solution^[119] as well as the formed Ru NPs itself, as they can also catalyze the reaction.^[120] Therefore, the pH of the incorporation reaction was adjusted by

the addition of acid (HCl, Table 3, entries 4-6, pH 0.3, 0.9, and 1.2, respectively) or base (KOH, Table 3, entry 7, pH 13). Another parameter that was modified was the addition speed of the reductant, as the initial concentration of reductant can also influence the NP formation.^[121] An addition in multiple portions would therefore reduce the initial concentration while still ensuring a complete reduction. As expected, in acidic media the reaction became significantly more violent due to the increased, rapid H₂ formation from the hydrolysis, although no change in incorporation was observed with only 1 equiv. of HCl (Table 3, entries 2 and 4). When larger amounts of acid were added in combination with a slow addition rate of NaBH₄, the incorporation gradually decreased down to 48% with 9 equiv. of HCl (Table 3, entry 6), showing the negative influence of a faster NaBH₄ hydrolysis. In contrast, the reaction became significantly less violent in basic media due to the diminished H₂ formation, although the incorporation remained largely unchanged at 75% (Table 3, entry 7). The slower addition of NaBH₄ seemed to have a negative influence in acidic media due to the rapid hydrolysis and therefore resulted in lower incorporations (Table 3, entries 5 and 6). However, under neutral conditions, the slow addition showed a positive effect, increasing incorporation up to 89% (Table 3, entry 8). Even though these studies showed interesting effects on the incorporation, none of the variations resulted in any catalytic activity in the hydrogenation test reaction. This suggested that rather than the NP synthesis process, the polymer itself could be responsible for the lack of reactivity. Thus the aforementioned differences in reactivity of catalysts derived from PEI systems using DCE or DCM as solvent were further investigated.

1.1.6. Effects of polymer variations on the hydrogenation performance

For the investigation of the effects of the different polymer properties on the hydrogenation performance, different polymers were subjected to identical incorporation conditions and the same amounts of the resulting catalysts were employed in the hydrogenation test reaction. While this approach disregards the individual incorporation differences, these were considered to be negligible due to the only small variations in nitrogen content (0.3 wt% N to 0.9 wt% N) of the PEI systems.

In order to study the effect of solvent choice during the polymerization on the reactivity and rule out other effects, the stoichiometric ratios of the polymerization were adjusted (See Table 1, entries 6 and 9). This resulted in two compounds with a very similar nitrogen content of 0.3 wt% from the reaction in DCE (**79i**) and in DCM (**79f**). Due to this, the compounds should both have a very thin polymer shell with the solvent being the only difference. Indeed, the catalyst derived from polymer **79f**, using DCM as solvent, showed excellent reactivity (Table 4, entry 7), while no reactivity was observed in the case of the DCE derived

polymer (**79i**) (Table 4, entry 8). Therefore it seemed conclusive, that the utilization of DCE as polymerization solvent seems to shut down the reactivity of the catalysts, which is also in line with previous observations (Tables 2 and 3). A possible mechanism for this deactivation is that DCE gets partially incorporated in the polymer through nucleophilic substitution since similar reactions have already been shown by Domingos *et al.*^[122] The resulting presence of C-Cl bonds in the polymer could then lead to the formation of HCl during the hydrogenation through hydrogenolysis of these bonds, leading to catalyst poisoning.^[123]

Table 4: Effects of different PEI polymers on the hydrogenation performance.

Entry	Co/C NP precursor	EA [wt% N]	Cat. [mg]	Conversion [%] (after 3 h) ^a
1	79c	0.5	4.0	93
2	79d	0.7	6.8	74
3	79d	0.7	6.8	78
4	79d	0.7	6.8	74
5	79e	0.9	6.8	46
6	79e	0.9	6.8	42
7	79f	0.3	6.8	100
8	79i	0.3	6.8	-
9	85	0.1	6.8	-
10	75	0	6.8	63

^a Reaction conditions: 10 mmol toluene (**88**), 0.4 mL isopropanol, catalyst (**87**), r.t., 30 bar H₂ pressure, 3 h reaction time, conversion determined by GC-FID.

With the focus consequently being shifted to the compounds derived from the polymerizations in DCM, the consequences of the reproducibility differences during the polymerization (See Table 1, entries 3-5) were investigated. As mentioned before, even under identical reaction conditions, polymers with nitrogen contents ranging from 0.5 wt% to 0.9 wt% (**79c-e**) were obtained from the synthesis in DCM. Due to this, the reproducibility of the incorporation reaction and its effects on the catalytic activity were also examined. Fortunately, only minor differences of around 4% conversion were observed when the same batches of polymer were used for the incorporation (Table 4, entries 2-4). In contrast, very significant changes were observed when different batches of polymer were utilized. Here, a clear trend of decreasing reactivity from 93% to only 42% with an increase in nitrogen content of the polymer from 0.5 wt% to 0.9 wt% was found (Table 4, entries 1-6). In line with these results, the polymer containing only 0.3 wt% N (**79f**), gave the best results of the PEI polymers by achieving 100% conversion (Table 4, entry 7). As part of

these investigations, the amino-functionalized Co/C NPs (**85**) as well as the unfunctionalized Co/C NPs (**75**) were also tested for the Ru NP immobilization. While the unfunctionalized particles (**75**) gave only mediocre results with 63% conversion (Table 4, entry 10), varying results were obtained with the amino NPs (**85**). It was found that with several different batches of Co/C NPs (**75**) used for the functionalization, catalytic activities ranging from no reaction to full conversion were observed. For that reason, research on the amino-functionalized NPs (**85**) was not continued and instead focused on the low nitrogen-containing PEI polymers.

1.1.7. Incorporation method improvements

After studying the effects of different PEI polymers on the hydrogenation performance, the Ru NP incorporation process was also revisited. The usual procedure for the immobilization of NPs in polymers involves the homogeneous distribution of a metal precursor in the polymer with subsequent reduction or decomposition. However, the violent nature of the Ru NP-catalyzed hydrolysis of NaBH₄ with rapid H₂ formation presumably hinders the homogeneous formation of NPs. Thus, the procedure was changed to dispersing the PEI@Co/C NPs (**79**) together with NaBH₄ in water, followed by the slow addition of a RuCl₃ solution. This process gave a much milder reaction without violent H₂ formation and improved the incorporation from originally only 10% with polymer **79a** to 67% using polymer **79f**, achieving a high loading of 10.6 wt% Ru. Additionally, it was possible to decrease the time to full conversion from 3 h to just 1 h with a catalyst loading of 0.07 mol%, resulting in a TOF 1,402 h⁻¹ of with the optimized catalyst.

1.1.8. Storage and oxidation stability

The stability of the catalysts was also briefly investigated using the catalysts derived from the PEI@Co/C NPs **79d**. It was found that when the catalysts were stored under air, their reactivity dropped significantly after only one day, giving about 20% less conversion. Within one week under air, the catalyst was completely inactive (Table 5, entry 1). In contrast, when the catalysts were stored under nitrogen atmosphere in a Schlenk flask only a minor drop in conversion of 7% was observed (Table 5, entry 3). These results show that the catalysts are prone to deactivation by oxygen, presumably due to the formation of catalytically inactive oxide species on the surface of the Ru-NPs.

Table 5: Storage stability of the catalysts derived from PEI@Co/C NPs (**79d**).

Entry	Conversion [%] (after 3 h) ^a		
	none ^b	1 day ^b	7 days ^b
1 ^c	74	53	n.r.
2 ^c	78	59	n.d.
3 ^d	74	n.d.	67

^a Reaction conditions: 10 mmol toluene (**88**), 0.4 mL isopropanol, 6.8 mg catalyst (**87**), r.t., 30 bar H₂ pressure, 3 h reaction time, conversion determined by GC-FID, ^b time after catalyst synthesis, ^c stored under air, ^d stored under nitrogen, n.r. = no reaction, n.d. = not determined.

1.2. Recycling and leaching studies

With the optimized catalyst system at hand, its recycling capabilities were investigated, as well as the Ru and Co leaching into the solution. Since both metals can be potentially toxic, the metal contamination of the final products needs to be analyzed precisely and is regulated to be below 10 ppm for Ru and 5 ppm for Co for pharmaceutical applications.^[124] Additionally, in the case of Ru, the leached metal can possibly play a role in reactivity loss of the catalyst. For this purpose, a standard 10 mmol hydrogenation reaction of toluene (**88**) was performed with an increased catalyst loading of 0.22 mol% Ru, to track small losses of Ru, and the corresponding reaction time was reduced to 20 min. When the reaction was complete, the solution was separated from the catalyst with the aid of a magnet, the catalyst was washed twice with *i*PrOH and subsequently recycled for the next run.

Table 6: Catalyst recycling and leaching of the optimized catalyst (**87**) in the hydrogenation of toluene (**88**).

Run	Conversion [%] ^a	Co leaching [ppm] ^b	Ru leaching [ppm] ^b	Ru leaching [%] ^b
1	>99	0.1	0.7	0.03
2	>99	0.1	0.7	0.03
3	>99	0.2	0.7	0.03
4	>99	<0.1	0.7	0.03
5	>99	<0.1	0.7	0.03
6	>99	<0.1	1.9	0.08
7	98	<0.1	7.2	0.30
8	>99	<0.1	0.7	0.03
9	>99	<0.1	0.7	0.03
10	>99	<0.1	0.7	0.03
11	96	<0.1	0.7	0.03
12	>99	<0.1	0.7	0.03
13	92	0.1	0.7	0.03
14	91	0.1	0.7	0.03
15	94	<0.1	0.7	0.03
16	88	0.2	0.7	0.03
Total Loss:				0.78

^a Reaction conditions: 10 mmol toluene (**88**), 0.4 mL isopropanol, 21 mg catalyst (**87**) (10.6 wt% Ru, 0.022 mmol Ru, 0.22 mol%), r.t., 30 bar H₂ pressure, 20 min reaction time, conversion determined by GC-FID, ^b determined by ICP-OES.

As can be seen in Table 6 and Figure 4, the catalyst showed excellent recycling as well as leaching results with only dropping to 88% conversion in the 16th run. For the first 10 runs, a TOF of 1,364 h⁻¹ was obtained, resulting in a TON of 7,048 within the 16 runs. The leaching of Ru and Co was even below 1 ppm in most of the runs with the exception of run 6 and 7, where the Ru contamination was 2 ppm and 7 ppm, respectively. However, even these statistical outliers are still within the limits of the abovementioned regulations for Ru (below 10 ppm). Overall it was found that only 0.78% of the Ru in the catalyst were leached out into the solution. Thus the loss in reactivity can not be attributed entirely to the loss of Ru. A partial oxidation of the Ru NPs seemed to be more likely since the recycling procedure was not performed under total oxygen exclusion.

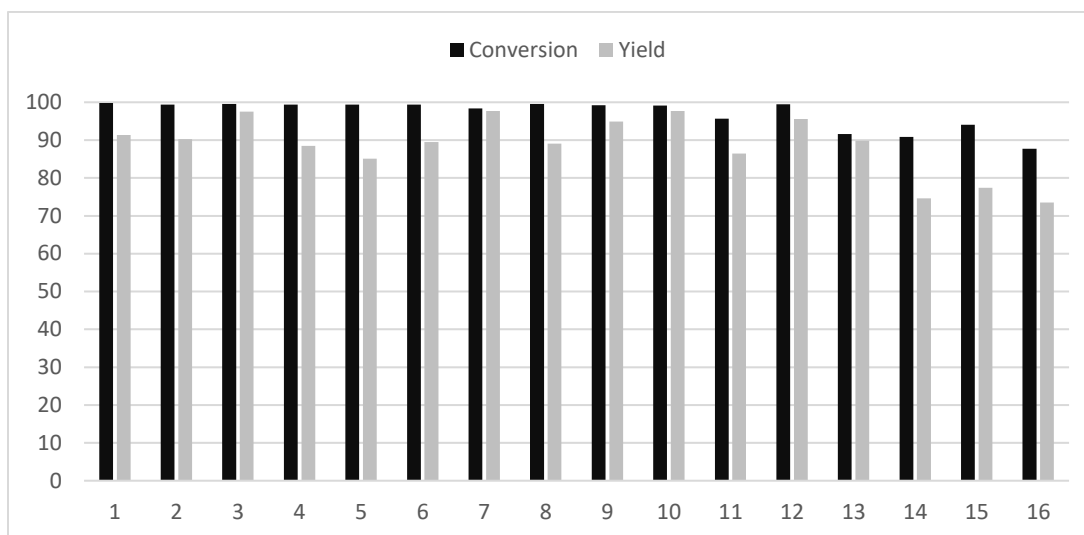


Figure 4: Catalyst recycling of the optimized catalyst (**87**) in the hydrogenation of toluene (**88**).

1.3. Substrate scope

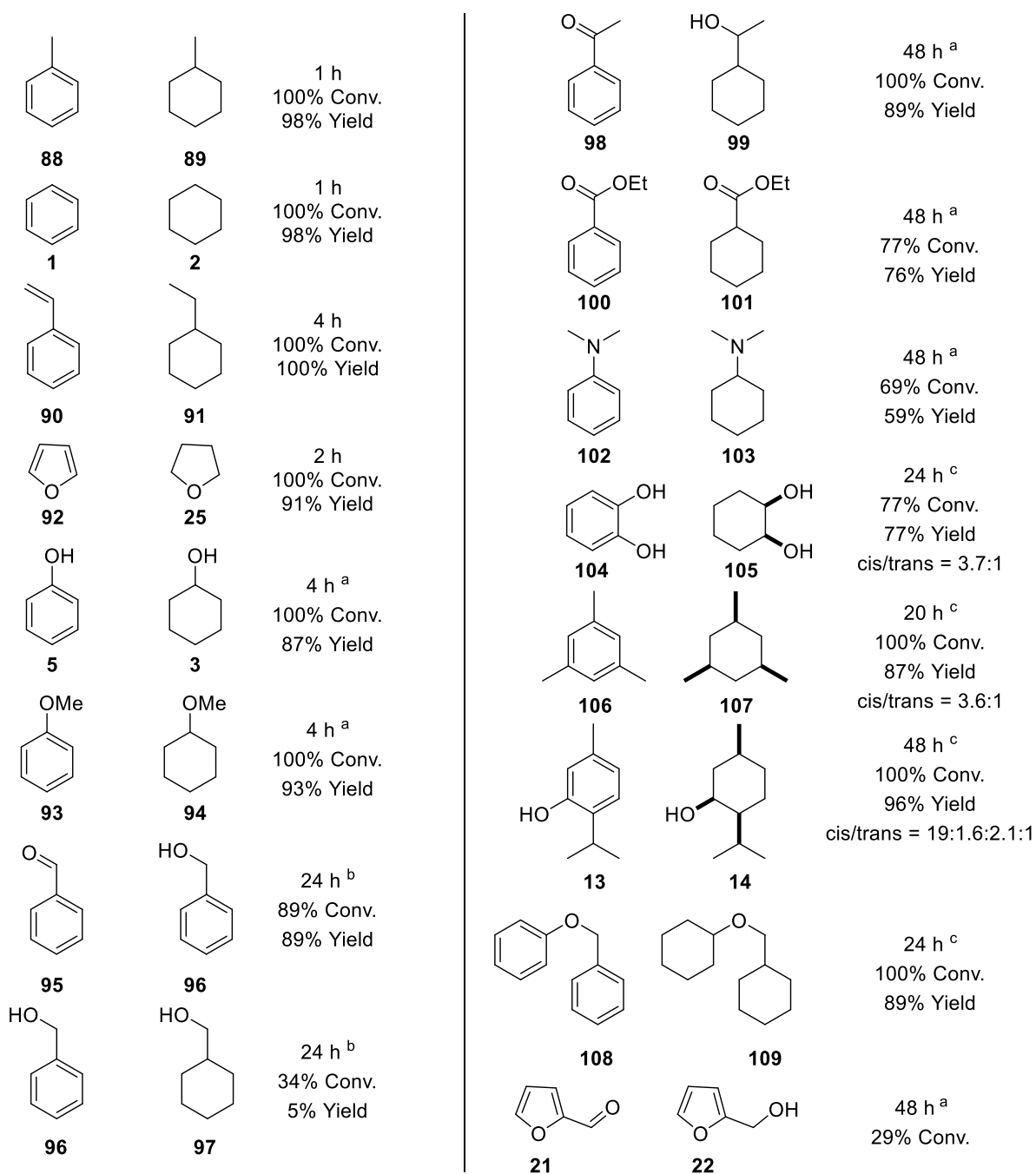
After successfully demonstrating the recycling capabilities of the catalyst, the substrate scope of the reaction was investigated (Scheme **30**). It was found that simple hydrocarbons like benzene (**1**) or styrene (**90**) performed best next to the model substrate toluene (**88**). A selective reduction of benzene (**1**) to cyclohexene (**8**) was also attempted, using a biphasic water/benzene reaction setup. While the catalyst still remained active under these conditions, no selectivity towards the formation of cyclohexene (**8**) was observed and the reactivity also decreased with only 24% conversion after 3 h reaction time. In the case of Styrene, full conversion to ethylbenzene could be observed after 2 h before the complete hydrogenation to ethylcyclohexane (**91**) within 4 h occurred. Noteworthy, also the heterocyclic substrate furan (**92**) could be reduced in only 2 h to THF (**25**), while furfural (**21**) only showed a mediocre conversion of 29% to furfuryl alcohol (**22**) in 48 h. Electron rich, oxygenated benzenes like phenol (**5**) and anisole (**93**) could also be reduced to the corresponding alcohol (**3**) or ether (**94**) within 4 h, respectively. In stark contrast to these results, electron-poor substrates generally required significantly longer reaction times of 24 h to 48 h. For benzaldehyde (**95**) a reaction time of 24 h was even only sufficient for a conversion of 89% to benzylic alcohol (**96**), while a fresh sample of benzylic alcohol showed almost no conversion to the corresponding cyclohexylmethanol (**97**) within 24 h. Interestingly, the free alcohol group in benzylic position seemed to be responsible for this diminished reactivity, since the reduction of benzylphenylether (**108**) achieved full conversion to the total hydrogenation product (**109**) after 24 h. One possible explanation could be that the hydrogenolysis of the alcohol group deactivates the catalyst which would

also justify the large discrepancy in conversion and yield found in that case. Other electron-poor substrates like acetophenone (**98**) or benzoic acid ethyl ester (**100**) required an even longer reaction time of 48 h. However, in the case of **98**, complete hydrogenation of the aromatic system as well as the ketone could be observed. For substrate **100** a conversion of 77% to the corresponding cyclohexyl derivative was observed with no reaction occurring on the ester group, as expected. Nitrogen-containing substrates also turned out to be very challenging to hydrogenate. For aniline (**112**), a test reaction showed, that it indeed acts as a catalyst poison as no conversion of either substrate was found in the reaction with toluene and 10 mol% aniline. This could also explain that no conversion occurred on nitrobenzene (**113**), as already small amounts of aniline could shut down the catalyst when the nitro group gets reduced. Interestingly, it was possible to hydrogenate dimethylaniline (**102**) in 48 h with 69% conversion, indicating that tertiary amines do not deactivate the catalyst. Pyridine (**115**) also could not be reduced successfully as no reaction occurred even after forming the corresponding pyridinium chloride or acetate before the reaction, which usually facilitates the reduction.^[125]

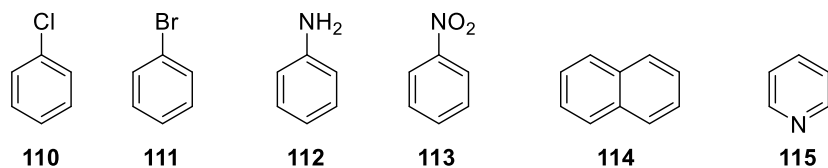
Annulated aromatic systems like naphthalene (**114**) and halogenated arenes like chloro- (**110**) or bromobenzene (**111**) also showed no conversion to the desired products. The reactions of the halogenated substrates both showed a color change of the solution to faint blue which could indicate the dissolving of the Ru NPs due to dehalogenation of the substrates and formation of the corresponding acids.

Because of the previous results, the investigation on higher substituted substrates was mainly focused on electron-rich systems. It was found that mesitylene (**106**) could be fully converted to the corresponding trimethylcyclohexane (**107**) within 20 h with a *cis/trans* ratio of 3.6:1. The hydrogenation of 1,2-dihydroxybenzene (**104**) also succeeded with 77% conversion after 24 h with a very similar *cis/trans* ratio of 3.7:1.

Gratifyingly it was also possible to completely hydrogenate thymol (**13**) within 48 h without the need for a higher reaction temperature and only 30 bar of H₂ pressure. As seen in Scheme 2 (See Introduction, Chapter 1.4.), four diastereomers (and their enantiomers) can be formed from this reaction. NMR analysis of the reaction mixture showed that the isomers were formed in a 19:2.1:1.6:1 ratio of neoisomenthol (**14d**) / isomenthol (**14b**) / neomenthol (**14c**) / menthol (**14a**) in that respective order. As expected, the main product was the all-*cis* (\pm)-neoisomenthol (**14d**), as higher reaction temperatures are required to form the thermodynamically more stable *trans*-products. Interestingly, this ratio also corresponds to a 4:1 ratio of the all-*cis* product to the rest of the *trans*-products and is therefore very similar to the other substrates.



Unsuccessful Substrates



Standard conditions: 10 mmol substrate, 0.07 mol% Ru cat.

^a 5 mmol substrate, 0.29 mol% Ru cat.

^b 10 mmol substrate, 0.14 mol% Ru cat.

^c 2 mmol substrate, 0.73 mol% Ru cat.

Scheme 30: Substrate scope of the optimized catalyst (**87**) for aromatic hydrogenations.

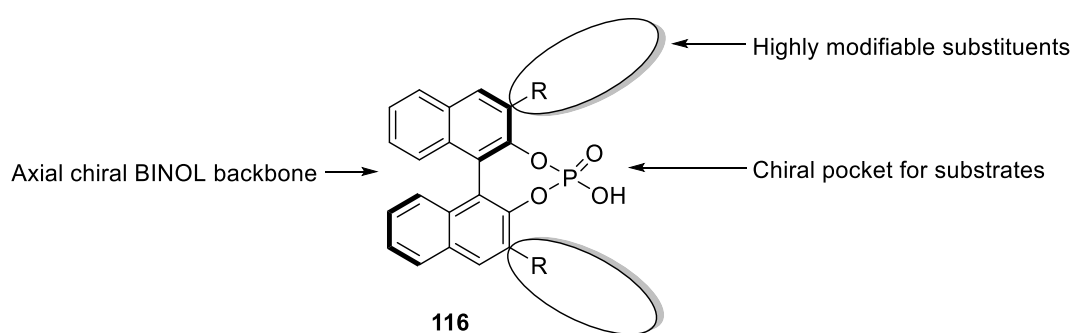
1.4. Conclusion

A new magnetically recoverable PEI@Co/C NP (**79**) supported Ru NP catalyst (**87**) for the hydrogenation of aromatic compounds was developed. The effects of the supporting PEI polymer were thoroughly investigated showing a correspondence between the nitrogen content of the polymer and the reactivity of the catalyst, with the highest catalytic activity being obtained with a low nitrogen content (0.3 wt% N). The optimized catalyst was able to achieve a TOF of $1,402 \text{ h}^{-1}$ in the hydrogenation of the model substrate toluene (**88**) at r.t. using 30 bar of H_2 pressure. During the exploration of the substrate scope, the catalyst was found to successfully reduce electron-rich arenes such as phenol (**5**) or anisole (**93**) as well as electron-poor systems like acetophenone (**98**) or ethyl benzoate (**100**). Di- or tri-substituted benzenes could also be hydrogenated giving products in a cis/trans ratio of around 4:1 with most remarkably thymol (**13**) being reduced to the corresponding menthol isomers (**14**). Limitations were discovered in the hydrogenation of nitrogen-containing compounds with the only successful example being the reduction of dimethylaniline (**102**). Polyaromatic systems like naphthalene (**114**), as well as chloro- (**110**) and bromobenzene (**111**), also showed no hydrogenation, with the latter two being suspected to hydrogenolysis induced catalyst poisoning. The catalyst showed excellent recycling capabilities and could be reused for 16 consecutive runs before dropping to 88% conversion in the last run, achieving a TOF of $1,364 \text{ h}^{-1}$ in the first 10 runs, corresponding to a TON of 7,048. Additionally, almost no metal leaching was found with an average of 1.1 ppm/cycle for Ru and 0.1 ppm/cycle for Co.

2. Magnetic Co/C nanoparticle supported chiral phosphoric acid catalysts

2.1. Chiral phosphoric acid catalysis

While transition metal-based catalysts were the main focus of this work until now, they are certainly not the only option for synthetic chemists to achieve (enantio-)selective transformations. The field of organocatalysis has emerged as an environmentally benign competitor to transition metals, using small organic molecules to achieve selective transformations *via* numerous activation modes.^[126,127] An important subclass in this field is the Brønsted acid catalysis.^[128] Brønsted acids can activate numerous electrophiles by lowering the LUMO energy through protonation, which facilitates the attack of a corresponding nucleophile.^[129] BINOL-derived chiral phosphoric acids (CPAs, **116**) have been established as one of the most promising candidates due to their structural versatility and widespread application in numerous transformations.^[130] The axial chirality of the BINOL backbone allows for the creation of a chiral pocket around the phosphoric acid moiety, simply by the installation of bulky substituents in the 3,3'-positions of the BINOL, which can be achieved *via* established crosscoupling reactions (Scheme 31).

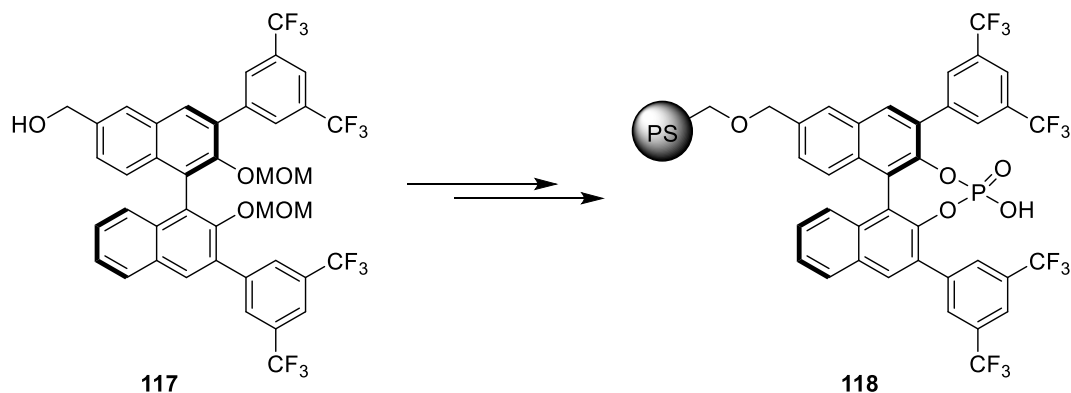


Scheme 31: Stereotypical features of BINOL-derived CPAs (**116**).

The structural versatility of these CPAs stems from the ability to individually adapt these substituents, to the desired substrates and reactions conditions. Thus, a plethora of different substituents have been investigated with a steadily increasing level of complexity.^[130] However, this complexity also comes at the cost of an often tedious synthesis, increasing the cost of those CPAs. Combined with the sometimes high catalyst loadings of up to 20 mol% used in some reactions, this has sparked the interest in developing reusable versions of these catalysts by immobilizing them on solid supports, which is often referred to as “heterogenization”. Fortunately, the high chemical stability and robustness of the CPAs make them well suited for reuse and several successful methods for their immobilization have been developed.

2.2. Immobilization methods for chiral phosphoric acids

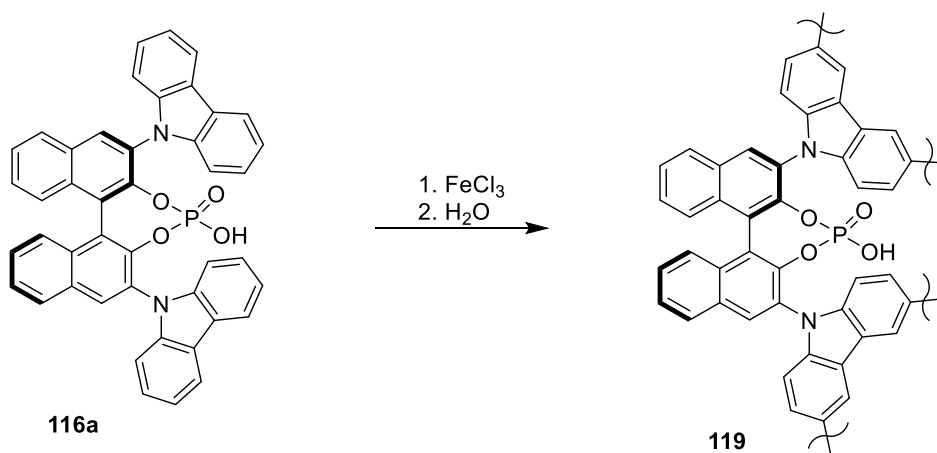
A very common approach for the immobilization of homogeneous catalysts is the attachment of a linker group in the periphery of the molecule, in order to not influence the catalytically active center. Pericàs *et al.* used this strategy by attaching a hydroxymethyl group to the BINOL backbone of the CPAs, which allowed the covalent connection to a Merrifield resin *via* a nucleophilic substitution reaction (Scheme 32).^[131]



Scheme 32: Immobilization of a CPA onto a Merrifield (PS) resin by Pericàs *et al.*^[131]

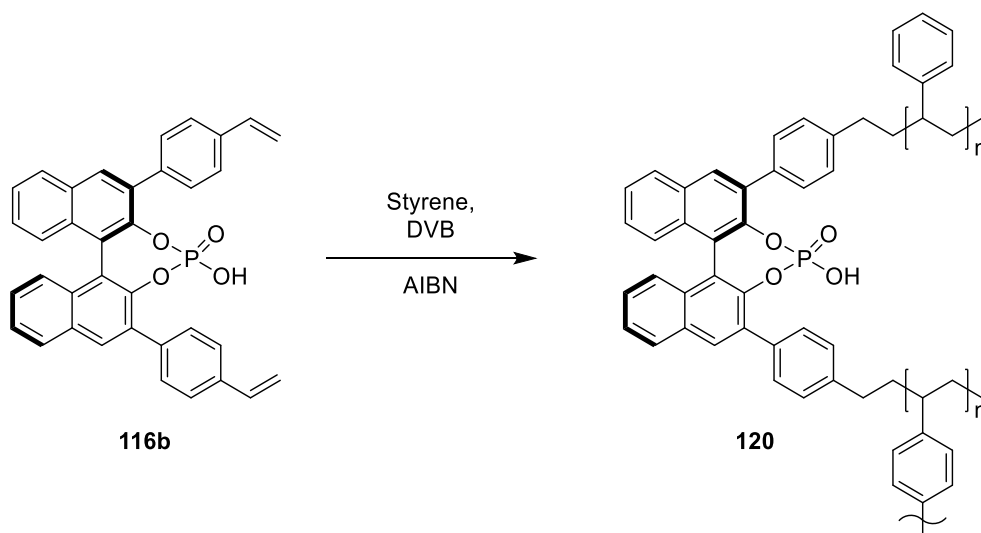
While quantitative immobilization of the modified CPA could be achieved with this method, the synthesis was a major drawback. Three additional steps were required for the introduction of the hydroxymethyl moiety, plus an additional protection/deprotection sequence of the hydroxyl group during the coupling with the 3,3' substituents. Although the developed catalyst was highly recyclable and could even be used in a continuous flow system, other procedures demanding less synthetic effort have been developed.

Another common motive in the heterogenization of homogeneous catalysts is the introduction of polymerizable groups. For the case of BINOL-based CPAs, several groups have applied this strategy in combination with exploiting the usual necessity of large substituents in the 3,3' positions of the BINOL to achieve satisfactory enantioselectivities.^[132–134] For example, Zhang *et al.* showed that the introduction of carbazole in the 3,3' positions could be used for a FeCl₃-promoted oxidative polymerization *via* homocoupling of the carbazoles, while also inducing good selectivities (Scheme 33).^[134]



Scheme 33: Oxidative polymerization of CPA **116a** by Zhang et al.^[134]

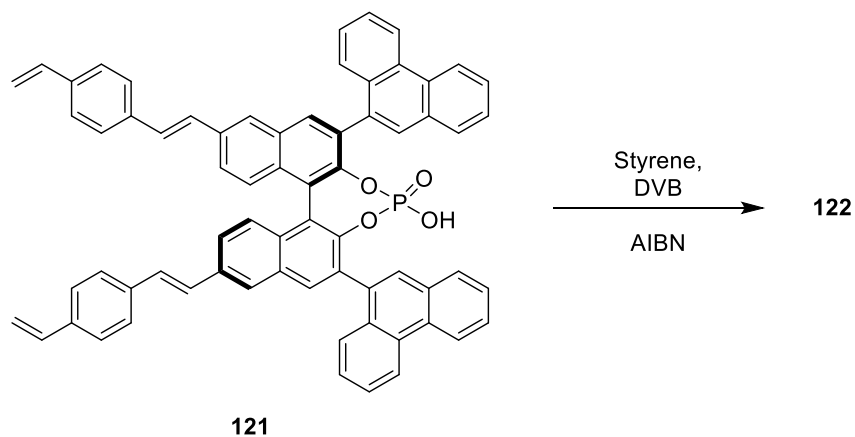
The catalyst was used amongst other reactions in the transfer hydrogenation of 2-phenylbenzoxazine giving high *ee*-values of up to 94% and could be recycled for at least 5 runs without loss of reactivity or selectivity. Interestingly, kinetic studies showed an atypical reactivity increase after the polymerization of the CPA. Since catalysts immobilized on polymeric support usually exert a reduced reactivity due to limited material transport, the authors attributed this unexpected result to an electronic effect. They concluded that the homocoupling of the carbazoles made them more electron-deficient which influences the Brønsted acidity of the CPA and thus can increase the reactivity.



Scheme 34: Radical polymerization of CPA **116b** by Rueping et al.^[133]

Rueping *et al.* also studied the introduction of styrene moieties and their utilization for a radical copolymerization with styrene and divinylbenzene (DVB) to achieve immobilization (Scheme 34).^[133] Using the polymerized CPA (**120**) with the styrene moieties 3,3'-positions, only moderate selectivities below 70%

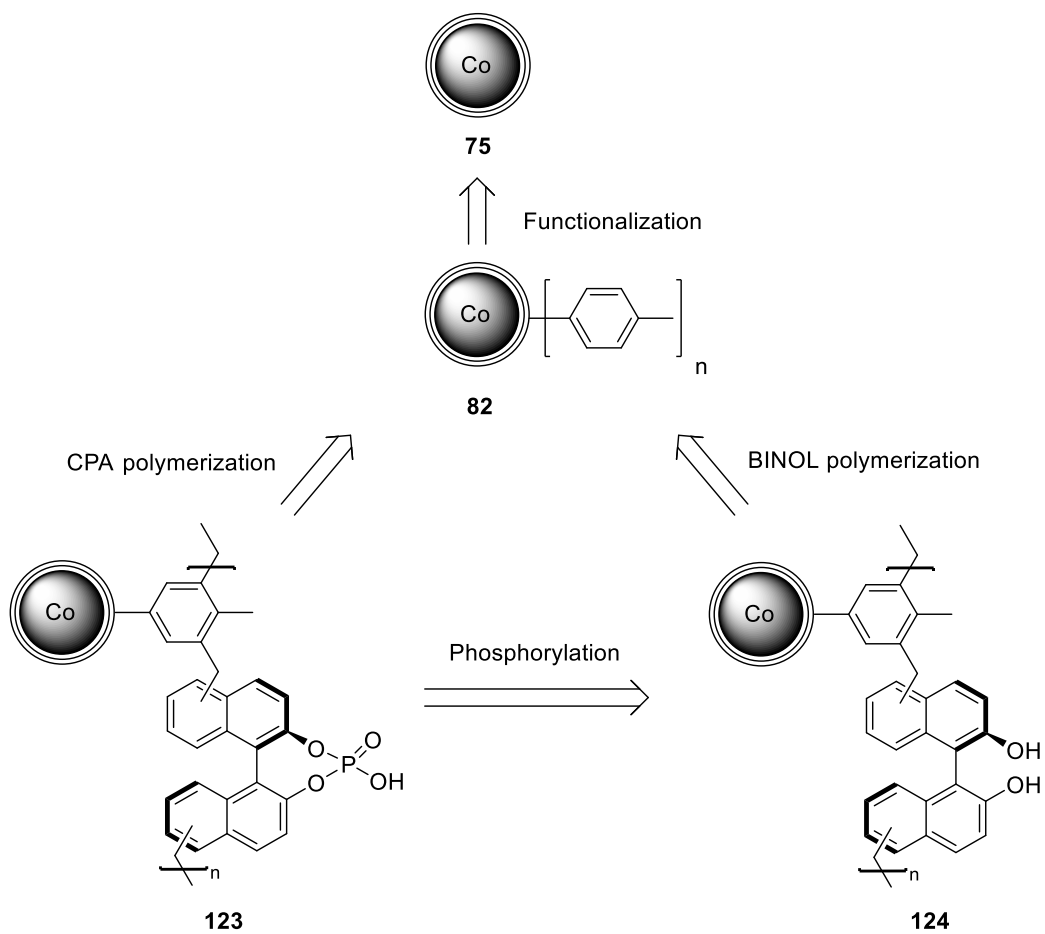
ee were observed in the transfer hydrogenation of 2-naphthylquinoline. For better results, CPA **121** had to be synthesized, bearing divinylbenzene moieties in the 6,6'-positions and 9-phenanthrene as bulkier substituents in the 3,3'-positions of the BINOL. The improved catalyst (**122**) was able to achieve high selectivities of up to 96% in the transfer hydrogenation of 2-phenylbenzoxazine and could be recycled for 12 runs.



Scheme 35: Optimized catalyst for the immobilization *via* radical polymerization.

This shows that often polymerizable substituents in the 3,3'-positions can not be used for an efficient chiral induction, which necessitates the synthesis of more complex monomers such as **121**, again increasing synthetic costs and effort.

In this work, a new immobilization approach was investigated that would allow the use of unmodified, commercially available CPAs and a straightforward immobilization procedure employing not more than 3 steps. Inspired by the polymerization method developed by Tan *et al.*^[115] for the formation of microporous organic polymer from simple arenes and the modification by Reiser *et al.*^[107] to covalently graft such polymers around magnetic Co/C NPs (see Scheme **24**, Chapter 1.1.1.), it was envisioned that the BINOL backbone could be exploited for immobilization purposes with this technique. Indeed, such a BINOL derived MOP (Without Co/C NPs) was already developed by Cooper *et al.* and researched mainly for its carbon dioxide capture potential.^[135] Knowing the polymerization can be applied to BINOL, the first idea was to immobilize the BINOL-MOP on the magnetic Co/C NPs with subsequent phosphorylation inside the polymer to obtain the immobilized CPAs in a three-step procedure. However, the direct utilization of unmodified CPAs for this polymerization technique was also explored, especially in regards to using commercially available CPAs, which would reduce the procedure to only two steps (Scheme **36**).

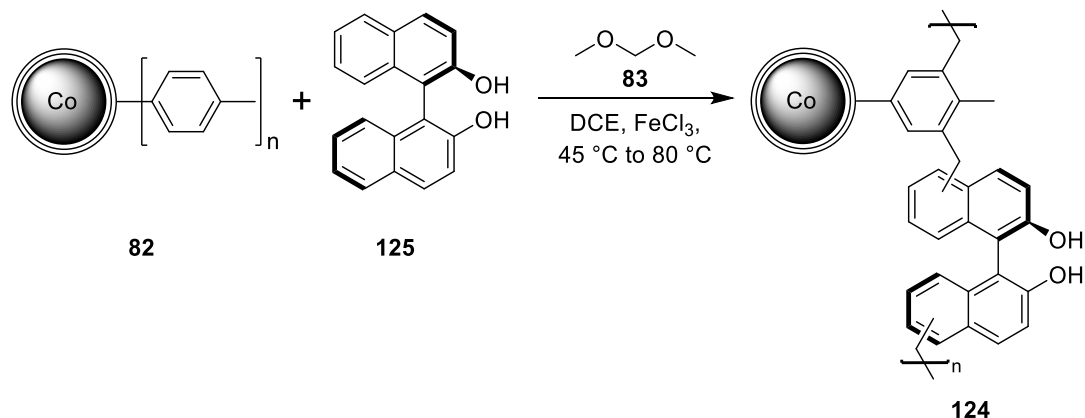


Scheme 36: New immobilization approach for CPAs investigated in this work.

2.3. Results and discussion

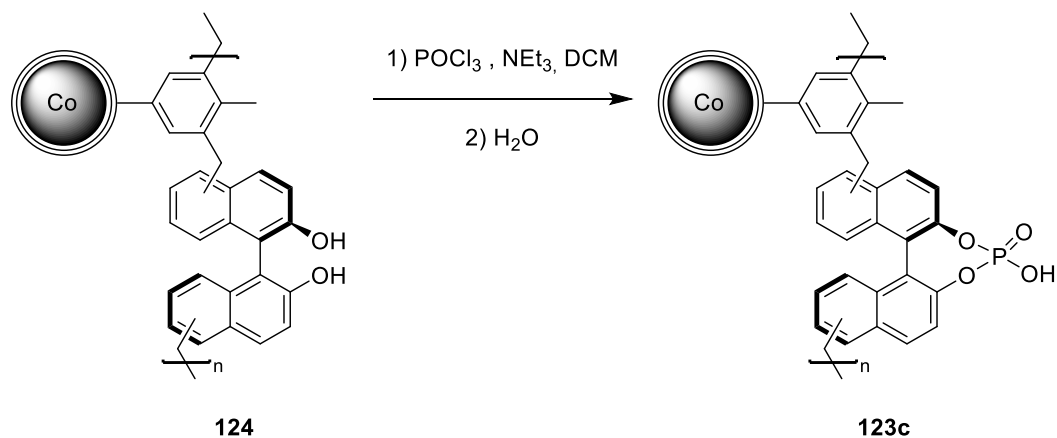
2.3.1. BINOL polymerization and subsequent phosphorylation

The first investigated approach was the immobilization of the BINOL derived MOP with subsequent phosphorylation similar to the methodology from Pericàs *et al.*^[131] Analogously to the previous attachment of MOPs to Co/C NPs, toluene functionalized Co/C NPs (**82**) were synthesized *via* diazonium chemistry (see Scheme **23**, Chapter 1.1.1.) and used as a covalent linker.



Scheme 37: Immobilization of BINOL (**125**) *via* a Friedel-Crafts type Polymerization.

For the immobilization, BINOL (**125**) was polymerized using formaldehyde dimethyl acetal (FDA, **83**) as an external crosslinker and FeCl₃ as a catalyst following the modified procedure^[107] of the Friedel-Crafts polymerization developed by Tan *et al.*^[115] (Scheme **37**). The arene moiety of the BINOL backbone would therefore be covalently connected to the toluene moiety on the Co/C NPs **82** *via* CH₂ bridges. The polymerization could successfully be used to immobilize BINOL on the Co/C NPs as shown by the increase in carbon content from 5 wt% C in the toluene functionalized NPs **82** to 51 wt% C in the resulting polymer (**124**).



Scheme 38: Phosphorylation of immobilized BINOL (**124**).

The phosphorylation was carried out using POCl_3 and NEt_3 in DCM as solvent followed by hydrolysis of the phosphoric acid chloride in water resulting in the immobilized CPA (**123c**) (Scheme 38). In order to confirm the presence of CPA on the magnetic NPs, IR spectra of **123c** and **124** were compared to the homogeneous, unsubstituted BINOL phosphoric acid (**116c**). The spectra show clear similarities in the fingerprint region between the immobilized CPA (**123c**) and the homogeneous phosphoric acid, confirming the successful phosphorylation.

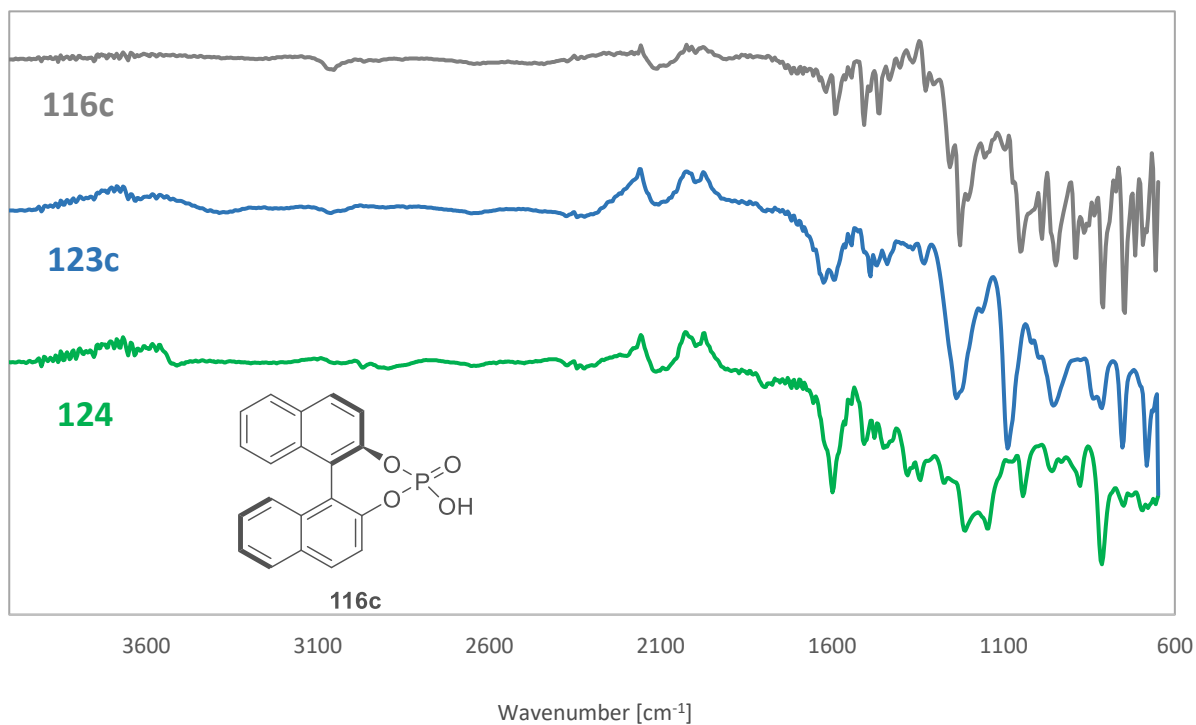
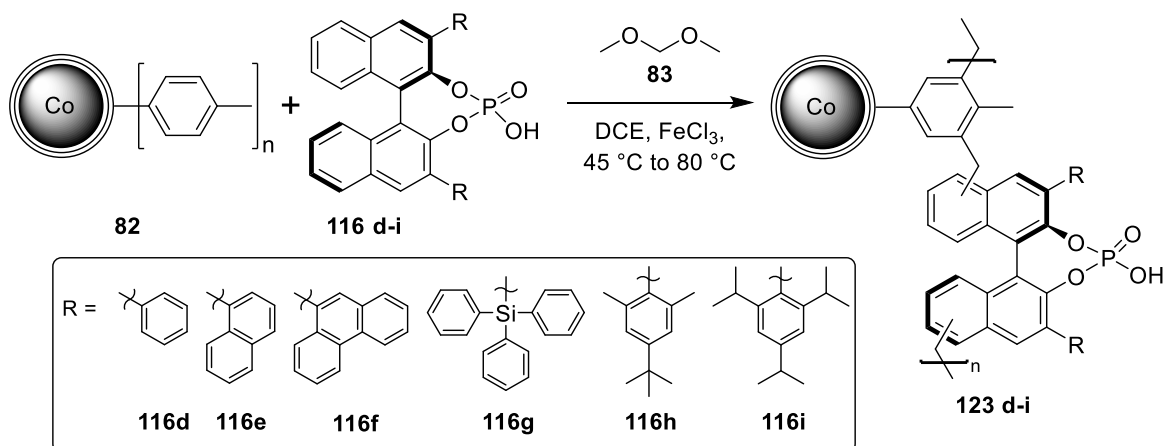


Figure 5: Stacked IR-spectra of BINOL phosphoric acid (**116c**), immobilized CPA (**123c**) and immobilized BINOL (**124**).

Elemental analysis also showed a decrease in carbon content from 52% to 46% as expected after the addition of non-carbon mass to the polymer. Unfortunately, the elemental analysis also revealed the presence of 1.2% nitrogen in the polymer coming from the NEt_3 . Since this could not be removed by aqueous washing under basic or acidic conditions nor by washing with organic solvents, further research on the CPA immobilization was focused on the direct polymerization of CPAs.

2.3.2. Direct polymerization of chiral phosphoric acids

For the direct polymerization, different CPAs were directly subjected to the Friedel-Crafts conditions together with the toluene functionalized Co/C NPs (**82**). Since most reactions require large substituents in the 3,3'-positions of the BINOL for good enantioselectivities and there was no way to introduce them after the polymerization, the effect of these substituents on the immobilization also had to be investigated (Scheme 39). For this purpose, the polymerization yield was considered. This was calculated from the mass balance of the isolated polymer compared to the starting materials. Each FDA (**83**) equivalent was taken into account as a $-\text{CH}_2-$ unit and all of the FeCl_3 was assumed to be removed from the polymer by washing. The experiments were set up using an equal amount of magnetic NPs and CPA by mass. Since the magnetic NPs would always be recovered by magnetic decantation a polymerization yield of 50% would therefore mean no successful immobilization of the CPA. Polymerization yields above 100% of the theoretical yield could be a result of incomplete removal of FeCl_3 , insufficient drying of the polymer or the presence of non-crosslinked "loose ends" of FDA containing $-\text{CH}_2-\text{OMe}$ groups. However, in an ICP-OES analysis of the polymer, almost no Iron (1.2 ppm) could be detected, leaving only the latter two options possible.



Scheme 39: Direct immobilization of different CPAs onto magnetic Co/C NPs.

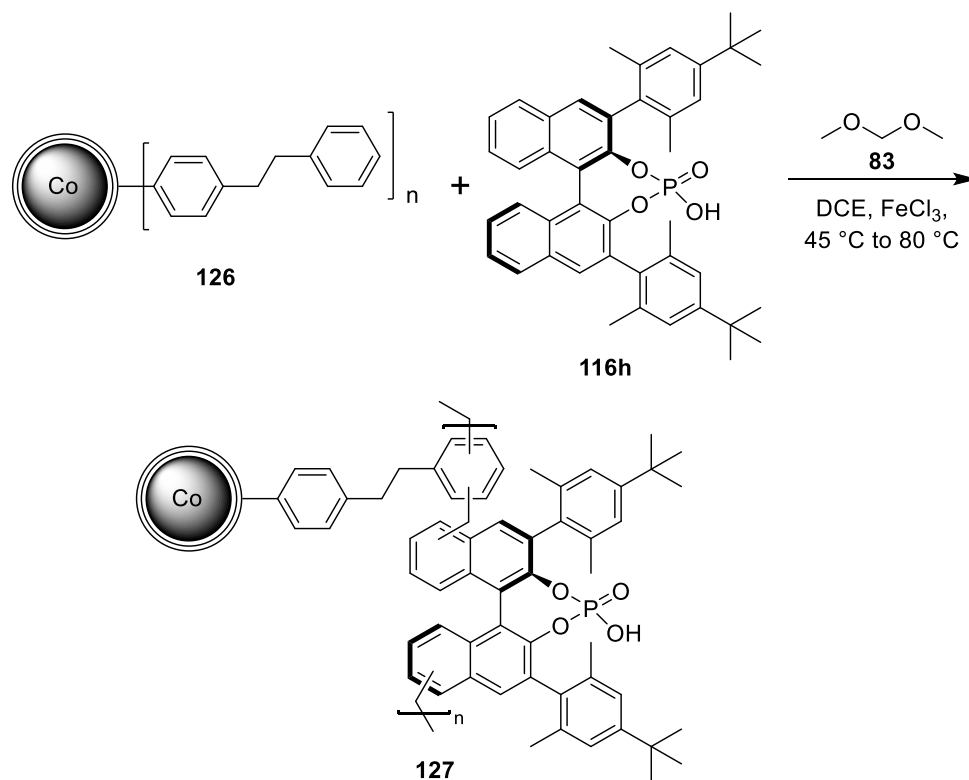
Gratifyingly the immobilization of CPAs containing sterically unhindered aryl substituents in the 3,3'-positions such as naphthyl (**116e**) or phenanthryl (**116f**) was successful in almost quantitative yields (Table 7, entries 1 and 2). Presumably, this is because crosslinking can occur on the substituents as well as on the BINOL backbone of the CPAs. However, CPAs containing sterically hindered substituents like 2,6-dimethyl-4-*tert*-butylphenyl (**116h**) or 2,4,6-triisopropylphenyl (**116i**) showed much lower immobilizations with 73% and 57% polymerization yield, respectively (Table 7, Entries 3 and 4).

Table 7: Effects of 3,3'-substituents on the direct immobilization of CPAs onto magnetic Co/C NPs.

Entry	Co/C-NPs	CPA	Polymerization yield ^a [%]
1	82	116e	97
2	82	116f	102
3 ^b	82	116h	73
4 ^b	82	116i	57
5	128	116h	89

^a Polymerization conditions: 10 mg functionalized Co/C NPs (**82/128**), 10 mg CPA (**116e-i**), 5 mg FeCl₃ (0.03 mmol), 3 μL FDA (0.03 mmol), 1 mL DCE, 5 h at 45 °C then 19 h at 80 °C, ^b Polymerization performed on 3x scale.

The first experiment to overcome this immobilization issue was to introduce a more flexible linker group to the surface of the magnetic NPs. Since these sterically more restricted CPAs polymerize predominantly on the BINOL backbone, a more flexible and also prolonged linker could therefore “catch” the CPAs better from the solution.

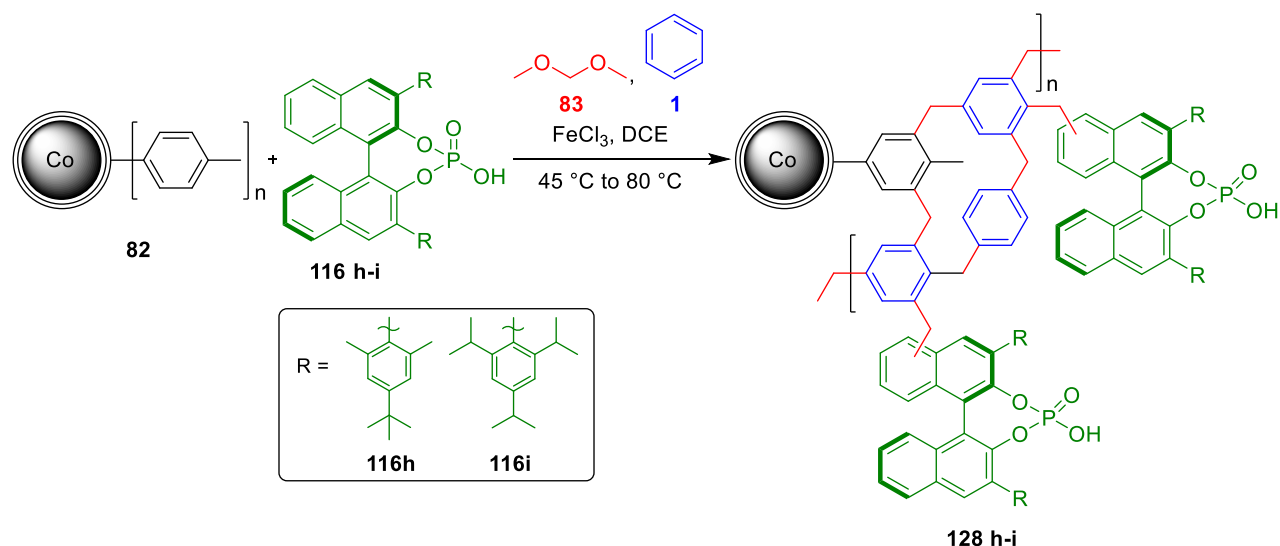


Scheme 40: Immobilization of CPA **116h** with an extended linker.

Therefore a dihydrostilbene moiety was attached to the surface of the Co/C NPs analogously to the toluene moiety before. The immobilization was then carried out using the new linker substituted NPs (**126**) and the CPA **116h** (Scheme **40**). The polymerization yield showed a significant increase from 73% without the extended linker to 89% using the linker, proving that the difficult connection of the CPAs to the surface of the NPs was an issue (Table **7**, entry 5). However, due to the high value of the CPAs, losses should be avoided during the immobilization process and higher polymerization yields are desired.

A different approach to improve the immobilization was to utilize a copolymerization strategy. It was already shown in earlier studies^[107] that several different substituted arenes can be used to grow polymers around the functionalized magnetic NPs (**82**). Therefore polymerizing a mixture of CPAs and benzene would lead to the growth of polymer around the NPs and automatically generate more connection sites for the CPAs to be immobilized (Scheme **41**). Fortunately, this approach proved to be very successful and CPA **116h** could be immobilized in almost quantitative yields with and even without the use of the

elongated linker NPs **126** (Table 8, entries 1 and 2). It was also possible to immobilize CPA **116i** with 95% polymerization yield which only achieved 57% before any improvement methods (Table 8, entry 3).



After accomplishing the immobilization of CPAs with sterically unhindered as well as sterically hindered substituents in 3,3'-positions the catalyst systems then had to be tested in a series of different CPA catalyzed reactions to investigate their applicability as well as their recyclability due to the magnetic NPs.

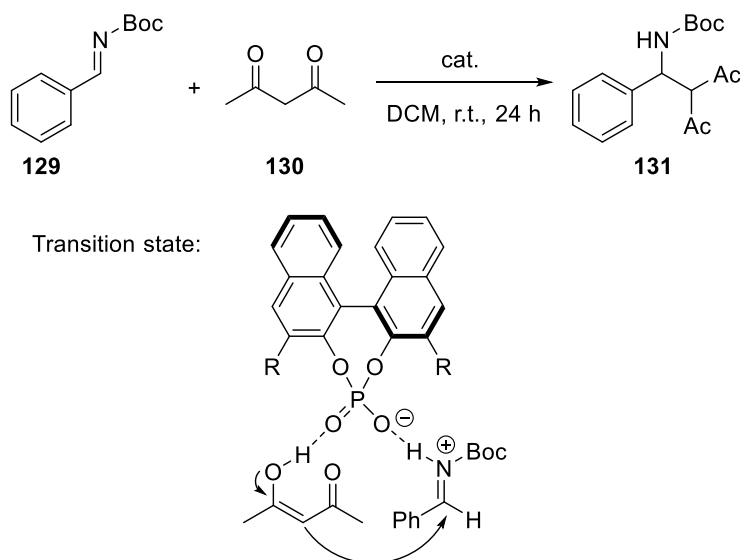
Table 8: Polymerization yields of the immobilization using a copolymerization strategy.

Entry	Co/C NPs	CPA	Additive	Polymerization yield ^a [%]
1	82	116h	Benzene (3 equiv.)	97
2	126	116h	Benzene (3 equiv.)	98
3	82	116i	Benzene (3 equiv.)	95

^a Polymerization conditions: 10 mg functionalized Co/C NPs (**82/128**), 10 mg CPA (0.02 mmol)(**116h-i**), 4 μ L benzene (0.05 mmol) 29 mg FeCl₃ (0.18 mmol), 16 μ L FDA (0.18 mmol), 1 mL DCE, 5 h at 45 °C then 19 h at 80 °C.

2.3.3. Direct Mannich reaction

The first reaction used to test the new immobilized CPAs was a direct Mannich reaction developed by Terada *et al.* in 2004.^[136] Together with a Mannich-type reaction developed by Akiyama *et al.*^[137] in the same year, this was one of the first reported reactions employing CPAs for enantioselective transformations. In Terada's protocol, N-Boc-protected imines (**129**) are reacted with acetylacetone (**130**). The CPA was first thought to only activate the imine by protonation, enabling the nucleophilic attack. However, it was later found by Goodman *et al.* that the CPA simultaneously activates the acetylacetone through hydrogen bonding with its enol resonance structure (Scheme 42).^[138]



Scheme 42: Direct Mannich reaction by Terada *et al.*^[136]

Employing the new immobilized CPA catalysts in this reaction under otherwise similar conditions resulted in almost no enantiomeric excess using the unsubstituted BINOL phosphoric acid catalyst **123c** or catalyst **123d** with phenyl substituents (Table 9, entries 1 and 2). Investigating this issue, it was found that while reproducing the homogeneous reaction with the phenyl CPA (**116d**) gave similar results to literature (45% *ee* to 56% *ee* in Lit.) (Table 9, entry 3), there was also a background reaction found when no catalyst was present in the reaction mixture giving comparable yields (Table 9, entry 4). It was therefore suspected that the heterogeneously catalyzed reaction was too slow to compete with this unselective background reaction. This was most likely also a result of the instability of the N-Boc protected imine which decomposes easily under moisture.

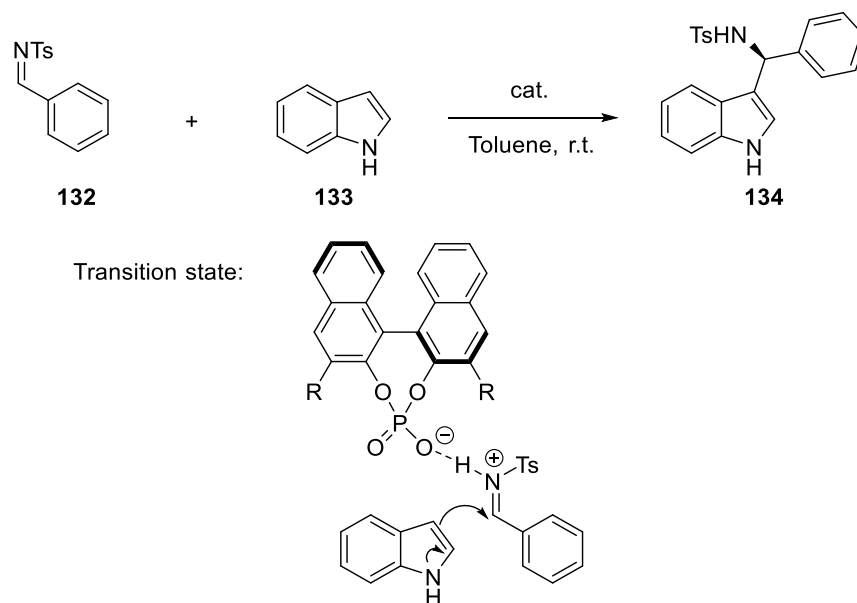
Table 9: Catalysis results for the direct Mannich developed by Terada *et al.*

Entry	Catalyst	Yield [%] ^a	ee [%] ^b
1	123c	96	4
2	123d	99	3
3	116d	96	45
4	-	95	-

^a Reaction conditions: 0.2 mmol N-Boc-protected imine (**129**), 0.2 mmol acetylacetone (**130**), 10 mg catalyst (**123c/123d**) or 1 mg **116d** (0.002 mmol, 1 mol%), 1 mL DCM, r.t., 24 h reaction time, ^b Enantiomeric excess determined by chiral HPLC.

2.3.4. Friedel-Crafts alkylation of indole

After recognizing the issue of an almost quantitative background reaction with the first test reaction, the Friedel-Crafts alkylation of indole (**133**) was investigated as an alternative (Scheme **43**).^[139] The here employed Tosyl-protected imines were considered to be much more stable towards hydrolysis and therefore expected to minimize the problem. In addition, the group of Pericàs *et al.* also performed this reaction very successfully with their aforementioned Merrifield resin supported CPA catalyst, showing that heterogenization can be achieved.^[131] From a synthetic point of view, the produced 3-indoylemethanamine core structure would also be highly desirable due to its presence in various biologically active compounds.^[140,141]



Scheme 43: Friedel-Crafts alkylation of indole (**135**).^[139]

Unfortunately, employing similar reaction conditions and the catalyst **128h** with the immobilized 2,6-Dimethyl-4-*tert*-butylphenyl substituted CPA (**116h**) resulted in only 53% isolated yield of the desired product. Also, no optical rotation could be measured, indicating that no enantioselectivity was induced by the catalyst (Table **10**, entry 1). Due to those unsatisfactory results, no further optimization of the reaction conditions was pursued and different reaction types were investigated.

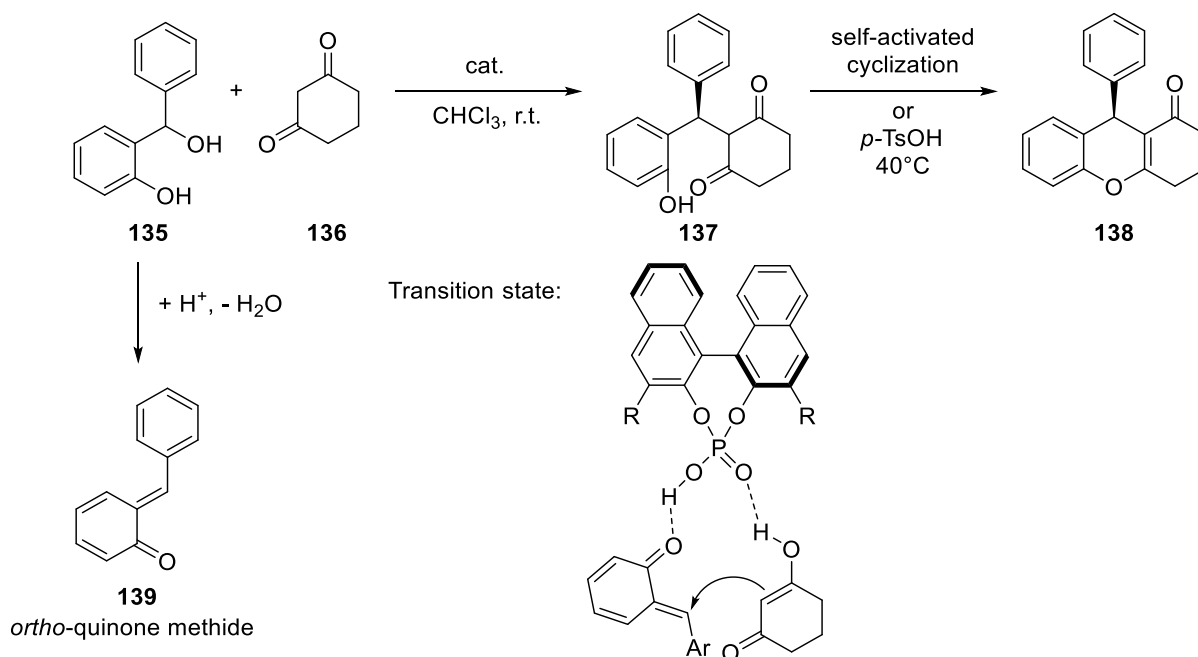
Table 10: Catalysis results for the Friedel-Crafts alkylation of indole (**133**) by developed You *et al.*

Entry	Catalyst	Conversion ^a	Yield [%]	Selectivity
1	128h	100%	53	$[\alpha]_D^{20} = 0^\circ$
2 ^b	118	100%	81	93% (<i>ee</i>)

^a Reaction conditions: 0.5 mmol N-tosyl-protected imine (**132**), 0.7 mmol indole (**133**), 25 mg catalyst (**128h**), 2.5 mL toluene, r.t., 72 h reaction time, ^b Literature results.^[131]

2.3.5. Conjugate addition to *ortho*-quinone methides

Since previous reactions using N-protected imines as activatable substrates showed no promising results, the focus was shifted towards other reaction types. One particularly interesting transformation was the conjugate addition of 1,3-dicarbonyls to *in situ* generated *ortho*-quinone methides (**139**) developed by Schneider *et al.* in 2014.^[142] In the proposed mechanism the catalyst generates the *ortho*-quinone methides (**139**) through acid-catalyzed water elimination from the starting material, while simultaneously activating the enol form of the 1,3-dicarbonyl through hydrogen bonding (Scheme **44**).



Scheme 44: Conjugate addition of 1,3-cyclohexadione to *in situ* generated *ortho*-quinone methide **139**.^[142]

The therefore highly ordered transition state allows for an enantioselective formation of the intermediate **137**. An additional intermolecular cyclization and water elimination, which in some cases requires *p*-T₂SOH and slightly elevated temperature (40 °C), then forms 4-aryl-4H-chromenes (**138**) as the final product. This 4H-chromene core structure is also present in many natural products and biologically active compounds^[143–145], which would give great synthetic value to the development of a recyclable, highly selective catalyst. In the selected example employing the cyclic 1,3-cyclohexanedione (**136**) as dicarbonyl compound, the final product directly forms without the need for additional reagents, which was thought to be ideal regarding recyclability and sustainability.

Table 11: Catalysis results for the conjugate addition developed by Schneider *et al.*

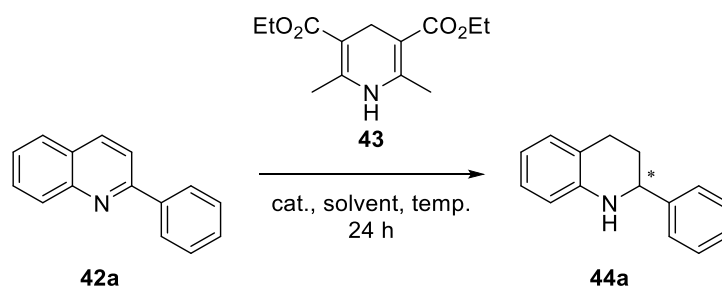
Entry	Catalyst	Conversion [%] ^a	Yield [%]	<i>Ee</i> [%] ^b
1	None	-	-	-
2	116h	100	80	81
3	123h	incomplete	n.d.	n.d.
4	123h (Run 2)	-	-	-
5	128h	100	74	40

^a Reaction conditions: 0.20 mmol 2-(hydroxy(phenyl)methyl)phenol (**135**), 0.24 mmol 1,3-cyclohexanedione (**136**), 25 mg catalyst (**123h/128h**) or 7 mg **116h** (0.01 mmol, 5 mol%), r.t., 48 h reaction time, ^b Enantiomeric excess determined by chiral HPLC, n.d. = not determined.

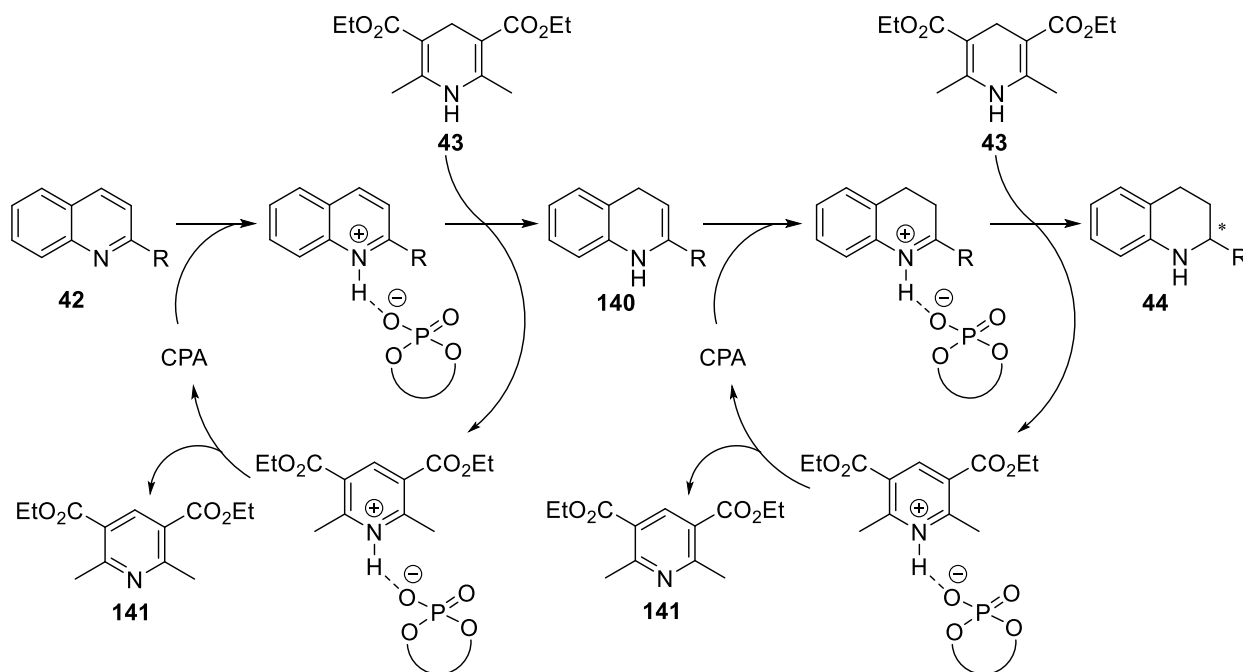
For the initial test on this reaction, catalyst **123h** was used, containing the immobilized 2,6-dimethyl-4-tert-butylphenyl substituted CPA (**116h**) which was polymerized without the addition of benzene. Interestingly, while the desired product could be detected on TLC, the reaction stopped at some point, never achieving full conversion (Table **11**, entry 3). Employing the same catalyst to a second run of the reaction then resulted in no formation of the desired product (Table **11**, entry 4). Due to the high stability of the CPA catalysts, it was concluded that rather than catalyst degradation, the problem would most likely lie in the microporous nature of the catalyst. Since the product of this addition reaction is much larger than the two starting materials, it is possible that the product was formed inside the pores of the catalyst, but at a certain point could no longer get out of the pores, inhibiting further material transport and thus shutting down the reaction. This hypothesis is further supported by the results achieved with the second catalyst **128h** tested, containing the identical CPA (**116h**) but with utilizing the copolymerization strategy for the immobilization. Here, the reaction did go to full conversion and 74% of the desired product could be isolated with 40% *ee* (Table **11**, entry 5). It is reported in literature^[146] that copolymerization with benzene in such Friedel-Crafts like polymerization indeed has a major influence on the porosity of the resulting polymer. Therefore, the copolymerization presumably could have increased the pore size of the polymer to a point where material transport of starting material as well as product through the polymer was possible. While unfortunately the selectivity of the new catalyst was not up to par with the literature results (90% *ee*) or the reproduced homogeneous reaction (81% *ee*, Table **11**, entry 2), this was still the first result where a significant enantioselectivity could be observed with this new type of immobilized catalysts, proving the viability of this polymerization method. Derived from the results with catalyst **123h**, it was concluded that any type of addition reaction could potentially lead to the same issue with material transport through the polymer. Therefore, the focus of finding a suitable reaction for those new catalysts had to be shifted towards different reaction types.

2.3.6. Transfer hydrogenation of 2-substituted Quinolines

One of the reaction types matching this criteria were asymmetric transfer hydrogenations. Here, the chiral information gets introduced *via* the selective transfer of a hydride ion. Therefore, the size increase of the product is minimized and mainly limited to conformational changes due to the shift in hybridization. The first enantioselective transfer hydrogenation employing CPAs was reported by Rueping *et al.* in 2005.^[147] In this procedure, N-protected ketimines were reduced using Hantzsch dihydropyridine (**43**) as a hydrogen source. However, due to the aforementioned concerns employing N-protected imines, a different variation of the reaction, also published by Rueping *et al.* in 2006 was considered instead (Scheme **45**).^[60] In this alteration, 2-substituted quinolines (**42**) were used as substrates and reduced to the corresponding 1,2,3,4-tetrahydroquinolines (**44**). In the proposed mechanism, the substrate is activated by the CPA through protonation of the nitrogen, which allows for the first transfer of a hydride from the Hantzsch dihydropyridine (**43**), reducing the substrate to the enamine species **140**. The resulting pyridinium cation then regenerates the CPA catalyst through reprotonation. After tautomerization of the enamine **140** to its imine form, the catalyst can therefore activate the substrate a second time through protonation, followed by a second hydride transfer to give the final product (Scheme **46**).

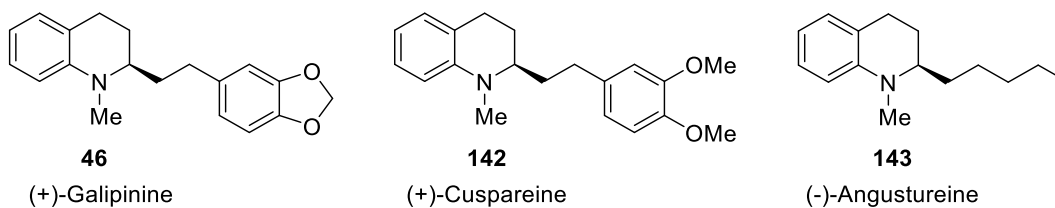


Scheme 45: Asymmetric transfer hydrogenation of 2-substituted quinolines (**42**).^[60]



Scheme 46: Proposed mechanism for the transfer hydrogenation of 2-substituted quinolines (**42**).^[60]

The resulting 1,2,3,4-tetrahydroquinolines (**44**) are of great significance as their core structure is present in many natural products. Specifically, several biologically active alkaloids can be directly obtained after a simple N-methylation of the products (Scheme **47**). Of those three, (+)-galipinine (**46**) is especially interesting due to its potential use as an anti-malarial drug.^[61]



Scheme 47: Natural products containing the 1,2,3,4-tetrahydroquinoline core structure.

For this reaction, the performance of several immobilized CPAs in the transfer hydrogenation of 2-phenyl substituted quinoline (**42a**) was evaluated. In order to investigate the effects of the immobilization, most reactions were carried out with the immobilized and the homogeneous catalyst under similar reaction conditions. Surprisingly, the CPAs with the highest homogeneous selectivities in literature, reported by Rueping *et al.*, gave only mediocre enantioselectivities of 24 or 30% (Table **12**, entries 2 and 3). From that, it was concluded that CPAs with sterically unhindered aromatic moieties in 3,3'-Positions were not well

suitable for this heterogeneous reaction. However, utilizing the copolymers with the sterically restricted aryl moieties, like the 2,6-DM4TB catalyst **128h** already gave a promising result of 61% *ee* which could be even improved to 72% *ee* by performing the reaction at room temperature (Table **12**, entries 5 and 6). After checking different commonly used solvents with this catalyst, it was found that DCM and THF showed no major impact on the selectivities, although the reaction time in THF increased significantly to 48 h (Table **12**, entries 7 and 8). Finally, using the TRIPS catalyst **128i**, DCM showed significantly better results than toluene as solvent, yielding 98% *ee* in the homogeneous reaction and 77% *ee* after the immobilization (Table **12**, entry 11).

Table 12: Solvent and catalyst screening for the transfer hydrogenation of 2-phenyl quinoline (**42a**).

Entry	CPA/NP-cat.	Solvent	Temp. [°C]	<i>ee</i> [%] ^a	
				Homo-geneous	Hetero-geneous
1	116d/123d	Toluene	60	5 ^b	17
2	116e/123e	Toluene	60	84 ^b	24
3	116f/123f	Toluene	60	97 ^b	30
4	116g/123g	DCM	r.t.	n.r.	9
5	116h/128h	Toluene	60	n.d.	61
6	116h/128h	Toluene	r.t.	85	72
7	116h/128h	THF	r.t.	89	70 ^c
8	116h/128h	DCM	r.t.	89	73
9	116i/128i	Toluene	r.t.	89	43
10	116i/128i	THF	r.t.	96	73 ^c
11	116i/128i	DCM	r.t.	98	77 (85 ^d)

^a Reaction conditions: 0.10 mmol 2-phenylquinoline (**42a**), 0.24 mmol Hantzsch dihydropyridine (**43**), 10 mg heterogeneous catalyst or 5 mol% homogeneous catalyst, 2 mL solvent, 24 h reaction time, enantiomeric excess determined by chiral HPLC, ^b literature results^[60], ^c 48 h reaction time, ^d after optimized catalyst washing procedure, n.r. = no reaction, n.d. = not determined.

With these first positive results, the reaction was also used to further investigate the effects of the immobilization, especially regarding the copolymerization strategy. It was found that the selectivity of the reaction correlated with the benzene content of the copolymer. The selectivity decreased from 83% *ee* with no benzene in the polymer to 37% *ee* when 50 equiv. of benzene were used in the copolymer (Table **13**, entries 1 and 3).

From a material scientific point of view it was also interesting to see that when the benzene equivalents in the copolymer were increased, the yield of the isolated polymer dropped to 56% with 50 equiv. of benzene and even no isolation was possible when 100 equiv. were used (Table 13, entries 3 and 4). Of course, this is a result of the lower overall magnetization of the polymer when more and more non-magnetic material is attached to the NPs. However, in contrast to those results it was found that when 80 equiv. benzene and 20 equiv. of phenyldodecane were employed in the polymerization, 80% of the polymer could be isolated (Table 13, entry 5). This suggests that the incorporation of a softener-type molecule, like phenyldodecane, into the polymer allows for the attachment of more non-magnetic material the NPs. This could possibly be the result of the polymer becoming less brittle, and therefore less completely non-magnetic polymer is formed through breaking off. Nevertheless, the trend of lower selectivity with higher benzene/phenyldodecane content is also observed here with only 19% *ee* when this catalyst was employed.

Table 13: Results on the correlation between copolymer benzene-content and selectivity.

Entry	CPA	Polymerization additive	Polymerization yield [%]	<i>ee</i> [%] ^a
1	116i	-	57	83
2	116i	Benzene (3 equiv.)	95	77
3	116i	Benzene (50 equiv.)	56	37
4	116i	Benzene (100 equiv.)	no isolation possible	-
5	116i	Benzene (80 equiv.) + Phenyldodecane (20 equiv.)	80	19

^a Reaction conditions: 0.10 mmol 2-phenylquinoline (**42a**), 0.24 mmol Hantzsch dihydropyridine (**43**), 10 mg heterogeneous catalyst, 2 mL DCM, 24 h reaction time, enantiomeric excess determined by chiral HPLC.

This trend indicates that the benzene-part of the copolymer might cause an asymmetric background reaction and therefore reduce the overall selectivity. Since these microporous organic structures have been reported to absorb various (heavy metal) ionic species^[148] as well as water^[135], this was suspected to be an effect of the adsorption of HCl (H₃O⁺, Cl⁻) into the benzene polymer during the acidification of the catalyst, which could not be removed in *vacuo*. To get further evidence for this hypothesis, a benzene polymer with magnetic NPs but no CPA was treated with the same acidification procedure as a normal CPA catalyst (Table 14, entry 2) while another sample of the polymer was neutralized by washing with water

after the acidification. Both samples were dried and then subjected to the transfer hydrogenation reaction of **42a** for 6 h. It was found that when no catalyst at all was present (Table **14**, entry 1) only minor amounts of 4% product could be detected *via* NMR. With the acidified polymer present in the reaction, 76% yield was detected, showing a major background reaction within only 6 h. However, it could also be shown that the neutralization successfully reduces the background reaction to only 14% yield within 6 h (Table **14**, entry 3). Employing this procedure to the catalyst with the optimized immobilization conditions (3 equiv. benzene) improved the selectivity from 77% *ee* to 85% *ee* (Table **12**, Entry 11, in brackets), which is similar to the selectivity without any benzene in the polymer.

Table 14: Results on the asymmetric background-reaction induced by the benzene polymer.

Entry	Cat.	Washing procedure	NMR-Yield [%] ^a
1	none	-	4
2	Benzene polymer	1 M HCl (10x) then dried	76
3	Benzene polymer	1 M HCl (10x), H ₂ O (15x) then dried	14

^a Reaction conditions: 0.10 mmol 2-phenylquinoline (**42a**), 0.24 mmol Hantzsch dihydropyridine (**43**), 10 mg benzene MOP@Co/C NPs, 2 mL DCM, 6 h reaction time, NMR-Yield determined using 1,3,5-trimethoxybenzene as internal standard.

To explore the synthetic utility and advantages of the immobilized system, the recyclability of the catalyst in regard to reactivity and selectivity was evaluated. With a reaction time of 5 h for substrate **42a** on a 0.5 mmol scale, the reactivity of the catalyst remained almost constant for the first 10 reaction cycles and thereafter only slightly degraded to 95% yield up to run 17. Also, the selectivity showed no significant degradation over the course of 17 cycles and constantly high *ee* values around 80% could be achieved (Figure **6**). Thus, a total of 1.7 g of product could be synthesized with only 25 mg of catalyst material. Additionally, it was possible to demonstrate that the *ee* values of the lowest selectivity 73% (Run 12) could be improved up to 99% by recrystallization from ethanol together with tartaric acid (2x). This proves that the catalyst system is not only capable of producing large amounts of product but also can be utilized when very high selectivities are required.

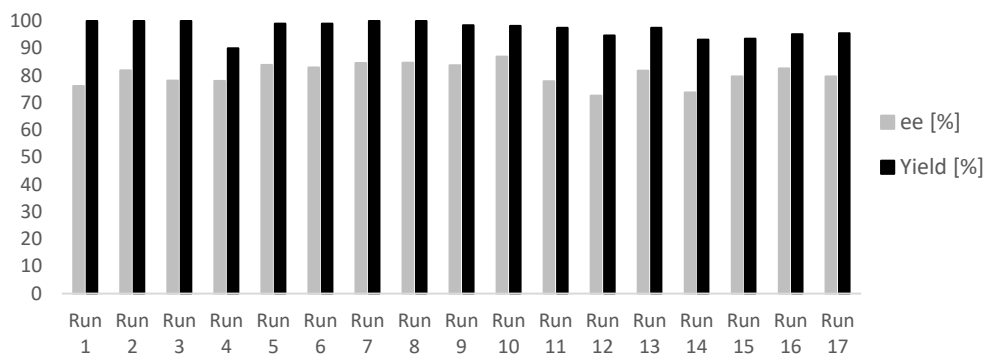


Figure 6: Recycling of the immobilized TRIPS (**128i**) in the transfer hydrogenation of substrate **42a**.

Since the catalyst could introduce potentially toxic cobalt metal into the product, the reaction solution was analyzed by ICP-OES for the first 10 runs. While the first run showed contamination of 39 ppm cobalt, all other runs showed only below 8 ppm levels of cobalt (Figure 7). Additionally, the contamination was measured in Run 1 after chromatographic workup and no cobalt could be detected (<1 ppm) showing that none of the leached cobalt ends up in the isolated product.

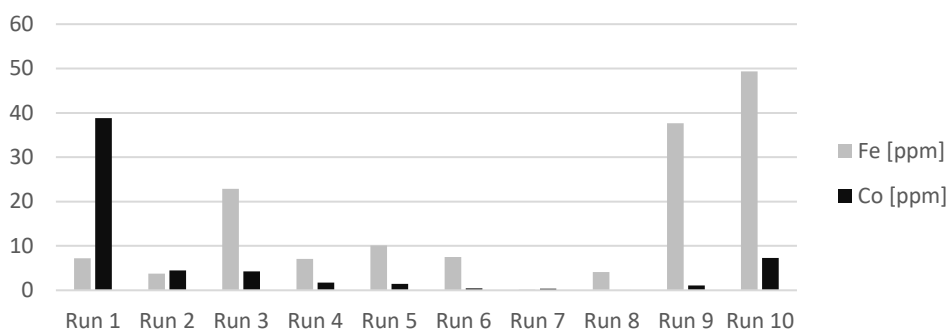


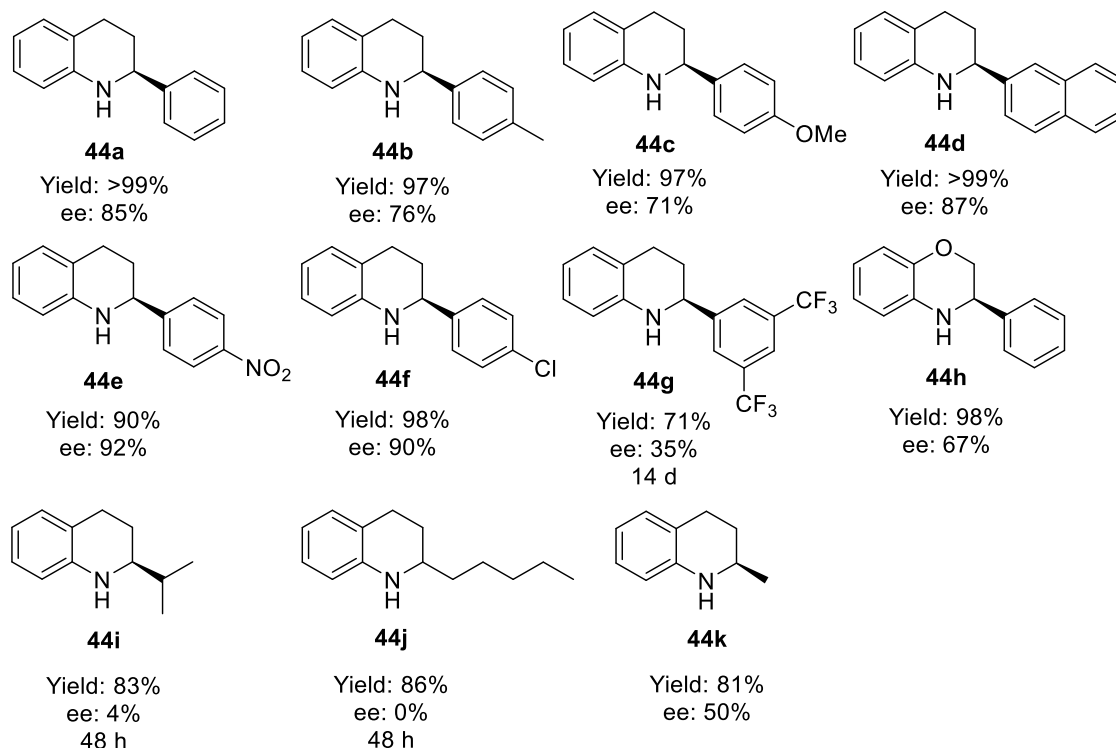
Figure 7: Cobalt and Iron contamination within the first ten runs of recycling the catalyst (**128i**).

Since it is known in literature that counterions can have a significant influence on the enantioselectivity of the catalyst^[149], the solution was also analyzed for its iron content. Potential iron sources could be from the catalyst polymerization as well as from the starting material synthesis. However, no iron could be detected in the catalyst, leaving the different batches of starting material as the only source, and no correlation between iron content and selectivity could be observed.

Exploring the substrate scope of the newly developed catalyst, also on a 0.5 mmol scale, revealed generally good selectivities for aryl-substituted quinolines (Scheme **48**). The introduction of electron-donating groups like a methyl- or a methoxy group (**44b** and **44c**) showed a slight decrease in selectivity down to 71% in the case of the methoxy group. Substrate **44d** with a naphthyl group showed a high selectivity of

87% *ee*, presumably due to sterical reasons. Electron withdrawing substituents such as nitro- or chloro groups (**44e** and **44f**) on the phenyl ring showed the best selectivities with 92% *ee* and 90% *ee*, respectively. Interestingly substrate **44g** containing a double CF₃ substituted phenyl ring could only be reduced in 35% *ee* and with a reaction time of 2 weeks. It is suspected that this could be the result of the product blocking the pores of the catalyst, resulting in lower selectivity and the higher reaction time. The catalyst could also be used for the reduction of 2-phenyl substituted 2H-1,4-benzoxazine (**44h**) in 67% *ee* although the selectivity was lower compared to the corresponding quinoline derivative **44a** (85% *ee*). Substrates with aliphatic substituents (**44i** and **44j**), however, could not be selectively reduced. It was found that for substrate **44i** this is also true for the homogeneous TRIPS-catalyst (**116i**) and thus is most likely a result of the high sterical hindrance of the alkyl chain with the isopropyl groups of the catalyst. Only Substrate **44k** could be converted with 50% *ee* due to the small size of the methyl group.

These results also show that the catalyst system can not be used for the synthesis of the aforementioned alkaloids since they all contain aliphatic substituents. As a control experiment, substrate **44i** was also reduced with catalyst **123f** containing the 9-phenanthrene substituted CPA (**116f**), which in literature could reduce aliphatically substituted substrates in good selectivity. However, after the immobilization of the CPA, only 8% *ee* could be achieved.



Scheme 48: Substrate scope of the immobilized CPA catalyst **130i**.

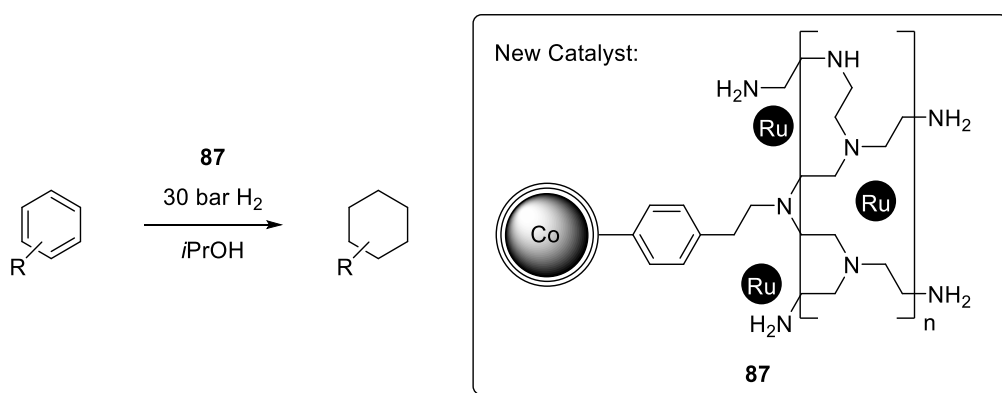
2.4. Conclusion

A new immobilization method for BINOL-derived chiral phosphoric acids (CPAs) on magnetic Co/C NPs has been developed. Without the need for prior functionalization, the CPAs were polymerized in high yields onto the NP surface using toluene moieties as the anchor point and formaldehyde dimethyl acetal as the crosslinker for the aromatic BINOL backbone. The new hybrid materials were tested for several CPA catalyzed reactions and were found to be successful in the asymmetric transfer hydrogenation of 2-substituted quinolones (**42**) achieving high yields as well as good enantioselectivities from 71% *ee* with electron-rich substituents such as *para*-methoxyphenyl (**44c**) up to 92% *ee* with electron-deficient substituents like *para*-nitrophenyl (**44e**). Unfortunately, aliphatic substituents were not well tolerated owing to the best performing TRIPS CPA **118i** that was also not able to selectively reduce these substrates before the immobilization. The only substrate with aliphatic residues where a decent chiral induction of 50% *ee* could be obtained was substrate **44k**, presumable due to the small size of the methyl substituent. The catalyst could be easily reused due to its magnetic properties for at least 17 runs without any loss in enantioselectivity and only minor loss in activity. The products were obtained in high purity and especially, no contamination with cobalt metal that could have leached from the NP platform was detected (<1 ppm). These results prove that the concept of this immobilization method is viable and could potentially also be expanded towards other organocatalysts or even metal complexes bearing polymerizable aromatic residues.

C. Summary

In this work, two different magnetically recoverable catalytic systems were developed and their synthetic utility was investigated. Both catalysts were supported by magnetic Co/C NPs (**75**), which rendered them highly reusable through quick and facile removal from the solution with an external magnet.

In the first chapter, a Ru NP-based catalyst for the aromatic hydrogenations was investigated. Three distinct strategies for the immobilization of Ru NPs on magnetic Co/C NPs were compared, and a poly(ethylenimine) (PEI)-based system (**87**) grafted onto the Co/C NPs proved to be superior in terms of reactivity and reusability (Scheme **49**).

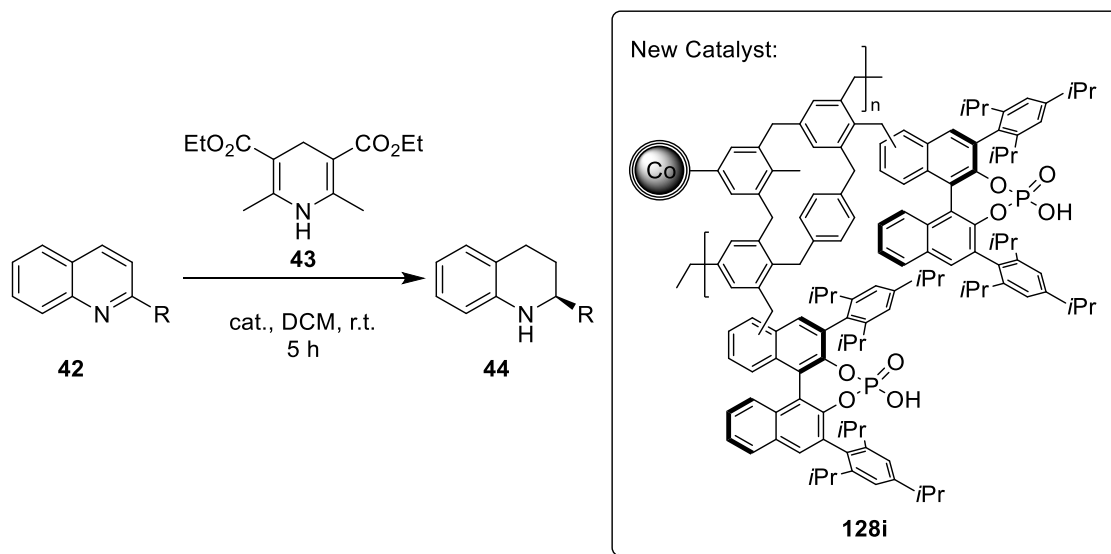


Scheme 49: New Ru NPs@PEI@Co/C NPs catalyst for the hydrogenation of arenes.

The effects of different PEI polymer variations on the catalytic performance were explored, revealing that materials with a lower nitrogen content (and therefore a smaller polymer coating) were ideal. For the final catalyst, a PEI@Co/C NPs system with only 0.3 wt% N was used and the incorporation of Ru NPs was optimized so that up to 67% of the employed Ru were immobilized, giving rise to a high Ru loading of 10.6 wt%. The catalytic activity was evaluated in the hydrogenation of toluene (**88**) as a model reaction and a TOF of 1,402 h⁻¹ was achieved using 30 bar H₂ pressure at room temperature. Reusability of the catalyst was also examined in this reaction, and the catalyst could be recovered and reused for at least 16 consecutive runs with only a minor loss in reactivity and an almost negligible amount of metal leaching with an average of 1.1 ppm/cycle for Ru and 0.1 ppm/cycle for Co. Lastly, the substrate scope of the newly developed catalyst was studied. In total the aromatic hydrogenation of 13 different substrates was shown, including electron-rich and electron-poor systems as well as highly substituted substrates such as thymol (**13**), which gives rise to the highly desired menthol isomers (**14**).

In the second chapter, a new method for the immobilization of BINOL-based chiral phosphoric acids (CPAs) onto the magnetic Co/C NPs was invented. Employing a procedure developed by Tan *et al.*^[115] for grafting

of microporous organic polymers from simple arenes, the aromatic moieties of the CPAs were polymerized using formaldehyde dimethyl acetal (FDA) as an external crosslinker. Since the substituents in the 3,3'-positions of the BINOL play a critical role for the chiral induction of the catalyst, the immobilization was tested for several different CPAs. While CPAs with sterically unhindered aromatic substituents such as a naphthyl moiety were immobilized quantitatively without issues, a copolymerization strategy with benzene had to be employed for CPAs with sterically hindered substituents to achieve the same goal. The resulting catalysts were tested in a number of Brønsted acid-catalyzed reactions with the most success being found in the enantioselective transfer hydrogenation of 2-substituted quinolines (**42**) (Scheme 50).



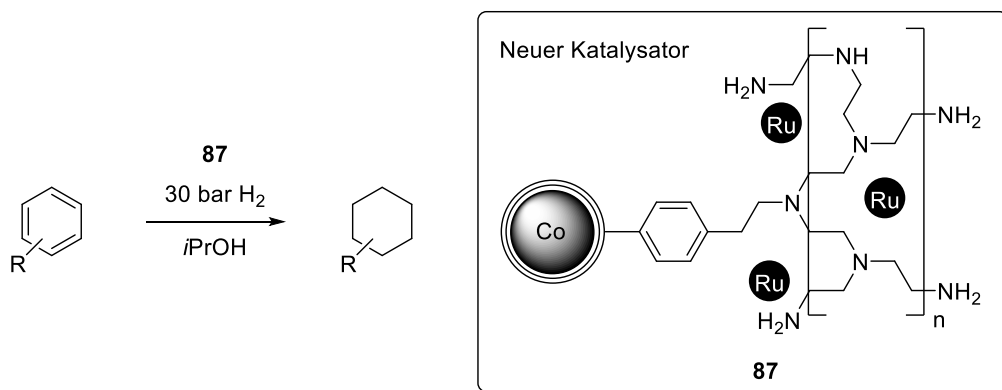
Scheme 50: Immobilized TRIPS catalyst **130i** for the transfer hydrogenation of 2-substituted quinolines (**42**).

Using the immobilized TRIPS catalyst **128i** resulted in the highest selectivity of 85% *ee* for the model substrate 2-phenylquinoline (**42a**). Other quinolines with aromatic substituents were also well tolerated reaching selectivities of up to 92% *ee* for 4-nitrophenyl-quinoline (**42e**). The recycling capabilities of the system were also explored for the model substrate (**42a**) and the catalyst could be reused for 17 consecutive runs with only negligible losses in reactivity and constantly high *ee* values of around 80%. Due to this excellent reusability, a total of 1.7 g product (**44a**) could be synthesized with only 25 mg of catalyst material.

D. Zusammenfassung

In dieser Dissertation wurden zwei neue magnetisch abtrennbare Katalysatorsysteme entwickelt und auf ihre Anwendungsmöglichkeiten getestet. Beide Katalysatoren wurden auf magnetischen Co/C Nanopartikeln (NP) als Immobilisierungsplattform aufgebaut, was ihnen eine hohe Wiederverwendbarkeit verleiht und die einfache Abtrennung innerhalb von wenigen Sekunden mit einem externen Magneten ermöglicht.

Im ersten Kapitel wurde ein auf Ru NP basierender Katalysator für die Hydrierung von aromatischen Verbindungen untersucht. Es wurden drei unterschiedliche Methoden für die Immobilisierung von Ru NP auf magnetischen Co/C NP verglichen. Ein auf einem Poly(ethylenimin) (PEI) polymer basierendes System (**87**) stellte sich dabei als idealer Kandidat in Bezug auf Reaktivität und Wiederverwendbarkeit heraus (Schema 1).

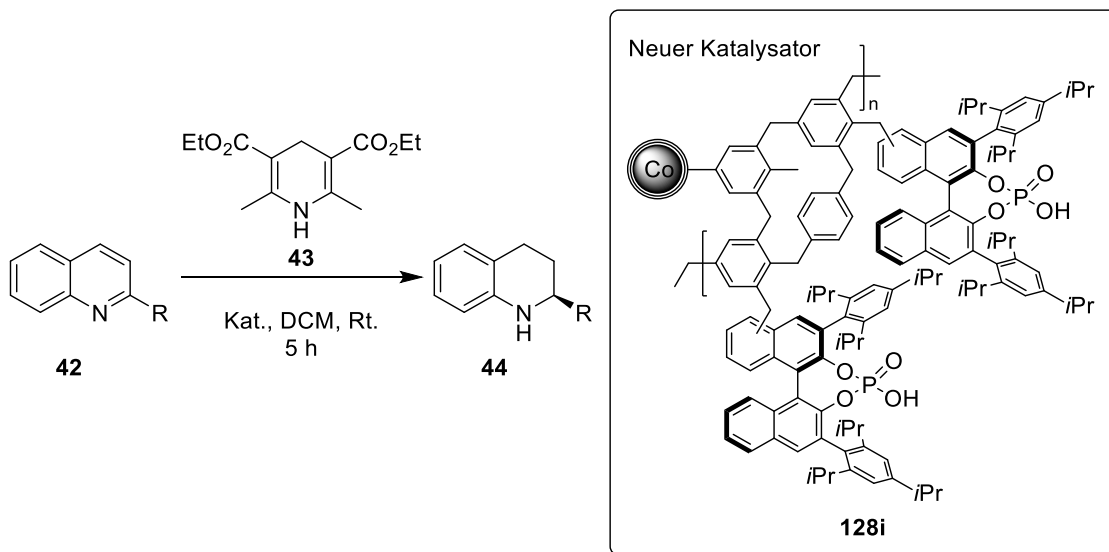


Schema 1: Neu entwickelter Ru NP@PEI@Co/C NP Katalysator für die Hydrierung aromatischer Verbindungen.

Die Auswirkungen von unterschiedlichen Variationen des PEI Polymers auf die katalytische Aktivität wurden untersucht, wobei sich zeigte, dass Verbindungen mit niedrigerem Stickstoffgehalt (und damit weniger Polymer) die besten Ergebnisse lieferten. Für den optimierten Katalysator wurde deshalb ein PEI@Co/C NP system mit nur 0.3 Gew.-% Stickstoff verwendet. Die Einlagerung der Ru NP konnte bis auf 67% des verwendeten Ru optimiert werden, wodurch der Katalysator mit 10.6 Gew.-% Ru eine hohe Beladung aufwies. Die katalytische Aktivität wurde in the Hydrierung von Toluol (**88**) als Modellreaktion evaluiert und eine TOF von 1.402 h⁻¹ bei Raumtemperatur und 30 bar H₂ Druck konnte erreicht werden. Die Wiederverwendbarkeit des Katalysators wurde ebenfalls in dieser Reaktion getestet und es konnten 16 aufeinanderfolgende Zyklen durchgeführt werden, mit nur geringem Reaktivitätsverlust und einem nahezu vernachlässigbarem Metall-Leaching von durchschnittlich 1.1 ppm/Zyklus für Ru und 0.1 ppm/Zyklus für Co. Zuletzt wurde die Substratbreite des neuen Katalysators analysiert und die

aromatische Hydrierung von 13 unterschiedlichen Substraten konnte gezeigt werden. Dabei konnten sowohl elektronenreiche als auch elektronenarme Verbindungen und sogar hoch substituierte Substrate wie Thymol (**13**) reduziert werden. Letzteres war dabei besonders interessant, da es die Synthese der hochbegehrten Mentholisomere (**14**) ermöglicht.

Im zweiten Kapitel wurde eine neue Methode für die Immobilisierung von BINOL basierten chiralen Phosphorsäuren (CPAs) auf magnetischen Co/C NP entwickelt. Dabei wurde auf ein von Tan *et al.*^[115] entwickeltes Verfahren zur Herstellung von mikroporösen organischen Polymeren aus einfachen Arenen zurückgegriffen. Die aromatischen Einheiten der CPAs wurden hierbei mithilfe von Formaldehyddimethylacetal (FDA) über CH₂ Brücken verbunden. Da die Substituenten in den 3,3'-Positionen des BINOLs eine große Rolle für die Enantioselektivität des Katalysators spielen, wurde die Immobilisierung für verschiedene CPAs verglichen. Während CPAs mit sterisch ungehinderten aromatischen Substituenten wie einer Naphthylgruppe dabei ohne Probleme quantitativ immobilisiert werden konnten, musste für CPAs mit sterisch gehinderten Resten eine Copolymerisierung mit Benzol durchgeführt werden um dies zu erreichen. Die immobilisierten Katalysatoren wurden in einer Reihe von Brønsted Säure katalysierten Reaktionen getestet, wobei sich die enantioselektive Transferhydrierung von 2-substituierten Chinolinen (**42**) als am Erfolgversprechensten herausstellte (Schema 2).



Schema 2: Immobilisierter TRIPS Katalysator für die Transferhydrierung von 2-substituierten Chinolinen (**42**).

Die höchsten Selektivitäten konnten durch den immobilisierten TRIPS Katalysator **128i** beobachtet werden, welcher 85% *ee* für das Modellsubstrat 2-Phenylchinolin (**42a**) erreichte. Bei der Reduktion

anderer aromatisch substituierter Chinoline konnten ebenfalls gute Selektivitäten von bis zu 92% *ee* für den Fall von 4-Nitrophenylchinolin (**42e**) erzielt werden. Die Wiederverwendbarkeit des Katalysators wurde für die Reduktion des Modellsubstrates **42a** untersucht, wobei 17 aufeinanderfolgende Zyklen durchgeführt werden konnten. Der Katalysator zeigte dabei nur einen geringen Verlust and Reaktivität bei konstant hohen Selektivitäten um 80% *ee*. Aufgrund dieser exzellenten Ergebnisse konnten 1.7 g des Produktes (**44a**) mit nur 25 mg des Katalysatormaterials hergestellt werden.

E. Experimental Part

1. General information

Chemicals and solvents

All commercially available chemicals were purchased in high quality and used without further purification. Technical grade ethyl acetate, hexanes (40/60) and DCM for workup and column chromatography were freshly distilled prior to usage. Anhydrous solvents were prepared following standard procedures.^[150]

All syntheses of literature known starting materials were performed according to or with slightly modified procedures of the corresponding references given in the synthesis section. (R)/(S)-BINOL were synthesized from students in the organic chemistry laboratory courses at the University of Regensburg according to literature^[151,152] and recrystallized in toluene before use. CPAs **116d** and **116g-i** were synthesized following the given literature references in the synthesis section, CPA **116e** and **116f** were purchased.

Carbon-coated cobalt nanoparticles (Co/C NPs, **75**) were obtained from the group of Prof. W. J. Stark from the ETH Zurich, Switzerland but are also commercially available from Turbobeads Llc. Prior to use, they were washed in a conc. HCl/ deionized water (Millipore) mixture (1:1) five times for 24 h. The acid residuals were removed by washing with Millipore water until neutral pH of the supernatant solution. Afterwards, the NPs were washed with acetone (3x) and Et₂O (2x) and dried at 50 °C *in vacuo*.

¹H-NMR Spectroscopy

¹H-NMR spectra were recorded either on a Bruker Avance 300 (300 MHz) or a Bruker Avance 400 (400 MHz) at room temperature. All spectra were recorded in CDCl₃ or acetone-d₆, the chemical shifts are reported as parts per million (ppm) and refer to the signal of CHCl₃ at 7.26 ppm or acetone-d₅ at 2.05 ppm. The multiplicity of the signals is described as follows: s = singlet, bs = broad singlet, d = doublet, t = triplet, q = quartet, sext = sextet, sept = septet, m = multiplet. The integrals represent the relative number of hydrogen atoms related to the corresponding signals.

¹³C-NMR Spectroscopy

¹³C-NMR spectra were recorded either on a Bruker Avance 300 (75.5 MHz) or a Bruker Avance 400 (101 MHz) at room temperature. All spectra were recorded in CDCl₃, the chemical shifts are reported as parts per million (ppm) and refer to the center of the triplet of CDCl₃ at 77.2 ppm.

³¹P-NMR Spectroscopy

³¹P-NMR spectra were recorded either on a Bruker Avance 300 (162 MHz) or a Bruker Avance 400 (121 MHz) at room temperature. All spectra were recorded in CDCl₃, the chemical shifts are reported as parts per million (ppm).

¹⁹F-NMR Spectroscopy

¹⁹F-NMR spectra was recorded on a Bruker Avance 400 (376 MHz) at room temperature. The spectra was recorded in CDCl₃, the chemical shift is reported as parts per million (ppm).

Elemental microanalysis

Elemental microanalysis was performed in the micro analytical department of the University of Regensburg ("Zentrale Analytik") using a Vario MICRO Cube.

Thin-layer chromatography (TLC)

Thin-layer chromatography was performed using silica-coated aluminum plates (Merck silica gel 60 F₂₅₄, d = 0.2 mm). Visualization was accomplished with UV light (λ = 254 nm or 366 nm) or through the use of stains such as KMnO₄, vanillin/sulfuric acid, or Iodine in silica.

Column Chromatography

(Flash-) Column chromatography was performed using silica gel (Merck Gerduran 60, 0.063 – 0.2 mm particle size) or Merck flash (0.040 – 0.063 mm) silica gel.

Infrared spectroscopy (IR)

Infrared spectra were recorded on an Agilent Cary 630 FT-IR spectrometer. All spectra were measured of neat compounds.

Gas chromatography (GC)

Gas chromatography was performed on a Fisons Instruments Gas Chromatograph GC8000 equipped with a capillary column (DB-1 100% dimethylpolysiloxane; 30 m x 250 μ m x 0.25 μ m, injection temperature 250 °C, detector temperature 300 °C) and a flame ionization detector (FID).

Chiral gas chromatography

Gas chromatography was performed on a Fisons Instruments Gas Chromatograph GC8000 equipped with a Cyclodex- β column (CP-chirasil-Dex CB; 25 m x 250 μ m x 0.25 μ m, injection temperature 250 °C, detector temperature 250 °C) and a flame ionization detector (FID).

Chiral high-performance liquid chromatography (HPLC)

Chiral HPLC was performed on a Varian LC-902 Liquid Chromatograph, using a Phenomenex Lux Cellulose 1 column (4.6 * 250 mm, 5 μ m), a Phenomenex Lux i-Amylose-3 column (4.6 * 100 mm, 5 μ m) or a Chiracel AS-H column (4.6 * 250 mm, 10 μ m). The absolute configuration of the products was determined by comparison to literature results.

Inductively coupled plasma optical emission spectrometry (ICP-OES)

Samples for ICP-OES were measured on a Spectro Analytical Instruments ICP Modula EOP or a Spectroblue FMX36 (Spectro) in acidic aqueous solution (aqua regia 32% (v/v)) after prior standardization and calibration.

Hydrogenations

All hydrogenation reactions were performed in a 100 mL Carl Roth Hockdruck-Laborautoklav Modell I with magnetic stirring at r.t. or 50 °C using a heating mantle (Figure 8).

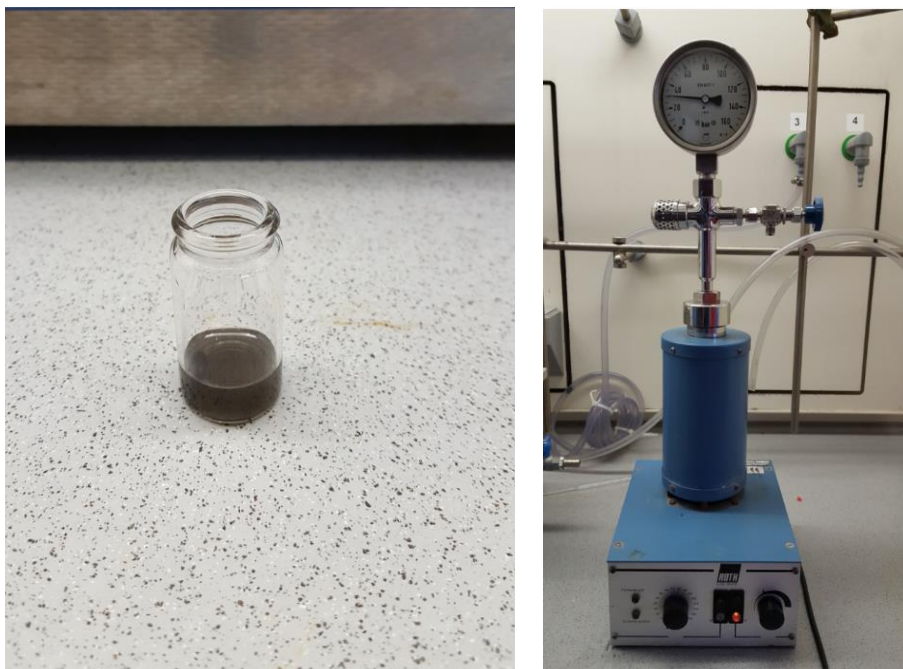


Figure 8: Typical reaction setup for aromatic hydrogenations (left), stainless-steel autoclave (right).

Working methods for magnetic Nanoparticles

Dispersion of the particles was achieved using an ultrasound bath (Sonorex RK 255 H-R, Bandelin). For the recovery of the NPs, commercially available neodymium-based magnets (12 x 12 mm) were used. Magnetic decantation was done by collecting the NPs with the magnet (within several seconds) and decanting the supernatant solution. On smaller scale reactions (<2 mL) the solution was removed with a Pasteur pipette instead. NPs were separated from magnetic stirring bars during the last washing step by stirring at maximum speed and removing the NP dispersion with a Pasteur pipette.

ICP sample preparation

Samples for the ICP-OES analysis were prepared by dissolving the incorporated metal in aqua regia. 5 mg of the corresponding particles were therefore treated with conc. HCl (2.4 mL) and conc. HNO₃ (0.8 mL) at 100 °C for 10 min. The solution was collected, and the remaining particles were treated with the same procedure a second time. The combined solutions were diluted to 10 mL, filtered through a syringe filter, and diluted by a factor of two (5 mL to 10 mL) to achieve the required 32 % (v/v) aqua regia.

For the analysis of transition metal contaminations, the reaction products were treated with conc. HCl (2.4 mL) and conc. HNO₃ (0.8 mL) at 100 °C for 10 min. The solution was collected, filtered through a syringe filter, and diluted to 10 mL to achieve the required 32 % (v/v) aqua regia.

2. General synthesis procedures

General procedures for the functionalization of Co/C NPs (75) via diazonium chemistry (GP1)^[102]

In a 50 mL round-bottom flask, Co/C NPs (75) were dispersed in a mixture of conc. HCl, amino compound and Millipore water (15 mL) with the aid of an ultrasonic bath for 15 min at r.t. The slurry was stirred and cooled to 0 °C with an ice bath and a precooled solution of sodium nitrite in Millipore water was slowly added. The reaction mixture was stirred for 30 min at 0 °C followed by sonication for 30 min at room temperature. The nanoparticles were recovered from the solution with the aid of a magnet and washed with 1 M NaOH (1 x 5 mL) Millipore water (2 x 5 mL) and acetone (5 x 5 mL) and the washed nanoparticles were dried *in vacuo*.

General procedure for the synthesis of microporous frameworks around Co/C NPs (GP2)^[107]

A 30 mL screw-capped vial was charged with all the given reaction components (see corresponding procedure). The nanoparticles were dispersed with the aid of an ultrasonic bath for 10 min at r.t. and the mixture was stirred for 5 h at 45 °C followed by 19 h at 80 °C. The solvent was decanted, the nanoparticles were washed with ethanol by magnetic decantation until the supernatant solution was clear and the nanoparticles were dried *in vacuo* for 4 h at 60 °C.

In the case of CPA containing frameworks, the compounds were also acidified by washing with 1 M HCl (10 x) before drying.

General procedure for the synthesis of PEI polymers around amino-functionalized Co/C NPs (GP3)^[100]

In a 30 mL pressure tube, amino-functionalized Co/C NPs (85) were dispersed in the solvent with the aid of an ultrasonic bath for 10 min at r.t. The mixture was stirred at r.t. and HCl conc. and aziridine (86) were added successively. After the addition, the pressure tube was placed in an oil bath heated to 40 °C if the solvent was DCM or 80 °C if the solvent was DCE and the slurry was stirred for the given reaction time. The reaction was allowed to cool to r.t. and the NPs were washed with DCM (3 x 5 mL) and Millipore water (3 x 5 mL) and dried *in vacuo* at 60 °C for 4 h.

General procedure for the incorporation of Ru NPs in PEI polymers *via* reduction of RuCl₃ (GP4)

A 25 mL round bottom flask was charged with the given PEI@Co/C NPs (**79**), RuCl₃ · x H₂O (36 wt% Ru), Millipore water (and additives if used) and the NPs were dispersed with the aid of an ultrasonic bath for 10 min at r.t. The slurry was stirred at r.t. and NaBH₄ was added in one portion unless stated otherwise (caution, rapid H₂ formation!). After the addition, the reaction was stirred for 30 min at r.t. and the NPs were collected with the aid of a magnet. The NPs were washed with Millipore water (2 x 5 mL) and acetone (2 x 5 mL) and dried *in vacuo*.

General procedure for the hydrogenation of arenes (GP5)

An open 5 mL vial was charged with substrate, solvent, catalyst and a stirring bar and the NPs were dispersed by stirring for approximately 1 min. The vial was placed in a stainless-steel autoclave and the apparatus was flushed twice with 20 bar H₂ before setting the reaction pressure of 30 bar H₂ and starting the magnetic stirring. After the reaction, the catalyst was collected with the aid of a magnet and the solution was analyzed by GC-FID or NMR.

Recycling procedure for the hydrogenation of toluene (88)

Following the general procedure **GP5**, a 5 mL vial was charged with toluene (1.06 mL, 10 mmol), isopropanol (0.4 mL) and the optimized catalyst **87** (21 mg, 10.6 wt% Ru, 0.022 mmol Ru, 0.22 mol%). After collecting the NP catalyst with the aid of a magnet, the product solution was separated and the catalyst was washed isopropanol (2 x 0.4 mL) *via* magnetic decantation before being subjected to the next reaction cycle.

General procedure for the synthesis of 2-substituted quinolines (42**) (GP6)^[153]**

A 100 mL round bottom flask was charged with 2-nitrobenzaldehyde (755 mg, 5 mmol), iron powder (1.2 g, 10 mmol), ethanol (15 mL) and while stirring at r.t. 0.1 M HCl (5 mL) was added. The mixture was heated to 95 °C for 2 h. After complete reduction of the nitro group as judged by TLC, KOH (337 mg, 6 mmol) and the corresponding ketone (10 mmol) was added subsequently. The mixture was heated to 95 °C for 18 h, cooled to r.t., diluted with DCM (30 mL), filtered through a plug of Celite and extracted with dist. H₂O. The aqueous layer was extracted with DCM (2x 30 mL) and the combined organic layers were dried over MgSO₄. The solvent was evaporated and the crude product was purified by flash column chromatography or recrystallization from ethanol.

General procedure for CPA catalyzed transfer hydrogenations (GP7)

A small vial was charged with Quinoline derivate (0.5 mmol), Hantzsch dihydropyridine (304 mg, 1.2 mmol), immobilized CPA catalyst (25 mg) and 10 mL of DCM and the mixture was stirred at r.t. until complete conversion of starting material as judged by TLC (5 – 48 h). The catalyst was separated from the reaction mixture *via* magnetic decantation and washed with DCM (2 x 10 mL). The organic solutions were combined and the solvent was evaporated. The crude product was purified by column chromatography.

Catalyst screening reactions

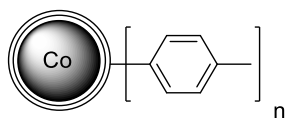
Screening reactions were performed following general procedure **GP7** using 2-phenylquinoline (**42a**) (20 mg, 0.1 mmol), Hantzsch dihydropyridine (61 mg, 0.24 mmol), 2 mL of the given solvent and 10 mg of the immobilized CPA catalyst, or 5 mol% of the homogeneous CPA. The reaction was stirred at the given temperature for 24 h or 48 h, for further details see Table **12**.

Recycling procedure for the transfer hydrogenation of 2-phenylquinoline (42a)

The recycling reactions were performed following general procedure **GP7** using 2-phenylquinoline (**42a**) (105 mg, 0.5 mmol). After the washing with DCM, the catalyst was directly subjected to the next reaction cycle without drying.

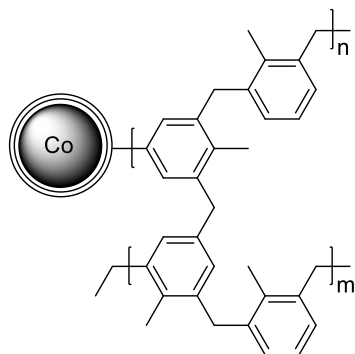
3. Co/C Nanocomposites

Toluene-functionalized Co/C NPs (**82**)



The compound was synthesized following general procedure **GP1** using 500 mg of Co/C NPs (**75**), conc. HCl (0.3 mL), *p*-Toluidine (80 mg, 0.75 mmol) and Millipore water (15 mL) as dispersion. A precooled solution of sodium nitrite (80 mg, 1.15 mmol) in Millipore water (6 mL) was added. 488 mg of **82** were recovered. Elemental microanalysis [%]: C, 5.14; H, 0.10.

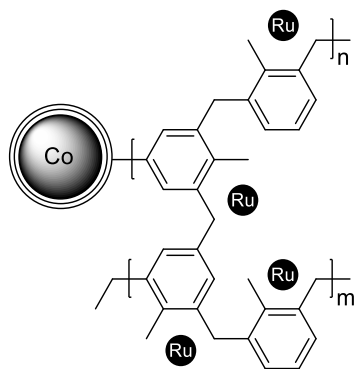
Toluene-MOP@Co/C NPs (**77**)



The compound was synthesized following general procedure **GP2**, using 200 mg of toluene functionalized Co/C NPs (**82**), toluene (106 μ L, 1 mmol), FeCl_3 (325 mg, 2 mmol), formaldehyde dimethyl acetal (176 μ L, 2 mmol) and DCE (18 mL). 241 mg of **77** were recovered.

Elemental microanalysis [%]: C, 36.4; H, 2.5.

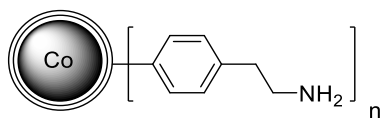
Ru NPs@toluene-MOP@Co/C NPs (**86**)



A 10 mL Schlenk tube was charged with 200 mg of the toluene-MOP@Co/C NPs (**77**), tetradecane (4 mL), and $\text{Ru}_3(\text{CO})_{12}$ (12 mg, 0.02 mmol). The mixture was degassed by repeated freeze-pump-thaw cycles (3 x), set under nitrogen atmosphere and dispersed with the aid of an ultrasonic bath for 10 min. The Schlenk tube was transferred to an oil bath preheated to 160 $^\circ\text{C}$ and the slurry was stirred for 30 min. The reaction was allowed to cool to room temperature and the NPs were collected with the aid of a magnet. Afterwards, the NPs were washed with DCM (4 x 5 mL) by magnetic decantation and dried *in vacuo*. 200 mg of **86** were recovered.

ICP-OES analysis: 1.65 wt% Ru (60% incorporation)

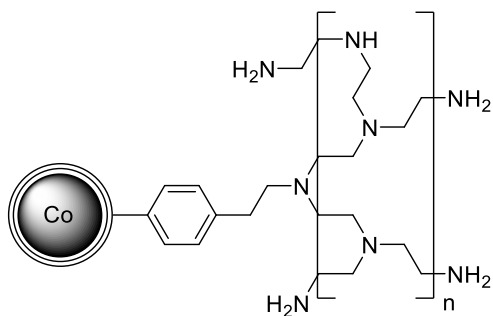
Amino-functionalized Co/C NPs (**85**)



The compound was synthesized following general procedure **GP1** using 250 mg of Co/C NPs (**75**), conc. HCl (0.25 mL), 4-(2-aminoethyl)-aniline (**84**) (34 mg, 0.25 mmol) and Millipore water (7.5 mL) as dispersion. A precooled solution of sodium nitrite (26 mg, 0.38 mmol) in Millipore water (7.5 mL) was added. 220 mg of **85** were recovered.

Elemental microanalysis [%]: C, 4.95; H, 0.12; N, 0.13

PEI@Co/C NPs (**79**)



Compound **79a**

Following general procedure **GP3**, 115 mg amino-functionalized NPs (**82**), 360 μ l (299 mg, 6.9 mmol) aziridine (**86**), 15 μ l HCl conc. and 10 mL DCM were used. The reaction time was 24 h. 113 mg of **79a** were recovered.

Elemental microanalysis [%]: C, 5.8; H, 0.4; N, 0.6

Compound **79b**

Following general procedure **GP3**, 100 mg amino-functionalized NPs (**82**), 360 μ l (299 mg, 6.9 mmol) aziridine (**86**), 15 μ l HCl conc. and 10 mL DCM were used. The reaction time was 72 h. 95 mg of **79b** were recovered.

Elemental microanalysis [%]: C, 9.6; H, 1.5; N, 3.1.

Compound 79c

Following general procedure **GP3**, 100 mg amino-functionalized NPs (**82**), 360 μ l (299 mg, 6.9 mmol) aziridine (**86**), 15 μ L HCl conc. and 15 mL DCM were used. The reaction time was 24 h. 100 mg of **79e** were recovered.

Elemental microanalysis [%]: C, 5.5; H, 0.3; N, 0.5.

Compound 79d

Following general procedure **GP3**, 150 mg amino-functionalized NPs (**82**), 540 μ l (448 mg, 10.4 mmol) aziridine (**86**), 23 μ L HCl conc. and 15 mL DCM were used. The reaction time was 24 h. 135 mg of **79f** were recovered.

Elemental microanalysis [%]: C, 5.8; H, 0.3; N, 0.7.

Compound 79e

Following general procedure **GP3**, 150 mg amino-functionalized NPs (**82**), 540 μ l (448 mg, 10.4 mmol) aziridine (**86**), 23 μ L HCl conc. and 15 mL DCM were used. The reaction time was 24 h. 145 mg of **79g** were recovered.

Elemental microanalysis [%]: C, 6.3; H, 0.4; N, 0.9.

Compound 79f

Following general procedure **GP3**, 100 mg amino-functionalized NPs (**82**), 60 μ l (50 mg, 1.2 mmol) aziridine (**86**), 10 μ L HCl conc. and 10 mL DCM were used. The reaction time was 24 h. 99 mg of **79i** were recovered.

Elemental microanalysis [%]: C, 8.0; H, 0.2; N, 0.3.

Compound 79g

Following general procedure **GP3**, 210 mg amino-functionalized NPs (**82**), 730 μ l (606 mg, 14.1 mmol) aziridine (**86**), 30 μ L HCl conc. and 30 mL DCE were used. The reaction time was 24 h. 350 mg of **79c** were recovered.

Elemental microanalysis [%]: C, 17.6; H, 3.8; N, 7.8.

Compound 79h

Following general procedure **GP3**, 150 mg amino-functionalized NPs (**82**), 540 μ l (448 mg, 10.4 mmol) aziridine (**86**), 23 μ l HCl conc. and 15 mL DCE were used. The reaction time was 72 h. 275 mg of **79d** were recovered.

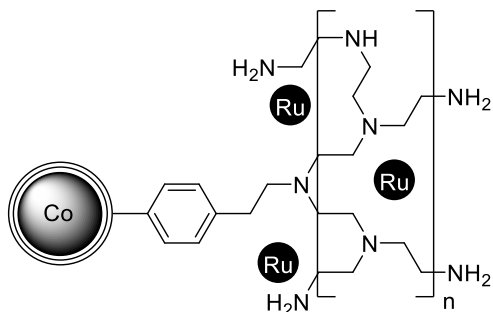
Elemental microanalysis [%]: C, 29.1; H, 6.6; N, 13.9.

Compound 79i

Following general procedure **GP3**, 50 mg amino-functionalized NPs (**82**), 5 μ l (4 mg, 0.1 mmol) aziridine (**86**), 7 μ l HCl conc. and 4 mL DCE were used. The reaction time was 24 h. 45 mg of **79h** were recovered.

Elemental microanalysis [%]: C, 5.5; H, 0.2; N, 0.3.

Ru NPs@PEI@Co/C NPs (**87**)



Ru₃(CO)₁₂ thermal decomposition method

A 10 mL Schlenk tube was charged with 65 mg of the PEI@Co/C NPs (**79a**), tetradecane (4 mL) and Ru₃(CO)₁₂ (12 mg, 0.02 mmol). The mixture was degassed by repeated freeze-pump-thaw cycles (3 x), set under nitrogen atmosphere and dispersed with the aid of an ultrasonic bath for 10 min at r.t. The Schlenk tube was transferred to an oil bath preheated to 160 °C and the slurry was stirred for 30 min. The reaction was allowed to cool to room temperature and the NPs were collected with the aid of a magnet. Afterwards, the NPs were washed with DCM (4 x 5 mL) by magnetic decantation and dried *in vacuo*. 65 mg were recovered

ICP-OES analysis: 1.28 wt% Ru (40% incorporation)

RuCl₃/NaBH₄ reduction method

All incorporations were performed following general procedure **GP4**, selected example (Table 2, entry 5): 50 mg PEI@Co/C NPs (**79a**), 26 mg (0.09 mmol Ru) RuCl₃ · x H₂O in 10 mL Millipore water and 113 mg (3.0 mmol) NaBH₄ were used. 50 mg were recovered.

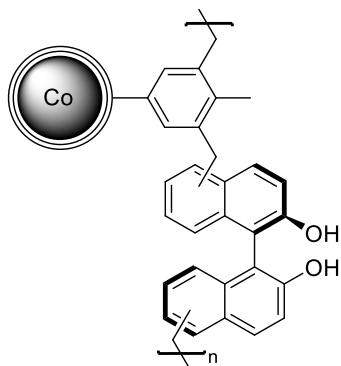
ICP-OES analysis: 1.67 wt% Ru (10% incorporation)

Improved synthesis method for the final catalyst

Prior to use, all solvents were degassed by nitrogen sparging for 10 min. In a 100 mL Schlenk flask, 25 mg PEI@Co/C NPs (**79i**) were dispersed in 15 ml Millipore water under nitrogen atmosphere. The slurry was stirred at r.t. and NaBH₄ (56 mg, 1.5 mmol) was added in one portion. The flask was sealed with a septum and a solution of RuCl₃ · x H₂O (13 mg, 0.04 mmol Ru) in 15 mL Millipore water was added with a syringe pump over 30 min. (flow rate: 30 mL/h). After the addition, the reaction was stirred for 30 min at r.t. and the NPs were collected with the aid of a magnet. The NPs were washed with Millipore water (2 x 5 mL) and acetone (2 x 5 mL) and dried *in vacuo*. 27 mg were recovered.

ICP-OES analysis: 10.6 wt% Ru (67% incorporation)

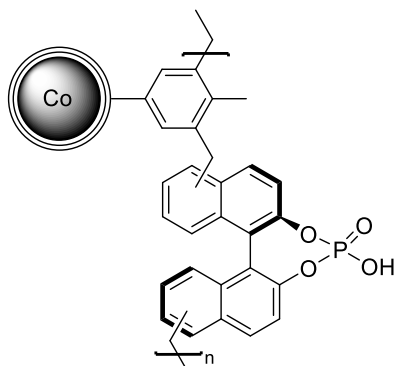
BINOL-MOP@Co/C NPs (**124**)



The compound was synthesized following general procedure **GP2**, using 100 mg of toluene functionalized Co/C NPs (**82**), R-BINOL (143 mg, 0.5 mmol), FeCl₃ (162 mg, 1 mmol), formaldehyde dimethyl acetal (88 μL, 1 mmol) and DCE (9 mL). 226 mg of **124** were recovered.

Elemental microanalysis [%]: C, 51; H, 3.2.

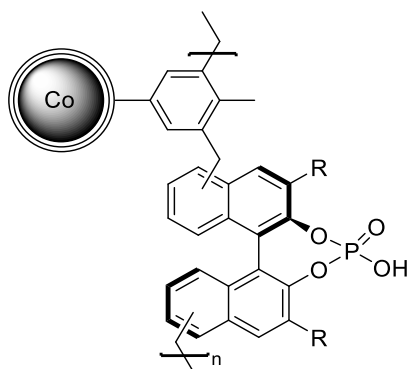
Immobilized CPA catalyst **123c**



In a 10 ml pressure tube, 100 mg BINOL-MOP@Co/C NPs (**124**) were dispersed in 2 mL DCM by stirring at r.t. for 30 min. POCl_3 (36 μL , 0.4 mmol) and Net_3 (166 μL , 1.2 mmol) were added and the mixture was heated to 50 $^\circ\text{C}$ for 3 h. After the reaction, the NPs were collected with the aid of a magnet, washed with DCM (2 x 4 mL), THF/Water (2:1, 1 x 4 mL) and THF (2 x 4 mL) and dried *in vacuo*. For acidification, the NPs were washed with 1 M HCl (5 x 5 mL) and dried again *in vacuo*. 99 mg of **123c** were recovered.

Elemental microanalysis [%]: C, 46.0; H, 3.1; N, 1.2.

Direct polymerization of CPAs onto functionalized Co/c NPs (**123d-i**)



Compound **123d**

The compound was synthesized following general procedure **GP2**, using 50 mg of toluene functionalized Co/C NPs (**82**), CPA **116d** (63 mg, 0.13 mmol), FeCl_3 (41 mg, 0.25 mmol), formaldehyde dimethyl acetal (22 μL , 0.25 mmol) and DCE (2.5 mL). 106 mg of **123d** were recovered.

Elemental microanalysis [%]: C, 39.1; H, 2.9.

Compounds 123e-g

The compounds were synthesized following general procedure **GP2**, using 10 mg of toluene functionalized Co/C NPs (**82**), CPA **116e-g** (10 mg), FeCl₃ (5 mg, 0.03 mmol), formaldehyde dimethyl acetal (3 μL, 0.03 mmol) and DCE (1 mL).

123e: 20 mg were recovered, elemental microanalysis [%]: C, 38.5; H, 2.4.

123f: 21 mg were recovered, elemental microanalysis [%]: C, 38.1; H, 2.2.

123g: 15 mg were recovered, elemental microanalysis [%]: C, 34.4; H, 2.2.

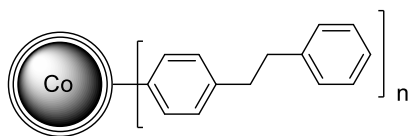
Compounds 123h-i

The compounds were synthesized following general procedure **GP2**, using 30 mg of toluene functionalized Co/C NPs (**82**), CPA **116h-i** (30 mg), FeCl₃ (15 mg, 0.09 mmol), formaldehyde dimethyl acetal (8 μL, 0.09 mmol) and DCE (1.5 mL).

123h: 44 mg were recovered, elemental microanalysis [%]: C, 30.0; H, 2.2.

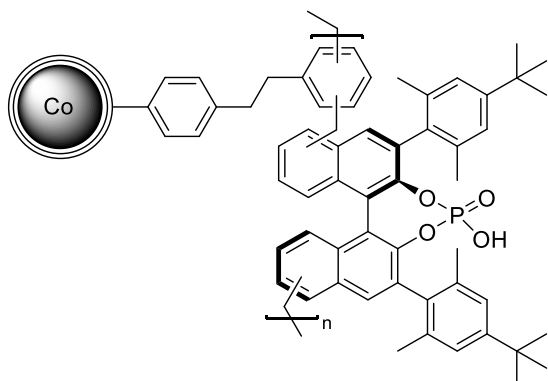
123i: 36 mg were recovered, elemental microanalysis [%]: n.d.

Dihydrostilbene-functionalized Co/C NPs (**126**)



The compound was synthesized following general procedure **GP1** using 200 mg of Co/C NPs, conc. HCl (0.1 mL), 4-phenethylamine (60 mg, 0.3 mmol) and Millipore water (6 mL) as dispersion. A precooled solution of sodium nitrite (32 mg, 0.5 mmol) in Millipore water (6 mL) was added. 192 mg of **126** were recovered. Elemental microanalysis [%]: C, 5.31; H, 0.12.

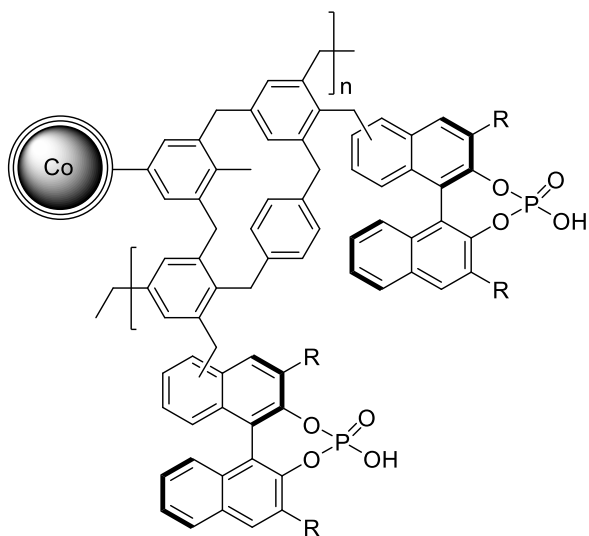
Direct polymerization of CPAs 118h onto dihydrostilbene-functionalized Co/c NPs (127)



The compound was synthesized following general procedure **GP2**, using 10 mg of dihydrostilbene-functionalized Co/C NPs (**126**), CPA **116h** (10 mg, 0.015 mmol), FeCl₃ (5 mg, 0.03 mmol), formaldehyde dimethyl acetal (6 μL, 0.03 mmol) and DCE (1 mL). 18 mg of **127** were recovered.

Elemental microanalysis [%]: C, 35.3; H, 2.8.

Direct polymerization of CPAs using the copolymerization strategy (128h-i)



Compounds 128h-i

The compounds were synthesized following general procedure **GP2**, using 10 mg of toluene functionalized Co/C NPs (**82**), CPA **116h-i** (10 mg), benzene (4 μL, 0.05 mmol) FeCl₃ (29 mg, 0.18 mmol), formaldehyde dimethyl acetal (16 μL, 0.18 mmol) and DCE (1 mL).

128h: 25 mg were recovered, elemental microanalysis [%]: C, 47.9; H, 3.6.

128i: 21 mg were recovered, elemental microanalysis [%]: C, 52.8; H, 4.0.

Copolymerization using dihydrostilbene-functionalized Co/C NPs (**126**)

The compound was synthesized following general procedure **GP2**, using 10 mg of dihydrostilbene functionalized Co/C NPs (**126**), CPA **116h** (10 mg, 0.01mmol), benzene (4 μ L, 0.05 mmol) FeCl₃ (29 mg, 0.18 mmol), formaldehyde dimethyl acetal (16 μ L, 0.18 mmol) and DCE (1 mL). 26 mg were recovered.

Elemental microanalysis [%]: C, 47.1; H, 3.5.

Large scale synthesis of **126i**

The compound was synthesized following general procedure **GP2**, using 75 mg of toluene functionalized Co/C NPs (**82**), CPA **116i** (75 mg, 0.1mmol), benzene (27 μ L, 0.3 mmol) FeCl₃ (194 mg, 1.2 mmol), formaldehyde dimethyl acetal (106 μ L, 1.2 mmol) and DCE (8 mL). 166 mg of **128i** were recovered.

Elemental microanalysis [%]: C, 47.6; H, 3.6.

CPA polymers with increased additive contents

Table **13**, entry 3: The compound was synthesized following general procedure **GP2**, using 10 mg of toluene functionalized Co/C NPs (**82**), CPA **116i** (5 mg, 0.007 mmol), benzene (30 μ L, 0.33 mmol) FeCl₃ (161 mg, 1.00 mmol), formaldehyde dimethyl acetal (88 μ L, 1.00 mmol) and DCE (5 mL). 31 mg were recovered.

Elemental microanalysis [%]: C, 69.4; H, 4.9.

Table **13**, entry 4: The compound was synthesized following general procedure **GP2**, using 10 mg of toluene functionalized Co/C NPs (**82**), CPA **116i** (5 mg, 0.007 mmol), benzene (59 μ L, 0.66 mmol) FeCl₃ (323 mg, 1.99 mmol), formaldehyde dimethyl acetal (176 μ L, 1.99 mmol) and DCE (5 mL). No isolation was possible.

Table **13**, entry 4: The compound was synthesized following general procedure **GP2**, using 10 mg of toluene functionalized Co/C NPs (**82**), CPA **116i** (5 mg, 0.007 mmol), benzene (47 μ L, 0.53 mmol), phenyldodecane (38 μ L, 0.13 mmol), FeCl₃ (323 mg, 1.99 mmol), formaldehyde dimethyl acetal (176 μ L, 1.99 mmol) and DCE (5 mL). 93 mg were recovered.

Elemental microanalysis [%]: C, 74.9; H, 6.3.

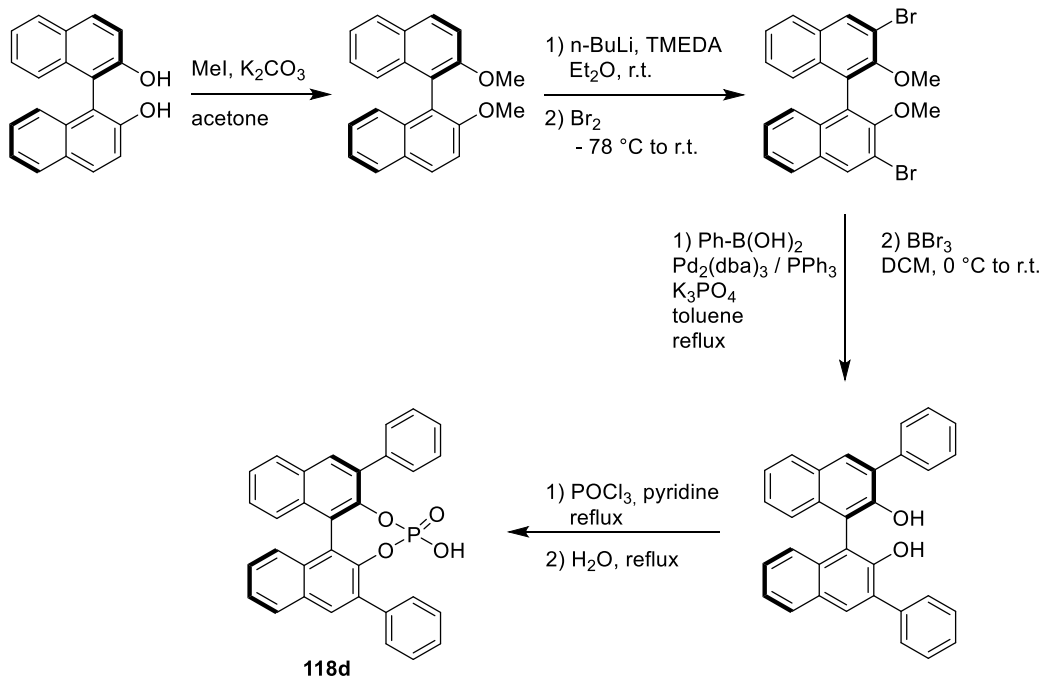
Benzene MOP for asymmetric background reaction tests

The compound was synthesized following general procedure **GP2**, using 100 mg of toluene functionalized Co/C NPs (**82**), benzene (44 μ L, 0.5 mmol), FeCl₃ (243 mg, 1.5 mmol), formaldehyde dimethyl acetal (132 μ L, 1.5 mmol) and DCE (9 mL). 135 mg were recovered

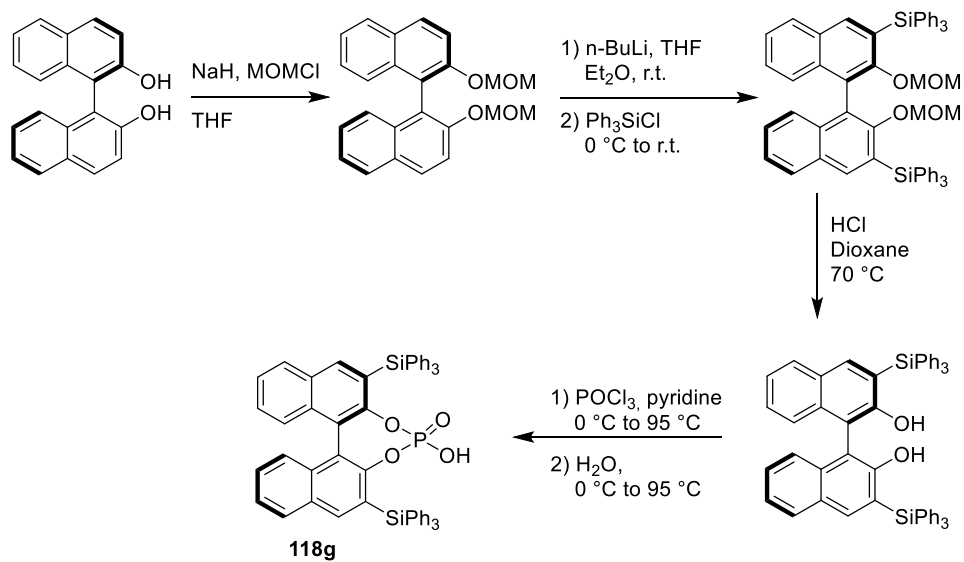
Elemental microanalysis [%]: C, 31.1; H, 1.9.

4. Chiral phosphoric acids

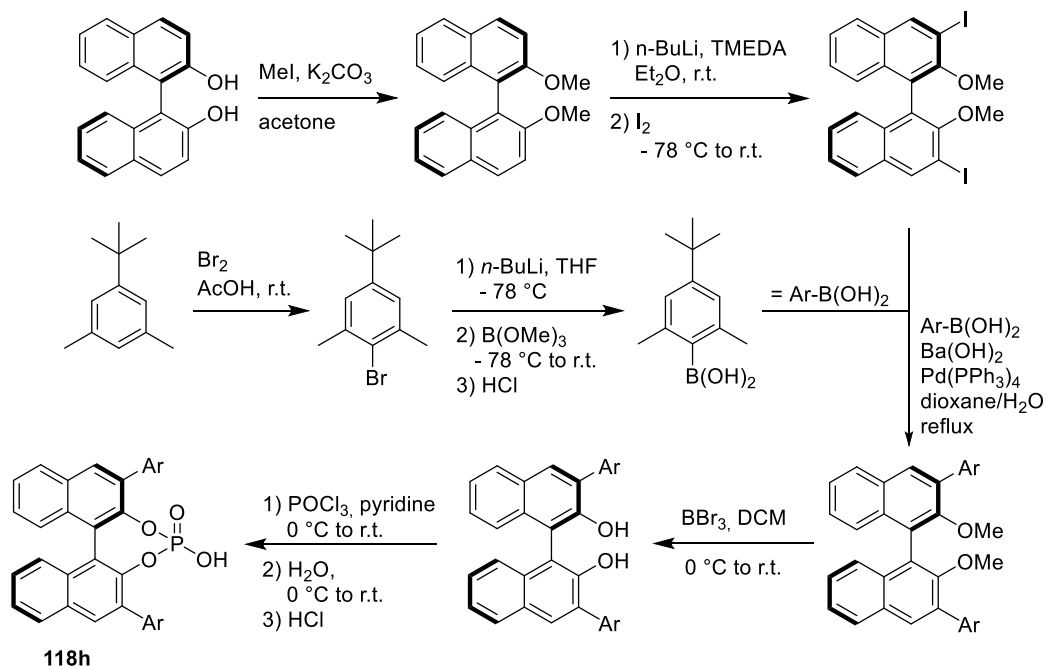
Synthesis route for CPA 116d



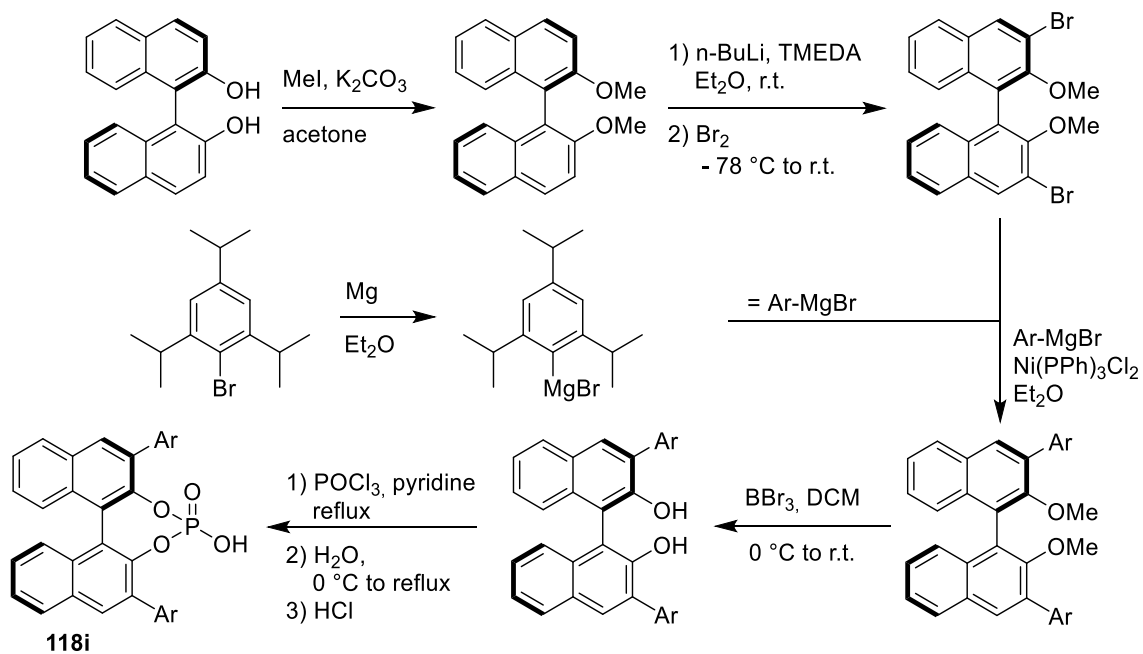
Synthesis route for CPA 116g



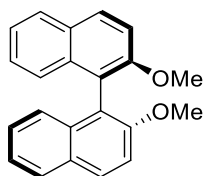
Synthesis route for CPA 116h



Synthesis route for CPA 116i



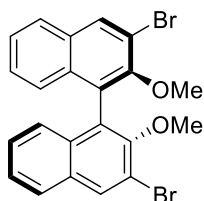
(R)-2,2'-dimethoxy-1,1'-binaphthalene^[154]



A 100 mL Flask was charged with (R)-BINOL (1.50 g, 5.4 mmol) and acetone (50 mL) the mixture was stirred until a homogeneous solution was formed, then methyl iodide (1.3 mL, 21 mmol) and K_2CO_3 (2.5 g, 18 mmol) were added and the mixture was refluxed for 24 h. Subsequently, additional methyl iodide (0.6 mL, 9 mmol) was added and the mixture was refluxed for 12 h. The solvent was distilled off to approx. 10 mL (caution methyl iodide!), after cooling to r.t. 50 mL dist. H_2O were added and the mixture was stirred for 6.5 h. The resulting solid was filtered, washed with dist. H_2O and dried in *vacuo*. The product was isolated as a white solid (1.53 g, 4.8 mmol, 93%).

¹H-NMR (300 MHz, $CDCl_3$) δ_H [ppm] = 7.98 (d, J = 9.0 Hz, 2H), 7.87 (d, J = 8.1 Hz, 2H), 7.47 (d, J = 9.0 Hz, 2H), 7.36 – 7.28 (m, 2H), 7.25 – 7.17 (m, 2H), 7.14 – 7.08 (m, 2H), 3.77 (s, 6H).

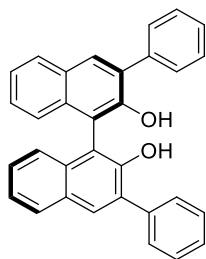
(R)-3,3'-dibromo-2,2'-dimethoxy-1,1'-binaphthalene^[154]



Under nitrogen atmosphere, a 250 mL Schlenk flask was charged with dry diethyl ether (29 mL), TMEDA (491 μ L, 3.3 mmol) and *n*-BuLi in hexanes (2.8 mL, 4.4 mmol, 1.6 M). The solution was stirred for 15 min. at r.t. and (R)-2,2'-dimethoxy-1,1'-binaphthalene (465 mg, 1.5 mmol) was added in one portion. The resulting suspension was stirred for 3 h at r.t. and then cooled to -78 °C. Bromine (0.9 mL, 17.9 mmol) was added slowly, the mixture was allowed to warm up to r.t. and stirred for 4 h. A saturated aqueous solution of $Na_2S_2O_3$ (30 mL) was added carefully and the mixture was stirred for 4 h. The reaction was diluted with water and diethyl ether, the organic layer was washed with Brine, dried over Na_2SO_4 and the solvent was evaporated. The crude product was purified by flash column chromatography (PE/EA 50:1 to PE/EA 19:1) to give the product (390 mg, 0.8 mmol, 56%) as a pale yellow solid.

¹H-NMR (300 MHz, CDCl₃) δ_H [ppm] = 8.27 (s, 2H), 7.83 (d, *J* = 8.2 Hz, 2H), 7.47 – 7.39 (m, 2H), 7.32 – 7.23 (m, 2H), 7.12 – 7.05 (m, 2H), 3.51 (s, 6H).

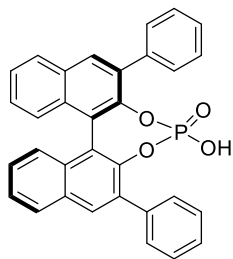
(R)-3,3'-diphenyl-[1,1'-binaphthalene]-2,2'-diol^[131]



A 10 mL pressure tube was charged with (R)-3,3'-dibromo-2,2'-dimethoxy-1,1'-binaphthalene (600 mg, 1.27 mmol), phenylboronic acid (387 mg, 3.18 mmol), Pd₂(dba)₃ (36 mg, 0.04 mmol), K₃PO₄ (1.34 g, 6.33 mmol) and toluene (3 mL). The mixture was degassed by 3 consecutive freeze-pump-thaw cycles and PPh₃ (41 mg, 0.16 mmol) was added under nitrogen atmosphere. The reaction was stirred at 110 °C for 17 h, cooled to r.t. and filtered through a plug of celite. The solvent was evaporated and the crude mixture was redissolved in DCM (65 mL). After cooling the mixture to 0 °C, BBr₃ (7.6 mL, 7.6 mmol, 1 M) was added slowly and the reaction was stirred at r.t. for 24 h. The reaction was carefully quenched with dist. H₂O (1 mL), extracted with a saturated aqueous solution of Na₂S₂O₃ (1x 30 mL), dist. H₂O (2x 30 mL) and brine (1x 30 mL) and the organic layer was dried over Na₂CO₃. The crude product was purified by flash column chromatography (PE/EA 9:1) to give the product (423 mg, 0.96 mmol, 76%) as a pale yellow solid.

¹H-NMR (300 MHz, CDCl₃) δ_H [ppm] = 8.04 (s, 2H), 7.93 (d, *J* = 7.4 Hz, 2H), 7.78 – 7.71 (m, 4H), 7.55 – 7.46 (m, 4H), 7.46 – 7.37 (m, 4H), 7.37 – 7.29 (m, 2H), 7.26 – 7.21 (m, 2H), 5.37 (s, 2H).

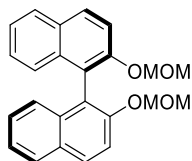
(R)-3,3'-diphenyl-[1,1'-binaphthyl]-2,2'-diyl hydrogenphosphate (118d)^[155]



A 10 mL pressure tube was charged with (R)-3,3'-diphenyl-[1,1'-binaphthalene]-2,2'-diol (450 mg, 1.0 mmol), pyridine (2.2 mL) and POCl₃ (280 μL, 3.1 mmol) was slowly added. The mixture was stirred at 115 °C for 14 h, cooled to r.t. and dist. H₂O was carefully added to quench the reaction. The reaction was stirred at 115 °C for 3 h, cooled to r.t., diluted with DCM (20 mL) and extracted 1 M HCl (5x 20 mL). The organic layer was dried over Na₂SO₄, the solvent was evaporated and the crude product was recrystallized in acetonitrile to give the product (156 mg, 0.3 mmol, 30%) as a white solid.

¹H-NMR (300 MHz, CDCl₃) δ_H [ppm] = 7.99 – 7.91 (m, 4H), 7.57 (d, *J* = 7.0 Hz, 4H), 7.52 – 7.45 (m, 2H), 7.39 (d, *J* = 8.5 Hz, 2H), 7.33 – 7.27 (m, 2H), 7.26 – 7.16 (m, 6H), 6.69 (bs, 1H).

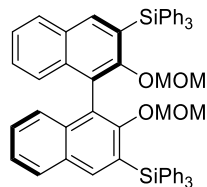
(R)-2,2'-bis(methoxymethoxy)-1,1'-binaphthalene^[156]



Under Nitrogen atmosphere, a 100 mL Schlenk flask was charged with dry THF (15 mL) and NaH (60% dispersion in mineral oil, 250 mg, 6.3 mmol, previously washed with pentane and filtered to remove mineral oil) and cooled to 0 °C. A solution of (R)-BINOL (650 mg, 2.3 mmol) in dry THF (5 mL) was added (careful, hydrogen formation) and the mixture was stirred for 30 min at r.t. The reaction was cooled back to 0 °C and chloro(methoxy)methane (MOMCl, 690 μL, 9 mmol) was added slowly. After stirring the mixture for 4 h at r.t. the reaction was quenched with a sat. NH₄Cl solution (20 mL) and extracted with DCM (3 x 20 mL). The organic layers were combined and dried over Na₂SO₄, the solvent was evaporated and the product was obtained as a white solid (828 mg, 2.2 mmol, 97%)

¹H-NMR (300 MHz, CDCl₃) δ_H [ppm] = 8.00 – 7.92 (m, 2H), 7.90 – 7.85 (m, 2H), 7.58 (d, *J* = 9.0 Hz, 2H), 7.38 – 7.31 (m, 2H), 7.25 – 7.19 (m, 2H), 7.18 – 7.13 (m, 2H), 5.09 (d, *J* = 6.8 Hz, 2H), 4.98 (d, *J* = 6.8 Hz, 2H), 3.14 (s, 6H).

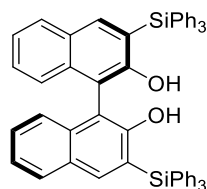
(R)-(2,2'-bis(methoxymethoxy)-[1,1'-binaphthalene]-3,3'-diyl)bis(triphenylsilane)^[157]



Under Nitrogen atmosphere, a 100 mL Schlenk flask was charged with dry Et₂O (33 mL) and (R)-2,2'-bis(methoxymethoxy)-1,1'-binaphthalene (700 mg, 1.9 mmol). A solution of *n*-BuLi in hexanes (2.9 mL, 4.7 mmol, 1.6 M) was added dropwise at r.t. and the mixture was stirred for 1.5 h. The reaction was cooled to 0 °C, THF (15 mL) was added and the mixture was stirred for 15 min. Still at 0 °C, a solution of Ph₃SiCl (1.5 g, 5.1 mmol) in THF (3.5 mL) was added and the mixture was stirred for 30 h at r.t. After the reaction, the brown suspension was quenched with a sat. NH₄Cl solution (30 mL) and extracted with DCM (3 x 30 mL). The organic layers were combined, washed with brine and dried over Na₂SO₄. The solvent was evaporated and the crude product was purified by flash column chromatography (PE to PE/EA 19:1) to give the product as a white solid (705 mg, 0.8 mmol, 42%). Unfortunately, the compound was still contaminated with unreacted Ph₃SiCl, as found by NMR but was used for further steps without extra purification.

¹H-NMR (300 MHz, CDCl₃) δ_H [ppm] = 7.88 (s, 2H), 7.72 – 7.62 (m, 20H), 7.46 – 7.31 (m, 34H), 3.82 (d, J = 5.1 Hz, 2H), 3.76 (d, J = 5.1 Hz, 2H), 2.26 (s, 6H).

(R)-3,3'-bis(triphenylsilyl)-[1,1'-binaphthalene]-2,2'-diol^[157]

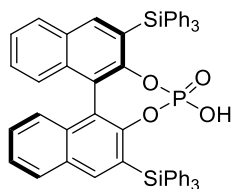


A 25 mL round bottom flask was charged with dioxane (5.5 mL), (R)-(2,2'-bis(methoxymethoxy)-[1,1'-binaphthalene]-3,3'-diyl)bis(triphenylsilane) (700 mg, 0.8 mmol) and conc. HCl (0.1 mL). The mixture was stirred at 70 °C (reflux condenser on) for 24 h. After the reaction, the mixture was quenched with a sat. NaHCO₃ solution (10 mL) and extracted with EA (3 x 10 mL). The organic layers were combined, washed with water and brine and dried over Na₂SO₄. The solvent was evaporated and the crude product was

trituated/washed with DCM/Et₂O (1:10) twice to give the product as a white solid (300 mg, 0.4 mmol, 47%).

¹H-NMR (300 MHz, CDCl₃) δ_H [ppm] = 7.91 (s, 2H), 7.67 – 7.62 (m, 12H), 7.47 – 7.28 (m, 26H), OH signals not observed.

(R)-3,3'-bis(triphenylsilyl)-[1,1'-binaphthyl]-2,2'-diyl hydrogenphosphate (118g)^[157]

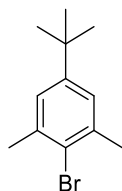


Under Nitrogen atmosphere, a dry 10 mL Schlenk pressure tube was charged with (R)-3,3'-bis(triphenylsilyl)-[1,1'-binaphthalene]-2,2'-diol (200 mg, 0.25 mmol) and pyridine (1 mL). A solution of POCl₃ (130 μL, 1.4 mmol) in pyridine (3 mL) was slowly added and the mixture was stirred at r.t. for 24 h. Due to no conversion on TLC, the mixture was stirred at 95 °C for 24 h after which additional POCl₃ (130 μL, 1.4 mmol) was added (at 0 °C, no solution) and the mixture was stirred at 95 °C for another 24 h. The reaction was cooled to 0 °C, carefully quenched with dist. H₂O (1 mL) and heated to 95 °C for 6 h. The mixture was diluted with DCM (20 mL) and extracted with 1 M HCl (3 x 10 mL). The organic layer was dried over Na₂SO₄, the solvent was evaporated and the crude product was purified by flash column chromatography (DCM/MeOH 24:1 to 19:1) to give the product as a white solid (115 mg, 0.13 mmol, 53%).

¹H-NMR (300 MHz, acetone-d₆) δ_H [ppm] = 7.97 (s, 2H), 7.79 – 7.72 (m, 2H), 7.63 – 7.56 (m, 12H), 7.43 – 7.35 (m, 2H), 7.36 – 7.22 (m, 20H), 7.14 – 7.08 (m, 2H).

³¹P NMR (121 MHz, acetone-d₆) δ_P [ppm]= 1.95.

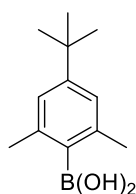
2-bromo-5-(tert-butyl)-1,3-dimethylbenzene^[158]



A 100 mL round bottom flask was charged with 1-(*tert*-butyl)-3,5-dimethylbenzene (5 mL, 27 mmol) and Acetic acid (38 mL) and cooled to 0 °C. Bromine (1.8 mL, 35 mmol) was added slowly *via* a syringe and the mixture was stirred at r.t. for 3 h. The precipitate was filtered off, washed with a saturated aqueous solution of Na₂S₂O₃ (20 mL), dist. H₂O (40 mL) and dried in *vacuo* to give the product as solid white needles (5.7 g, 24 mmol, 89%).

¹H-NMR (300 MHz, CDCl₃) δ_H [ppm] = 7.09 (s, 2H), 2.41 (s, 6H), 1.30 (s, 9H).

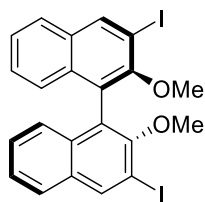
(4-(*tert*-butyl)-2,6-dimethylphenyl)boronic acid^[159]



A dried 250 mL Schlenk flask was charged with 2-bromo-5-(*tert*-butyl)-1,3-dimethylbenzene (3.5 g, 15 mmol), dry THF (140 mL) and cooled to -78 °C. *n*-BuLi in hexanes (14 mL, 22 mmol, 1.6 M) was added slowly *via* a syringe and the mixture was stirred at -78 °C for 2 h. B(OMe)₃ (4.9 mL, 44 mmol) was added dropwise *via* a syringe and the mixture was stirred at -78 °C for 2h and at r.t. for 15 h. 1 M HCl (50 mL) was added carefully and the mixture was stirred at r.t. for 5 h. The mixture was extracted with DCM (3x 50 mL), the combined organic layers were washed with 1 M HCl (1x 50 mL), dried over MgSO₄ and the solvent was removed in *vacuo*. The oily residue was cooled to -30 °C and carefully treated with hexanes (6x 3 mL). After drying in *vacuo* the product was isolated as a white solid (1.0 g, 4.8 mmol, 33%).

¹H-NMR (300 MHz, CDCl₃) δ_H [ppm] = 7.04 (s, 2H), 4.61 (bs, 2H), 2.39 (s, 6H), 1.30 (s, 9H).

(R)-3,3'-diiodo-2,2'-dimethoxy-1,1'-binaphthalene^[160]

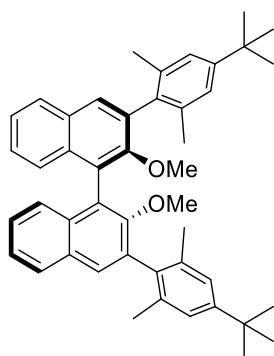


Under Nitrogen atmosphere, a 250 mL Schlenk flask was charged with dry diethyl ether (140 mL), TMEDA (3.6, 24 mmol) and *n*-BuLi in hexanes (15 mL, 24 mmol, 1.6 M). The solution was stirred for 15 min. at r.t.

and (R)-2,2'-dimethoxy-1,1'-binaphthalene (2.52 g, 8 mmol) was added in one portion. The resulting suspension was stirred for 3 h at r.t. and then cooled to -78 °C. Iodine (6.10 g, 24 mmol) dissolved in diethyl ether (60 mL) was added slowly, the mixture was allowed to warm up to r.t. and stirred for 17 h. A saturated aqueous solution of Na₂S₂O₅ (60 mL) was added carefully and the mixture was stirred for 4 h. The reaction was diluted with water and diethyl ether, the organic layer was washed with brine, dried over Na₂SO₄ and the solvent was evaporated. The crude product was purified by flash column chromatography (PE/EA 99:1 to PE/EA 19:1) to give the product (2.37 g, 4.2 mmol, 52%) as a pale-yellow solid.

¹H-NMR (300 MHz, CDCl₃) δ_H [ppm] = 8.54 (s, 1H), 7.80 (d, *J* = 8.2 Hz, 1H), 7.46 – 7.36 (m, 1H), 7.32 – 7.22 (m, 1H), 7.08 (d, *J* = 8.5 Hz, 1H), 3.42 (s, 3H).

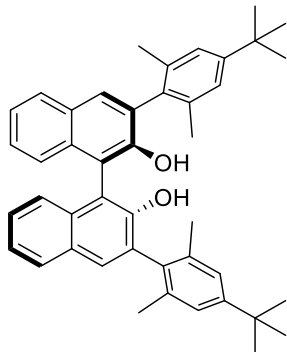
(R)-3,3'-bis(4-(*tert*-butyl)-2,6-dimethylphenyl)-2,2'-dimethoxy-1,1'-binaphthalene^[160]



Under Nitrogen atmosphere, a 30 mL Schlenk-Pressure tube was charged with (R)-3,3'-diiodo-2,2'-dimethoxy-1,1'-binaphthalene (894 mg, 1.6 mmol), (4-(*tert*-butyl)-2,6-dimethylphenyl)boronic acid (980 mg, 4.8 mmol), Ba(OH)₂•8 H₂O (1.50 g, 4.8 mmol), Pd(PPh₃)₄ (72 mg, 0.06 mmol) and a mixture of dioxane/H₂O (12 mL, 3:1 (v/v)). The reaction was heated to 105 °C for 72 h, cooled to r.t. and the solvent was evaporated. The residue was dissolved in DCM (20 mL) and 1 M HCl (20 mL), the layers were separated and the aqueous phase was extracted with DCM (2x 20 mL). The combined organic layers were washed with brine (1x 20 mL) dried over Na₂SO₄ and the solvent was evaporated. The crude product was purified by flash column chromatography (PE/EA 19:1) to give the product (636 mg, 1.0 mmol, 63%) as a white solid.

¹H-NMR (300 MHz, CDCl₃) δ_H [ppm] = 7.86 (d, *J* = 8.2 Hz, 2H), 7.73 (s, 2H), 7.44 – 7.37 (m, 2H), 7.30 – 7.26 (m, 4H), 7.15 (s, 4H), 3.10 (s, 6H), 2.22 (s, 6H), 2.17 (s, 6H), 1.36 (s, 18H).

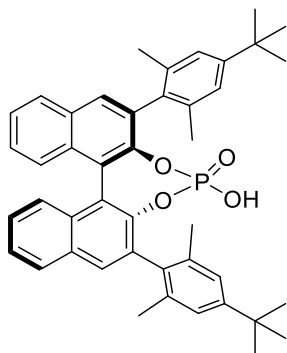
(R)-3,3'-bis(4-(*tert*-butyl)-2,6-dimethylphenyl)-[1,1'-binaphthalene]-2,2'-diol^[160]



A 50 mL round bottom flask was charged with 3,3'-bis(4-(*tert*-butyl)-2,6-dimethylphenyl)-2,2'-dimethoxy-1,1'-binaphthalene (355 mg, 0.56 mmol), DCM (25 mL) and cooled to 0 °C. A solution of BBr₃ in DCM (2 mL, 2 mmol, 1 M) was added slowly *via* syringe and the mixture was stirred for 2 h at r.t. The reaction was quenched carefully with 1 mL dist. H₂O, the organic layer was then extracted with a saturated aqueous solution of Na₂S₂O₃ (1x 25 mL) and brine (1x 25 mL) and dried over Na₂CO₃. The crude product was purified by column chromatography (PE/EA 19:1) and the product was isolated as a yellowish solid (114 mg, 0.19 mmol, 34%).

¹H-NMR (300 MHz, CDCl₃) δ_H [ppm] = 7.87 (d, *J* = 7.4 Hz, 2H), 7.77 (s, 2H), 7.42 – 7.35 (m, 2H), 7.35 – 7.29 (m, 2H), 7.28 – 7.23 (m, 2H), 7.19 (s, 4H), 5.01 (s, 2H), 2.19 (s, 6H), 2.11 (s, 6H), 1.35 (s, 18H).

(R)-3,3'-bis(4-(*tert*-butyl)-2,6-dimethylphenyl)-[1,1'-binaphthyl]-2,2'-diyl hydrogenphosphate (118h)^[160]



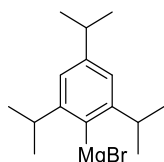
Under Nitrogen atmosphere, a 25 mL Schlenk flask was charged with (R)-3,3'-bis(4-(*tert*-butyl)-2,6-dimethylphenyl)-[1,1'-binaphthalene]-2,2'-diol (104 mg, 0.17 mmol) and pyridine (0.5 mL) and cooled to 0 °C. A solution of POCl₃ (48 μL, 0.53 mmol) in pyridine (3 mL) was slowly added *via* syringe and the mixture was stirred at r.t. for 24 h. The reaction was cooled to 0 °C, carefully quenched with dist. H₂O (10 mL) and

stirred at r.t. for an additional 24 h. 1 M HCl (5 mL) was added and the mixture was stirred at r.t. for 5 h. The mixture was extracted with diethyl ether (2x 20 mL), the combined organic layers were washed with 1 M HCl (5x 12 mL) and dried over MgSO₄. The solvent was evaporated and the product was isolated as a pale yellow solid (84 mg, 0.13 mmol, 74%).

¹H-NMR (300 MHz, CDCl₃) δ_H [ppm] = 7.93 (d, *J* = 8.2 Hz, 2H), 7.89 (s, 1H), 7.83 (s, 2H), 7.56 – 7.49 (m, 2H), 7.44 – 7.30 (m, 4H), 7.01 (s, 4H), 2.20 (s, 6H), 2.06 (s, 6H), 1.03 (s, 18H).

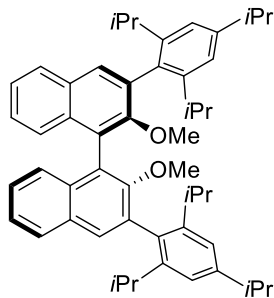
³¹P NMR (121 MHz, CDCl₃) δ_P [ppm]= 6.21.

(2,4,6-triisopropylphenyl)magnesium bromide^[155]



Under nitrogen atmosphere, a dried 25 mL Schlenk flask was charged with Magnesium turnings (1.84 g, 13 mmol), diethyl ether (10 mL), and a spatula tip of iodine. Two syringes were connected via a septal containing 2-bromo-1,3,5-triisopropylbenzene (1.7 mL, 6.5 mmol) in diethyl ether (10 mL) and 1,2-dibromoethane (0.1 mL) respectively. To start the exothermic reaction several drops of 1,2-dibromoethane and 10% (v/v) of the 2-bromo-1,3,5-triisopropylbenzene solution were added and the flask was heated gently. Upon activation of the reaction as seen by gentle boiling of the solvent, the solution was added in a manner of keeping the reaction active. After complete addition, the mixture was refluxed for 24 h and used in the next step without further purification.

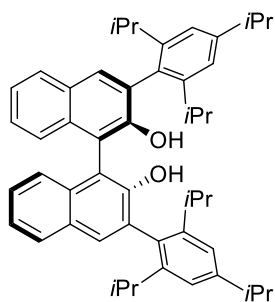
(R)-2,2'-dimethoxy-3,3'-bis(2,4,6-triisopropylphenyl)-1,1'-binaphthalene^[155]



Under Nitrogen atmosphere, a 30 mL pressure tube was charged with Ni(PPh₃)₂Cl₂ (60 mg, 0.23 mmol), (R)-3,3'-dibromo-2,2'-dimethoxy-1,1'-binaphthalene (218 mg, 0.46 mmol) and diethyl ether (7 mL). The Grignard solution was added slowly *via* syringe and the mixture was refluxed for 6 h. The reaction was cooled to 0 °C and quenched with 1 M HCl (10 mL). The layers were separated, the organic layer was extracted with 1 M HCl (2x 10 mL) and the combined aqueous phases were extracted with diethyl ether (3x 10 mL). The combined organic layers were dried over MgSO₄, the solvent was evaporated and the crude product was purified by column chromatography (PE/EA 19:1). The product was isolated as a white solid (260 mg, 0.36 mmol, 78%)

¹H-NMR (300 MHz, CDCl₃) δ_H [ppm] = 7.85 (d, *J* = 8.1 Hz, 2H), 7.74 (s, 2H), 7.46 – 7.36 (m, 2H), 7.36 – 7.27 (m, 4H), 7.15 – 7.05 (m, 4H), 3.08 (s, 6H), 3.01 – 2.74 (m, 6H), 1.32 (d, *J* = 6.9 Hz, 12H), 1.18 (dd, *J* = 8.8, 6.9 Hz, 12H), 1.10 (dd, *J* = 14.2, 6.8 Hz, 12H).

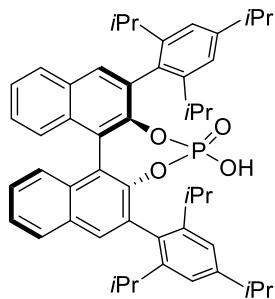
(R)-3,3'-bis(2,4,6-triisopropylphenyl)-[1,1'-binaphthalene]-2,2'-diol^[155]



A 50 mL round bottom flask was charged with (R)-2,2'-dimethoxy-3,3'-bis(2,4,6-triisopropylphenyl)-1,1'-binaphthalene (200 mg, 0.28 mmol), DCM (10 mL) and cooled to 0 °C. A solution of BBr₃ in DCM (2.2 mL, 2.2 mmol, 1 M) was added slowly *via* syringe and the mixture was stirred for 2 h at r.t. The reaction was quenched carefully with 1 mL dist. H₂O, the organic layer was then extracted with a saturated aqueous solution of Na₂S₂O₃ (1x 25 mL) and brine (1x 25 mL) and dried over Na₂CO₃. The crude product was purified by column chromatography (PE/EA 19:1) and the product was isolated as a yellowish solid (168 mg, 0.24 mmol, 87%).

¹H-NMR (300 MHz, CDCl₃) δ_H [ppm] = 7.87 (d, *J* = 7.6 Hz, 2H), 7.77 (s, 2H), 7.41 – 7.34 (m, 2H), 7.34 – 7.27 (m, 4H), 7.13 (dd, *J* = 5.9, 1.6 Hz, 4H), 4.92 (s, 2H), 2.96 (sept, *J* = 6.9 Hz, 2H), 2.85 (sept, *J* = 6.8 Hz, 2H), 2.68 (sept, *J* = 6.8 Hz, 2H), 1.32 (d, *J* = 6.9 Hz, 12H), 1.20 (d, *J* = 6.8 Hz, 6H), 1.11 (d, *J* = 6.6 Hz, 6H), 1.09 (d, *J* = 6.7 Hz, 8H), 1.03 (d, *J* = 6.9 Hz, 6H).

(R)-3,3'-bis(2,4,6-triisopropylphenyl)-[1,1'-binaphthyl]-2,2'-diyl hydrogenphosphate (118i)^[155]



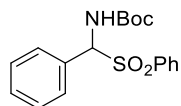
Under Nitrogen atmosphere, a 10 mL pressure tube was charged with (R)-3,3'-bis(2,4,6-triisopropylphenyl)-[1,1'-binaphthalene]-2,2'-diol (200 mg, 0.29 mmol) and pyridine (0.5 mL). A solution of POCl₃ (80 μL, 0.87 mmol) in pyridine (2 mL) was slowly added *via* syringe and the mixture was refluxed for 24 h. The reaction was cooled to 0 °C, carefully quenched with dist. H₂O (1 mL) and refluxed for an additional 24 h. The reaction was cooled to r.t., 1 M HCl (5 mL) was added and the mixture was refluxed for 5 h. After cooling the reaction back to r.t. the mixture was extracted with diethyl ether (2x 20 mL), the combined organic layers were washed with 1 M HCl (2x 12 mL) and dried over MgSO₄. The solvent was evaporated and the product was isolated as a pale brown solid (158 mg, 0.21 mmol, 72%). Further purification could be achieved by recrystallization in Acetonitrile.

¹H-NMR (400 MHz, CDCl₃) δ_H [ppm] = (d, *J* = 8.2 Hz, 2H), 7.80 (s, 2H), 7.54 – 7.45 (m, 2H), 7.37 – 7.28 (m, 4H), 6.92 (d, *J* = 12.1 Hz, 4H), 6.23 (s, 1H), 2.83 (sept, *J* = 6.8 Hz, 2H), 2.58 (sept, *J* = 6.8 Hz, 2H), 2.50 (sept, *J* = 6.6 Hz, 2H), 1.23 (d, *J* = 3.0 Hz, 6H), 1.21 (d, *J* = 3.0 Hz, 3H), 1.01 (d, *J* = 6.7 Hz, 6H), 0.97 (d, *J* = 6.8 Hz, 6H), 0.90 (d, *J* = 6.8 Hz, 6H), 0.66 (d, *J* = 6.6 Hz, 6H).

³¹P NMR (162 MHz, CDCl₃) δ_P [ppm]= 3.20.

5. Starting materials

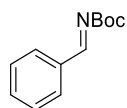
***tert*-butyl (phenyl(phenylsulfonyl)methyl)carbamate^[161]**



A 250 mL round bottom flask was charged with benzaldehyde (3.2 g, 20 mmol), *tert*-butylcarbamate (2.4 g, 20 mmol), sodium benzenesulfinate (6.6 g, 40 mmol), MeOH (21.6 mL), water (43.2 mL) and formic acid (14.4 mL). The mixture was stirred at r.t. for 72 h, the solid was filtered off, washed with water and PE and dried *in vacuo* to give the product as a white solid (6.8 g, 19.6 mmol, 98%)

¹H-NMR (300 MHz, CDCl₃) δ_H [ppm] = 7.95 – 7.87 (m, 2H), 7.69 – 7.61 (m, 1H), 7.57 – 7.50 (m, 2H), 7.48 – 7.37 (m, 5H), 5.86 (dd, J = 30.8, 10.4 Hz, 2H), 1.26 (s, 9H).

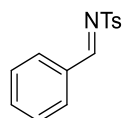
***tert*-butyl (Z)-benzylidenecarbamate (129)^[161]**



Prior to the reaction, 2 g finely crushed molecular sieves (4 Å) were activated by heating under vacuum in a 50 mL dry Schlenk flask. After cooling to r.t. *tert*-butyl (phenyl(phenylsulfonyl)methyl)carbamate (0.5 g, 1.4 mmol) and dry THF (25 mL) were added and the slurry was stirred at r.t. for 15 min. Afterwards dried Na₂SO₄ (1.5 g, 11 mmol) and dried K₂CO₃ (1.3 g, 9 mmol) were added and the mixture was refluxed for 18 h. After the reaction, the dispersion was cooled to r.t. the solids were removed by filtration and the solvent was evaporated. The residue was dried *in vacuo* to give the product as a colorless oil (244 mg, 1.2 mmol, 85%).

¹H-NMR (300 MHz, CDCl₃) δ_H [ppm] = 8.88 (s, 1H), 7.96 – 7.86 (m, 2H), 7.62 – 7.52 (m, 1H), 7.52 – 7.40 (m, 2H), 1.59 (s, 9H).

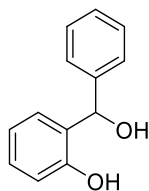
N-benzylidene-4-methylbenzenesulfonamide (132)^[162]



A 50 mL round bottom flask was charged with benzaldehyde (3.7 mL, 37 mmol), tetraethyl orthosilicate (8.5 mL, 39 mmol) and *p*-toluenesulfonamide (6.3 g, 37 mmol). The flask was equipped with a distillation bridge and the mixture was heated to 160 °C under nitrogen atmosphere for 6 h. After cooling to r.t. the residue was dissolved in EA (125 mL), pentane (300 mL) was added and the product crystallized after storing the mixture for 15 h at 7 °C. After filtration and drying in *vacuo*, the product (5.4 g, 21 mmol, 57%) was isolated as white crystals.

¹H-NMR (300 MHz, CDCl₃) δ_H [ppm] = 9.03 (s, 1H), 7.98 – 7.85 (m, 4H), 7.66 – 7.57 (m, 1H), 7.55 – 7.42 (m, 2H), 7.39 – 7.30 (m, 2H), 2.44 (s, 3H).

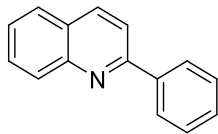
2-(hydroxy(phenyl)methyl)phenol (135)^[163]



A dried 100 mL Schlenk flask, under nitrogen atmosphere, was charged with Magnesium turnings (1.0 g, 40 mmol), dry THF (14 mL), a spatula tip of iodine and 2 drops of 1,2-dibromoethane. Bromobenzene (4.2 mL, 40 mmol) was dissolved in dry THF (18 mL) and 2 mL of the solution were added to the mixture *via* a syringe connected to a septal. The reaction was started by gentle heating and the bromobenzene solution was added in a manner of keeping the reaction active as indicated by evaporation of the solvent on the Magnesium turnings. After the complete addition, the mixture was stirred at r.t. for 30 min followed by heating to reflux for 1 h. The reaction was cooled to 0 °C, salicylaldehyde (1.6 mL, 16 mmol) dissolved in dry THF (18 mL) was slowly added and the mixture was stirred at r.t. for 3 h. Afterwards, the reaction was carefully quenched with a saturated aqueous solution of NH₄Cl (30 mL), extracted with DCM (2x 30 mL), the organic layer was dried over Na₂SO₄. The solvent was evaporated and the crude product was purified by flash column chromatography (PE/EA 19:1 to PE/EA 5:1) to give the product (2.6 g, 13 mmol, 82%) as a white solid.

¹H-NMR (300 MHz, CDCl₃) δ_H [ppm] = 7.94 (bs, 1H), 7.42 – 7.29 (m, 5H), 7.23 – 7.16 (m, 1H), 6.92 – 6.78 (m, 3H), 6.00 (s, 1H), 3.05 (bs, 1H).

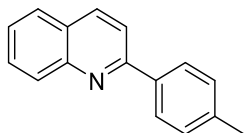
2-phenylquinoline (42a)



Prepared according to the general procedure **GP6** at double scale, acetophenone (2.4 mL, 20 mmol) was used as ketone. The crude product was purified by flash column chromatography (PE/EA 19:1) to give the product (1.7 g, 8.4 mmol, 84%) as a white solid.

$^1\text{H-NMR}$ (300 MHz, CDCl_3) δ_{H} [ppm] = 8.28 – 8.13 (m, 4H), 7.93 – 7.80 (m, 2H), 7.79 – 7.70 (m, 1H), 7.59 – 7.42 (m, 4H).

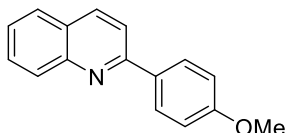
2-(4-methylphenyl)quinoline (42b)



Prepared according to the general procedure **GP6**, 4-methylacetophenone (1.3 g, 10 mmol) was used as ketone. The crude product was purified by flash column chromatography (PE/EA 19:1) to give the product (466 mg, 2.1 mmol, 47%) as a white solid.

$^1\text{H-NMR}$ (300 MHz, CDCl_3) δ_{H} [ppm] = 8.24 – 8.15 (m, $J = 8.9$ Hz, 2H), 8.12 – 8.04 (m, 2H), 7.87 (d, $J = 8.6$ Hz, 1H), 7.82 (dd, $J = 8.1, 1.3$ Hz, 1H), 7.76 – 7.69 (m, 1H), 7.56 – 7.48 (m, 1H), 7.37 – 7.31 (m, 2H), 2.44 (s, 3H).

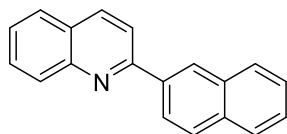
2-(4-methoxyphenyl)quinoline (42c)



Prepared according to the general procedure **GP6**, 4-methoxyacetophenone (1.5 g, 10 mmol) was used as ketone. The crude product was purified by recrystallization from ethanol to give the product (995 mg, 4.2 mmol, 85%) as a white solid.

¹H-NMR (300 MHz, CDCl₃) δ_H [ppm] = 8.23 – 8.12 (m, 4H), 7.87 – 7.79 (m, 2H), 7.75 – 7.68 (m, 1H), 7.54 – 7.47 (m, 1H), 7.09 – 7.02 (m, 2H), 3.89 (s, 3H).

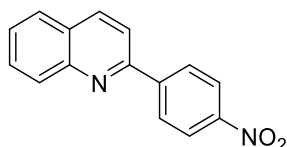
2-(2-naphthyl)quinoline (42d)



Prepared according to the general procedure **GP6**, 2-acetonaphthone (1.5 mL, 10 mmol) was used as ketone. The crude product was purified by flash column chromatography (PE/EA 49:1) to give the product (307 mg, 1.2 mmol, 24%) as a white solid.

¹H-NMR (300 MHz, CDCl₃) δ_H [ppm] = 8.63 (d, *J* = 1.2 Hz, 1H), 8.38 (dd, *J* = 8.6, 1.8 Hz, 1H), 8.31 – 8.22 (m, 2H), 8.05 (d, *J* = 8.6 Hz, 1H), 8.03 – 7.98 (m, 2H), 7.94 – 7.89 (m, 1H), 7.86 (dd, *J* = 8.2, 1.2 Hz, 1H), 7.80 – 7.73 (m, 1H), 7.59 – 7.51 (m, 3H).

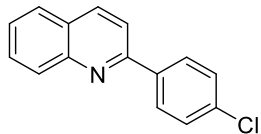
2-(4-nitrophenyl)quinoline (42e)



Prepared according to the general procedure **GP6**, 4-nitroacetophenone (1.7 g, 10 mmol) was used as ketone. The crude product was purified by flash column chromatography (PE/EA 19:1) to give the product (194 mg, 0.8 mmol, 16%) as a yellow solid.

¹H-NMR (300 MHz, CDCl₃) δ_H [ppm] = 8.42 – 8.34 (m, 4H), 8.31 (d, *J* = 8.6 Hz, 1H), 8.20 (d, *J* = 8.6 Hz, 1H), 7.94 (d, *J* = 8.6 Hz, 1H), 7.91 – 7.85 (m, 1H), 7.84 – 7.74 (m, 1H), 7.64 – 7.56 (m, 1H).

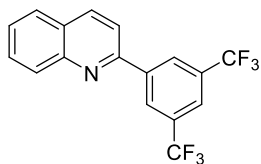
2-(4-chlorophenyl)quinoline (42f)



Prepared according to the general procedure **GP6**, 4-chloroacetophenone (1.5 g, 10 mmol) was used as ketone. The crude product was purified by recrystallization from ethanol to give the product (946 mg, 3.9 mmol, 79%) as a white solid.

$^1\text{H-NMR}$ (300 MHz, CDCl_3) δ_{H} [ppm] = 8.23 (d, J = 8.7 Hz, 1H), 8.19 – 8.09 (m, 3H), 7.87 – 7.81 (m, 2H), 7.78 – 7.70 (m, 1H), 7.58 – 7.47 (m, 3H).

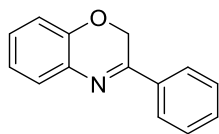
2-(3,5-bis(trifluoromethyl)phenyl)quinoline (42g)



Prepared according to the general procedure **GP6**, 3,5-bis(trifluoromethyl)acetophenone (1.1 mL, 6 mmol) was used as ketone. The crude product was purified by recrystallization from ethanol to give the product (214 mg, 0.6 mmol, 12%) as a white solid.

$^1\text{H-NMR}$ (300 MHz, CDCl_3) δ_{H} [ppm] = 8.69 – 8.64 (m, 2H), 8.36 – 8.29 (m, 1H), 8.24 – 8.18 (m, 1H), 7.99 – 7.96 (m, 1H), 7.94 (d, J = 8.6 Hz, 1H), 7.88 (dd, J = 8.0, 1.4 Hz, 1H), 7.83 – 7.76 (m, 1H), 7.64 – 7.57 (m, 1H).

3-phenyl-2H-benzo[b][1,4]oxazine (42h)^[164]

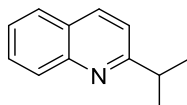


A 250 mL round bottom flask was charged with 2-aminophenol (2.18 g, 20 mmol), DCM (50 mL), an aqueous solution of K_2CO_3 (16 g, 115 mmol in 80 mL) and tetrabutylammonium hydrogensulfate (340 mg, 1 mmol) and the mixture was stirred at r.t. for 2 h. A solution of 2-chloroacetophenone (3.98 g, 20 mmol) in DCM (20 mL) was added over 15 min and the mixture was heated to 40 °C for 17 h. After cooling the

reaction to r.t., the mixture was extracted with DCM (2x 40 mL), the combined organic layers were dried over Na₂SO₄ and the solvent was evaporated. The crude product was recrystallized in ethanol (2x) to give the product (2.32 g, 11 mmol, 55%) as a yellow solid.

¹H-NMR (300 MHz, CDCl₃) δ_H [ppm] = 7.99 – 7.88 (m, 2H), 7.55 – 7.41 (m, 4H), 7.20 – 7.12 (m, 1H), 7.09 – 6.99 (m, 1H), 6.97 – 6.88 (m, 1H), 5.07 (s, 2H).

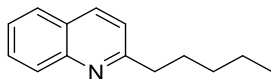
2-isopropylquinoline (42i)



Prepared according to the general procedure **GP6** at double scale, 3-methylbutanone (2.2 mL, 20 mmol) was used as ketone. The crude product was purified by flash column chromatography (PE/EA 19:1) to give the product (1.4 g, 8 mmol, 80%) as a colorless oil.

¹H-NMR (300 MHz, CDCl₃) δ_H [ppm] = 8.09 (t, *J* = 8.2 Hz, 2H), 7.78 (dd, *J* = 8.1, 1.3 Hz, 1H), 7.73 – 7.64 (m, 1H), 7.53 – 7.44 (m, 1H), 7.36 (d, *J* = 8.5 Hz, 1H), 3.28 (sept, *J* = 7.0 Hz, 1H), 1.40 (d, *J* = 7.0 Hz, 6H).

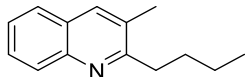
2-pentylquinoline (42j)



Prepared according to the general procedure **GP6**, heptanone (1.4 mL, 10 mmol) was used as ketone. The crude product was purified by flash column chromatography (PE/EA 19:1) to give the product (310 mg, 1.6 mmol, 31%) as a colorless oil.

¹H-NMR (300 MHz, CDCl₃) δ_H [ppm] = 8.09 (d, *J* = 8.4 Hz, 2H), 7.79 (dd, *J* = 8.1, 1.3 Hz, 1H), 7.74 – 7.65 (m, 1H), 7.53 – 7.45 (m, 1H), 7.32 (d, *J* = 8.4 Hz, 1H), 3.05 – 2.95 (m, 2H), 1.90 – 1.73 (m, 2H), 1.46 – 1.30 (m, 4H), 0.93 – 0.87 (m, 3H).

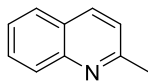
2-butyl-3-methylquinoline



Byproduct of the 2-pentylquinoline (**42j**) synthesis, isolated after flash column chromatography (PE/EA 19:1) as a colorless oil (483 mg, 2.4 mmol, 24%)

¹H-NMR (300 MHz, CDCl₃) δ_H [ppm] = 8.01 (d, *J* = 8.4 Hz, 1H), 7.84 (s, 1H), 7.72 (d, *J* = 8.1 Hz, 1H), 7.65 – 7.58 (m, 1H), 7.50 – 7.41 (m, 1H), 2.81 – 2.74 (m, 2H), 2.74 (s, 3H), 1.75 – 1.59 (m, 2H), 1.46 (sext, *J* = 7.2 Hz, 2H), 0.99 (t, *J* = 7.3 Hz, 3H).

2-methylquinoline (42k)



Prepared according to the general procedure **GP6**, acetone (1.5 mL, 20 mmol) was used as ketone. The crude product was purified by flash column chromatography (PE/EA 19:1) to give the product (594 mg, 4.2 mmol, 83%) as a colorless oil.

¹H-NMR (300 MHz, CDCl₃) δ_H [ppm] = 8.06 (d, *J* = 8.3 Hz, 2H), 7.78 (d, *J* = 8.1 Hz, 1H), 7.74 – 7.65 (m, 1H), 7.55 – 7.44 (m, 1H), 7.29 (d, *J* = 8.4 Hz, 1H), 2.77 (s, 3H).

6. Catalysis products

Methylcyclohexane (89)



The compound was synthesized following the general procedure **GP5**, using toluene (1.06 mL, 10 mmol), isopropanol (0.4 mL) and the optimized catalyst **87** (7 mg, 10.6 wt% Ru, 0.007 mmol Ru, 0.07 mol%). The reaction was run for 1 h and the product solution was analyzed by GC-FID. GC-Yield: 98%.

GC conditions: 60 °C (0 min) – 10 °C/min – 200 °C. Retention times: Methylcyclohexane (2.15 min), toluene (2.35 min), ethylbenzene (3.14 min, standard).

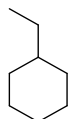
Cyclohexane (2)



The compound was synthesized following the general procedure **GP5**, using benzene (0.89 mL, 10 mmol), isopropanol (0.4 mL) and the optimized catalyst **87** (7 mg, 10.6 wt% Ru, 0.007 mmol Ru, 0.07 mol%). The reaction was run for 1 h and the product solution was analyzed by GC-FID. GC-Yield: 98%.

GC conditions: 35 °C (5 min) – 10 °C/min – 155 °C. Retention times: Benzene (2.62 min), cyclohexane (2.75 min), ethylbenzene (7.92 min, standard)

Ethylcyclohexane (91)



The compound was synthesized following the general procedure **GP5**, using styrene (1.14 mL, 10 mmol), isopropanol (0.4 mL) and the optimized catalyst **87** (7 mg, 10.6 wt% Ru, 0.007 mmol Ru, 0.07 mol%). The reaction was run for 4 h and the product solution was analyzed by GC-FID. GC-Yield: 100%.

GC conditions: 60 °C (0 min) – 10 °C/min – 200 °C. Retention times: Ethylcyclohexane (2.98 min), ethylbenzene (3.12 min), styrene (3.42 min), dodecane (7.89 min, standard).

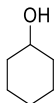
Tetrahydrofuran (25)



The compound was synthesized following the general procedure **GP5**, using furan (0.72 mL, 10 mmol), no solvent and the optimized catalyst **87** (7 mg, 10.6 wt% Ru, 0.007 mmol Ru, 0.07 mol%). The reaction was run for 2 h and the product solution was separated analyzed by NMR. 653 mg THF (9.1 mmol, 91%) were recovered, “relatively low” yield due to small scale and volatility.

$^1\text{H-NMR}$ (300 MHz, CDCl_3) δ_{H} [ppm] = 3.79 – 3.67 (m, 2H), 1.88 – 1.79 (m, 2H).

Cyclohexanol (3)

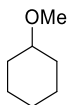


The compound was synthesized following the general procedure **GP5**, using phenol (470 mg, 5 mmol), isopropanol (0.8 mL) and the optimized catalyst **87** (14 mg, 10.6 wt% Ru, 0.014 mmol Ru, 0.29 mol%). The reaction was run for 4 h and the product solution was analyzed by GC-FID. Due to similar retention times of cyclohexanol and cyclohexanone, the product was identified by NMR. GC-Yield: 87%.

GC conditions: 60 °C (0 min) – 10 °C/min – 200 °C. Retention times: Cyclohexanol (3.28 min), phenol (4.42 min), dodecane (7.88 min, standard)

$^1\text{H-NMR}$ (300 MHz, CDCl_3) δ_{H} [ppm] = 3.67 – 3.49 (m, 1H), 1.98 – 1.80 (m, 3H), 1.78 – 1.66 (m, 2H), 1.59 – 1.46 (m, 1H), 1.35 – 1.08 (m, 5H).

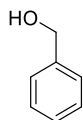
Methoxycyclohexane (94)



The compound was synthesized following the general procedure **GP5**, using anisole (0.55 mL, 5 mmol), isopropanol (0.2 mL) and the optimized catalyst **87** (14 mg, 10.6 wt% Ru, 0.014 mmol Ru, 0.29 mol%). The reaction was run for 4 h and the product solution was analyzed by GC-FID. GC-Yield: 93%

GC conditions: 60 °C (0 min) – 10 °C/min – 200 °C. Retention times: Methoxycyclohexane (3.18 min), anisole (3.65 min), dodecane (7.88 min).

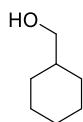
Phenylmethanol (96)



The compound was synthesized following the general procedure **GP5**, using benzaldehyde (1.01 mL, 10 mmol), no solvent and the optimized catalyst **87** (14 mg, 10.6 wt% Ru, 0.014 mmol Ru, 0.14 mol%). The reaction was run for 24 h and the product solution was analyzed by GC-FID. GC-Yield: 89%.

GC conditions: 60 °C (0 min) – 15 °C/min – 250 °C. Retention times: Ethylbenzene (2.87 min, standard), benzaldehyde (3.60 min), cyclohexylmethanol (4.09 min) phenylmethanol (4.32 min).

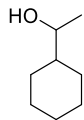
Cyclohexylmethanol (97)



The compound was synthesized following the general procedure **GP5**, using phenylmethanol (1.04 mL, 10 mmol), no solvent and the optimized catalyst **87** (14 mg, 10.6 wt% Ru, 0.014 mmol Ru, 0.14 mol%). The reaction was run for 24 h and the product solution was analyzed by GC-FID. GC-Yield: 5%

GC conditions: 60 °C (0 min) – 15 °C/min – 250 °C. Retention times: Ethylbenzene (2.87 min, standard), cyclohexylmethanol (4.09 min) phenylmethanol (4.32 min).

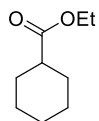
1-Cyclohexylethanol (99)



The compound was synthesized following the general procedure **GP5**, using acetophenone (0.85 mL, 5 mmol), isopropanol (0.2 mL) and the optimized catalyst **87** (14 mg, 10.6 wt% Ru, 0.014 mmol Ru, 0.29 mol%). The reaction was run for 48 h and the product solution was analyzed by GC-FID. GC-Yield: 89%.

GC conditions: 60 °C (0 min) – 5 °C/min – 110 °C (0 min) – 20 °C/min – 250 °C. Retention times: Ethylbenzene (3.58 min, standard), 1-cyclohexylethanol (7.19 min), acetophenone (7.33 min).

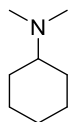
Ethyl cyclohexanecarboxylate (101)



The compound was synthesized following the general procedure **GP5**, using ethyl benzoate (0.71 mL, 5 mmol), isopropanol (0.2 mL) and the optimized catalyst **87** (14 mg, 10.6 wt% Ru, 0.014 mmol Ru, 0.29 mol%). The reaction was run for 48 h and the product solution was analyzed by GC-FID. GC-Yield: 76%.

GC conditions: 60 °C (0 min) – 10 °C/min – 250 °C. Retention times: Ethylbenzene (3.15 min, standard), ethyl cyclohexanecarboxylate (6.60 min), ethyl benzoate (7.08 min).

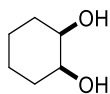
N,N-Dimethylcyclohexanamine (103)



The compound was synthesized following the general procedure **GP5**, using N,N-dimethylaniline (0.63 mL, 5 mmol), no solvent and the optimized catalyst **87** (14 mg, 10.6 wt% Ru, 0.014 mmol Ru, 0.29 mol%). The reaction was run for 48 h and the product solution was analyzed by GC-FID. GC-Yield: 59%.

GC conditions: 60 °C (0 min) – 10 °C/min – 250 °C. Retention times: Ethylbenzene (3.12 min, standard), N,N-dimethylcyclohexanamine (4.55 min), N,N-dimethylaniline (5.92 min).

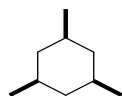
1,2-Cyclohexanediol (105)



The compound was synthesized following the general procedure **GP5**, using 1,2-dihydroxybenzene (220 mg, 2 mmol), isopropanol (2 mL) and the optimized catalyst **87** (14 mg, 10.6 wt% Ru, 0.014 mmol Ru, 0.73 mol%). The reaction was run for 24 h and the product was isolated by column chromatography (PE/EA = 7:1). The product was isolated as a white solid (178 mg, 1.5 mmol, 77%), 3.7:1 cis/trans ratio, determined by NMR.

¹H-NMR (300 MHz, CDCl₃) δ_H [ppm] = 3.80 – 3.73 (m, 2H), 2.30 (s, 2H), 1.81 – 1.68 (m, 2H), 1.64 – 1.48 (m, 4H), 1.40 – 1.20 (m, 2H). (Cis isomer)

1,3,5-Trimethylcyclohexane (107)

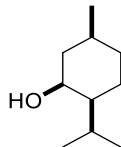


The compound was synthesized following the general procedure **GP5**, using mesitylene (0.27 mL, 2 mmol), isopropanol (2 mL) and the optimized catalyst **87** (14 mg, 10.6 wt% Ru, 0.014 mmol Ru, 0.73 mol%). The reaction was run for 20 h and the conversion was analyzed by GC-FID. The solvent was evaporated to give the isolated product as a colorless liquid (220 mg, 1.7 mmol, 87%), 3.6:1 cis/trans ratio, determined by NMR.

GC conditions: 60 °C (0 min) – 10 °C/min – 200 °C. Retention times: 1,3,5-trimethylcyclohexane (2.96 min (cis), 3.19 min (trans)), mesitylene (4.40 min), dodecane (7.89 min, standard).

¹H-NMR (300 MHz, CDCl₃) δ_H [ppm] = 1.64 – 1.56 (m, 3H), 1.46 – 1.33 (m, 3H), 0.86 (d, J = 6.6 Hz, 9H), 0.47 (q, J = 11.5 Hz, 3H). (Cis isomer)

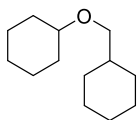
2-Isopropyl-5-methyl-cyclohexan-1-ol (**14**)



The compound was synthesized following the general procedure **GP5**, using thymol (300 mg, 2 mmol), isopropanol (2 mL) and the optimized catalyst **87** (14 mg, 10.6 wt% Ru, 0.014 mmol Ru, 0.73 mol%). The reaction was run for 48 h and the solvent was evaporated to give the isolated product as a colorless liquid (288 mg, 1.8 mmol, 96%), 19:1.6:2.1:1 ratio of neoisomenthol (**14d**)/isomenthol (**14b**)/neomenthol (**14c**)/menthol (**14a**) in that respective order, determined by NMR.

¹H-NMR (400 MHz, CDCl₃) δ_H [ppm] = 4.05 – 3.99 (m, 1H), 1.81 – 1.32 (m, 9H), 1.29 (s, 1H), 1.07 (d, J = 7.1 Hz, 3H), 1.00 (d, J = 6.6 Hz, 3H), 0.93 (d, J = 6.7 Hz, 4H). (**14d** isomer)

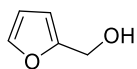
(Cyclohexylmethoxy)cyclohexane (**109**)



The compound was synthesized following the general procedure **GP5**, using benzyl phenyl ether (368 mg, 2 mmol), isopropanol (2 mL) and the optimized catalyst **87** (14 mg, 10.6 wt% Ru, 0.014 mmol Ru, 0.73 mol%). The reaction was run for 24 h and the product was isolated by column chromatography (PE/EA = 19:1). The product was isolated as a white solid (349 mg, 1.8 mmol, 89%).

¹H-NMR (300 MHz, CDCl₃) δ_H [ppm] = 3.22 (d, J = 6.6 Hz, 2H), 3.20 – 3.11 (m, 1H), 1.94 – 1.82 (m, 2H), 1.82 – 1.61 (m, 7H), 1.60 – 1.45 (m, 2H), 1.34 – 1.11 (m, 8H), 0.97 – 0.80 (m, 2H).

Furfuryl alcohol (**22**)



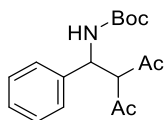
The compound was synthesized following the general procedure **GP5**, using furfural (0.41 mL, 5 mmol), no solvent and the optimized catalyst **87** (14 mg, 10.6 wt% Ru, 0.014 mmol Ru, 0.29 mol%). The reaction

was run for 48 h and the product solution was analyzed by NMR, 29% conversion to furfuryl alcohol (**22**) detected.

Furfural: $^1\text{H-NMR}$ (300 MHz, CDCl_3) δ_{H} [ppm] = 9.65 (d, $J = 0.8$ Hz, 1H), 7.71 – 7.65 (m, 1H), 7.25 (dd, $J = 3.6$, 0.8 Hz, 1H), 6.60 (dd, $J = 3.6$, 1.7 Hz, 1H).

Furfuryl alcohol: $^1\text{H-NMR}$ (300 MHz, CDCl_3) δ_{H} [ppm] = 7.38 (dd, $J = 1.8$, 0.9 Hz, 1H), 6.32 (dd, $J = 3.2$, 1.8 Hz, 1H), 6.29 – 6.26 (m, 1H), 4.60 (s, 2H), 1.98 (s, 1H).

Tert-butyl (2-acetyl-3-oxo-1-phenylbutyl)carbamate (131)



Under nitrogen atmosphere, a dried 10 mL Schlenk pressure tube was charged with *tert*-butyl (*Z*)-benzylidenecarbamate (**129**) (40 mg, 0.2mmol), acetylacetone (23 μL , 0.2 mmol), dry DCM (1 mL) and 10 mg of immobilized CPA cat (**123c/123d**) or CPA **116d** (1 mg, 0.002 mmol) and the reaction was stirred at r.t. for 24 h. The solvent was evaporated and the residue was dried *in vacuo* to give the product as a white solid.

123c cat.: Yield: 59 mg, 0.19 mmol, 96%, 4% *ee*.

123d cat.: Yield: 60 mg, 0.20 mmol, 99%, 3% *ee*

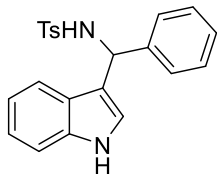
116d cat: Yield: 59 mg, 0.19 mmol, 96%, 45% *ee*.

No cat.: Yield: 58 mg, 0.19 mmol, 95%.

HPLC conditions: Chiracel AS-H column, *n*-heptane/*i*-PrOH 99:1, flow rate 1 mL/min, $\lambda = 215$ nm, t_{R} (major) = 29.4 min, t_{R} (minor) = 43.9 min.

$^1\text{H-NMR}$ (300 MHz, CDCl_3) δ_{H} [ppm] = 7.35 – 7.23 (m, 5H), 5.80 (bs, 1H), 5.49 (bs, 1H), 4.21 (d, $J = 6.8$ Hz, 1H), 2.19 (bs, 3H), 2.11 (s, 3H), 1.39 (s, 9H).

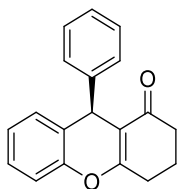
N-((1H-indol-3-yl)(phenyl)methyl)-4-methylbenzenesulfonamide (**134**)



A 10 mL vial was charged with N-benzylidene-4-methylbenzenesulfonamide (**132**) (130 mg, 0.5 mmol), indole (84 mg, 0.7 mmol), toluene (2.5 mL) and the immobilized CPA **128i** (25 mg). The reaction was stirred at r.t. for 72 h, after which the catalyst was separated with the aid of a magnet, the solvent was evaporated and the crude mixture was purified by flash column chromatography (PE/EA 19:1 to PE/EA 9:1) to give the product (100 mg, 0.27 mmol, 53%, $\alpha_D^{20} = 0^\circ$) as a white solid.

¹H-NMR (300 MHz, CDCl₃) δ_H [ppm] = 8.00 (bs, 1H), 7.60 – 7.53 (m, 2H), 7.34 – 7.28 (m, 1H), 7.25 – 7.14 (m, 7H), 7.14 – 7.09 (m, 2H), 7.04 – 6.95 (m, 1H), 6.68 (dd, $J = 2.6, 0.8$ Hz, 1H), 5.85 (d, $J = 6.3$ Hz, 1H), 5.04 (d, $J = 6.8$ Hz, 1H), 2.37 (s, 3H).

(R)-9-Phenyl-2,3,4,9-tetrahydro-1H-xanthen-1-one (**138**)



A 10 mL round bottom flask was charged with 2-(hydroxy(phenyl)methyl)phenol (**135**) (40 mg, 0.2 mmol), 1,3-cyclohexanedione (27 mg, 0.24 mmol), chloroform (1.5 mL) and in the case of a homogeneous reaction CPA **116h** (7 mg, 0.01 mmol) or in the case of a heterogeneous reaction the immobilized CPA cat **123h/128h** (25 mg). The reaction was stirred at r.t. for 48 h, after which the catalyst was removed with the aid of a magnet in the case of a heterogeneous reaction. The crude mixture was filtered through a pad of silica using PE/EA 3:1 as eluent and the solvent were evaporated. The residue was redissolved in chloroform (1 mL), *p*-toluenesulfonic acid (8 mg, 0.05 mmol) was added and the mixture was heated to 40 °C for 2 h. The solvent was evaporated and the crude product was purified by flash column chromatography (PE/EA 6:1 to PE/EA 3:1) to give the product as a white solid.

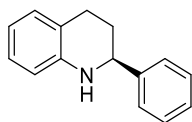
116h cat.: Yield: 44 mg, 0.16 mmol, 80%, -81% *ee*, ((S)-**116h** was used).

128h cat.: Yield: 41 mg, 0.15 mmol, 74%, 40% *ee*.

HPLC conditions: Phenomenex Lux Cellulose-1 column, *n*-heptane/*i*-PrOH 95:5, flow rate 1.0 mL/min, λ = 254 nm, t_R (minor) = 9.3 min, t_R (major) = 11.4 min.

¹H-NMR (300 MHz, CDCl₃) δ_H [ppm] = 7.25 – 7.20 (m, 4H), 7.19 – 7.12 (m, 2H), 7.11 – 6.98 (m, 3H), 5.06 (s, 1H), 2.80 – 2.57 (m, 2H), 2.48 – 2.28 (m, 2H), 2.12 – 1.91 (m, 2H).

(S)-2-phenyl-1,2,3,4-tetrahydroquinoline (44a)



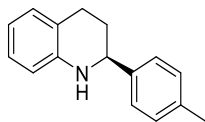
The compound was synthesized following general procedure **GP7**, the Product was obtained as a white solid (104 mg, 99%, 76% *ee*) after flash chromatography (PE/ EA = 49:1).

HPLC conditions: Phenomenex Lux Cellulose-1 column, *n*-heptane/*i*-PrOH 95:5, flow rate 0.5 mL/min, λ = 254 nm, t_R (major) = 20.7 min, t_R (minor) = 20.8 min.

¹H-NMR (300 MHz, CDCl₃) δ_H [ppm] = 7.46 – 7.27 (m, 5H), 7.09 – 6.97 (m, 2H), 6.68 (t, *J* = 7.4 Hz, 1H), 6.57 (d, *J* = 8.2 Hz, 1H), 4.46 (d, *J* = 9.2 Hz, 1H), 4.21 (bs, 1H), 3.03 – 2.87 (m, 1H), 2.83 – 2.69 (m, 1H), 2.21 – 2.09 (m, 1H), 2.09 – 1.93 (m, 1H).

¹³C-NMR (75 MHz, CDCl₃) δ_C [ppm] = 144.72, 129.35, 128.62, 127.50, 126.95, 126.62, 121.02, 117.33, 114.14, 56.32, 30.97, 26.41.

(S)-2-(*p*-tolyl)-1,2,3,4-tetrahydroquinoline (44b)



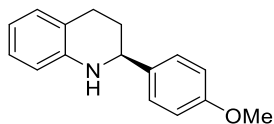
The compound was synthesized following general procedure **GP7**, the Product was obtained as a white solid (109 mg, 97%, 76% *ee*) after flash chromatography (PE/ EA = 19:1).

HPLC conditions: Phenomenex Lux Cellulose-1 column, *n*-heptane/*i*-PrOH 90:10, flow rate 0.5 mL/min, λ = 254 nm, t_R (major) = 14.1 min, t_R (minor) = 23.9 min.

¹H-NMR (300 MHz, CDCl₃) δ_H [ppm] = 7.31 (d, *J* = 8.1 Hz, 4H), 7.19 (d, *J* = 7.9 Hz, 4H), 7.07 – 6.99 (m, 4H), 6.68 (td, *J* = 7.4, 1.1 Hz, 2H), 6.60 – 6.51 (m, 2H), 4.42 (dd, *J* = 9.4, 3.3 Hz, 2H), 4.10 (bs, 1H), 2.95 (ddd, *J* = 16.3, 10.7, 5.6 Hz, 2H), 2.76 (dt, *J* = 16.4, 4.7 Hz, 2H), 2.38 (s, 6H), 2.19 – 1.92 (m, 4H).

¹³C-NMR (75 MHz, CDCl₃) δ_C [ppm] = 144.69, 141.75, 137.15, 129.33, 129.28, 126.91, 126.53, 121.03, 117.26, 114.11, 56.08, 31.01, 26.52, 21.15.

(S)-2-(4-methoxyphenyl)-1,2,3,4-tetrahydroquinoline (44c)



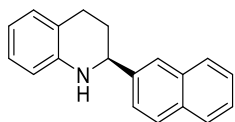
The compound was synthesized following general procedure **GP7**, the Product was obtained as a white solid (122 mg, >99%, 44% *ee*) after flash chromatography (PE/ EA = 19:1).

HPLC conditions: Phenomenex Lux Cellulose-1 column, *n*-heptane/*i*-PrOH 90:10, flow rate 0.5 mL/min, λ = 215 nm, t_R (major) = 17.3 min, t_R (minor) = 27.1 min.

$^1\text{H-NMR}$ (300 MHz, CDCl_3) δ_H [ppm] = 7.42 – 7.31 (m, 6H), 7.12 – 7.02 (m, 6H), 7.00 – 6.89 (m, 6H), 6.71 (td, J = 7.4, 1.1 Hz, 3H), 6.61 – 6.53 (m, 3H), 4.43 (dd, J = 9.4, 3.3 Hz, 3H), 3.99 (bs, 2H), 3.86 (s, 9H), 2.99 (ddd, J = 16.3, 10.8, 5.6 Hz, 3H), 2.79 (dt, J = 16.4, 4.6 Hz, 3H), 2.20 – 1.92 (m, 6H).

$^{13}\text{C-NMR}$ (75 MHz, CDCl_3) δ_C [ppm] = 159.03, 144.88, 136.95, 129.38, 127.74, 126.95, 120.98, 117.23, 114.10, 113.99, 55.79, 55.39, 31.18, 26.64.

(S)-2-(naphthalen-2-yl)-1,2,3,4-tetrahydroquinoline (44d)



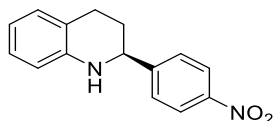
The compound was synthesized following general procedure **GP7**, the Product was obtained as a white solid (131 mg, >99%, 87% *ee*) after flash chromatography (PE/ EA = 19:1).

HPLC conditions: Phenomenex Lux Cellulose-1 column, *n*-heptane/*i*-PrOH 90:10, flow rate 0.5 mL/min, λ = 254 nm, t_R (major) = 24.8 min, t_R (minor) = 45.6 min.

$^1\text{H-NMR}$ (400 MHz, CDCl_3) δ_H [ppm] = 7.88 – 7.78 (m, 4H), 7.53 (dd, J = 8.5, 1.6 Hz, 1H), 7.51 – 7.45 (m, 2H), 7.07 – 6.94 (m, 2H), 6.70 (t, J = 7.3 Hz, 1H), 6.61 (d, J = 7.9 Hz, 1H), 4.61 (dd, J = 9.2, 3.4 Hz, 1H), 2.97 (ddd, J = 16.2, 10.5, 5.6 Hz, 1H), 2.78 (dt, J = 16.3, 4.7 Hz, 1H), 2.27 – 2.05 (m, 2H).

$^{13}\text{C-NMR}$ (75 MHz, CDCl_3) δ_C [ppm] = 144.61, 142.16, 133.45, 133.01, 129.38, 128.39, 127.91, 127.72, 127.00, 126.21, 125.82, 125.18, 124.92, 121.09, 117.38, 114.18, 56.41, 30.95, 26.46.

(S)-2-(4-nitrophenyl)-1,2,3,4-tetrahydroquinoline (44e)



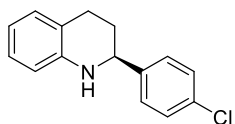
The compound was synthesized following general procedure **GP7**, the Product was obtained as a yellow solid (113 mg, 90%, 92% *ee*) after flash chromatography (PE/ DCM = 6:1).

HPLC conditions: Phenomenex Lux Cellulose-1 column, *n*-heptane/*i*-PrOH 70:30, flow rate 0.5 mL/min, λ = 254 nm, t_R (major) = 29.7 min, t_R (minor) = 39.6 min.

$^1\text{H-NMR}$ (300 MHz, CDCl_3) δ_H [ppm] = 8.24 – 8.16 (m, 2H), 7.61 – 7.52 (m, 2H), 7.11 – 6.97 (m, 2H), 6.70 (td, J = 7.4, 1.0 Hz, 1H), 6.61 (d, J = 7.9 Hz, 1H), 4.59 (dd, J = 8.5, 3.5 Hz, 1H), 4.18 (bs, 1H), 3.01 – 2.82 (m, 1H), 2.69 (dt, J = 16.4, 5.3 Hz, 1H), 2.24 – 2.08 (m, 1H), 2.07 – 1.91 (m, 1H).

$^{13}\text{C-NMR}$ (75 MHz, CDCl_3) δ_C [ppm] = 152.46, 147.29, 143.83, 129.41, 127.39, 127.18, 123.90, 120.75, 117.89, 114.32, 55.58, 30.75, 25.67.

(S)-2-(4-chlorophenyl)-1,2,3,4-tetrahydroquinoline (44f)



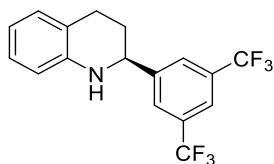
The compound was synthesized following general procedure **GP7**, the Product was obtained as a white solid (106 mg, 87%, 89% *ee*) after flash chromatography (PE/ EA = 19:1).

HPLC conditions: Phenomenex Lux Cellulose-1 column, *n*-heptane/*i*-PrOH 95:5, flow rate 0.5 mL/min, λ = 254 nm, t_R (major) = 23.3 min, t_R (minor) = 46.7 min.

$^1\text{H-NMR}$ (300 MHz, CDCl_3) δ_H [ppm] = 7.34 (s, 4H), 7.09 – 6.98 (m, 2H), 6.69 (td, J = 7.4, 1.1 Hz, 1H), 6.57 (d, J = 7.9 Hz, 1H), 4.43 (dd, J = 7.0 Hz, 1H), 4.20 (bs, 1H), 2.93 (ddd, J = 16.0, 10.4, 5.6 Hz, 1H), 2.73 (dt, J = 16.4, 4.9 Hz, 1H), 2.18 – 2.06 (m, 1H), 2.05 – 1.89 (m, 1H).

$^{13}\text{C-NMR}$ (75 MHz, CDCl_3) δ_C [ppm] = 144.31, 143.27, 133.06, 129.38, 128.73, 127.99, 127.02, 120.93, 117.58, 114.22, 55.64, 30.97, 26.17.

(S)-2-(3,5-bis(trifluoromethyl)phenyl)-1,2,3,4-tetrahydroquinoline (44g)



The compound was synthesized following general procedure **GP7**, the reaction was performed on a 0.3 mmol scale and the reaction time was 14 d, the Product was obtained as a colorless oil (73 mg, 71%, 35% *ee*) after flash chromatography (PE/ EA = 19:1).

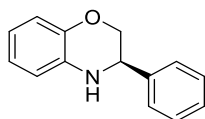
HPLC conditions: Phenomenex Lux Cellulose-1 column, *n*-heptane/*i*-PrOH 95:5, flow rate 0.5 mL/min, λ = 215 nm, t_R (major) = 21.1 min, t_R (minor) = 52.9 min.

¹H-NMR (400 MHz, CDCl₃) δ_H [ppm] = 7.89 (s, 2H), 7.83 (s, 1H), 7.05 (dd, J = 14.2, 7.3 Hz, 2H), 6.73 (t, J = 7.3 Hz, 1H), 6.62 (d, J = 7.9 Hz, 1H), 4.59 (dd, J = 9.4, 3.0 Hz, 1H), 4.06 (s, 1H), 3.04 – 2.91 (m, 1H), 2.76 (dt, J = 16.4, 4.6 Hz, 1H), 2.23 – 2.11 (m, J = 12.9, 8.5, 4.5 Hz, 1H), 2.08 – 1.94 (m, 1H).

¹³C-NMR (101 MHz, CDCl₃) δ_C [ppm] = 147.59, 143.86, 131.94 (q), 129.39, 127.19, 126.85 – 127.00 (m), 124.72, 122.01, 121.53 (sept), 120.78, 118.21, 114.55, 55.79, 31.40, 26.17.

¹⁹F-NMR (376 MHz, CDCl₃) δ_F[ppm] = -63.27.

(R)-3-phenyl-3,4-dihydro-2H-benzo[b][1,4]oxazine (44h)



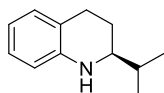
The compound was synthesized following general procedure **GP7**, the product was obtained as a colorless oil (103 mg, 98%, 67% ee) after flash chromatography (PE/ EA = 19:1).

HPLC conditions: Phenomenex Lux i-Amylose-1 column, *n*-heptane/*i*-PrOH 80:20, flow rate 0.5 mL/min, λ = 215 nm, t_R(minor) = 11.0 min, t_R(major) = 12.6 min.

¹H-NMR (300 MHz, CDCl₃) δ_H [ppm] = 7.48 – 7.30 (m, 10H), 6.92 – 6.78 (m, 4H), 6.77 – 6.66 (m, 4H), 4.52 (dd, J = 8.6, 3.0 Hz, 2H), 4.30 (dd, J = 10.6, 3.0 Hz, 2H), 4.23 – 4.06 (m, 1H), 4.01 (dd, J = 10.6, 8.6 Hz, 2H).

¹³C-NMR (75 MHz, CDCl₃) δ_C [ppm] = 143.55, 139.16, 133.94, 128.87, 128.39, 127.24, 121.53, 118.97, 116.64, 115.42, 71.01, 54.24.

(S)-2-isopropyl-1,2,3,4-tetrahydroquinoline (44i)



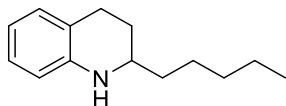
The compound was synthesized following general procedure **GP7**, the reaction time was 48 h, the product was obtained as a colorless oil (72 mg, 82%, 4% ee) after flash chromatography (PE/ EA = 19:1).

HPLC conditions: Phenomenex Lux Cellulose-1 column, *n*-heptane/*i*-PrOH 95:5, flow rate 0.5 mL/min, λ = 254 nm, t_R(minor) = 11.0 min, t_R(major) = 13.7 min.

¹H-NMR (300 MHz, CDCl₃) δ_H [ppm] = 7.06 – 6.93 (m, 2H), 6.62 (td, J = 7.4, 1.1 Hz, 1H), 6.56 – 6.47 (m, 1H), 3.72 (bs, 1H), 3.06 (ddd, J = 9.8, 5.8, 2.9 Hz, 1H), 2.92 – 2.69 (m, 2H), 1.94 (dddd, J = 12.4, 5.4, 3.9, 3.0 Hz, 1H), 1.82 – 1.60 (m, 2H), 1.02 (dd, J = 7.7, 6.9 Hz, 6H).

¹³C-NMR (75 MHz, CDCl₃) δ_C [ppm] = 145.02, 129.20, 126.76, 121.50, 116.81, 114.06, 57.34, 32.56, 26.69, 24.53, 18.66, 18.31.

(R)-2-pentyl-1,2,3,4-tetrahydroquinoline (44j)



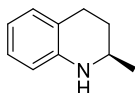
The compound was synthesized following general procedure **GP7**, the reaction time was 48 h, the product was obtained as a colorless oil (87 mg, 86%, 0% *ee*) after flash chromatography (PE/ EA = 19:1).

HPLC conditions: Phenomenex Lux Cellulose-1 column, *n*-heptane/*i*-PrOH 95:5, flow rate 0.5 mL/min, λ = 254 nm, t_R (minor) = 10.2 min, t_R (major) = 10.8 min.

$^1\text{H-NMR}$ (300 MHz, CDCl_3) δ_H [ppm] = 7.03 – 6.93 (m, 2H), 6.68 – 6.56 (m, 1H), 6.55 – 6.44 (m, 1H), 3.52 (bs, 1H), 3.32 – 3.19 (m, 1H), 2.92 – 2.69 (m, 2H), 2.04 – 1.91 (m, 1H), 1.71 – 1.57 (m, 1H), 1.56 – 1.25 (m, 8H), 1.02 – 0.88 (m, 3H).

$^{13}\text{C-NMR}$ (75 MHz, CDCl_3) δ_C [ppm] = 144.64, 129.30, 126.74, 121.52, 117.02, 114.16, 51.67, 36.67, 32.00, 28.12, 26.47, 25.45, 22.70, 14.12.

(R)-2-methyl-1,2,3,4-tetrahydroquinoline (44k)



The compound was synthesized following general procedure **GP7**, the product was obtained as a colorless oil (59 mg, 81%, 50% *ee*) after flash chromatography (PE/ EA = 19:1).

GC conditions: CP-Chirasil-Dex CB column, He carrier Gas, 135 °C isothermic, 13 min, t_R (minor) = 10.8 min, t_R (major) = 11.0 min.

$^1\text{H-NMR}$ (400 MHz, CDCl_3) δ_H [ppm] = 7.02 – 6.93 (m, 2H), 6.68 – 6.58 (m, 1H), 6.56 – 6.48 (m, 1H), 4.13 (bs, 1H), 3.47 – 3.37 (m, 1H), 2.90 – 2.80 (m, 1H), 2.78 – 2.69 (m, 1H), 2.00 – 1.89 (m, 1H), 1.70 – 1.53 (m, 1H), 1.29 – 1.18 (m, 3H).

$^{13}\text{C-NMR}$ (75 MHz, CDCl_3) δ_C [ppm] = 129.34, 126.75, 117.48, 114.42, 47.33, 30.03, 26.55, 22.46.

F. References

- [1] M. P. Wiesenfeldt, Z. Nairoukh, T. Dalton, F. Glorius, *Angew. Chem. Int. Ed.* **2019**, *58*, 10460.
- [2] Z. X. Giustra, J. S.A. Ishibashi, S.-Y. Liu, *Coord. Chem. Rev.* **2016**, *314*, 134.
- [3] D.-S. Wang, Q.-A. Chen, S.-M. Lu, Y.-G. Zhou, *Chem. Rev.* **2012**, *112*, 2557.
- [4] G. Chacón, J. Dupont, *ChemCatChem* **2019**, *11*, 333.
- [5] L. Foppa, J. Dupont, *Chem. Soc. Rev.* **2015**, *44*, 1886.
- [6] A. Gual, C. Godard, S. Castellón, C. Claver, *Dalton Trans.* **2010**, *39*, 11499.
- [7] P. Sabatier, J. B. Senderens, *C. R. Acad. Sci.* **1901**, *132*, 1254.
- [8] B. H. Cooper, B. B.L. Donniss, *Appl. Catal. A-Gen.* **1996**, *137*, 203.
- [9] J. P. van den Berg, J. P. Lucien, G. Germaine, G.L.B. Thielemans, *Fuel Process. Technol.* **1993**, *35*, 119.
- [10] A. Stanislaus, B. H. Cooper, *Catal. Rev.* **1994**, *36*, 75.
- [11] C. Song, X. Ma, *Appl. Catal. B-Environ.* **2003**, *41*, 207.
- [12] A. Corma, A. Martínez, V. Martínez-Soria, *J. Catal.* **1997**, *169*, 480.
- [13] J. A. Widegren, R. G. Finke, *J. Mol. Catal. A Chem.* **2003**, *191*, 187.
- [14] K. Weissermel, H. J. Arpe, *Industrial Organic Chemistry*, Wiley-VCH, Weinheim, Germany, **2003**.
- [15] E. A. Martynenko, I. L. Glazko, S. V. Levanova, *Russ Chem Bull* **2016**, *65*, 2513.
- [16] C. Amen-Chen, H. Pakdel, C. Roy, *Bioresour. Technol.* **2001**, *79*, 277.
- [17] M. P. Pandey, C. S. Kim, *Chem. Eng. Technol.* **2011**, *34*, 29.
- [18] Y. Z. Chen, C. W. Liaw, L. I. Lee, *Appl. Catal. A-Gen.* **1999**, *177*, 1.
- [19] X. Kong, Y. Gong, S. Mao, Y. Wang, *ChemNanoMat* **2018**, *4*, 432.
- [20] H. Liu, T. Jiang, B. Han, S. Liang, Y. Zhou, *Science* **2009**, *326*, 1250.
- [21] D. J. W. Charles, J. W. C. O. T. U. Drinkard, DE2221137 (A1) **1972**.
- [22] J. Struijk, M. d'Angremond, W.J.M. L.-d. Regt, J.J.F. Scholten, *Appl. Catal. A-Gen.* **1992**, *83*, 263.
- [23] H. Nagahara, M. Ono, M. Konishi, Y. Fukuoka, *Appl. Surf. Sci.* **1997**, *121-122*, 448.
- [24] C. Sell, *The chemistry of fragrances. From perfumer to consumer*, RSC Publishing, Cambridge, UK, **2006**.
- [25] G. S. Clark, *Perfumer Flavorist* **2007**, *32*, 38.
- [26] W. Biedermann, DE2314813 (A1) **1973**.
- [27] I. L. Gatfield, J. M. Hilmer, U. Bornscheuer, R. Schmidt, S. Vorlova, US2002182674 (A1) **2002**.
- [28] B. Etzold, A. Jess, M. Nobis, *Catal. Today* **2009**, *140*, 30.
- [29] P. Preuster, C. Papp, P. Wasserscheid, *Acc. Chem. Res.* **2017**, *50*, 74.
- [30] N. Brückner, K. Obesser, A. Bösmann, D. Teichmann, W. Arlt, J. Dungs, P. Wasserscheid, *ChemSusChem* **2014**, *7*, 229.
- [31] K. Müller, K. Stark, V. N. Emel'yanenko, M. A. Varfolomeev, D. H. Zaitsau, E. Shoifet, C. Schick, S. P. Verevkin, W. Arlt, *Ind. Eng. Chem. Res.* **2015**, *54*, 7967.
- [32] G. P. Pez, A. R. Scott, A. C. Cooper, H. Cheng, US2004223907 (A1) **2003**.
- [33] K. Müller, J. Völkl, W. Arlt, *Energy Technol.* **2013**, *1*, 20.
- [34] J.-P. Lange, E. van der Heide, J. van Buijtenen, R. Price, *ChemSusChem* **2012**, *5*, 150.
- [35] K. Yan, G. Wu, T. Lafleur, C. Jarvis, *Renew. Sust. Energ. Rev.* **2014**, *38*, 663.
- [36] S. Dutta, S. De, B. Saha, M. I. Alam, *Catal. Sci. Technol.* **2012**, *2*, 2025.
- [37] R. Mariscal, P. Maireles-Torres, M. Ojeda, I. Sádaba, M. López Granados, *Energy Environ. Sci.* **2016**, *9*, 1144.
- [38] M. H. Schneider, J. G. Phillips, US2002173564 (A1) **2002**.
- [39] S. Chen, R. Wojcieszak, F. Dumeignil, E. Marceau, S. Royer, *Chem. Rev.* **2018**, *118*, 11023.

- [40] X. Chen, W. Sun, N. Xiao, Y. Yan, S. Liu, *Chem. Eng. J.* **2007**, *126*, 5.
- [41] S. Koso, I. Furikado, A. Shimao, T. Miyazawa, K. Kunimori, K. Tomishige, *Chem. Commun.* **2009**, 2035.
- [42] T. Lacombe, X. Montagne, B. Delfort, F. Paille, US2002053161 (A1) **2001**.
- [43] H. E. Hoydonckx, W. M. van Rhijn, W. van Rhijn, D. E. de Vos, P. A. Jacobs in *Ullmann's encyclopedia of industrial chemistry*, Wiley-VCH, Weinheim, Germany, **2007**, p. 285.
- [44] C. Li, G. Xu, X. Liu, Y. Zhang, Y. Fu, *Ind. Eng. Chem. Res.* **2017**, *56*, 8843.
- [45] M. G. Al-Shaal, A. Dzierbinski, R. Palkovits, *Green Chem* **2014**, *16*, 1358.
- [46] A. Irshad, AU2582602 (A) **2001**.
- [47] F. Dong, Y. Zhu, G. Ding, J. Cui, X. Li, Y. Li, *ChemSusChem* **2015**, *8*, 1534.
- [48] W. W. Gilbert, B. W. Howk, US2772293 (A) **1953**.
- [49] E. J. García-Suárez, A. M. Balu, M. Tristany, A. B. García, K. Philippot, R. Luque, *Green Chem* **2012**, *14*, 1434.
- [50] M. P. Wiesenfeldt, Z. Nairoukh, W. Li, F. Glorius, *Science* **2017**, *357*, 908.
- [51] D. O'Hagan, *Chem. Soc. Rev.* **2008**, *37*, 308.
- [52] K. Müller, C. Faeh, F. Diederich, *Science* **2007**, *317*, 1881.
- [53] B. E. Smart, *J. Fluor. Chem.* **2001**, *109*, 3.
- [54] N. S. Keddie, A. M. Z. Slawin, T. Lebl, D. Philp, D. O'Hagan, *Nat. Chem.* **2015**, *7*, 483.
- [55] Z. Nairoukh, M. Wollenburg, C. Schleppehorst, K. Bergander, F. Glorius, *Nat. Chem.* **2019**, *11*, 264.
- [56] M. P. Wiesenfeldt, T. Knecht, C. Schleppehorst, F. Glorius, *Angew. Chem. Int. Ed.* **2018**, *57*, 8297.
- [57] M. Wollenburg, D. Mook, F. Glorius, *Angew. Chem. Int. Ed.* **2019**, *58*, 6549.
- [58] F. Glorius, N. Spielkamp, S. Holle, R. Goddard, C. W. Lehmann, *Angew. Chem. Int. Ed.* **2004**, *43*, 2850.
- [59] X. Wei, B. Qu, X. Zeng, J. Savoie, K. R. Fandrick, J.-N. Desrosiers, S. Tcyrulnikov, M. A. Marsini, F. G. Buono, Z. Li et al., *J. Am. Chem. Soc.* **2016**, *138*, 15473.
- [60] M. Rueping, A. P. Antonchick, T. Theissmann, *Angew. Chem. Int. Ed.* **2006**, *45*, 3683.
- [61] I. Jacquemond-Collet, F. Benoit-Vical, A. Valentin, E. Stanislas, M. Mallié, I. Fourasté, *Planta Med.* **2002**, *68*, 68.
- [62] D. Mook, M. P. Wiesenfeldt, M. Freitag, S. Muratsugu, S. Ikemoto, R. Knitsch, J. Schneidewind, W. Baumann, A. H. Schäfer, A. Timmer et al., *ACS Catal.* **2020**, *10*, 6309.
- [63] D. Astruc, F. Lu, J. R. Aranzaes, *Angew. Chem. Int. Ed.* **2005**, *44*, 7852.
- [64] A. Roucoux, J. Schulz, H. Patin, *Chem. Rev.* **2002**, *102*, 3757.
- [65] Y. Berkovich, N. Garti, *Colloid Surface A* **1997**, *128*, 91.
- [66] J. Seo, S. Lee, B. Koo, W. Jung, *CrystEngComm* **2018**, *20*, 2010.
- [67] K. R. Januszkiewicz, H. Alper, *Organometallics* **1983**, *2*, 1055.
- [68] P. Migowski, J. Dupont, *Chem. Eur. J.* **2007**, *13*, 32.
- [69] J. Dupont, G. S. Fonseca, A. P. Umpierre, P. F. P. Fichtner, S. R. Teixeira, *J. Am. Chem. Soc.* **2002**, *124*, 4228.
- [70] N. U. D. Reshi, A. G. Samuelson, *Appl. Catal. A-Gen.* **2020**, *598*, 117561.
- [71] P. Lara, K. Philippot, B. Chaudret, *ChemCatChem* **2013**, *5*, 28.
- [72] B. Léger, A. Denicourt-Nowicki, H. Olivier-Bourbigou, A. Roucoux, *Inorg. Chem.* **2008**, *47*, 9090.
- [73] D. Gonzalez-Galvez, P. Lara, O. Rivada-Wheelaghan, S. Conejero, B. Chaudret, K. Philippot, P. W. N. M. van Leeuwen, *Catal. Sci. Technol.* **2013**, *3*, 99.
- [74] Z. B. Shifrina, V. G. Matveeva, L. M. Bronstein, *Chem. Rev.* **2020**, *120*, 1350.
- [75] C. Zhao, H. Wang, N. Yan, C. Xiao, X. Mu, P. Dyson, Y. Kou, *J. Catal.* **2007**, *250*, 33.
- [76] N. Yan, J.-g. Zhang, Y. Tong, S. Yao, C. Xiao, Z. Li, Y. Kou, *Chem. Commun.* **2009**, 4423.

- [77] J.-L. Pellegatta, C. Blandy, V. Collière, R. Choukroun, B. Chaudret, P. Cheng, K. Philippot, *J. Mol. Catal. A Chem.* **2002**, *178*, 55.
- [78] X.-d. Mu, J.-q. Meng, Z.-c. Li, Y. Kou, *J. Am. Chem. Soc.* **2005**, *127*, 9694.
- [79] F. Lu, J. Liu, J. Xu, *Adv. Synth. Catal.* **2006**, *348*, 857.
- [80] S. Noël, B. Léger, A. Ponchel, K. Philippot, A. Denicourt-Nowicki, A. Roucoux, E. Monflier, *Catal. Today* **2014**, *235*, 20.
- [81] R. Herbois, S. Noël, B. Léger, L. Bai, A. Roucoux, E. Monflier, A. Ponchel, *Chem. Commun.* **2012**, *48*, 3451.
- [82] M. Chen, Q. Dong, W. Ni, X. Zhao, Q. Gu, G. Tang, D. Li, W. Ma, Z. Hou, *ChemistrySelect* **2017**, *2*, 10537.
- [83] S. Kuklin, A. Maximov, A. Zolotukhina, E. Karakhanov, *Catal. Commun.* **2016**, *73*, 63.
- [84] A. Nowicki, Y. Zhang, B. Léger, J.-P. Rolland, H. Bricout, E. Monflier, A. Roucoux, *Chem. Commun.* **2006**, 296.
- [85] A. Maximov, A. Zolotukhina, V. Murzin, E. Karakhanov, E. Rosenberg, *ChemCatChem* **2015**, *7*, 1197.
- [86] L. M. Bronstein, Z. B. Shifrina, *Chem. Rev.* **2011**, *111*, 5301.
- [87] A.-H. Lu, E. L. Salabas, F. Schüth, *Angew. Chem. Int. Ed.* **2007**, *46*, 1222.
- [88] S. Shylesh, V. Schünemann, W. R. Thiel, *Angew. Chem. Int. Ed.* **2010**, *49*, 3428.
- [89] D. Wang, D. Astruc, *Chem. Rev.* **2014**, *114*, 6949.
- [90] P. Büschelberger, E. Reyes-Rodriguez, C. Schöttle, J. Treptow, C. Feldmann, A. Jacobi von Wangelin, R. Wolf, *Catal. Sci. Technol.* **2018**, *8*, 2648.
- [91] D. Cantillo, M. M. Moghaddam, C. O. Kappe, *J. Org. Chem.* **2013**, *78*, 4530.
- [92] A. Schätz, O. Reiser, W. J. Stark, *Chem. Eur. J.* **2010**, *16*, 8950.
- [93] S. Sun, H. Zeng, *J. Am. Chem. Soc.* **2002**, *124*, 8204.
- [94] Y. Lu, Y. Yin, B. T. Mayers, Y. Xia, *Nano Lett.* **2002**, *2*, 183.
- [95] M. J. Jacinto, P. K. Kiyohara, S. H. Masunaga, R. F. Jardim, L. M. Rossi, *Appl. Catal. A-Gen.* **2008**, *338*, 52.
- [96] M. J. Jacinto, O. H.C.F. Santos, R. Landers, P. K. Kiyohara, L. M. Rossi, *Appl. Catal. B-Environ.* **2009**, *90*, 688.
- [97] M. Nasiruzzaman Shaikh, M. A. Aziz, A. N. Kalanthoden, A. Helal, A. S. Hakeem, M. Bououdina, *Catal. Sci. Technol.* **2018**, *8*, 4709.
- [98] C.-H. Pélisson, A. Denicourt-Nowicki, A. Roucoux, *ACS Sustain. Chem. Eng.* **2016**, *4*, 1834.
- [99] C.-H. Pélisson, L. L.R. Vono, C. Hubert, A. Denicourt-Nowicki, L. M. Rossi, A. Roucoux, *Catal. Today* **2012**, *183*, 124.
- [100] Q. M. Kainz, S. Fernandes, C. M. Eichenseer, F. Besostri, H. Körner, R. Müller, O. Reiser, *Faraday Discuss.* **2014**, *175*, 27.
- [101] Q. M. Kainz, O. Reiser, *Acc. Chem. Res.* **2014**, *47*, 667.
- [102] R. N. Grass, E. K. Athanassiou, W. J. Stark, *Angew. Chem. Int. Ed.* **2007**, *46*, 4909.
- [103] S. Wittmann, A. Schätz, R. N. Grass, W. J. Stark, O. Reiser, *Angew. Chem. Int. Ed.* **2010**, *49*, 1867.
- [104] G. Purohit, D. S. Rawat, O. Reiser, *ChemCatChem* **2020**, *12*, 569.
- [105] C. M. Eichenseer, B. Kastl, M. A. Pericàs, P. R. Hanson, O. Reiser, *ACS Sustain. Chem. Eng.* **2016**, *4*, 2698.
- [106] Q. M. Kainz, R. Linhardt, R. N. Grass, G. Vilé, J. Pérez-Ramírez, W. J. Stark, O. Reiser, *Adv. Funct. Mater.* **2014**, *24*, 2020.
- [107] L. Stadler, M. Homafar, A. Hartl, S. Najafshirtari, M. Colombo, R. Zboril, P. Martin, M. B. Gawande, J. Zhi, O. Reiser, *ACS Sustain. Chem. Eng.* **2019**, *7*, 2388.

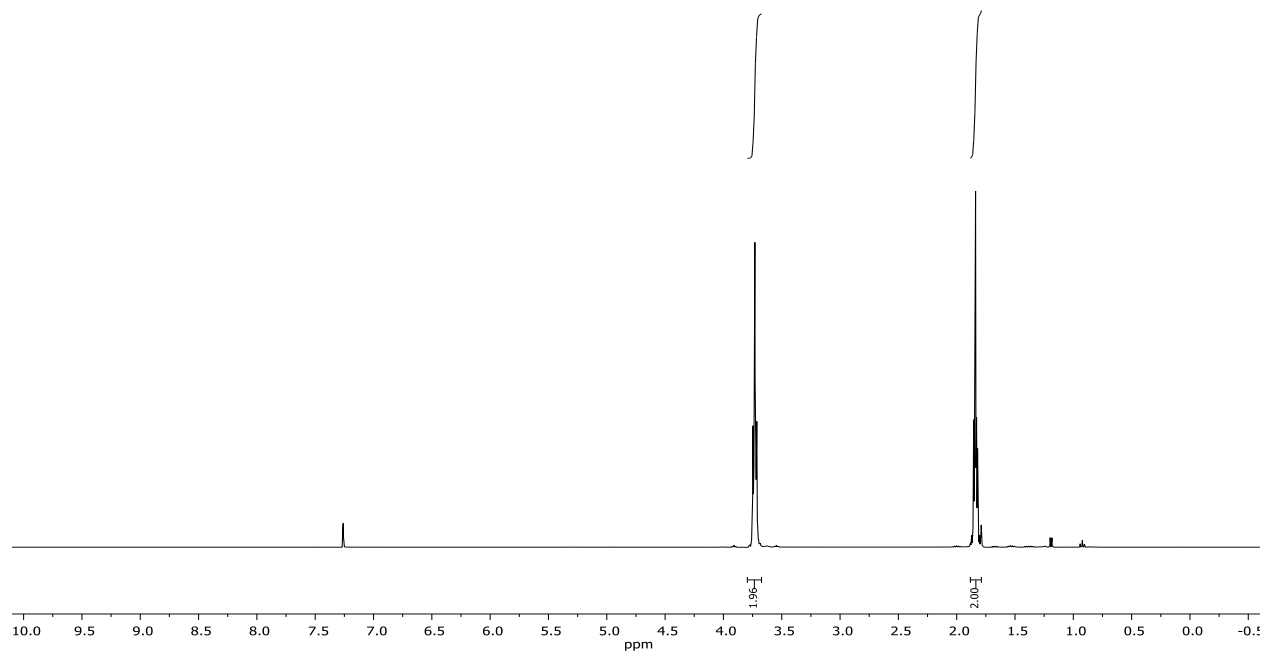
- [108] Q. Sun, Z. Dai, X. Meng, F.-S. Xiao, *Chem. Soc. Rev.* **2015**, *44*, 6018.
- [109] B. Kastl, *Dissertation*, Universität Regensburg, Regensburg, **2018**.
- [110] S. Fernandes, C. M. Eichenseer, P. Kreitmeier, J. Rewitzer, V. Zlateski, R. N. Grass, W. J. Stark, O. Reiser, *RSC Adv.* **2015**, *5*, 46430.
- [111] L. Gao, K. Kojima, H. Nagashima, *Tetrahedron* **2015**, *71*, 6414.
- [112] A. Maximov, A. Zolotukhina, L. Kulikov, Y. Kardasheva, E. Karakhanov, *Reac. Kinet. Mech. Cat.* **2016**, *117*, 729.
- [113] C. Moreno-Marrodan, F. Liguori, E. Mercadé, C. Godard, C. Claver, P. Barbaro, *Catal. Sci. Technol.* **2015**, *5*, 3762.
- [114] M. Siebels, C. Schlüsener, J. Thomas, Y.-X. Xiao, X.-Y. Yang, C. Janiak, *J. Mater. Chem. A* **2019**, *7*, 11934.
- [115] B. Li, R. Gong, W. Wang, X. Huang, W. Zhang, H. Li, C. Hu, B. Tan, *Macromolecules* **2011**, *44*, 2410.
- [116] R. Marcos Esteban, K. Schütte, D. Marquardt, J. Barthel, F. Beckert, R. Mülhaupt, C. Janiak, *Nano-Struct. Nano-Objects* **2015**, *2*, 28.
- [117] C. Ortiz-Cervantes, I. Iyañez, J. J. García, *J. Phys. Org. Chem.* **2012**, *25*, 902.
- [118] M. Zahmakiran, Y. Tonbul, S. Ozkar, *J. Am. Chem. Soc.* **2010**, *132*, 6541.
- [119] L. Yu, M. A. Matthews, *Int. J. Hydrogen Energ.* **2011**, *36*, 7416.
- [120] M. Zahmakiran, S. Ozkar, *Langmuir* **2009**, *25*, 2667.
- [121] A. Dikhtiarenko, S. A. Khainakov, J. R. García, J. Gimeno, I. de Pedro, J. R. Fernández, J. A. Blanco, *J. Alloy. Compd.* **2012**, *536S*, 437.
- [122] A. M. Signori, K. d. O. Santos, R. Eising, B. L. Albuquerque, F. C. Giacomelli, J. B. Domingos, *Langmuir* **2010**, *26*, 17772.
- [123] F. J. Urbano, J. M. Marinas, *J. Mol. Catal. A Chem.* **2001**, *173*, 329.
- [124] European Medicines Agency, *ICH guideline Q3D (R1) on elemental impurities*, **2019**.
- [125] R. M. Skomoroski, A. Schriesheim, *J. Phys. Chem.* **1961**, *65*, 1340.
- [126] D. W. C. MacMillan, *Nature* **2008**, *455*, 304.
- [127] J. Seayad, B. List, *Org. Biomol. Chem.* **2005**, *3*, 719.
- [128] T. Akiyama, J. Itoh, K. Fuchibe, *Adv. Synth. Catal.* **2006**, *348*, 999.
- [129] D. Parmar, E. Sugiono, S. Raja, M. Rueping, *Chem. Rev.* **2014**, *114*, 9047.
- [130] A. Zamfir, S. Schenker, M. Freund, S. B. Tsogoeva, *Org. Biomol. Chem.* **2010**, *8*, 5262.
- [131] L. Osorio-Planes, C. Rodríguez-Esrich, M. A. Pericàs, *Chem. Eur. J.* **2014**, *20*, 2367.
- [132] D. S. Kundu, J. Schmidt, C. Bleschke, A. Thomas, S. Blechert, *Angew. Chem. Int. Ed.* **2012**, *51*, 5456.
- [133] M. Rueping, E. Sugiono, A. Steck, T. Theissmann, *Adv. Synth. Catal.* **2010**, *352*, 281.
- [134] X. Zhang, A. Kormos, J. Zhang, *Org. Lett.* **2017**, *19*, 6072.
- [135] R. Dawson, L. A. Stevens, T. C. Drage, C. E. Snape, M. W. Smith, D. J. Adams, A. I. Cooper, *J. Am. Chem. Soc.* **2012**, *134*, 10741.
- [136] D. Uraguchi, M. Terada, *J. Am. Chem. Soc.* **2004**, *126*, 5356.
- [137] T. Akiyama, J. Itoh, K. Yokota, K. Fuchibe, *Angew. Chem. Int. Ed.* **2004**, *43*, 1566.
- [138] L. Simón, J. M. Goodman, *J. Org. Chem.* **2011**, *76*, 1775.
- [139] Q. Kang, Z.-A. Zhao, S.-L. You, *J. Am. Chem. Soc.* **2007**, *129*, 1484.
- [140] J. P. Kutney in *Total Synthesis of Natural Products*, John Wiley & Sons, Ltd, **2007**, pp. 273–438.
- [141] S. Hibino, T. Choshi, *Nat. Prod. Rep.* **2002**, *19*, 148.
- [142] O. El-Sepelgy, S. Haseloff, S. K. Alamsetti, C. Schneider, *Angew. Chem. Int. Ed.* **2014**, *53*, 7923.

- [143] K. C. Nicolaou, J. A. Pfefferkorn, A. J. Roecker, G.-Q. Cao, S. Barluenga, H. J. Mitchell, *J. Am. Chem. Soc.* **2000**, *122*, 9939.
- [144] D. Tian, S. G. Das, J. M. Doshi, J. Peng, J. Lin, C. Xing, *Cancer Lett.* **2008**, *259*, 198.
- [145] D. Salni, M. V. Sargent, B. W. Skelton, I. Soediro, M. Sutisna, A. H. White, E. Yulinah, *Aust. J. Chem.* **2002**, *55*, 229.
- [146] R. Dawson, T. Ratvijitvech, M. Corker, A. Laybourn, Y. Z. Khimiyak, A. I. Cooper, D. J. Adams, *Polym. Chem.* **2012**, *3*, 2034.
- [147] M. Rueping, E. Sugiono, C. Azap, T. Theissmann, M. Bolte, *Org. Lett.* **2005**, *7*, 3781.
- [148] B. Li, F. Su, H.-K. Luo, L. Liang, B. Tan, *Microporous and Mesoporous Materials* **2011**, *138*, 207.
- [149] M. Hatano, K. Moriyama, T. Maki, K. Ishihara, *Angew. Chem. Int. Ed.* **2010**, *49*, 3823.
- [150] S. Hünig, G. Märkl, J. Sauer, P. Kreitmeier, *Arbeitsmethoden in der organischen Chemie*, Verlag Lehmanns Media, Köln, **2019**.
- [151] M. Noji, M. Nakajima, K. Koga, *Tetrahedron Lett.* **1994**, *35*, 7983.
- [152] Qiao-Sheng Hu, D. Vitharana, Lin Pu, *Tetrahedron Asymmetry* **1995**, *6*, 2123.
- [153] A.-H. Li, D. Beard, H. Coate, A. Honda, M. Kadalbajoo, A. Kleinberg, R. Laufer, K. Mulvihill, A. Nigro, P. Rastogi et al., *Synthesis* **2010**, *2010*, 1678.
- [154] P. Wipf, J. K. Jung, *J. Org. Chem.* **2000**, *65*, 6319.
- [155] M. Klussmann, L. Ratjen, S. Hoffmann, V. Wakchaure, R. Goddard, B. List, *Synlett* **2010**, *2010*, 2189.
- [156] S. Kobayashi, K.-i. Kusakabe, S. Komiyama, H. Ishitani, *J. Org. Chem.* **1999**, *64*, 4220.
- [157] R. I. Storer, D. E. Carrera, Y. Ni, D. W. C. MacMillan, *J. Am. Chem. Soc.* **2006**, *128*, 84.
- [158] M. Anryu, D. Fukushima, US2013270544 (A1) **2011**.
- [159] M. Sickert, F. Abels, M. Lang, J. Sieler, C. Birkemeyer, C. Schneider, *Chem. Eur. J.* **2010**, *16*, 2806.
- [160] S. Saha, C. Schneider, *Chem. Eur. J.* **2015**, *21*, 2348.
- [161] A. G. Wenzel, E. N. Jacobsen, *J. Am. Chem. Soc.* **2002**, *124*, 12964.
- [162] B. E. Love, P. S. Raje, T. C. Williams II, *Synlett* **1994**, *1994*, 493.
- [163] N. Meisinger, L. Roiser, U. Monkowius, M. Himmelsbach, R. Robiette, M. Waser, *Chem. Eur. J.* **2017**, *23*, 5137.
- [164] B. C. Das, A. V. Madhukumar, J. Anguiano, S. Mani, *Bioorg. Med. Chem. Lett.* **2009**, *19*, 4204.

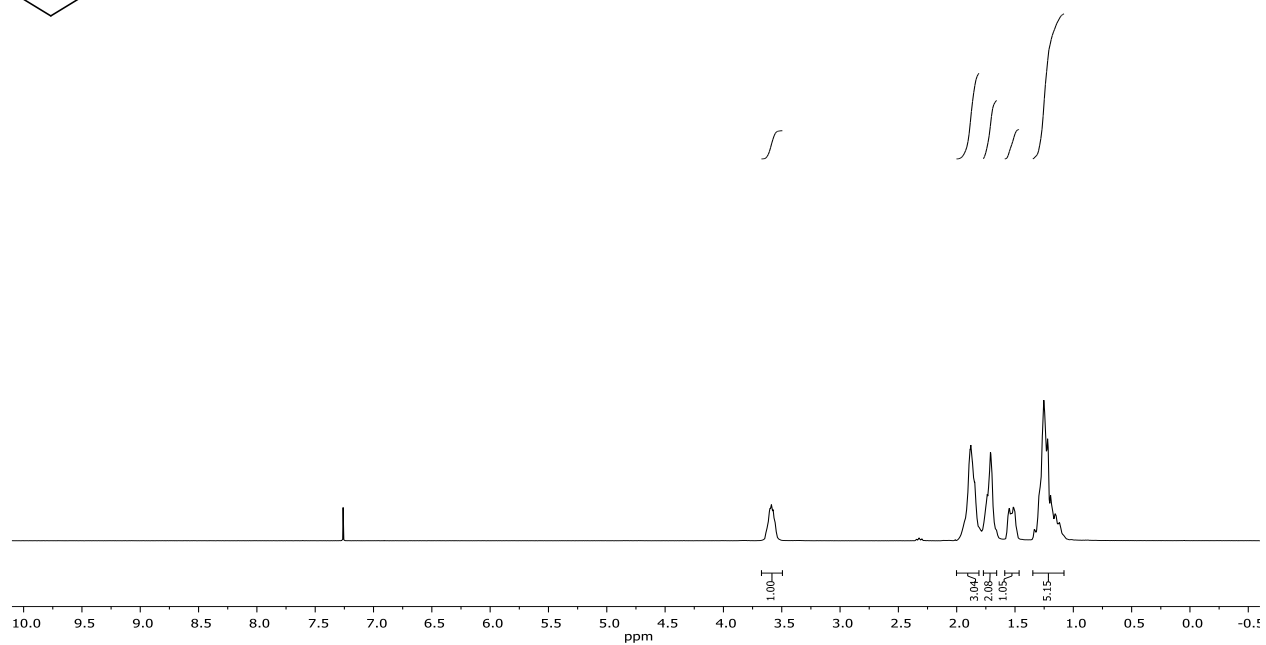
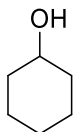
G. Appendix

1. NMR Spectra

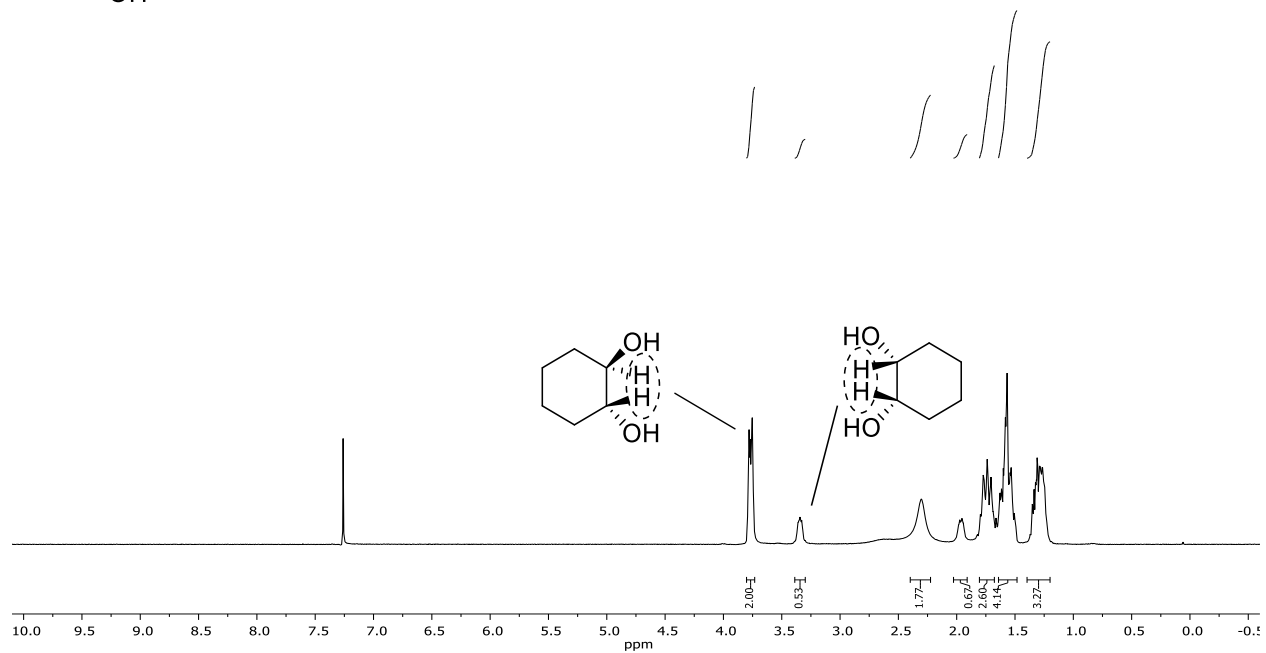
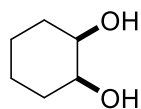
Tetrahydrofuran (25)



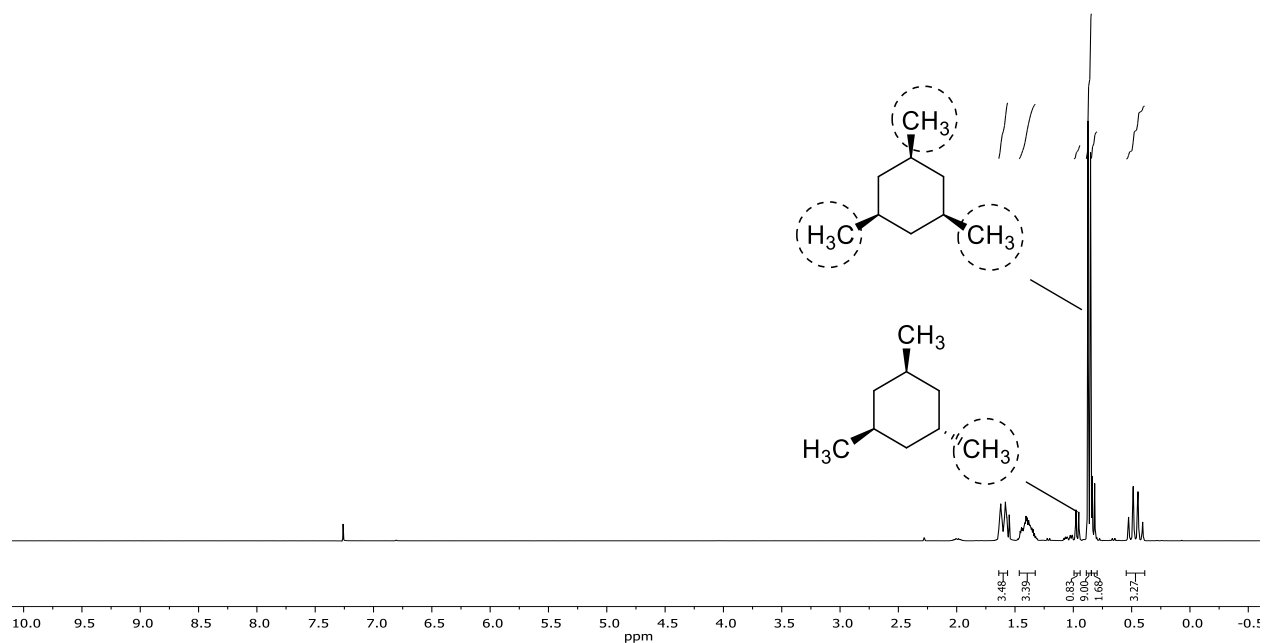
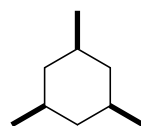
Cyclohexanol (3)



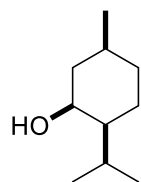
1,2-cyclohexanediol (105)



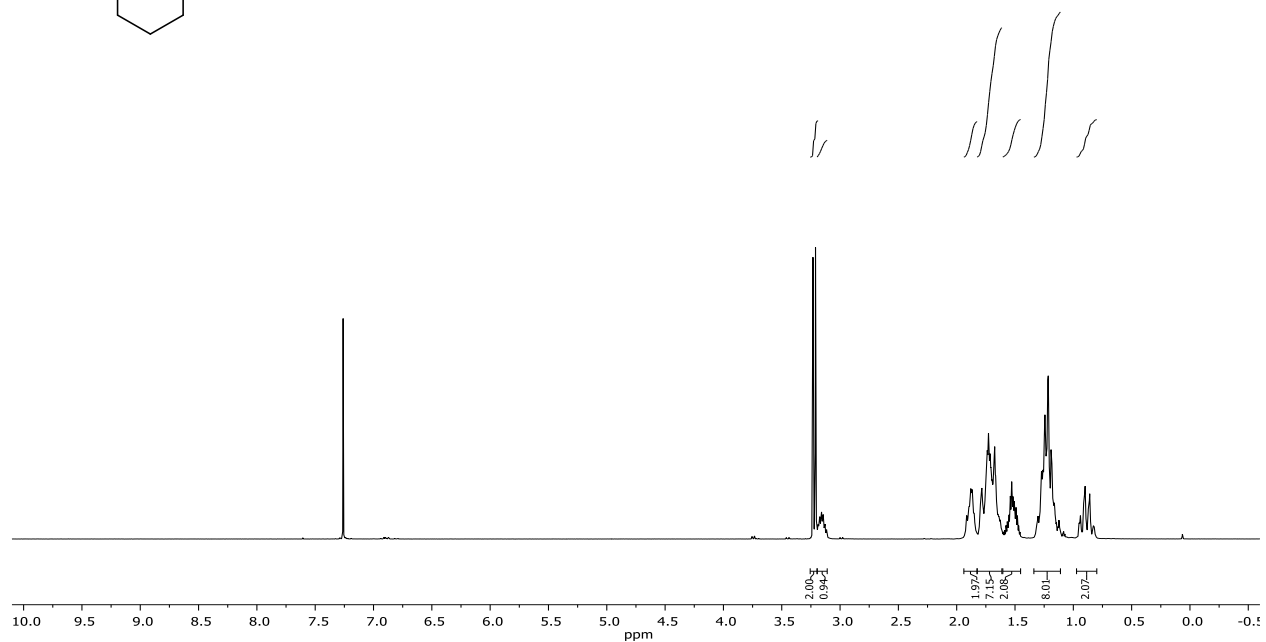
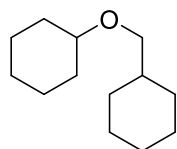
1,3,5-trimethylcyclohexane (107)



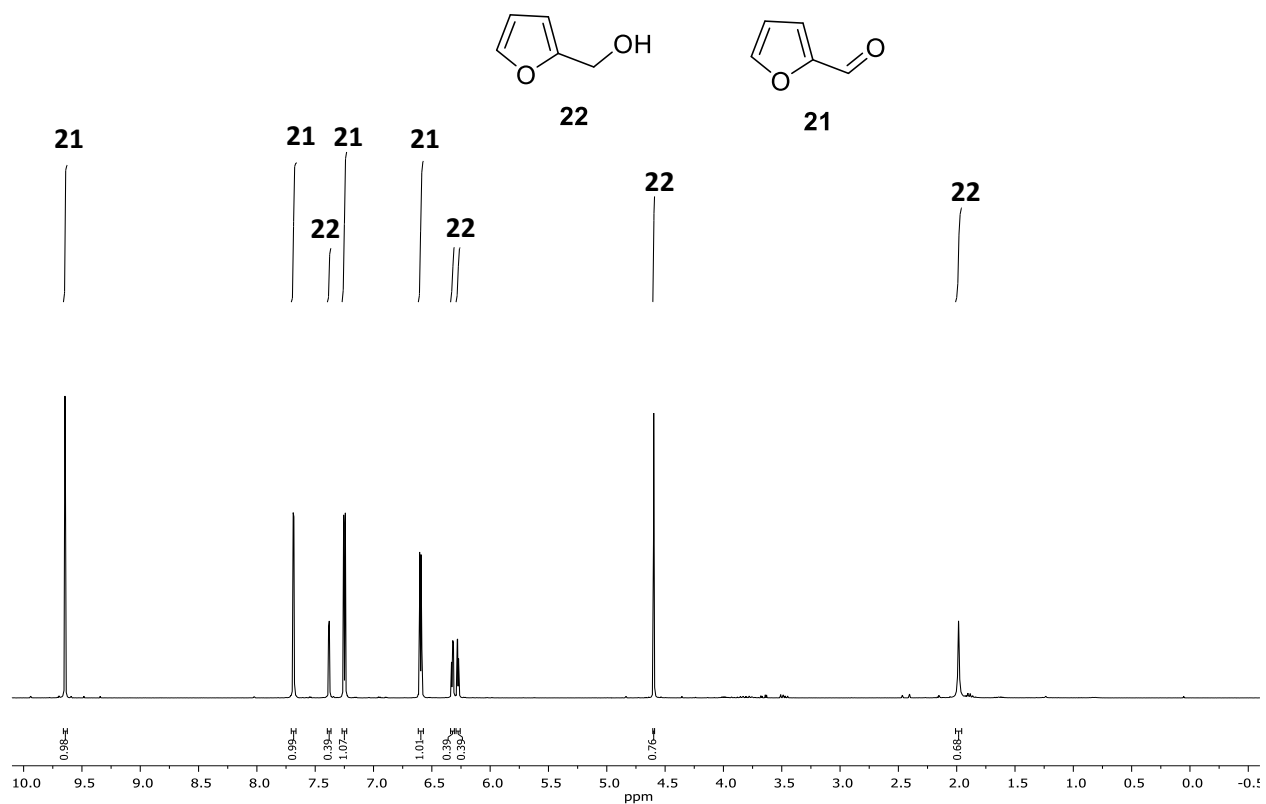
2-isopropyl-5-methyl-cyclohexan-1-ol (14)



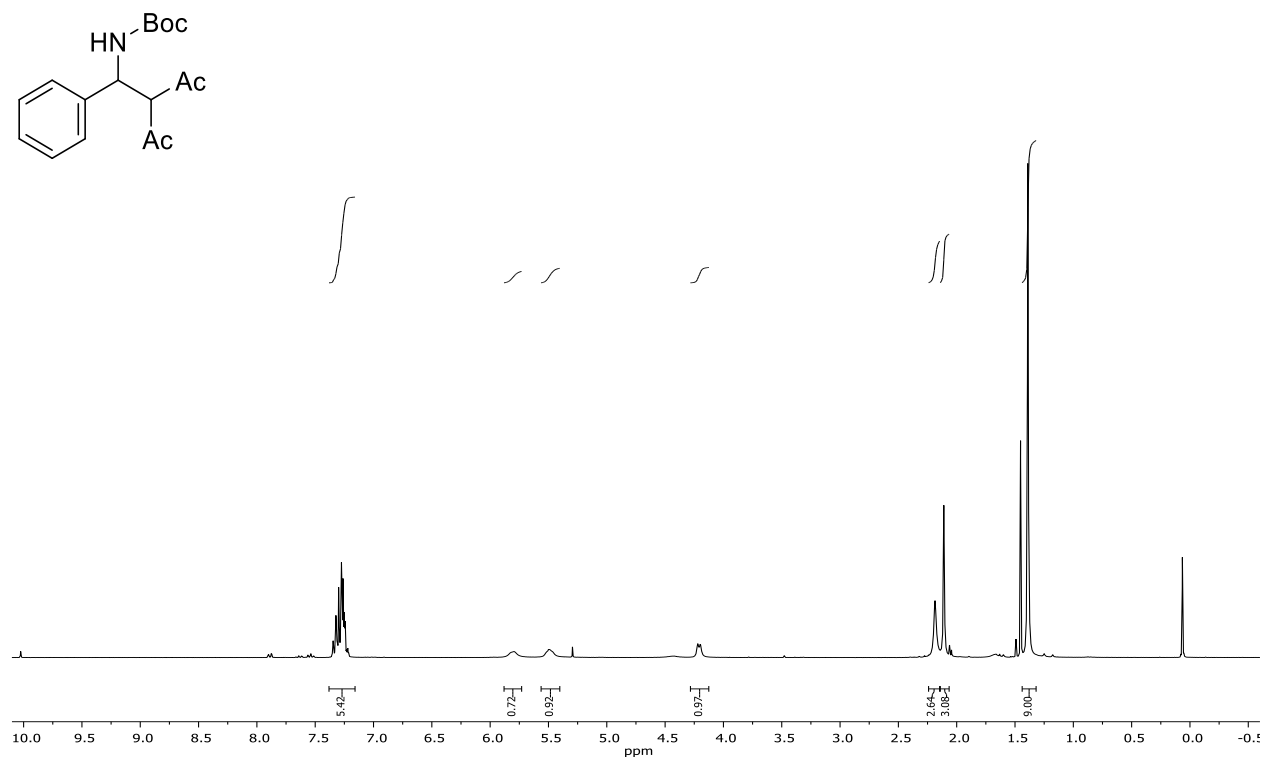
(Cyclohexylmethoxy)cyclohexane (109)



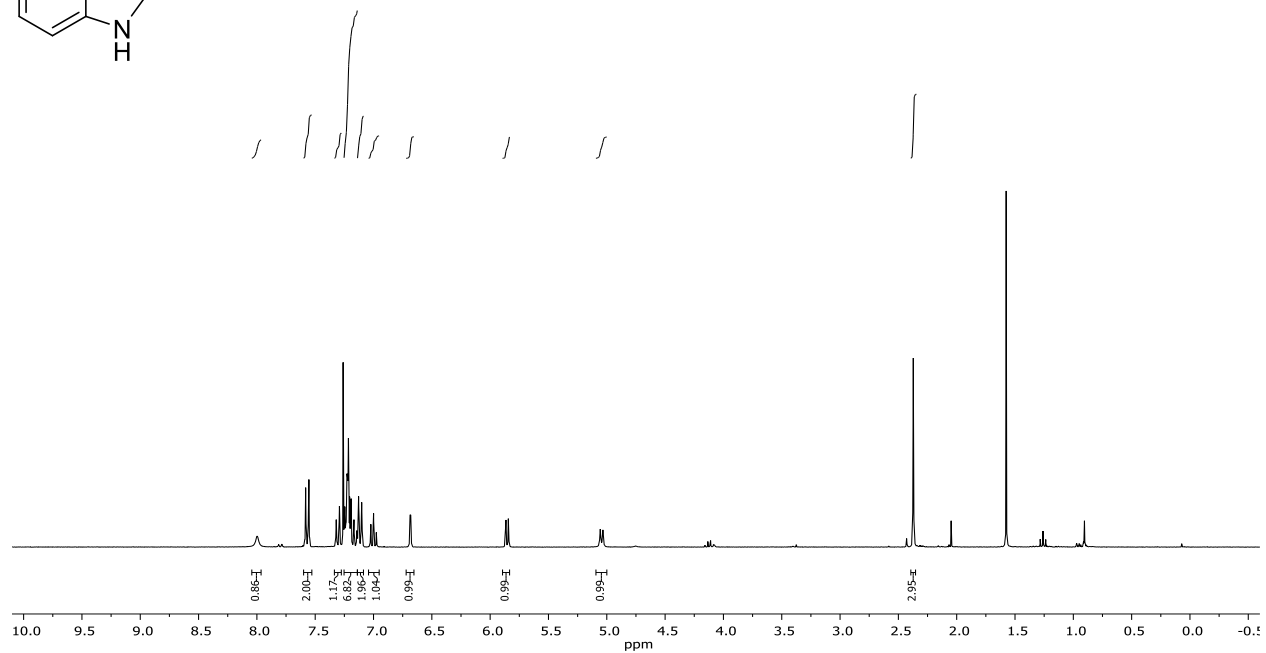
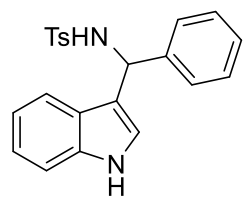
Furfuryl alcohol (22)



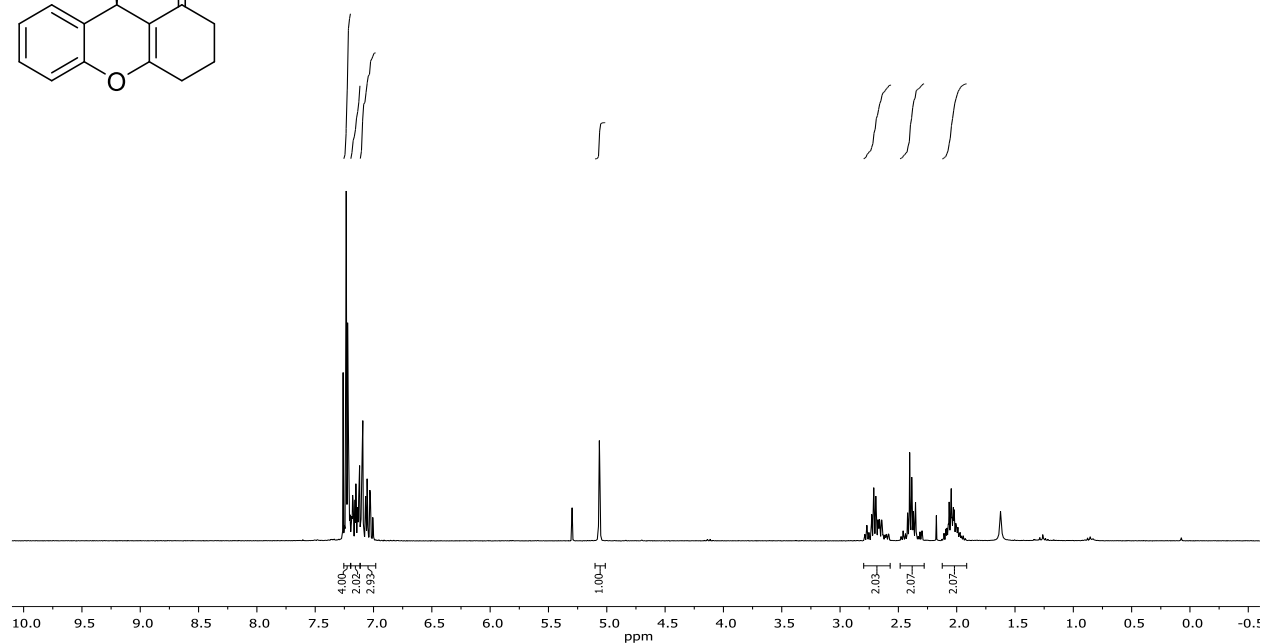
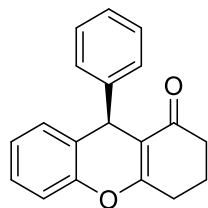
tert-butyl (2-acetyl-3-oxo-1-phenylbutyl)carbamate (131)



N-((1H-indol-3-yl)(phenyl)methyl)-4-methylbenzenesulfonamide (134)

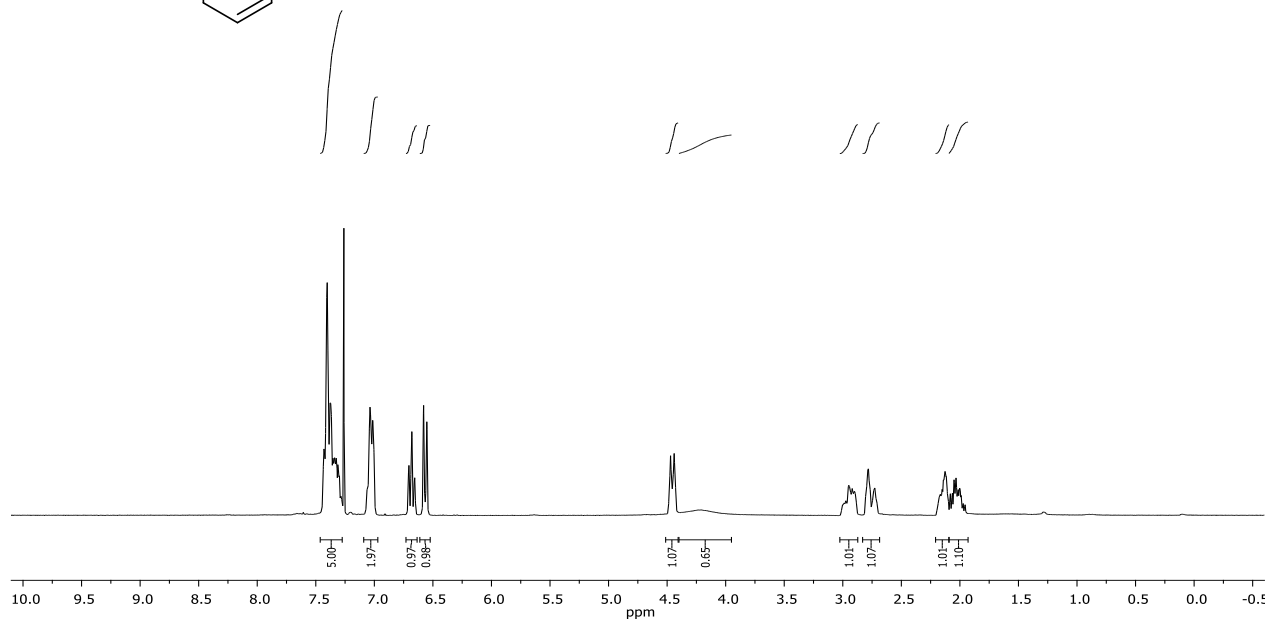
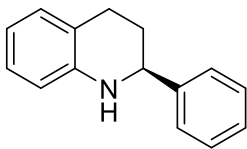


(R)-9-phenyl-2,3,4,9-tetrahydro-1H-xanthen-1-one (138)

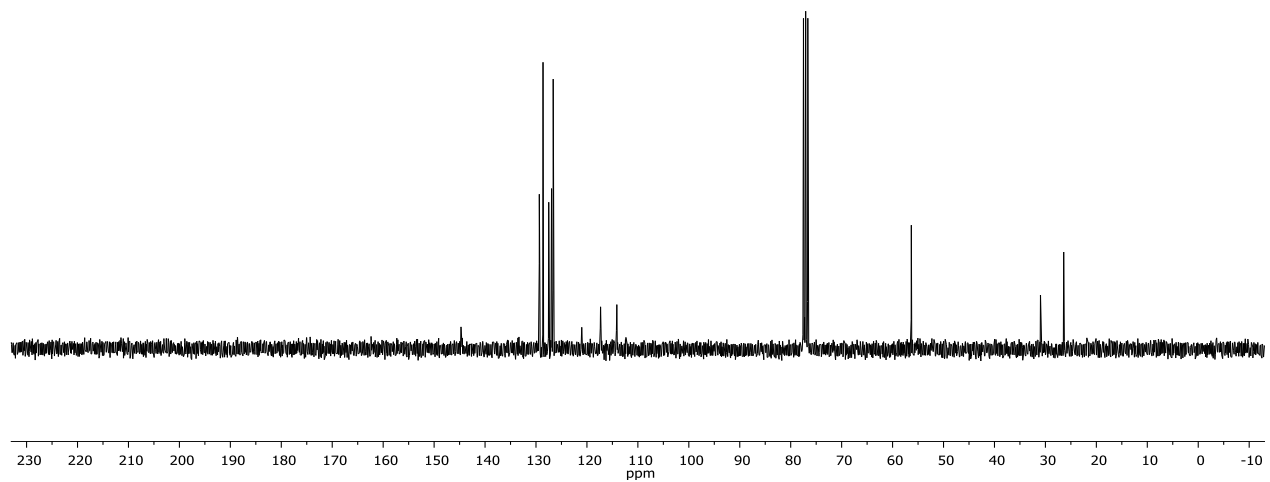


(S)-2-phenyl-1,2,3,4-tetrahydroquinoline (44a)

¹H-NMR (300 MHz, CDCl₃)

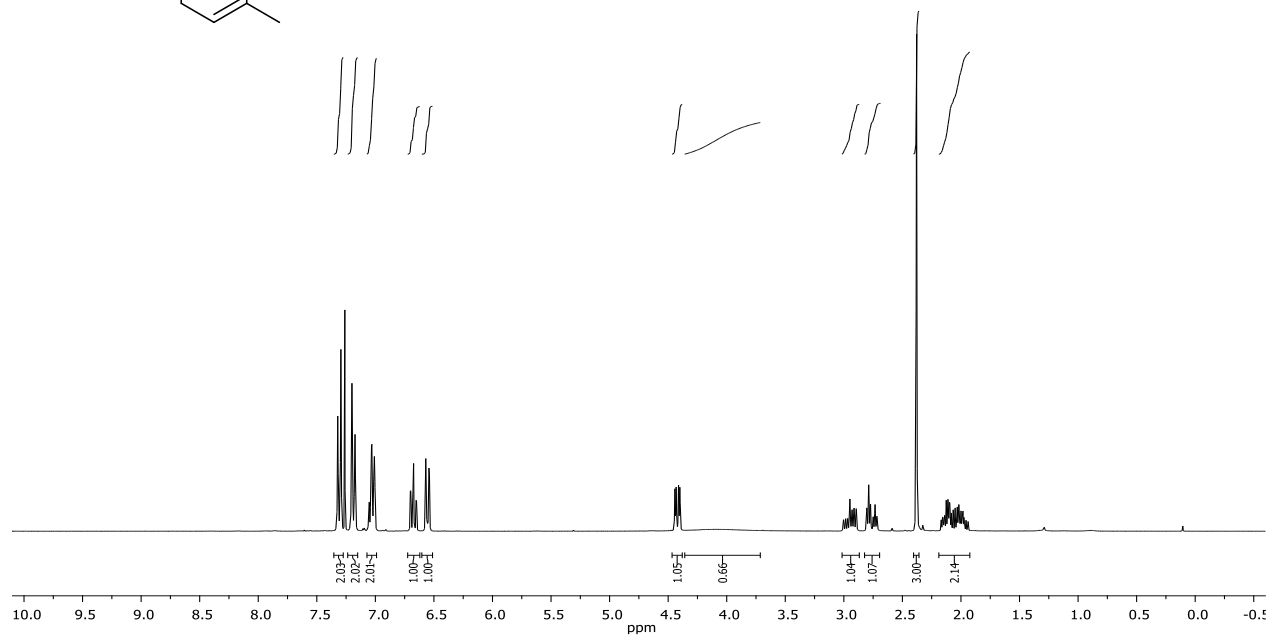
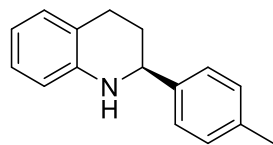


¹³C-NMR (75 MHz, CDCl₃)

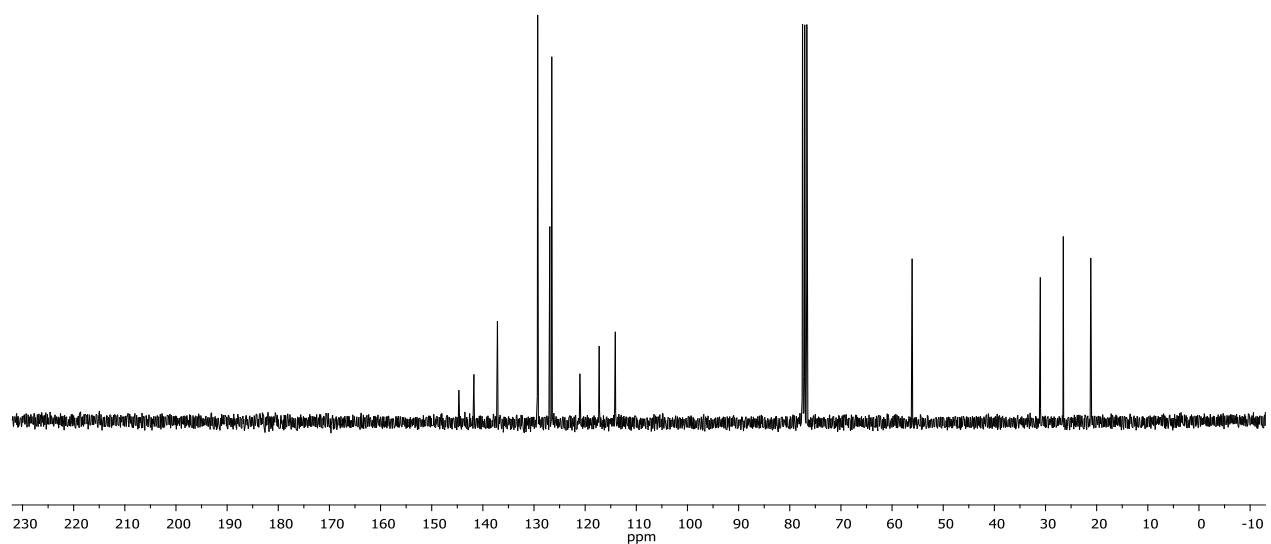


(S)-2-(p-tolyl)-1,2,3,4-tetrahydroquinoline (44b)

¹H-NMR (300 MHz, CDCl₃)

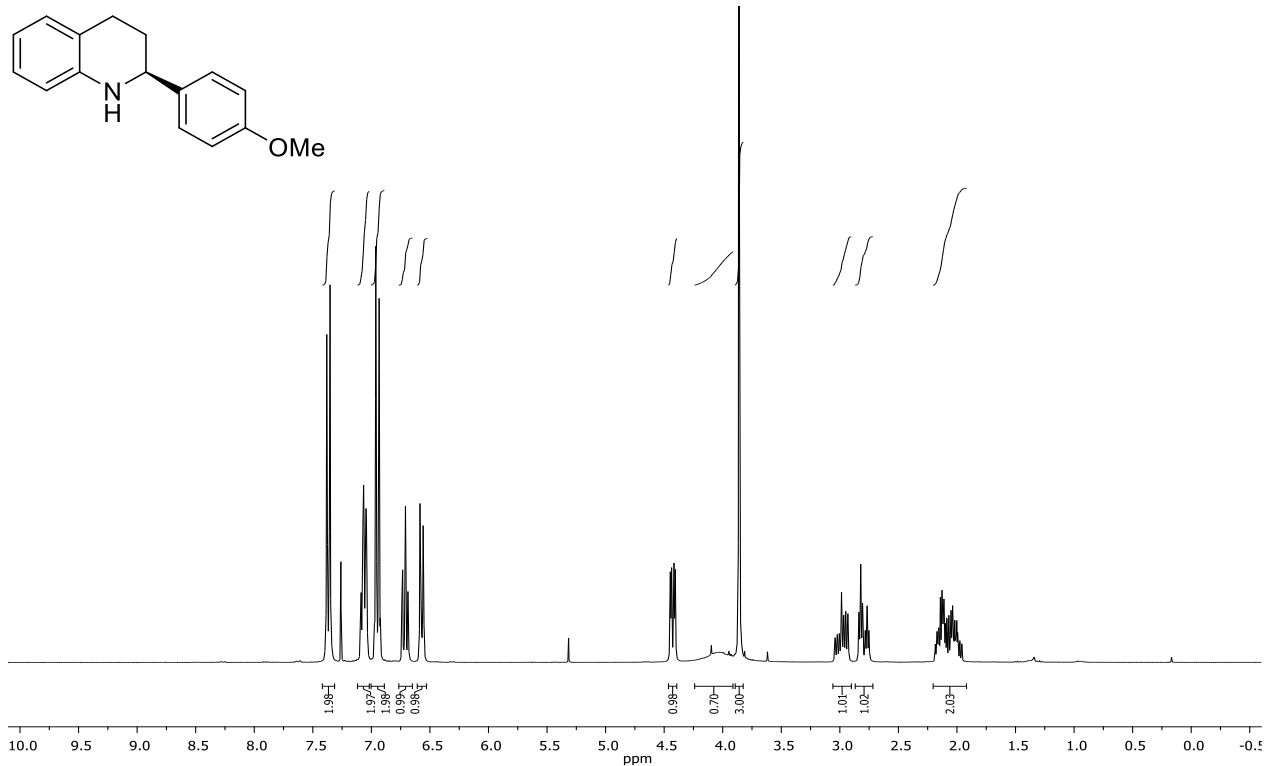


¹³C-NMR (75 MHz, CDCl₃)

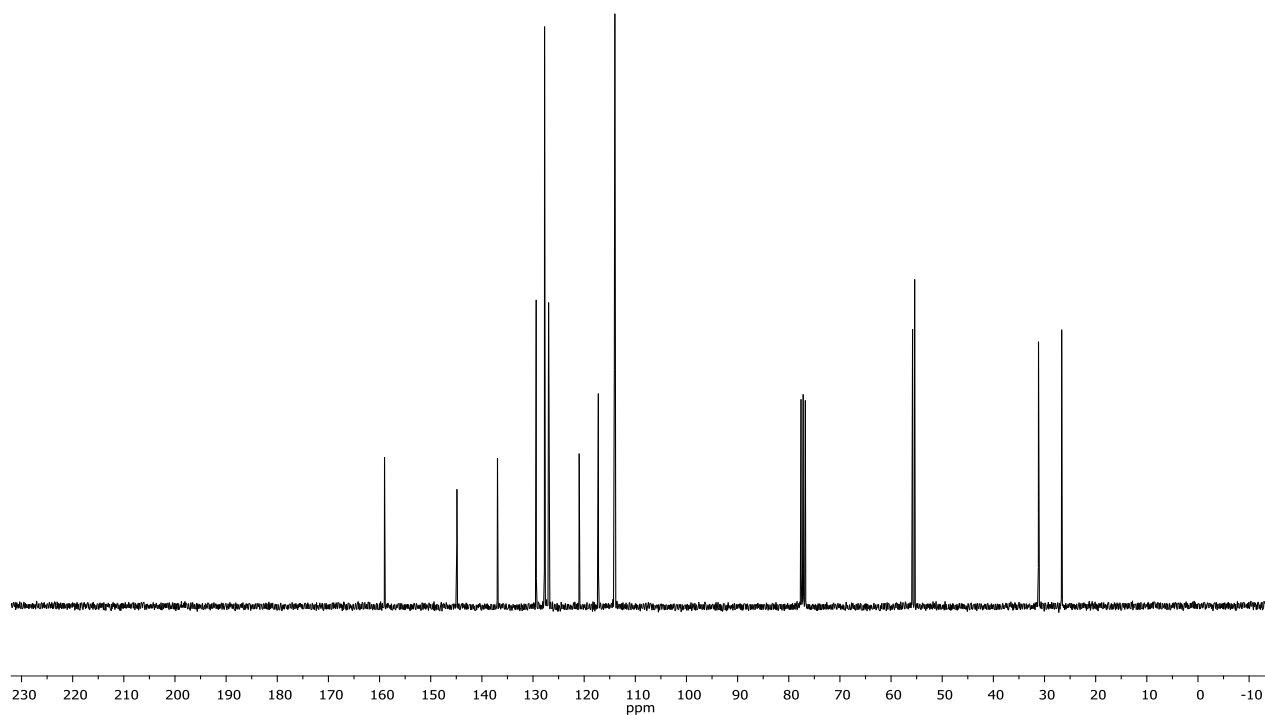


(S)-2-(4-methoxyphenyl)-1,2,3,4-tetrahydroquinoline (44c)

¹H-NMR (300 MHz, CDCl₃)

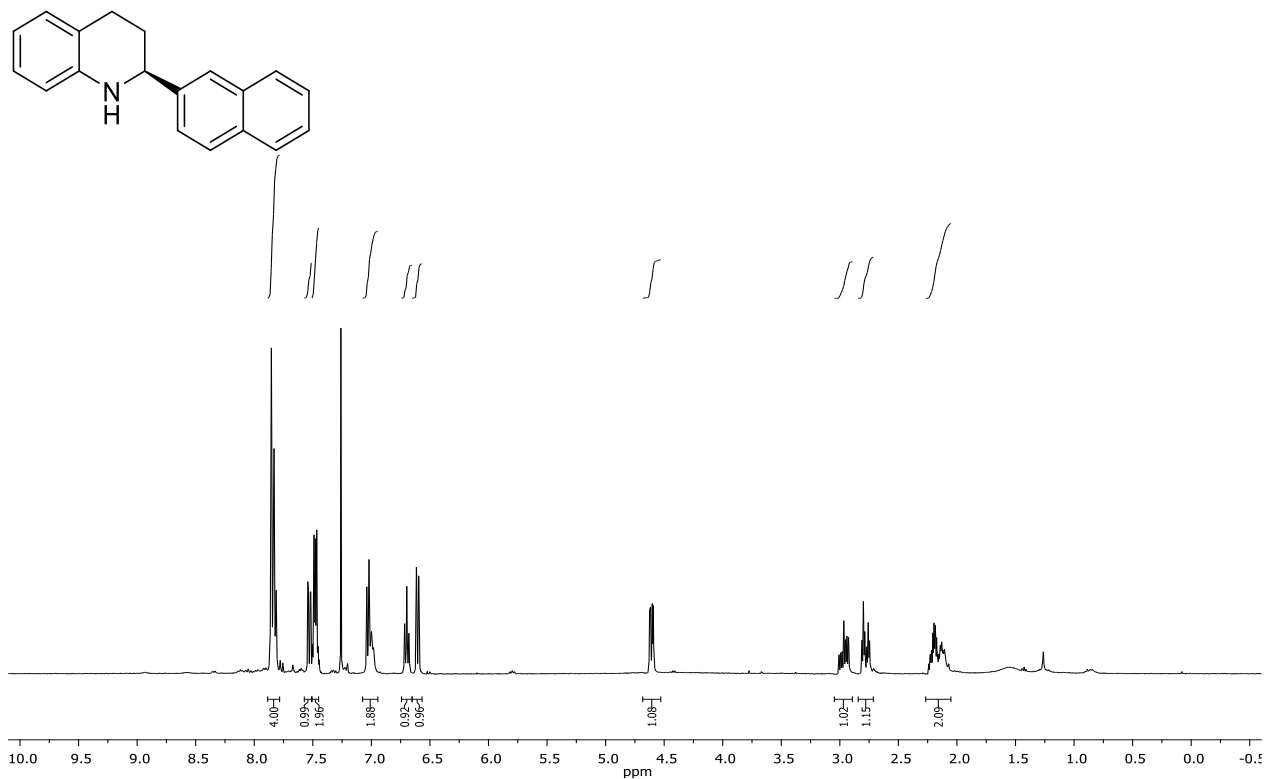


¹³C-NMR (75 MHz, CDCl₃)

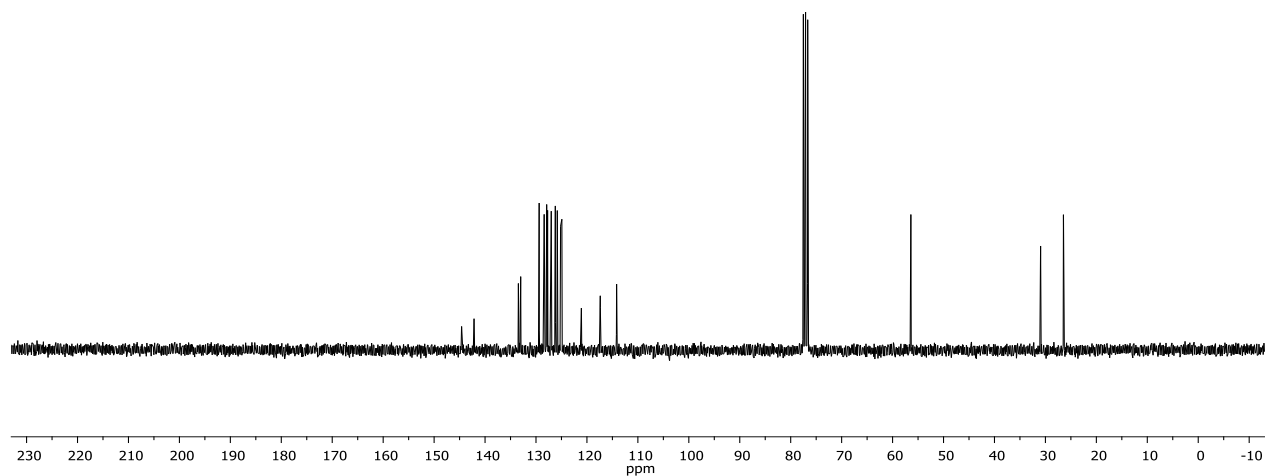


(S)-2-(naphthalen-2-yl)-1,2,3,4-tetrahydroquinoline (44d)

¹H-NMR (300 MHz, CDCl₃)

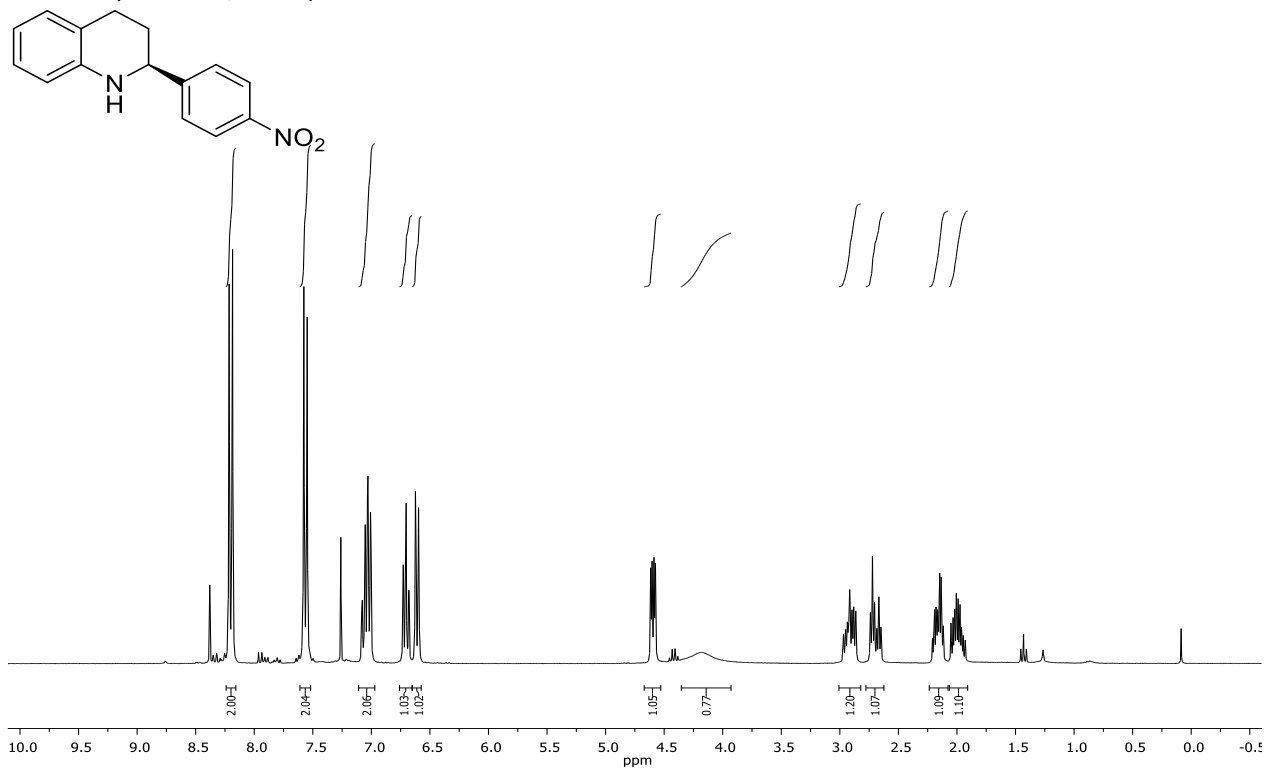


¹³C-NMR (75 MHz, CDCl₃)

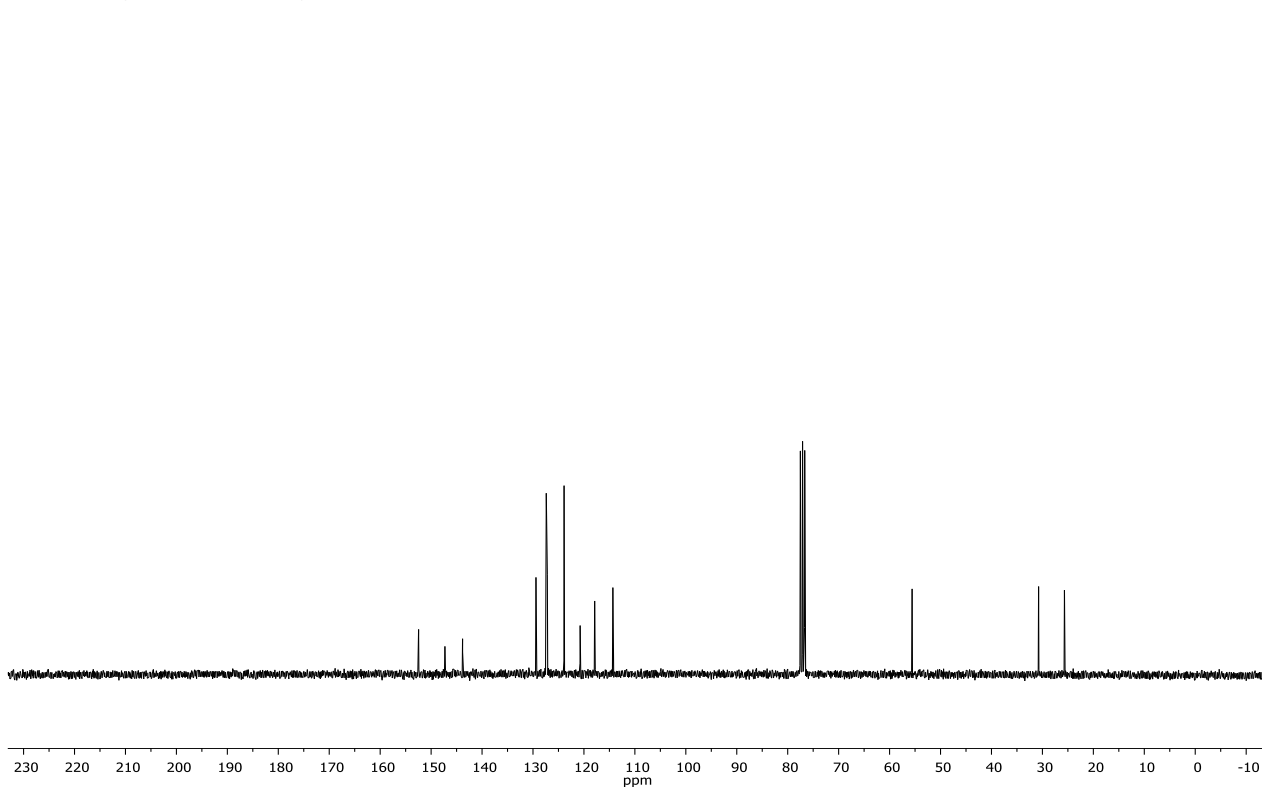


(S)-2-(4-nitrophenyl)-1,2,3,4-tetrahydroquinoline (44e)

¹H-NMR (300 MHz, CDCl₃)

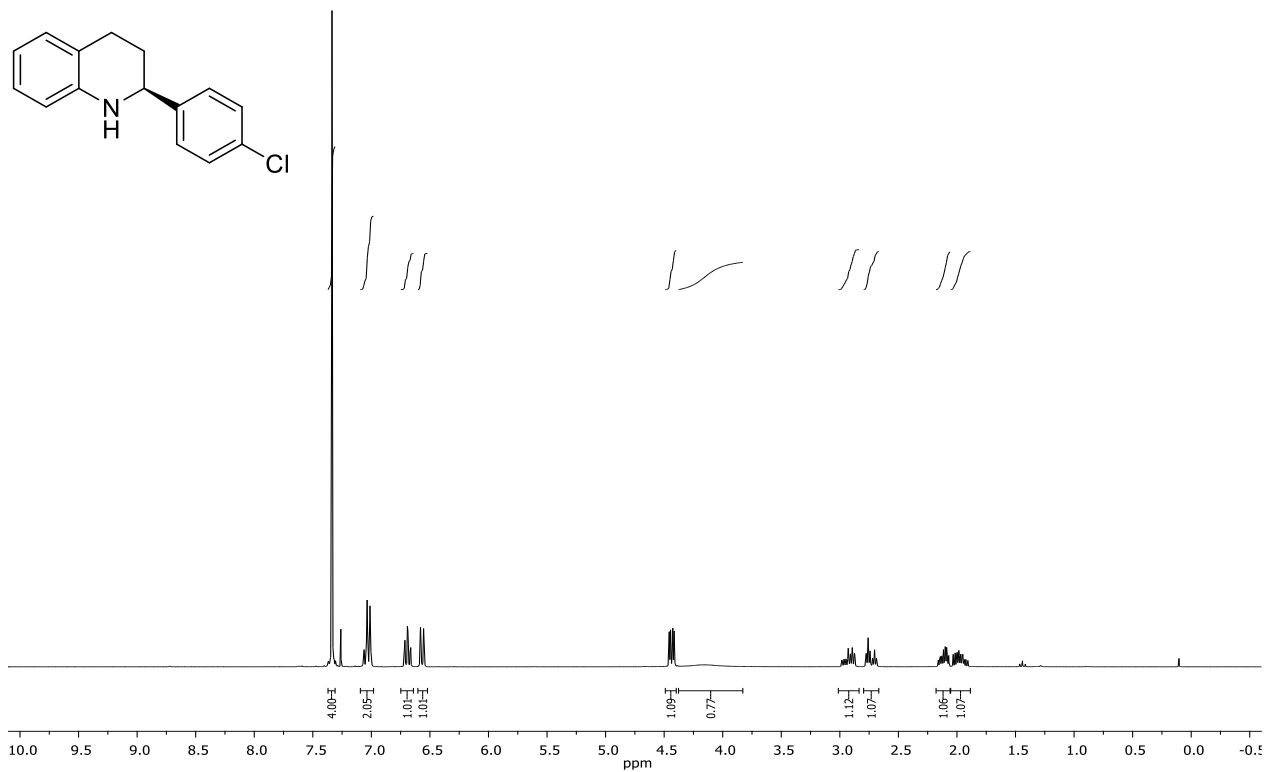


¹³C-NMR (75 MHz, CDCl₃)

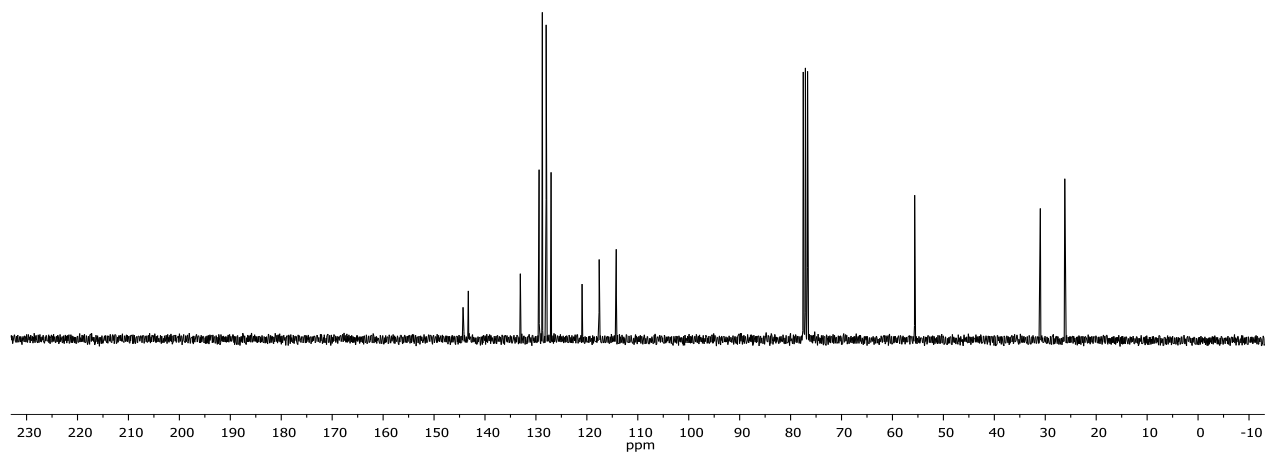


(S)-2-(4-chlorophenyl)-1,2,3,4-tetrahydroquinoline (44f)

¹H-NMR (300 MHz, CDCl₃)

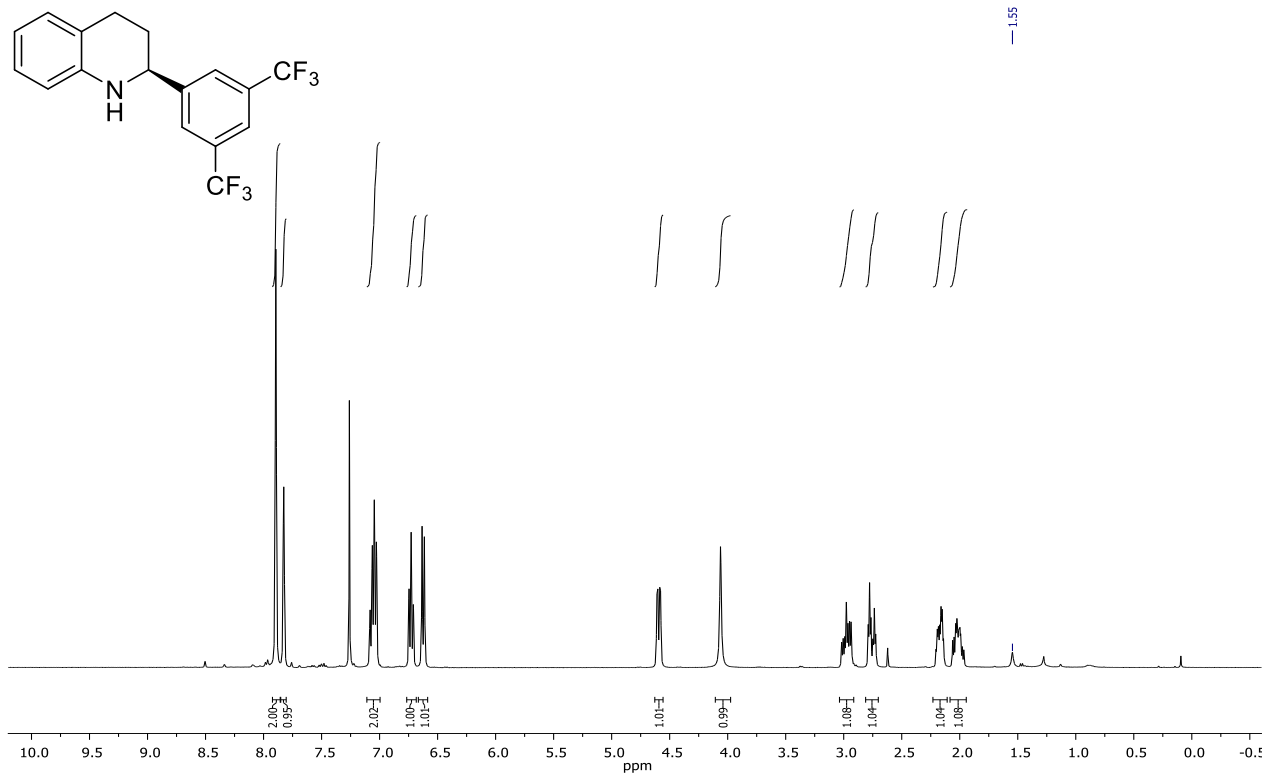


¹³C-NMR (75 MHz, CDCl₃)

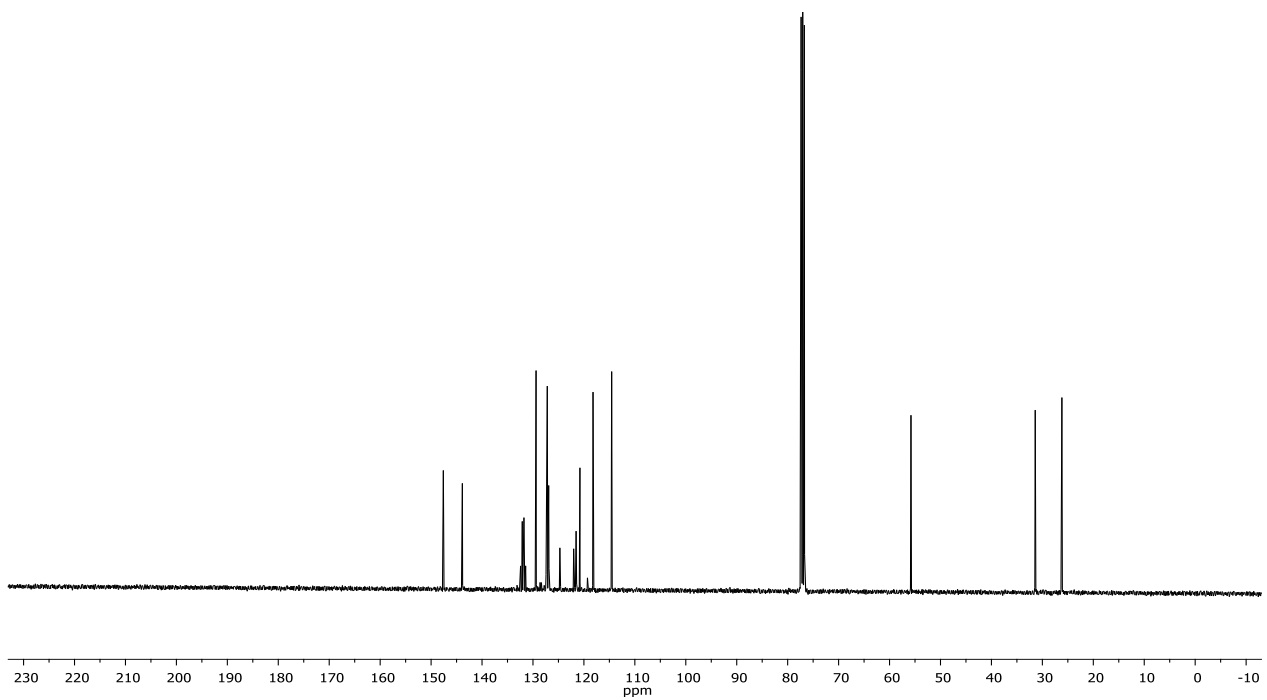


(S)-2-(3,5-bis(trifluoromethyl)phenyl)-1,2,3,4-tetrahydroquinoline (44g)

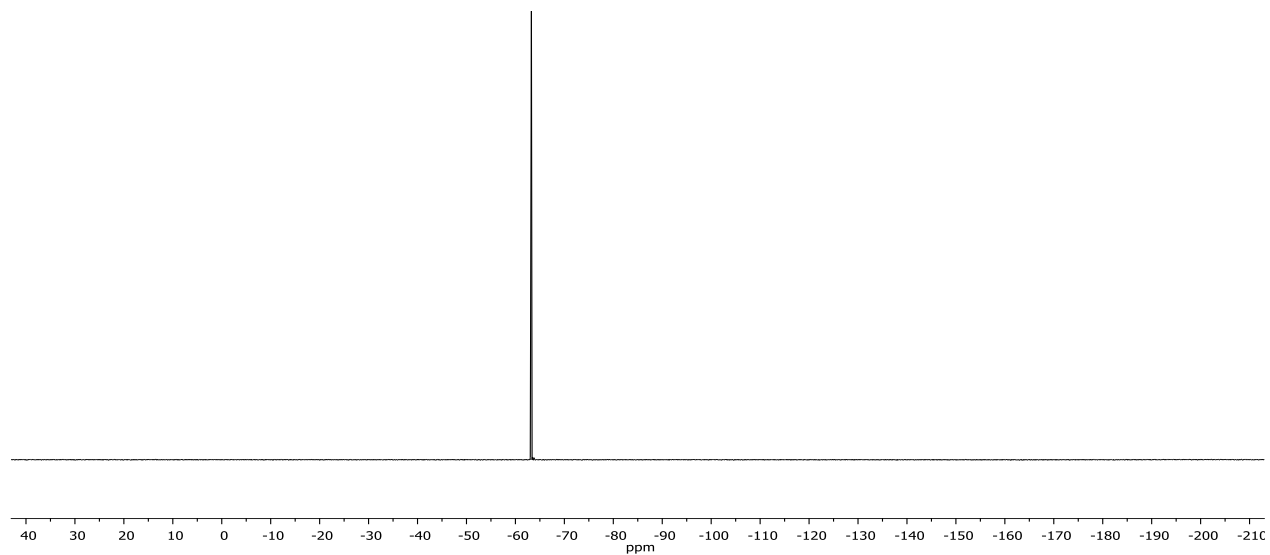
¹H-NMR (400 MHz, CDCl₃)



¹³C-NMR (101 MHz, CDCl₃)

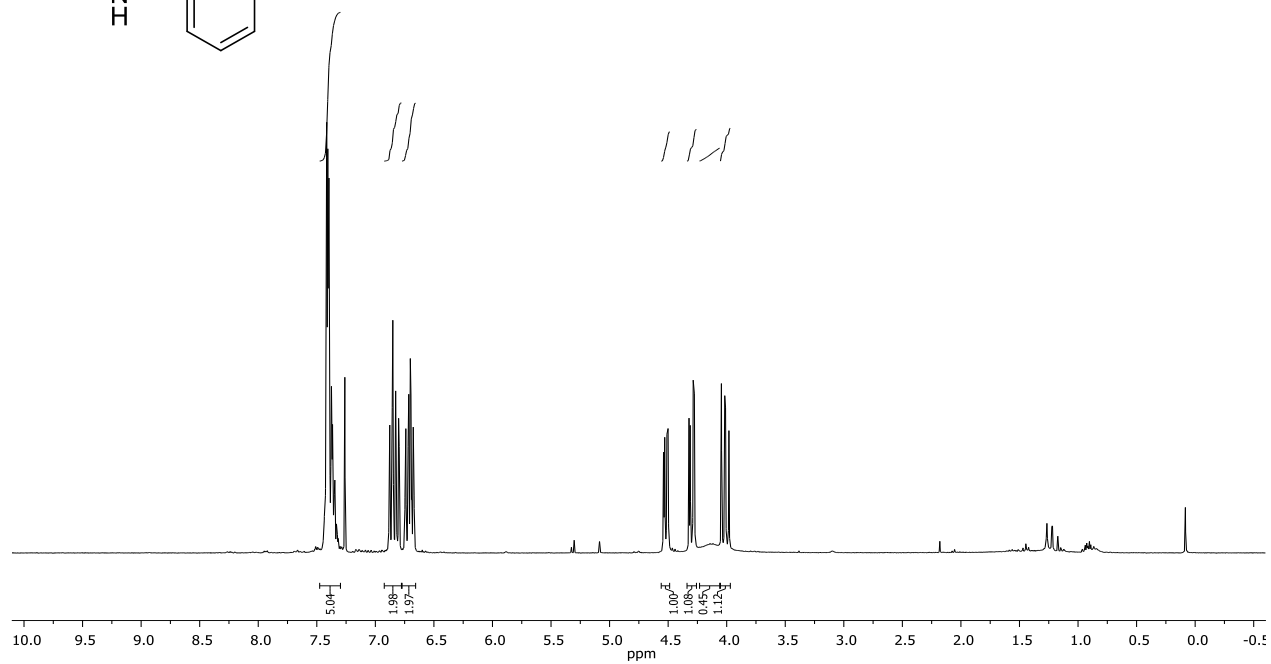
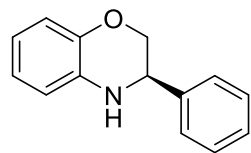


^{19}F -NMR (376 MHz, CDCl_3)

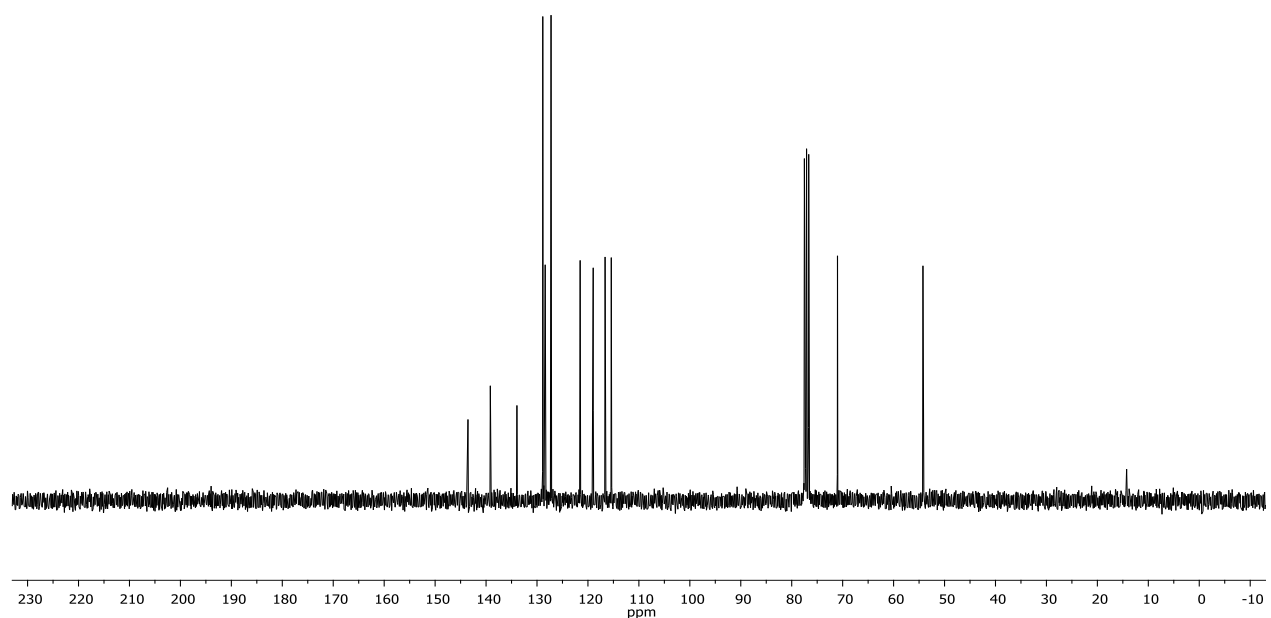


(R)-3-phenyl-3,4-dihydro-2H-benzo[b][1,4]oxazine (44h)

¹H-NMR (300 MHz, CDCl₃)

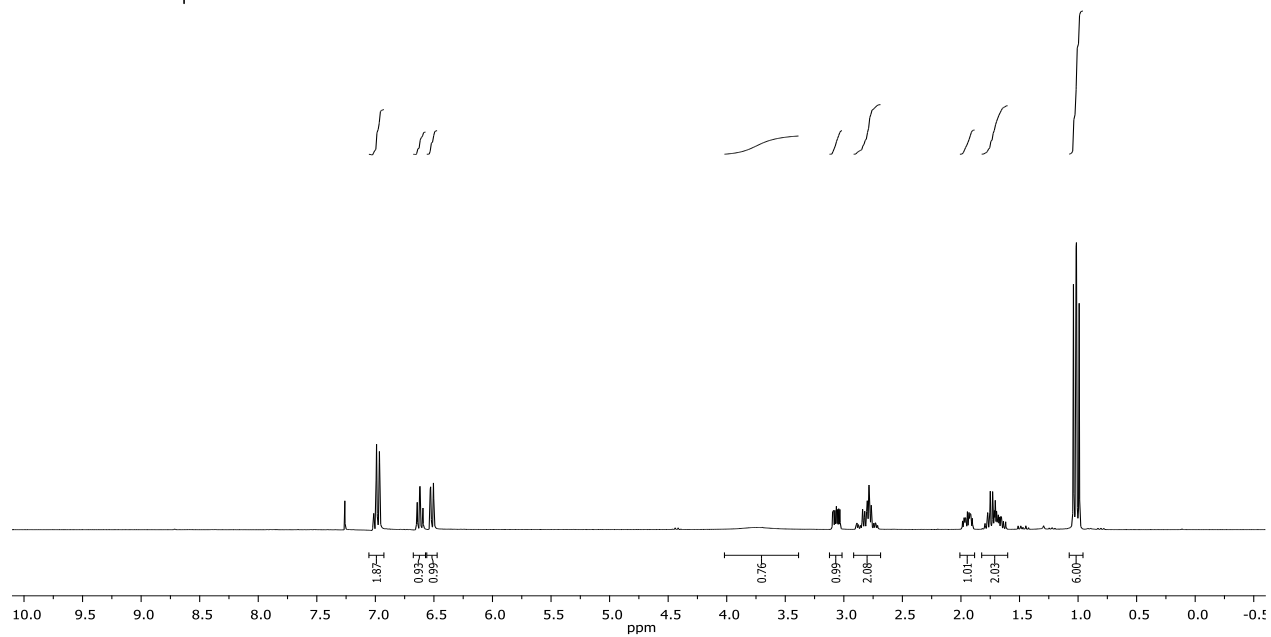
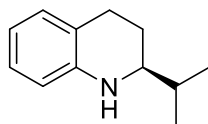


¹³C-NMR (75 MHz, CDCl₃)

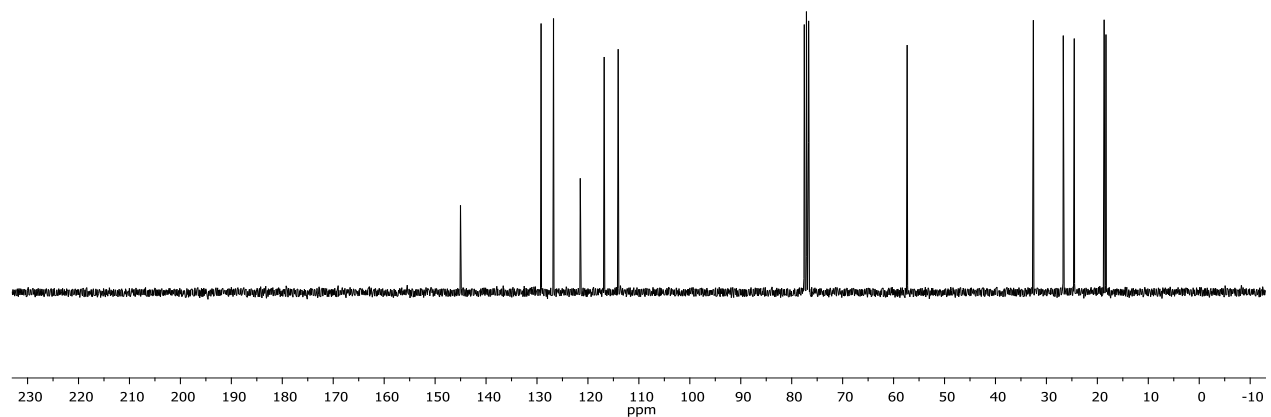


(S)-2-isopropyl-1,2,3,4-tetrahydroquinoline (44i)

¹H-NMR (300 MHz, CDCl₃)

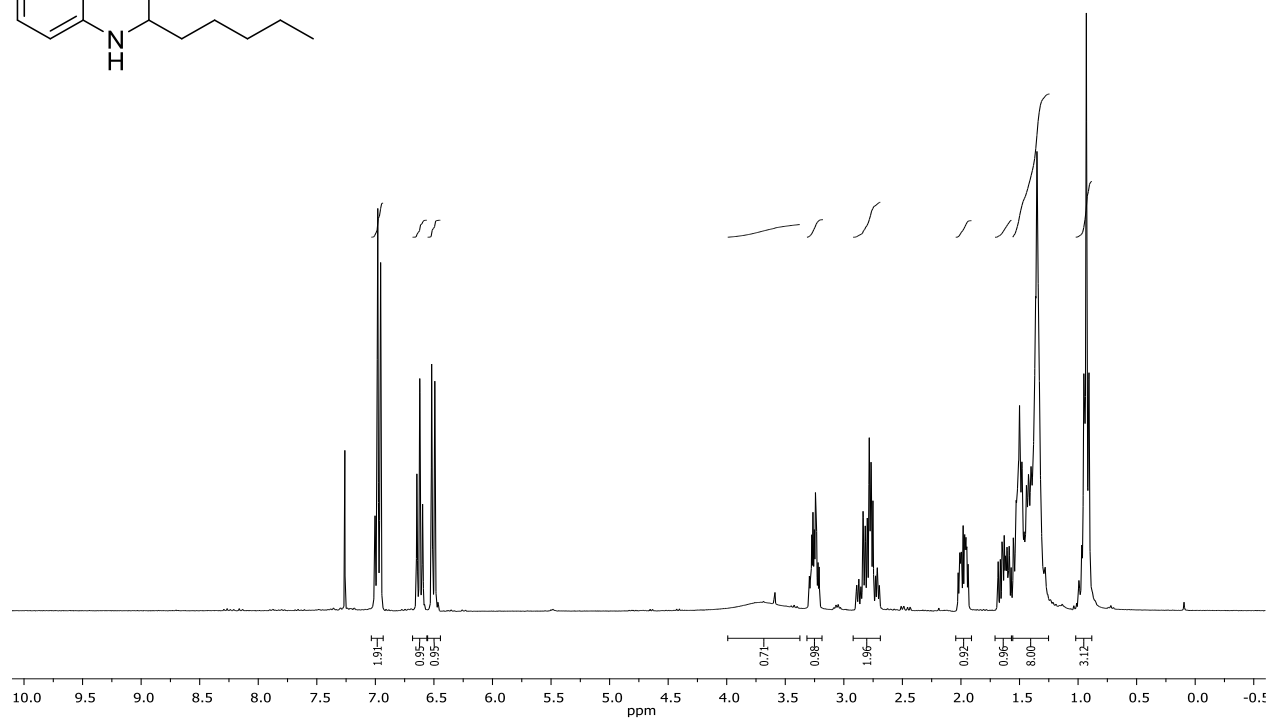
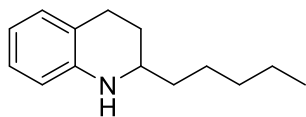


¹³C-NMR (75 MHz, CDCl₃)

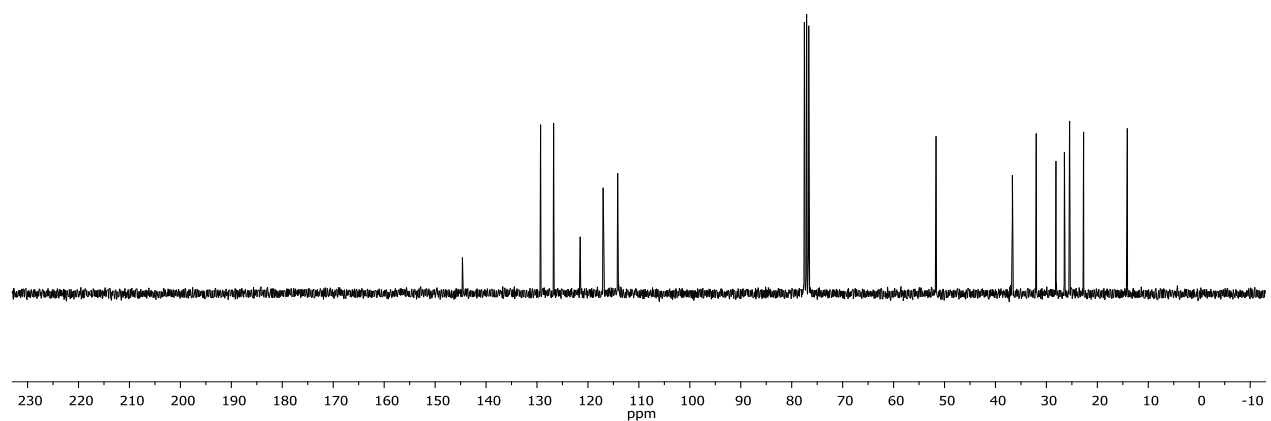


2-pentyl-1,2,3,4-tetrahydroquinoline (44j)

¹H-NMR (300 MHz, CDCl₃)

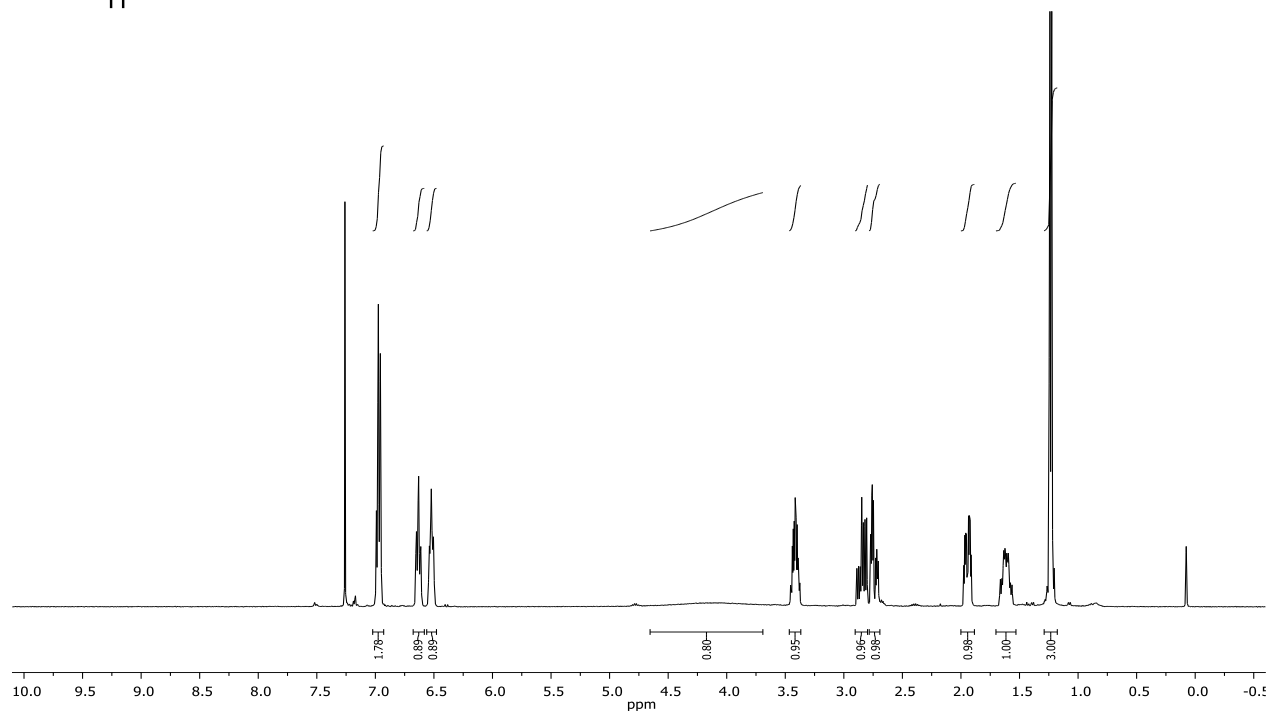
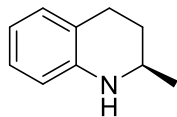


¹³C-NMR (75 MHz, CDCl₃)

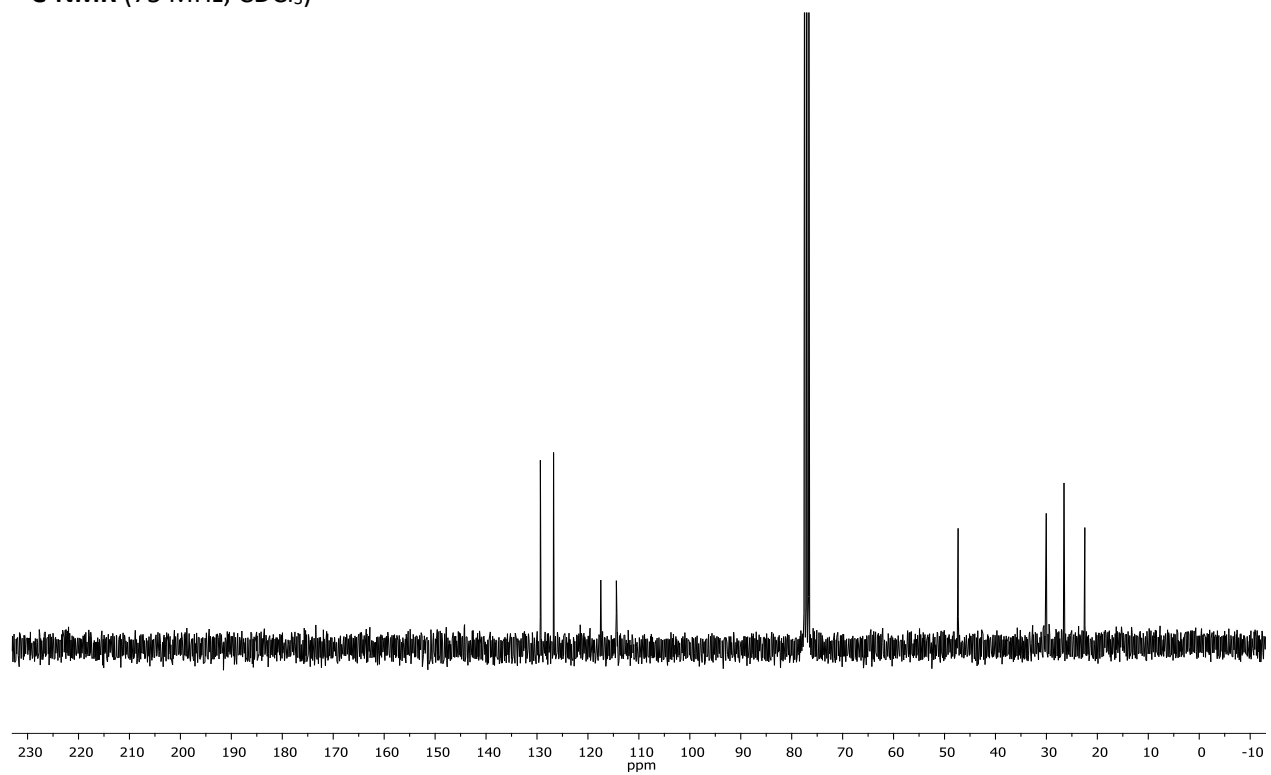


(R)-2-methyl-1,2,3,4-tetrahydroquinoline (6k)

¹H-NMR (300 MHz, CDCl₃)



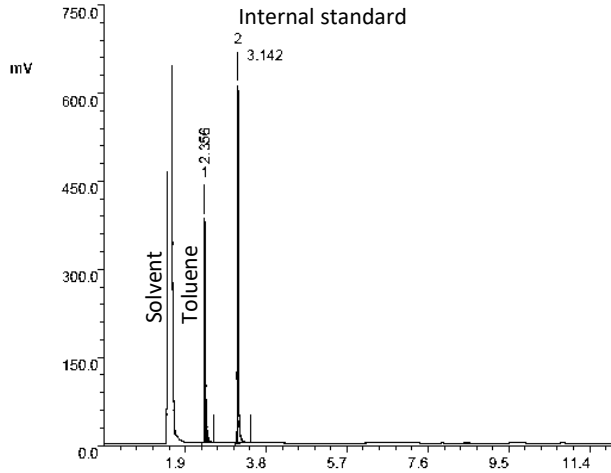
¹³C-NMR (75 MHz, CDCl₃)



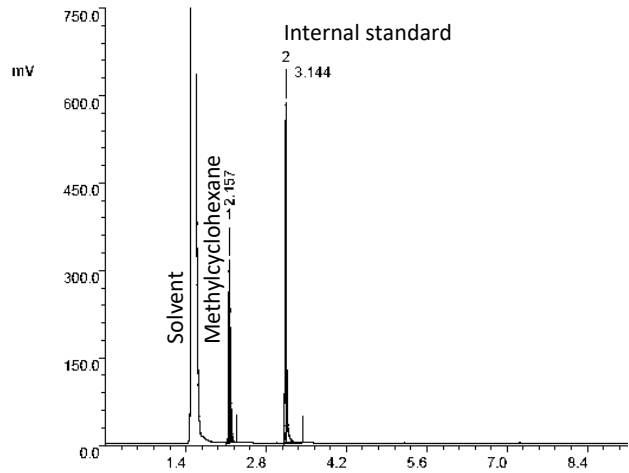
2. GC chromatograms

Methylcyclohexane (89)

Calibrations with ethylbenzene as internal standard, toluene (left), methylcyclohexane (right).



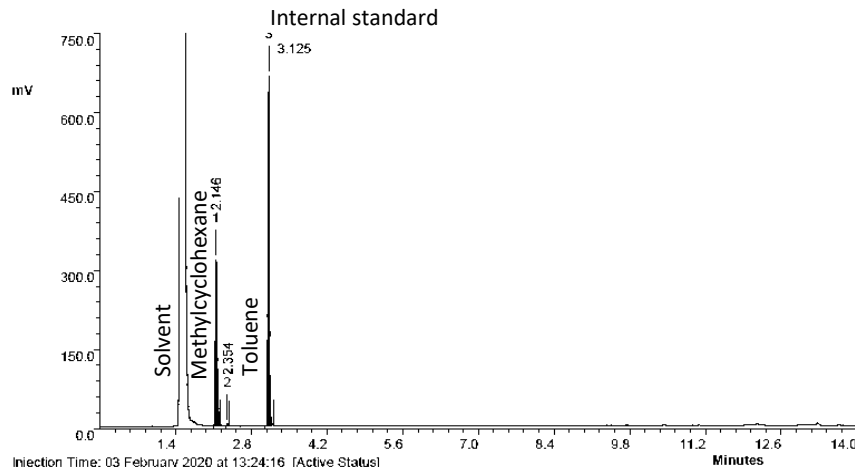
Injection Time: 29 May 2020 at 13:52:12 [Active Status]
 Type: AUTOINJ Injection Number: 106 Channel: Channel A Acquisition Rate: 16Hz
 Method File: C:\PW4\haa16352new\0001_haa16352new.mth Baseline noise: (not calculated)
 Standard File: (none) Sequence File: C:\PW4\haa16352new\haa16352new.seq



Injection Time: 02 June 2020 at 12:35:18 [Active Status]
 Type: AUTOINJ Injection Number: 111 Channel: Channel A Acquisition Rate: 16Hz
 Method File: C:\PW4\haa16352new\0001_haa16352new.mth Baseline noise: (not calculated)
 Standard File: (none) Sequence File: C:\PW4\haa16352new\haa16352new.seq

Peak	RT	Area	%Ar	Conc. (Ar)	Height	M	Units	Peak	RT	Area	%Ar	Conc. (Ar)	Height	M	Units
1	2.356	807.470	43.33	Not Calculated	381.551	1		1	2.157	671.431	41.30	Not Calculated	312.740	1	
2	3.142	1055.954	56.67	Not Calculated	608.210	1		2	3.144	954.436	58.70	Not Calculated	583.662	1	

Reaction sample with ethylbenzene as internal standard.

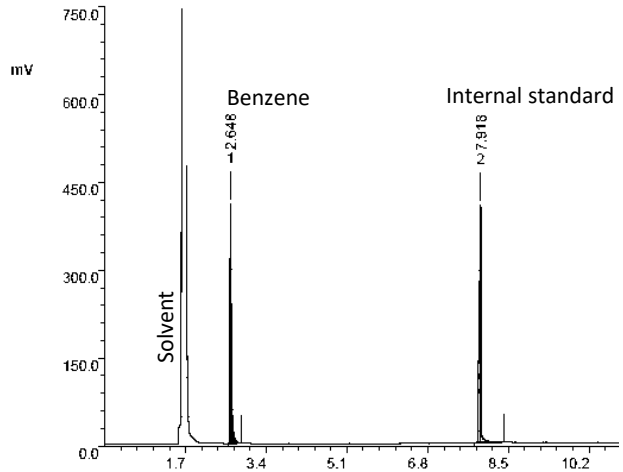


Injection Time: 03 February 2020 at 13:24:16 [Active Status]
 Type: AUTOINJ Injection Number: 20 Channel: Channel A Acquisition Rate: 16Hz
 Method File: C:\PW4\haa16352new\0001_haa16352new.mth Baseline noise: (not calculated)
 Standard File: (none) Sequence File: C:\PW4\haa16352new\haa16352new.seq

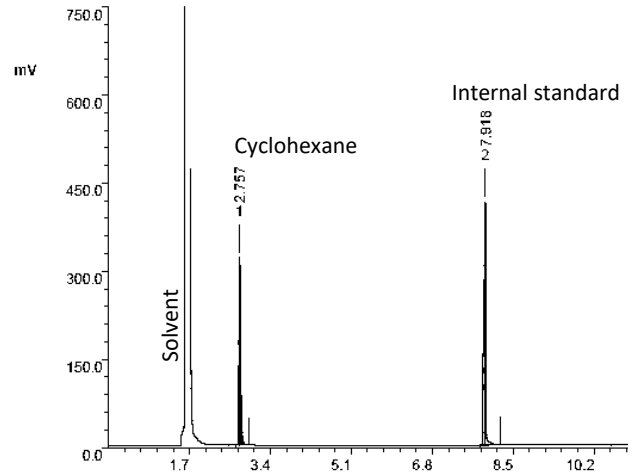
Peak	RT	Area	%Ar	Conc. (Ar)	Height	M	Units	Name
1	2.146	720.626	38.73	Not Calculated	314.458	1		
2	2.354	5.478	0.29	Not Calculated	2.860	1		
3	3.125	1134.656	60.98	Not Calculated	663.751	1		

Benzene (1)

Calibrations with ethylbenzene as internal standard, benzene (left), cyclohexane (right).



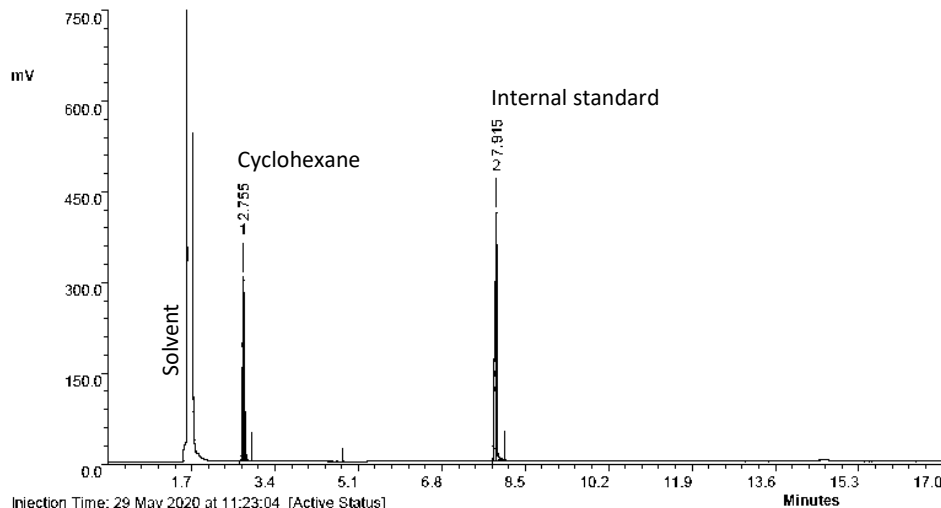
Injection Time: 02 June 2020 at 10:41:30 [Active Status]
 Type: AUTOINJ Injection Number: 108 Channel: Channel A Acquisition Rate: 16Hz
 Method File: C:\PW4\haa16352new\0001_haa16352new.mth Baseline noise: (not calculated)
 Standard File: (none) Sequence File: C:\PW4\haa16352new\haa16352new.seq



Injection Time: 02 June 2020 at 11:26:05 [Active Status]
 Type: AUTOINJ Injection Number: 109 Channel: Channel A Acquisition Rate: 16Hz
 Method File: C:\PW4\haa16352new\0001_haa16352new.mth Baseline noise: (not calculated)
 Standard File: (none) Sequence File: C:\PW4\haa16352new\haa16352new.seq

Peak	RT	Area	%Ar	Conc. (Ar)	Height	M	Units	Peak	RT	Area	%Ar	Conc. (Ar)	Height	M	Units
1	2.648	896.849	45.62	Not Calculated	408.212	1		1	2.757	810.005	40.04	Not Calculated	318.847	1	
2	7.918	1069.153	54.38	Not Calculated	404.300	1		2	7.918	1212.855	59.96	Not Calculated	413.666	1	

Reaction sample with ethylbenzene as internal standard.

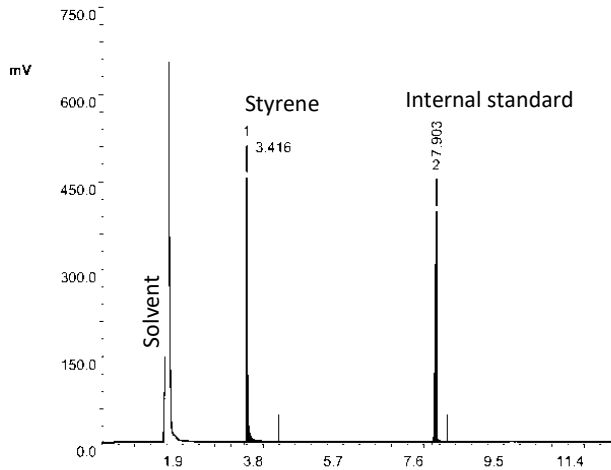


Injection Time: 29 May 2020 at 11:23:04 [Active Status]
 Type: AUTOINJ Injection Number: 101 Channel: Channel A Acquisition Rate: 16Hz
 Method File: C:\PW4\haa16352new\0001_haa16352new.mth Baseline noise: (not calculated)
 Standard File: (none) Sequence File: C:\PW4\haa16352new\haa16352new.seq

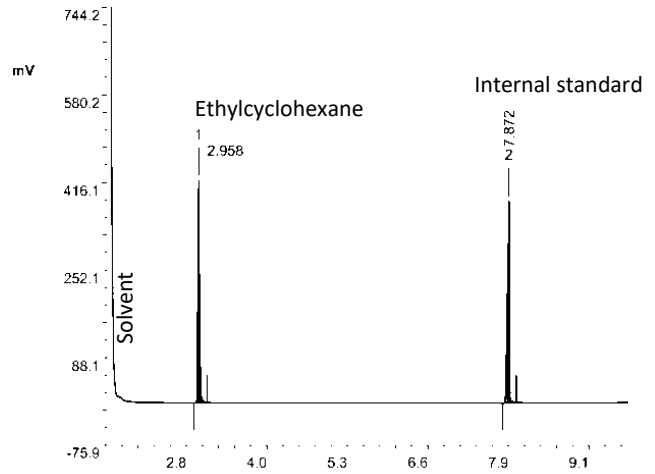
Peak	RT	Area	%Ar	Conc. (Ar)	Height	M	Units	Name
1	2.755	781.229	39.61	Not Calculated	304.277	1		
2	7.915	1190.965	60.39	Not Calculated	410.038	1		

Ethylcyclohexane (91)

Calibrations with dodecane as internal standard, styrene (left), ethylcyclohexane (right).



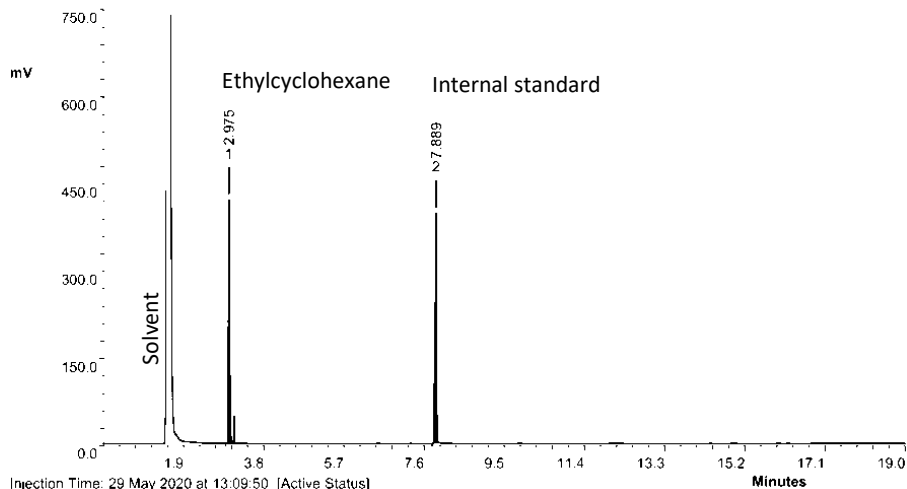
Injection Time: 02 June 2020 at 16:45:17 [Active Status]
 Type: AUTOINJ Injection Number: 115 Channel: Channel A Acquisition Rate: 16Hz
 Method File: C:\PW4\haa16352new\0001_haa16352new.mth Baseline noise: (not calculated)
 Standard File: (none) Sequence File: C:\PW4\haa16352new\haa16352new.seq



Injection Time: 03 June 2020 at 12:47:03 [Active Status]
 Type: AUTOINJ Injection Number: 119 Channel: Channel A Acquisition Rate: 16Hz
 Method File: C:\PW4\haa16352new\0001_haa16352new.mth Baseline noise: (not calculated)
 Standard File: (none) Sequence File: C:\PW4\haa16352new\haa16352new.seq

Peak	RT	Area	%Ar	Conc. (Ar)	Height	M	Units	Peak	RT	Area	%Ar	Conc. (Ar)	Height	M	Units
1	3.416	779.787	45.98	Not Calculated	453.313	1		1	2.958	731.589	46.28	Not Calculated	415.758	1	
2	7.903	915.965	54.02	Not Calculated	395.896	1		2	7.872	849.348	53.72	Not Calculated	377.173	1	

Reaction sample with dodecane as internal standard.

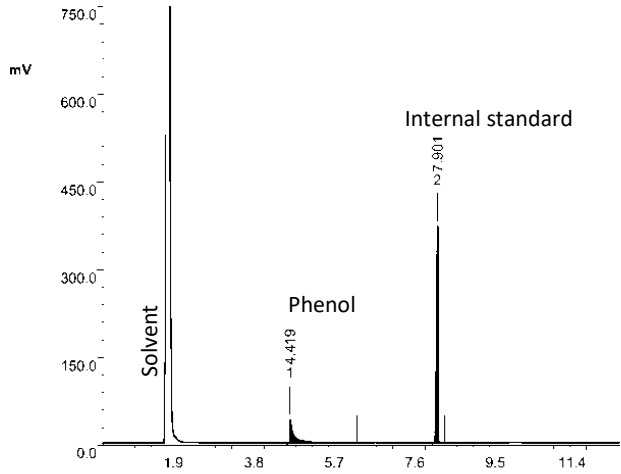


Injection Time: 29 May 2020 at 13:09:50 [Active Status]
 Type: AUTOINJ Injection Number: 105 Channel: Channel A Acquisition Rate: 16Hz
 Method File: C:\PW4\haa16352new\0001_haa16352new.mth Baseline noise: (not calculated)
 Standard File: (none) Sequence File: C:\PW4\haa16352new\haa16352new.seq

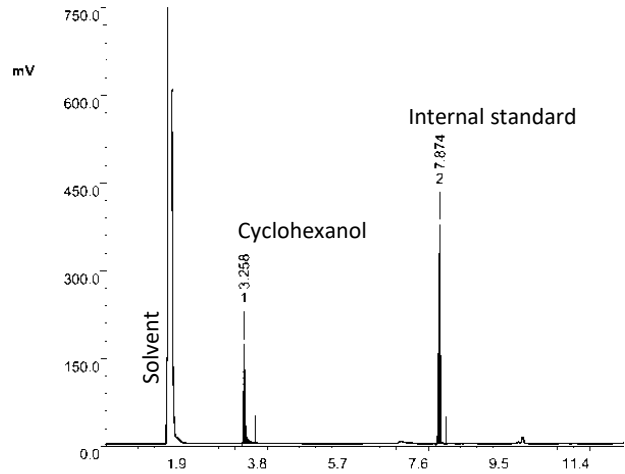
Peak	RT	Area	%Ar	Conc. (Ar)	Height	M	Units	Name
1	2.975	825.588	46.50	Not Calculated	418.320	1		
2	7.889	950.054	53.50	Not Calculated	394.326	1		

Cyclohexanol (3)

Calibrations with dodecane as internal standard, phenol (left), cyclohexanol (right).



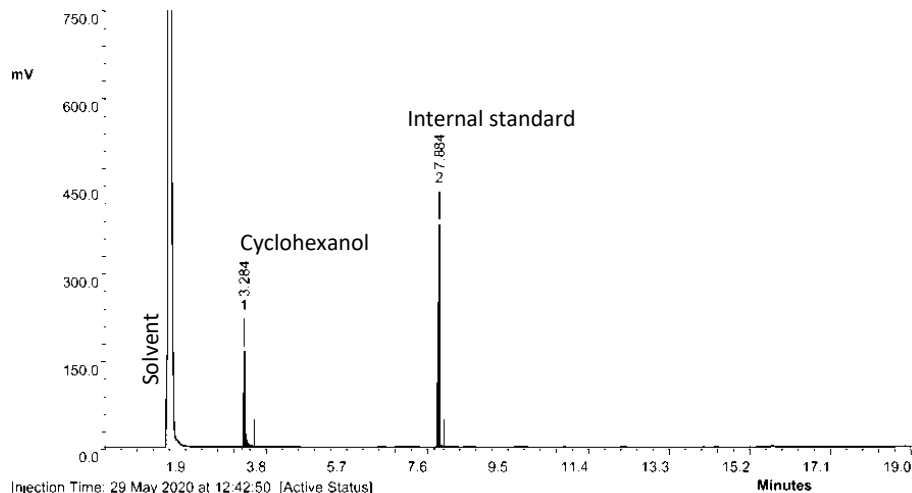
Injection Time: 02 June 2020 at 15:06:59 [Active Status]
 Type: AUTOINJ Injection Number: 113 Channel: Channel A Acquisition Rate: 16Hz
 Method File: C:\PW4\haa16352new\0001_haa16352new.mth Baseline noise: (not calculated)
 Standard File: (none) Sequence File: C:\PW4\haa16352new\haa16352new.seq



Injection Time: 03 June 2020 at 11:29:08 [Active Status]
 Type: AUTOINJ Injection Number: 117 Channel: Channel A Acquisition Rate: 16Hz
 Method File: C:\PW4\haa16352new\0001_haa16352new.mth Baseline noise: (not calculated)
 Standard File: (none) Sequence File: C:\PW4\haa16352new\haa16352new.seq

Peak	RT	Area	%Ar	Conc. (Ar)	Height	M	Units	Peak	RT	Area	%Ar	Conc. (Ar)	Height	M	Units
1	4.419	284.596	25.06	Not Calculated	40.275	1		1	3.258	303.879	26.64	Not Calculated	168.743	1	
2	7.901	851.031	74.94	Not Calculated	370.338	1		2	7.874	836.689	73.36	Not Calculated	374.148	1	

Reaction sample with dodecane as internal standard.

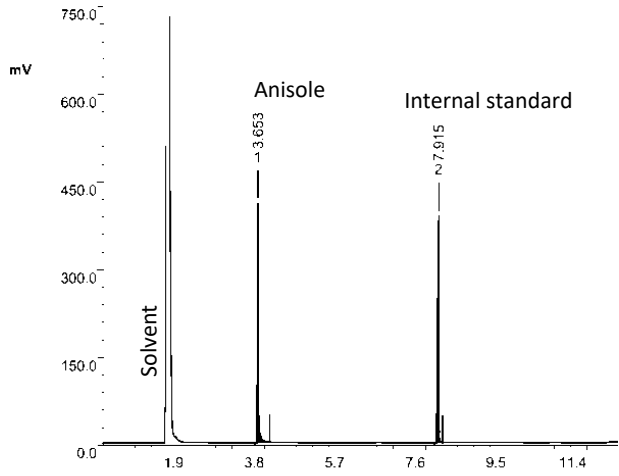


Injection Time: 29 May 2020 at 12:42:50 [Active Status]
 Type: AUTOINJ Injection Number: 104 Channel: Channel A Acquisition Rate: 16Hz
 Method File: C:\PW4\haa16352new\0001_haa16352new.mth Baseline noise: (not calculated)
 Standard File: (none) Sequence File: C:\PW4\haa16352new\haa16352new.seq

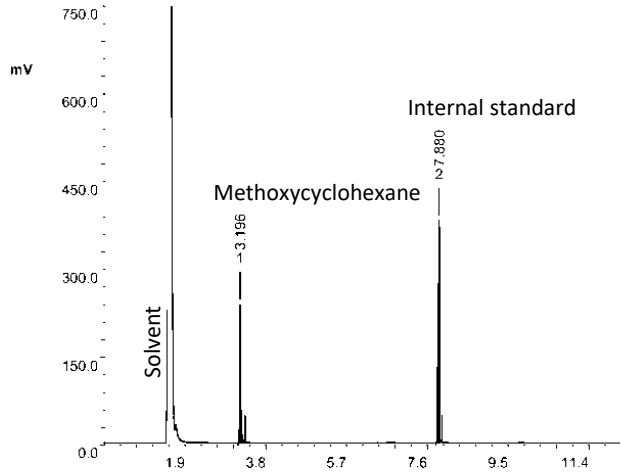
Peak	RT	Area	%Ar	Conc. (Ar)	Height	M	Units	Name
1	3.284	285.454	24.10	Not Calculated	162.927	1		
2	7.884	898.785	75.90	Not Calculated	380.309	1		

Methoxycyclohexane (94)

Calibrations with dodecane as internal standard, anisole (left), methoxycyclohexane (right).



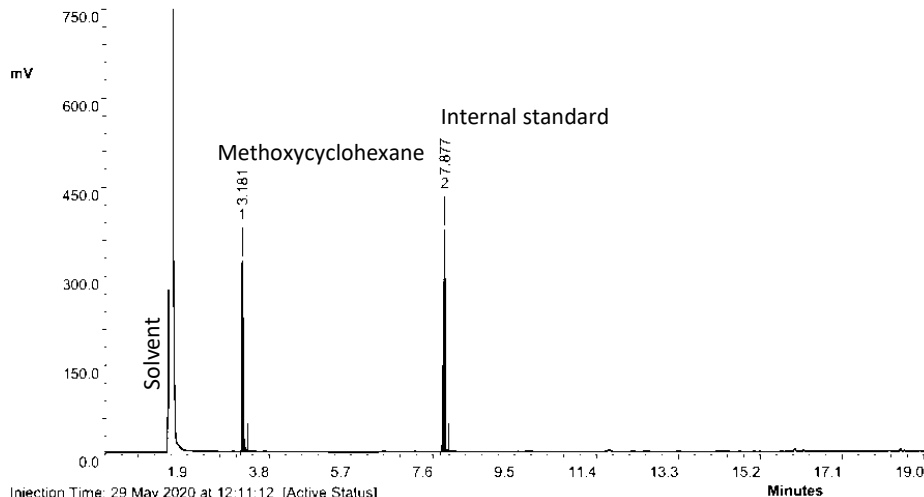
Injection Time: 02 June 2020 at 14:20:46 [Active Status]
 Type: AUTOINJ Injection Number: 112 Channel: Channel A Acquisition Rate: 16Hz
 Method File: C:\PW4\haa16352new\0001_haa16352new.mth Baseline noise: (not calculated)
 Standard File: (none) Sequence File: C:\PW4\haa16352new\haa16352new.seq



Injection Time: 03 June 2020 at 12:03:51 [Active Status]
 Type: AUTOINJ Injection Number: 118 Channel: Channel A Acquisition Rate: 16Hz
 Method File: C:\PW4\haa16352new\0001_haa16352new.mth Baseline noise: (not calculated)
 Standard File: (none) Sequence File: C:\PW4\haa16352new\haa16352new.seq

Peak	RT	Area	%Ar	Conc. (Ar)	Height	M	Units	Peak	RT	Area	%Ar	Conc. (Ar)	Height	M	Units
1	3.653	683.856	42.84	Not Calculated	408.970	1		1	3.196	369.538	29.79	Not Calculated	235.535	1	
2	7.915	912.541	57.16	Not Calculated	387.781	1		2	7.880	871.136	70.21	Not Calculated	378.472	1	

Reaction sample with dodecane as internal standard.

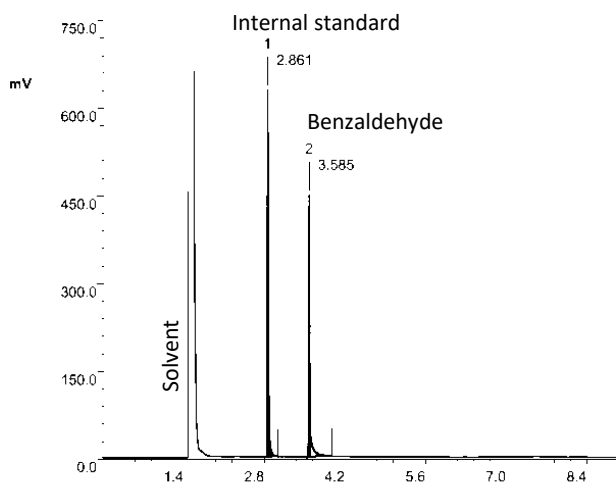


Injection Time: 29 May 2020 at 12:11:12 [Active Status]
 Type: AUTOINJ Injection Number: 103 Channel: Channel A Acquisition Rate: 16Hz
 Method File: C:\PW4\haa16352new\0001_haa16352new.mth Baseline noise: (not calculated)
 Standard File: (none) Sequence File: C:\PW4\haa16352new\haa16352new.seq

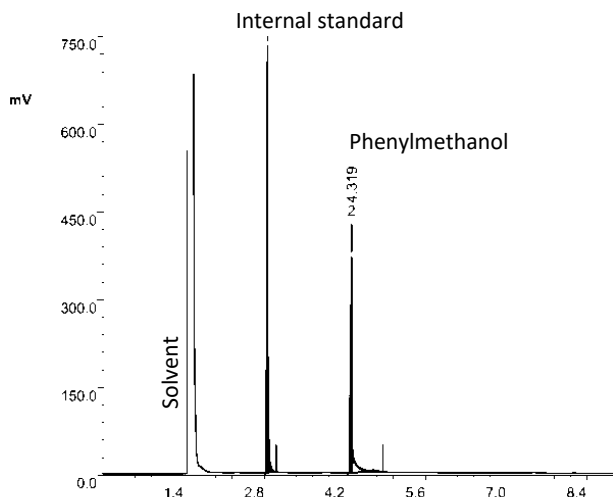
Peak	RT	Area	%Ar	Conc. (Ar)	Height	M	Units	Name
1	3.181	525.672	37.85	Not Calculated	320.512	1		
2	7.877	863.149	62.15	Not Calculated	372.132	1		

Phenylmethanol (96)

Calibrations with ethylbenzene as internal standard, benzaldehyde (left), phenylmethanol (right).



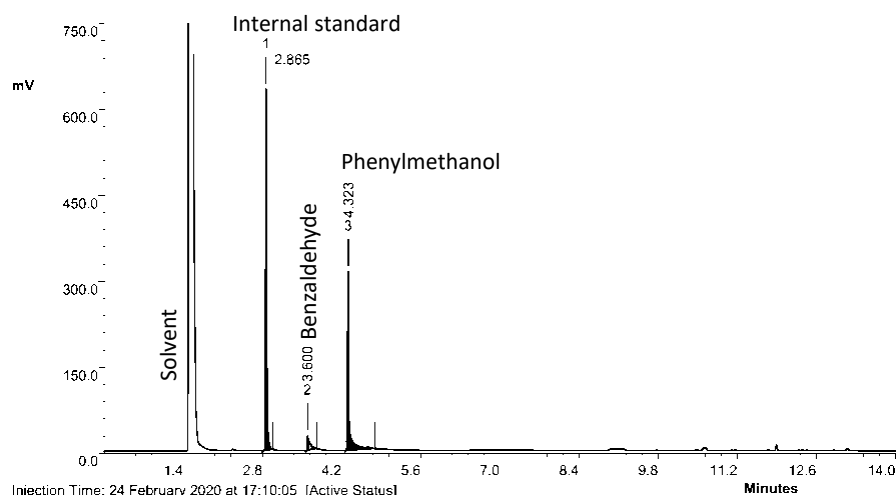
Injection Time: 03 June 2020 at 15:50:33 [Active Status]
 Type: AUTOINJ Injection Number: 123 Channel: Channel A Acquisition Rate: 16Hz
 Method File: C:\PW4\haa16352new\0001_haa16352new.mth Baseline noise: (not calculated)
 Standard File: (none) Sequence File: C:\PW4\haa16352new\haa16352new.seq



Injection Time: 03 June 2020 at 15:22:09 [Active Status]
 Type: AUTOINJ Injection Number: 122 Channel: Channel A Acquisition Rate: 16Hz
 Method File: C:\PW4\haa16352new\0001_haa16352new.mth Baseline noise: (not calculated)
 Standard File: (none) Sequence File: C:\PW4\haa16352new\haa16352new.seq

Peak	RT	Area	%Ar	Conc. (Ar)	Height	M	Units	Peak	RT	Area	%Ar	Conc. (Ar)	Height	M	Units
1	2.861	966.971	56.21	Not Calculated	626.955	1		1	2.855	1079.178	54.90	Not Calculated	730.257	1	
2	3.585	753.419	43.79	Not Calculated	447.634	1		2	4.319	886.479	45.10	Not Calculated	368.726	1	

Reaction sample with ethylbenzene as internal standard.

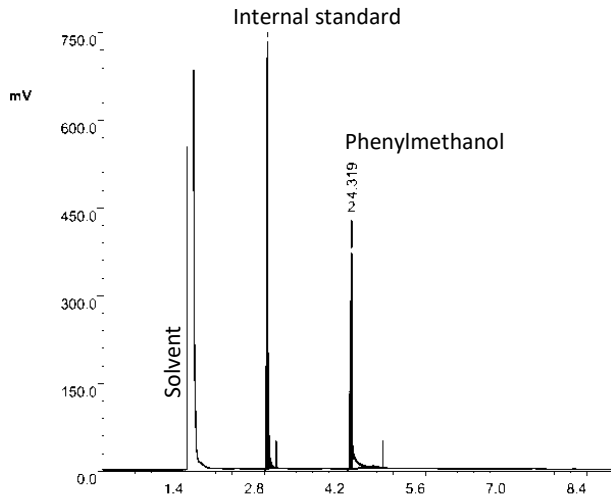


Injection Time: 24 February 2020 at 17:10:05 [Active Status]
 Type: AUTOINJ Injection Number: 43 Channel: Channel A Acquisition Rate: 16Hz
 Method File: C:\PW4\haa16352new\0001_haa16352new.mth Baseline noise: (not calculated)
 Standard File: (none) Sequence File: C:\PW4\haa16352new\haa16352new.seq

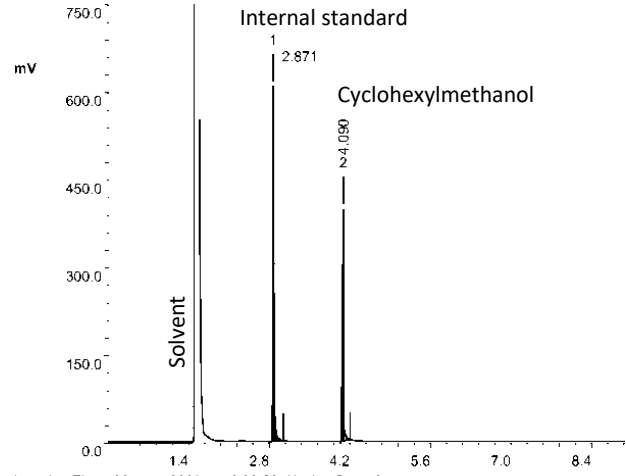
Peak	RT	Area	%Ar	Conc. (Ar)	Height	M	Units	Name
1	2.865	983.380	54.95	Not Calculated	630.011	1		
2	3.600	88.047	4.92	Not Calculated	25.946	1		
3	4.323	718.140	40.13	Not Calculated	312.182	1		

Cyclohexylmethanol (97)

Calibrations with ethylbenzene as internal standard, phenylmethanol (left), cyclohexylmethanol (right).



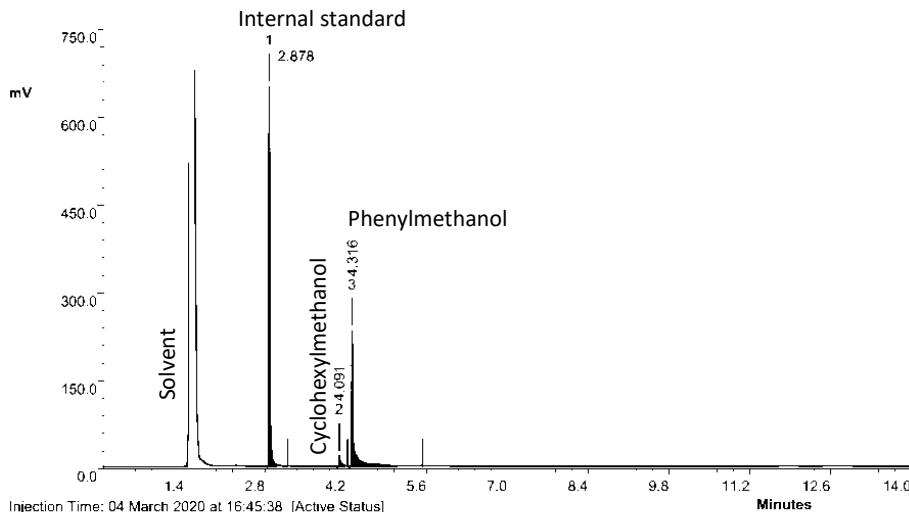
Injection Time: 03 June 2020 at 15:22:09 [Active Status]
 Type: AUTOINJ Injection Number: 122 Channel: Channel A Acquisition Rate: 16Hz
 Method File: C:\PW4\haa16352new\0001_haa16352new.mth Baseline noise: (not calculated)
 Standard File: (none) Sequence File: C:\PW4\haa16352new\haa16352new.seq



Injection Time: 03 June 2020 at 16:20:53 [Active Status]
 Type: AUTOINJ Injection Number: 124 Channel: Channel A Acquisition Rate: 16Hz
 Method File: C:\PW4\haa16352new\0001_haa16352new.mth Baseline noise: (not calculated)
 Standard File: (none) Sequence File: C:\PW4\haa16352new\haa16352new.seq

Peak	RT	Area	%Ar	Conc. (Ar)	Height	M	Units	Peak	RT	Area	%Ar	Conc. (Ar)	Height	M	Units
1	2.855	1079.178	54.90	Not Calculated	730.257	1		1	2.871	901.541	55.42	Not Calculated	606.573	1	
2	4.319	886.479	45.10	Not Calculated	368.726	1		2	4.090	725.206	44.58	Not Calculated	395.361	1	

Reaction sample with ethylbenzene as internal standard.

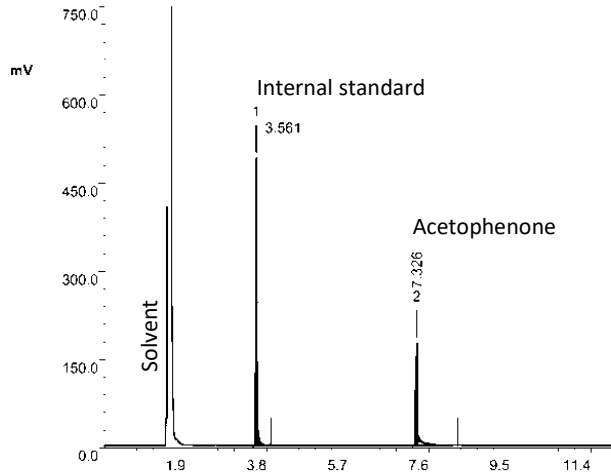


Injection Time: 04 March 2020 at 16:45:38 [Active Status]
 Type: AUTOINJ Injection Number: 56 Channel: Channel A Acquisition Rate: 16Hz
 Method File: C:\PW4\haa16352new\0001_haa16352new.mth Baseline noise: (not calculated)
 Standard File: (none) Sequence File: C:\PW4\haa16352new\haa16352new.seq

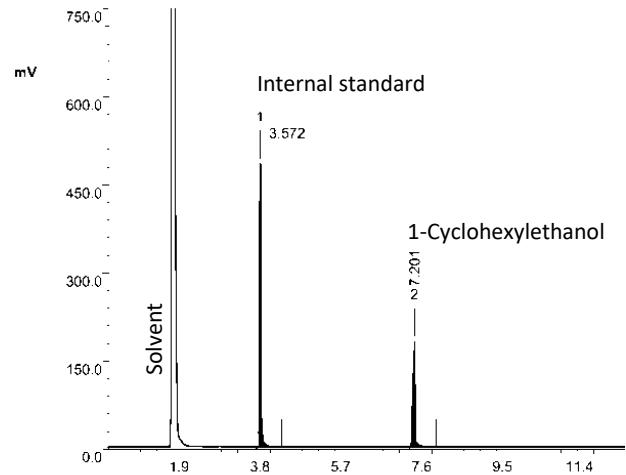
Peak	RT	Area	%Ar	Conc. (Ar)	Height	M	Units	Name
1	2.878	994.451	62.97	Not Calculated	648.675	1		
2	4.091	42.874	2.71	Not Calculated	17.687	1		
3	4.316	542.014	34.32	Not Calculated	231.474	1		

1-Cyclohexylethanol (99)

Calibrations with ethylbenzene as internal standard, acetophenone (left), 1-cyclohexylethanol (right).



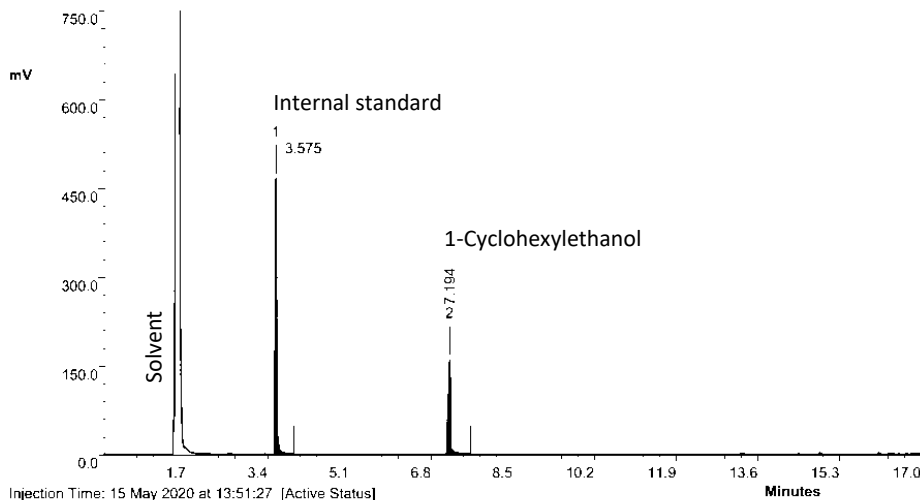
Injection Time: 02 June 2020 at 16:00:17 [Active Status]
 Type: AUTOINJ Injection Number: 114 Channel: Channel A Acquisition Rate: 16Hz
 Method File: C:\PW4\haa16352new\0001_haa16352new.mth Baseline noise: (not calculated)
 Standard File: (none) Sequence File: C:\PW4\haa16352new\haa16352new.seq



Injection Time: 03 June 2020 at 14:04:49 [Active Status]
 Type: AUTOINJ Injection Number: 120 Channel: Channel A Acquisition Rate: 16Hz
 Method File: C:\PW4\haa16352new\0001_haa16352new.mth Baseline noise: (not calculated)
 Standard File: (none) Sequence File: C:\PW4\haa16352new\haa16352new.seq

Peak	RT	Area	%Ar	Conc. (Ar)	Height	M	Units	Peak	RT	Area	%Ar	Conc. (Ar)	Height	M	Units
1	3.561	1017.514	60.87	Not Calculated	489.239	1		1	3.572	1064.281	62.79	Not Calculated	483.050	1	
2	7.326	654.053	39.13	Not Calculated	174.776	1		2	7.201	630.767	37.21	Not Calculated	180.286	1	

Reaction sample with ethylbenzene as internal standard.

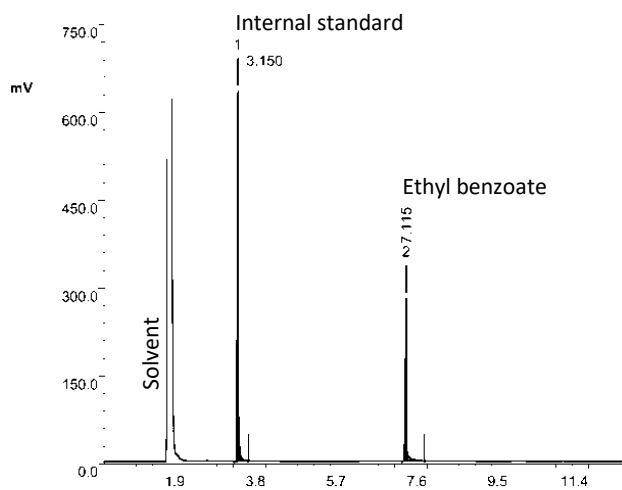


Injection Time: 15 May 2020 at 13:51:27 [Active Status]
 Type: AUTOINJ Injection Number: 98 Channel: Channel A Acquisition Rate: 16Hz
 Method File: C:\PW4\haa16352new\0001_haa16352new.mth Baseline noise: (not calculated)
 Standard File: (none) Sequence File: C:\PW4\haa16352new\haa16352new.seq

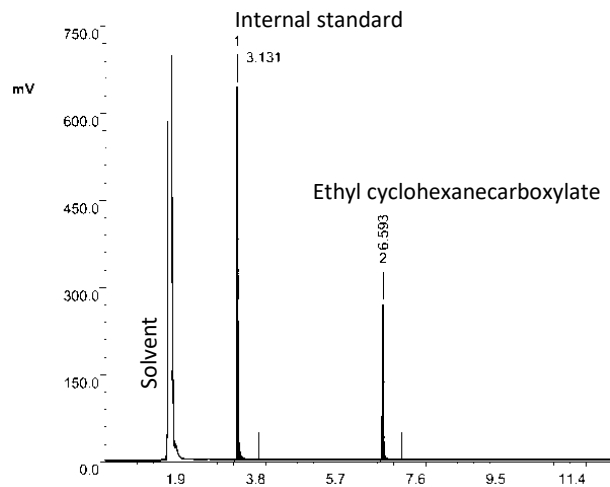
Peak	RT	Area	%Ar	Conc. (Ar)	Height	M	Units	Name
1	3.575	966.650	65.37	Not Calculated	465.101	1		
2	7.194	511.981	34.63	Not Calculated	159.295	1		

Ethyl cyclohexanecarboxylate (101)

Calibrations with ethylbenzene as internal standard, ethyl benzoate (left), ethyl cyclohexanecarboxylate (right).



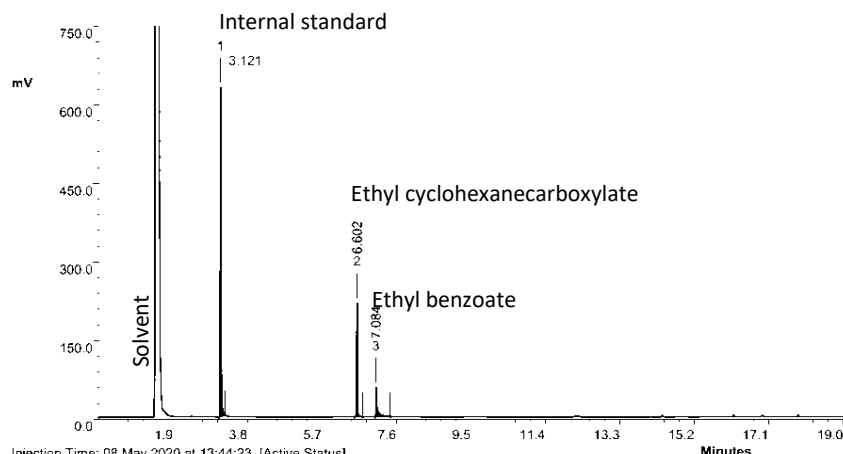
Injection Time: 29 May 2020 at 14:22:54 [Active Status]
 Type: AUTOINJ Injection Number: 107 Channel: Channel A Acquisition Rate: 16Hz
 Method File: C:\PW4\haa16352new\0001_haa16352new.mth Baseline noise: (not calculated)
 Standard File: (none) Sequence File: C:\PW4\haa16352new\haa16352new.seq



Injection Time: 03 June 2020 at 14:46:17 [Active Status]
 Type: AUTOINJ Injection Number: 121 Channel: Channel A Acquisition Rate: 16Hz
 Method File: C:\PW4\haa16352new\0001_haa16352new.mth Baseline noise: (not calculated)
 Standard File: (none) Sequence File: C:\PW4\haa16352new\haa16352new.seq

Peak	RT	Area	%Ar	Conc. (Ar)	Height	M	Units	Peak	RT	Area	%Ar	Conc. (Ar)	Height	M	Units
1	3.150	1053.771	61.68	Not Calculated	632.172	1		1	3.131	1093.814	68.51	Not Calculated	641.720	1	
2	7.115	654.589	38.32	Not Calculated	278.814	1		2	6.593	502.785	31.49	Not Calculated	267.325	1	

Reaction sample with ethylbenzene as internal standard.

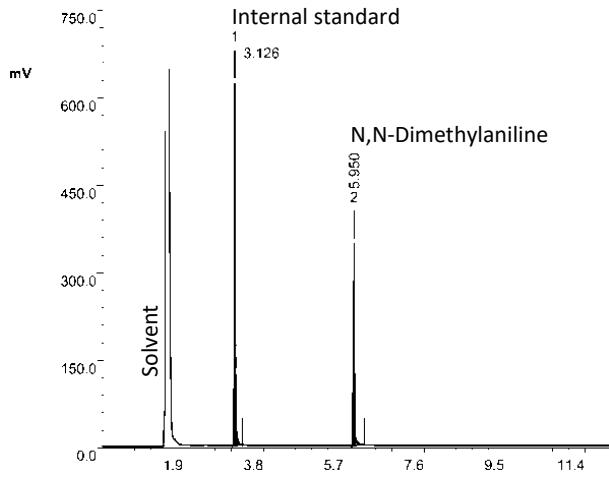


Injection Time: 08 May 2020 at 13:44:23 [Active Status]
 Type: AUTOINJ Injection Number: 94 Channel: Channel A Acquisition Rate: 16Hz
 Method File: C:\PW4\haa16352new\0001_haa16352new.mth Baseline noise: (not calculated)
 Standard File: (none) Sequence File: C:\PW4\haa16352new\haa16352new.seq

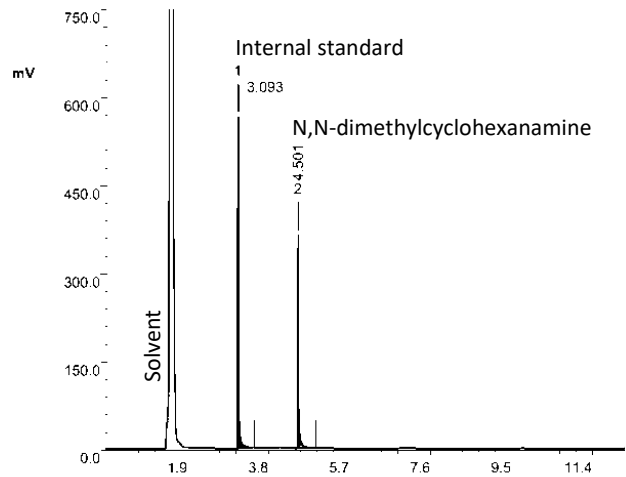
Peak	RT	Area	%Ar	Conc. (Ar)	Height	M	Units	Name
1	3.121	1078.198	67.15	Not Calculated	628.215	1		
2	6.602	374.796	23.34	Not Calculated	217.913	1		
3	7.084	152.522	9.50	Not Calculated	56.772	1		

N,N-Dimethylcyclohexanamine (103)

Calibrations with ethylbenzene as internal standard, N,N-dimethylaniline (left), N,N-dimethylcyclohexanamine (right).



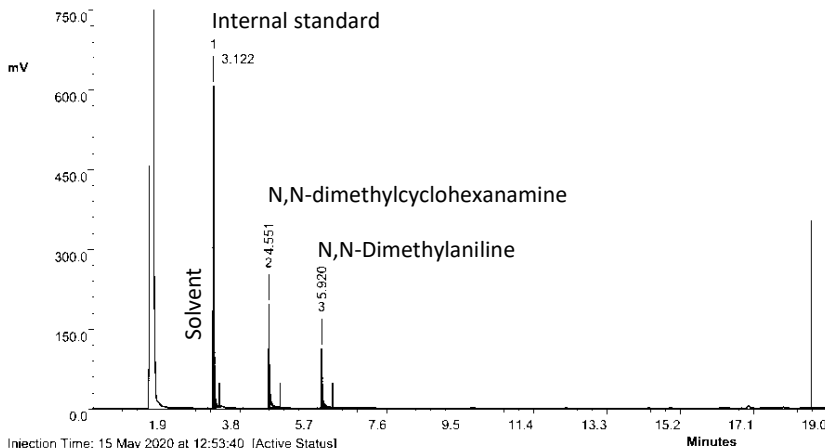
Injection Time: 02 June 2020 at 17:32:41 [Active Status]
 Type: AUTOINJ Injection Number: 116 Channel: Channel A Acquisition Rate: 16Hz
 Method File: C:\PW4\haa16352new\0001_haa16352new.mth Baseline noise: (not calculated)
 Standard File: (none) Sequence File: C:\PW4\haa16352new\haa16352new.seq



Injection Time: 08 July 2020 at 12:51:49 [Active Status]
 Type: AUTOINJ Injection Number: 129 Channel: Channel A Acquisition Rate: 16Hz
 Method File: C:\PW4\haa16352new\0001_haa16352new.mth Baseline noise: (not calculated)
 Standard File: (none) Sequence File: C:\PW4\haa16352new\haa16352new.seq

Peak	RT	Area	%Ar	Conc. (Ar)	Height	M	Units	Peak	RT	Area	%Ar	Conc. (Ar)	Height	M	Units
1	3.126	1079.320	60.08	Not Calculated	621.113	1		1	3.093	1050.764	64.43	Not Calculated	564.159	1	
2	5.950	717.155	39.92	Not Calculated	346.015	1		2	4.501	580.093	35.57	Not Calculated	362.315	1	

Reaction sample with ethylbenzene as internal standard.

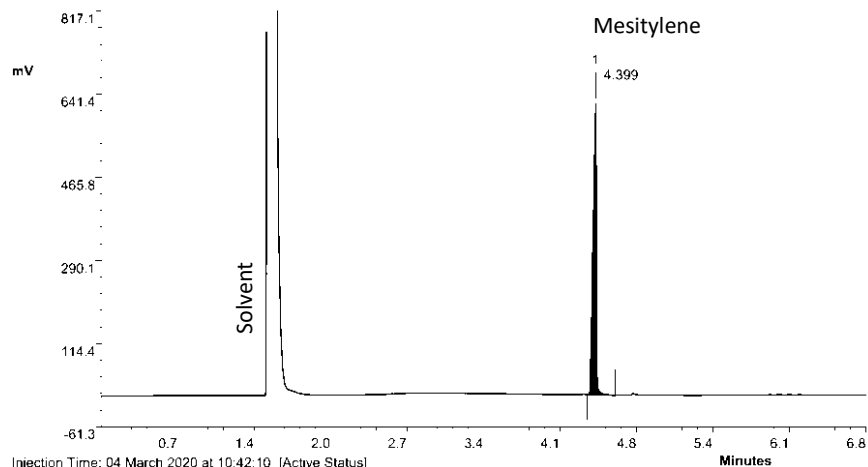


Injection Time: 15 May 2020 at 12:53:40 [Active Status]
 Type: AUTOINJ Injection Number: 96 Channel: Channel A Acquisition Rate: 16Hz
 Method File: C:\PW4\haa16352new\0001_haa16352new.mth Baseline noise: (not calculated)
 Standard File: (none) Sequence File: C:\PW4\haa16352new\haa16352new.seq

Peak	RT	Area	%Ar	Conc. (Ar)	Height	M	Units	Name
1	3.122	1019.850	65.38	Not Calculated	604.871	1		
2	4.551	329.575	21.13	Not Calculated	194.282	1		
3	5.920	210.567	13.50	Not Calculated	111.346	1		

1,3,5-Trimethylcyclohexane (107)

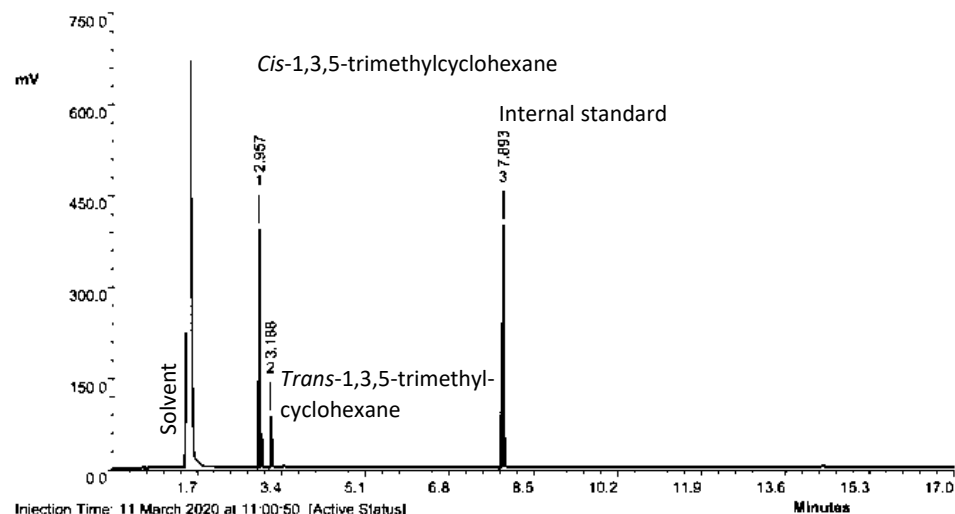
Mesitylene sample.



Injection Time: 04 March 2020 at 10:42:10 [Active Status]
Type: AUTOINJ Injection Number: 47 Channel: Channel A Acquisition Rate: 16Hz
Method File: C:\PW4\haa16352new\0001_haa16352new.mth Baseline noise: (not calculated)
Standard File: (none) Sequence File: C:\PW4\haa16352new\haa16352new.seq

Peak	RT	Area	%Ar	Conc. (Ar)	Height	M	Units	Name
1	4.399	1234.005	100.00	Not Calculated	614.817	1		

Reaction sample with dodecane as internal standard (No quantification *via* GC was performed).

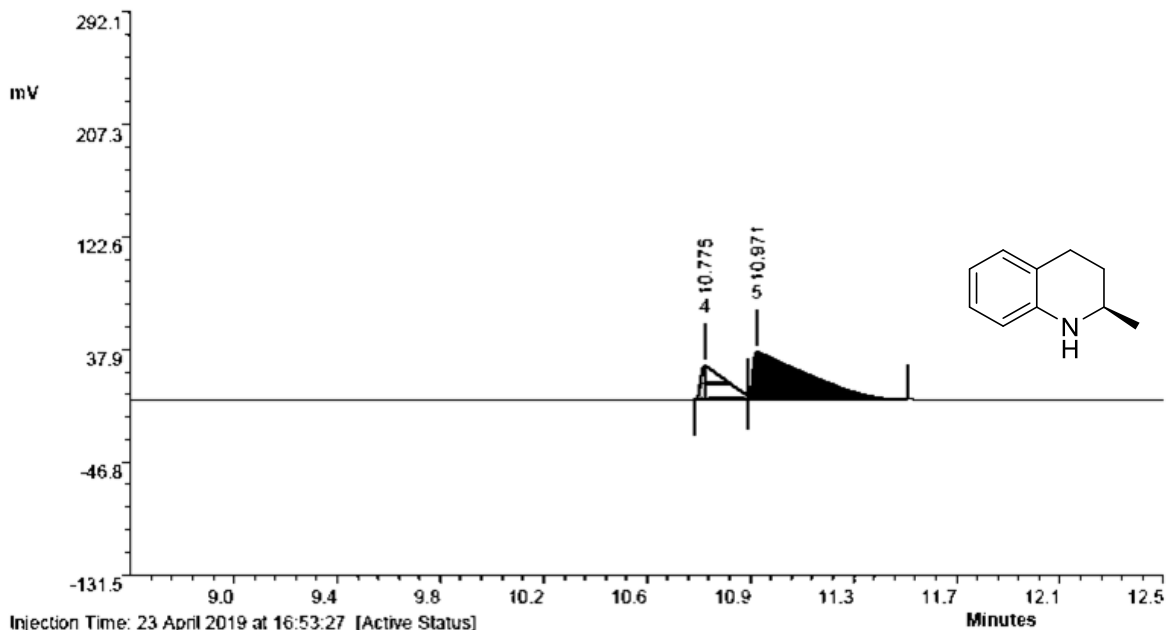


Injection Time: 11 March 2020 at 11:00:50 [Active Status]
Type: AUTOINJ Injection Number: 62 Channel: Channel A Acquisition Rate: 16Hz
Method File: C:\PW4\haa16352new\0001_haa16352new.mth Baseline noise: (not calculated)
Standard File: (none) Sequence File: C:\PW4\haa16352new\haa16352new.seq

Peak	RT	Area	%Ar	Conc. (Ar)	Height	M	Units	Name
1	2.957	670.281	39.00	Not Calculated	390.157	1		
2	3.188	135.635	7.89	Not Calculated	83.806	1		
3	7.893	912.565	53.10	Not Calculated	396.796	1		

3. Chiral GC chromatogram

(R)-2-methyl-1,2,3,4-tetrahydroquinoline (**44k**)

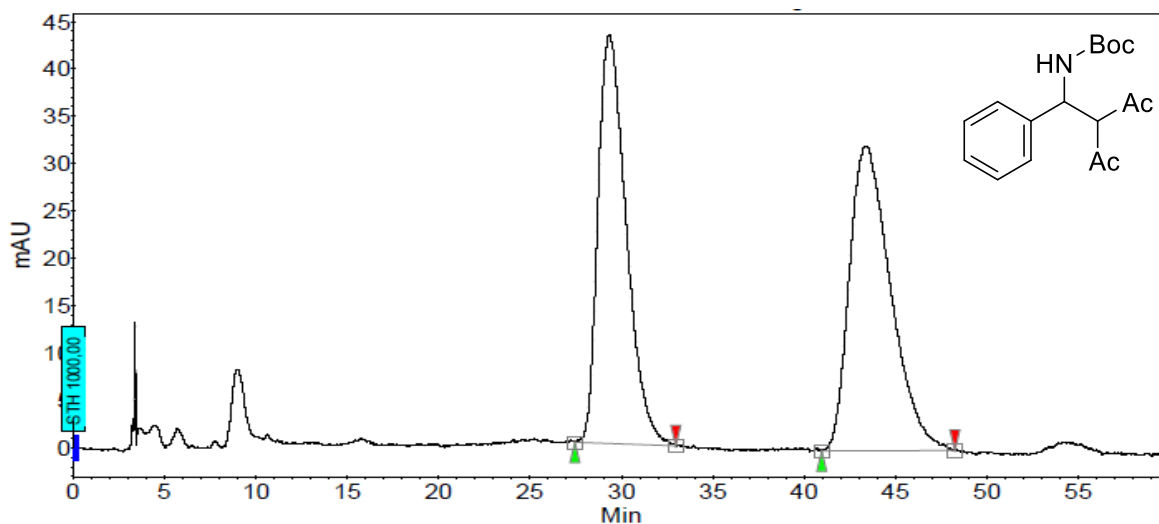


Injection Time: 23 April 2019 at 16:53:27 [Active Status]
 Type: AUTOINJ Injection Number: 63 Channel: Channel A Acquisition Rate: 4Hz
 Method File: C:\PW4\stf53059\0001_stf53059.mth Baseline noise: (not calculated)
 Standard File: (none) Sequence File: C:\PW4\stf53059\stf53059.seq

Peak	RT	Area	%Ar	Conc. (Ar)	Height	M	Units	Name
1	2.342	0.854	0.12	Not Calculated	0.354	0		
2	7.188	0.340	0.05	Not Calculated	0.183	0		
3	8.071	6.154	0.90	Not Calculated	0.832	0		
4	10.775	171.074	24.91	Not Calculated	25.552	0		
5	10.971	508.332	74.02	Not Calculated	36.079	0		

4. HPLC Chromatograms

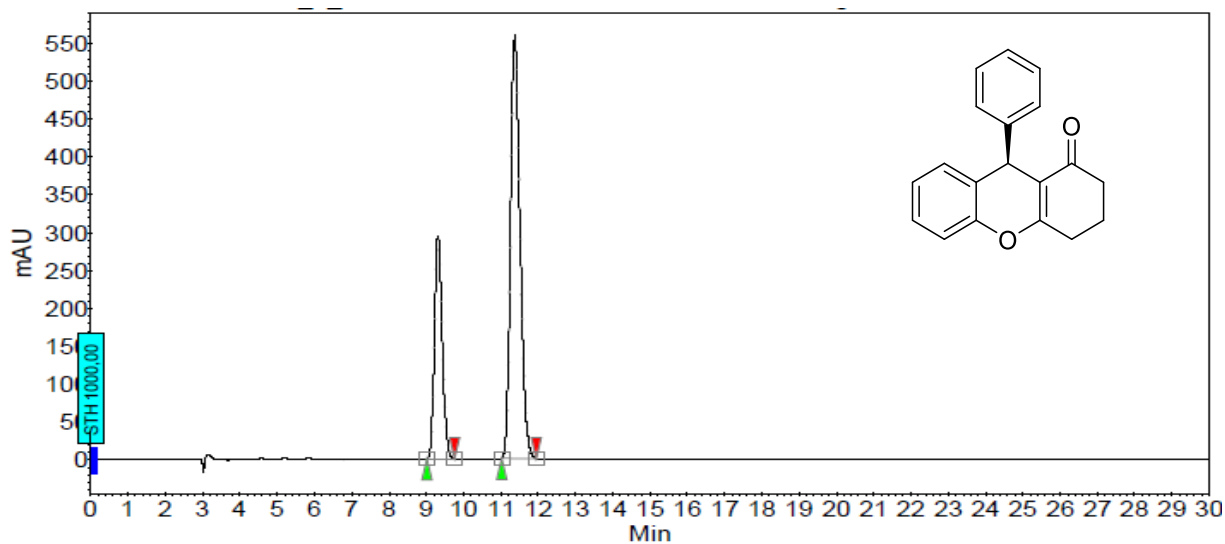
Tert-butyl (2-acetyl-3-oxo-1-phenylbutyl)carbamate (131)



Peak Results :

Index	Name	Time [Min]	Quantity [% Area]	Height [mAU]	Area [mAU.Min]	Area % [%]
1	UNKNOWN	29.35	47.90	43.2	77.6	47.895
2	UNKNOWN	43.35	52.10	32.2	84.4	52.105
Total			100.00	75.4	162.0	100.000

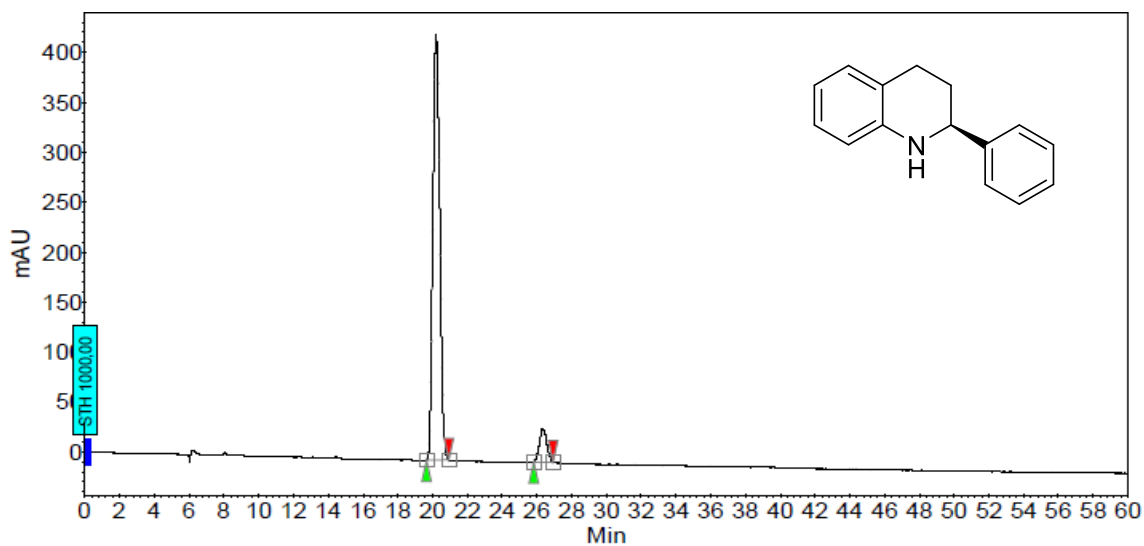
(*R*)-9-Phenyl-2,3,4,9-tetrahydro-1H-xanthen-1-one (138)



Peak Results :

Index	Name	Time [Min]	Quantity [% Area]	Height [mAU]	Area [mAU.Min]	Area % [%]
1	UNKNOWN	9.31	29.97	295.3	70.9	29.968
2	UNKNOWN	11.37	70.03	559.8	165.8	70.032
Total			100.00	855.1	236.7	100.000

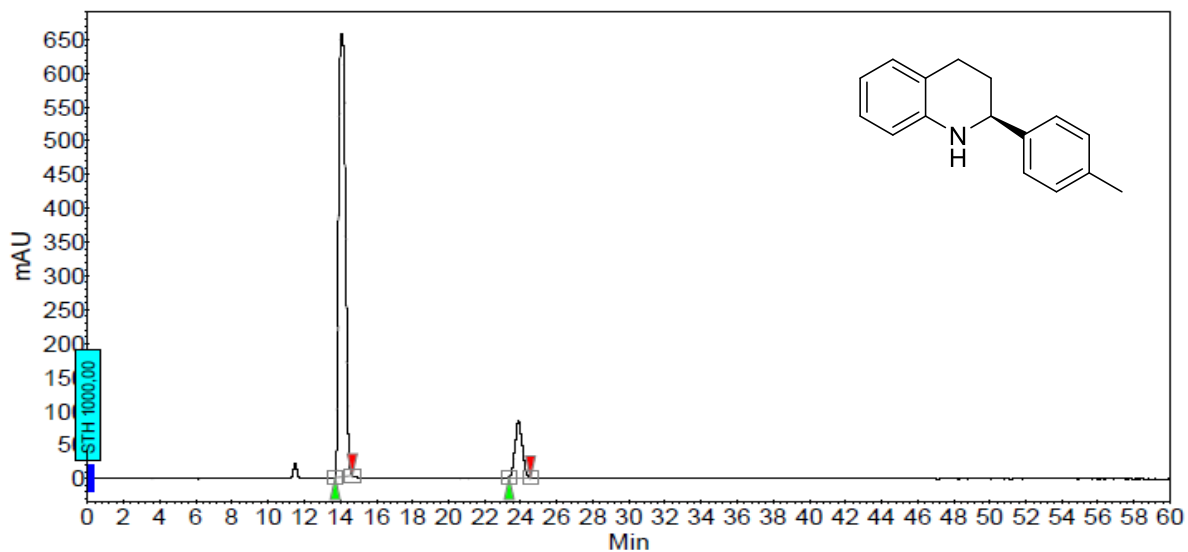
(S)-2-phenyl-1,2,3,4-tetrahydroquinoline (44a)



Peak Results :

Index	Name	Time [Min]	Quantity [% Area]	Height [mAU]	Area [mAU.Min]	Area % [%]
1	UNKNOWN	20.20	92.26	425.9	197.0	92.264
2	UNKNOWN	26.35	7.74	33.7	16.5	7.736
Total			100.00	459.5	213.5	100.000

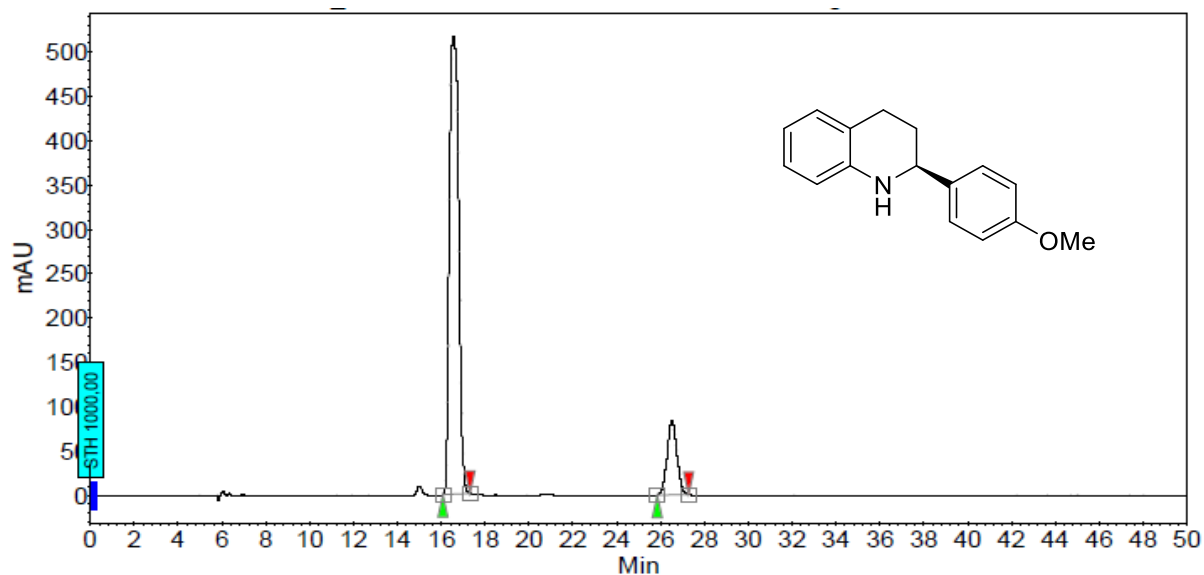
(S)-2-(p-tolyl)-1,2,3,4-tetrahydroquinoline (44b)



Peak Results :

Index	Name	Time [Min]	Quantity [% Area]	Height [mAU]	Area [mAU.Min]	Area % [%]
1	UNKNOWN	14.07	87.78	655.8	285.1	87.781
2	UNKNOWN	23.87	12.22	85.1	39.7	12.219
Total			100.00	740.9	324.8	100.000

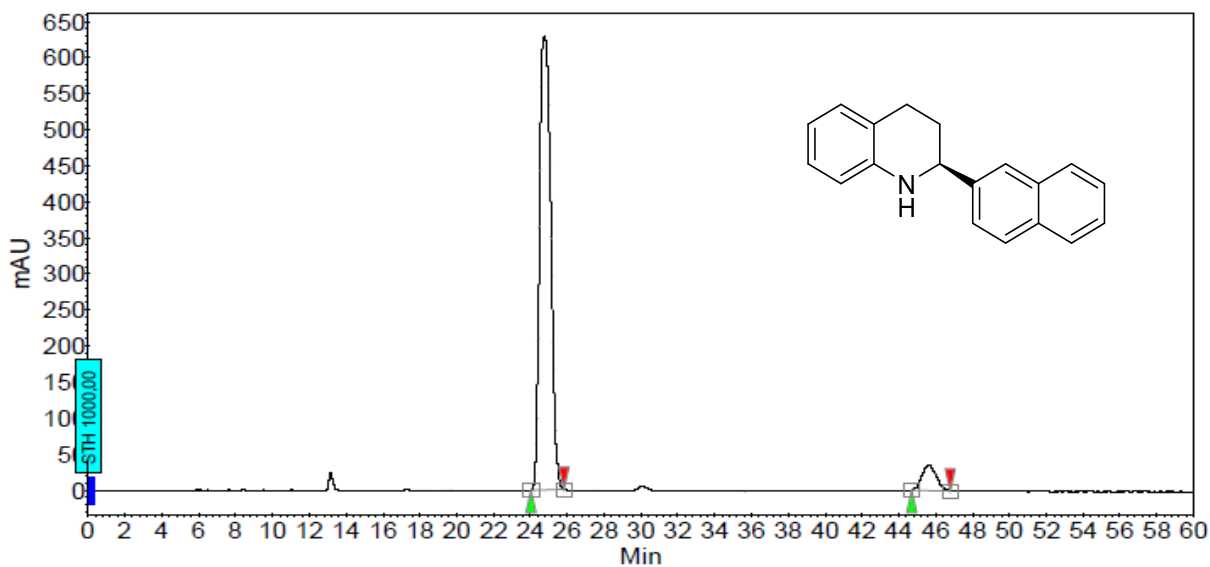
(S)-2-(4-methoxyphenyl)-1,2,3,4-tetrahydroquinoline (44c)



Peak Results :

Index	Name	Time [Min]	Quantity [% Area]	Height [mAU]	Area [mAU·Min]	Area % [%]
1	UNKNOWN	16.55	85.51	517.0	256.0	85.512
2	UNKNOWN	26.51	14.49	83.0	43.4	14.488
Total			100.00	600.0	299.3	100.000

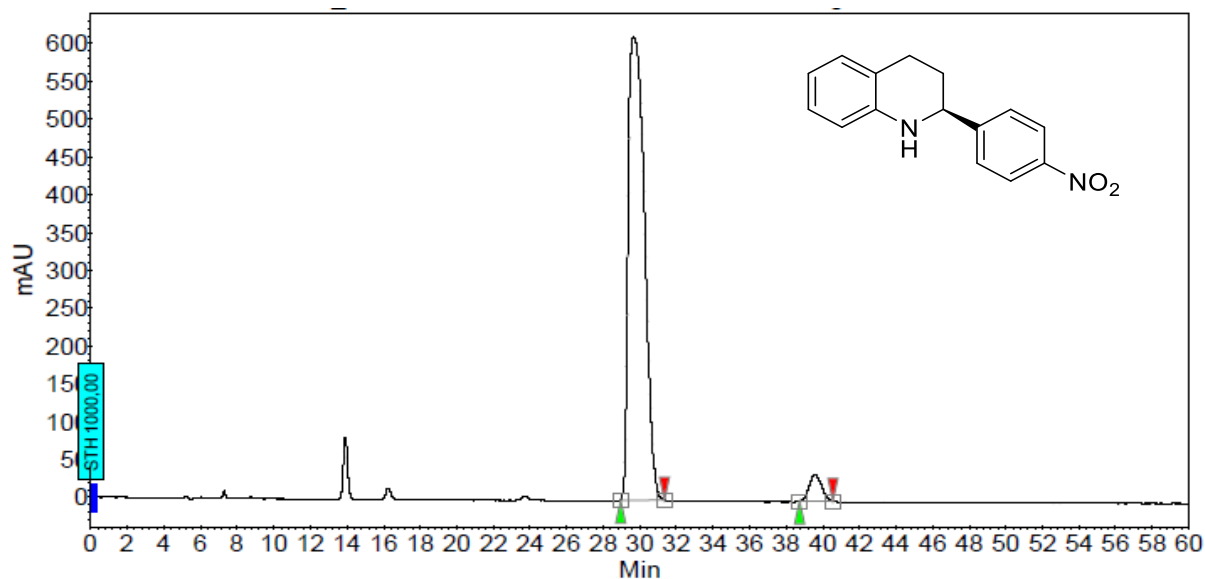
(S)-2-(naphthalen-2-yl)-1,2,3,4-tetrahydroquinoline (44d)



Peak Results :

Index	Name	Time [Min]	Quantity [% Area]	Height [mAU]	Area [mAU·Min]	Area % [%]
1	UNKNOWN	24.76	93.25	629.3	444.4	93.255
2	UNKNOWN	45.63	6.75	35.5	32.1	6.745
Total			100.00	664.9	476.6	100.000

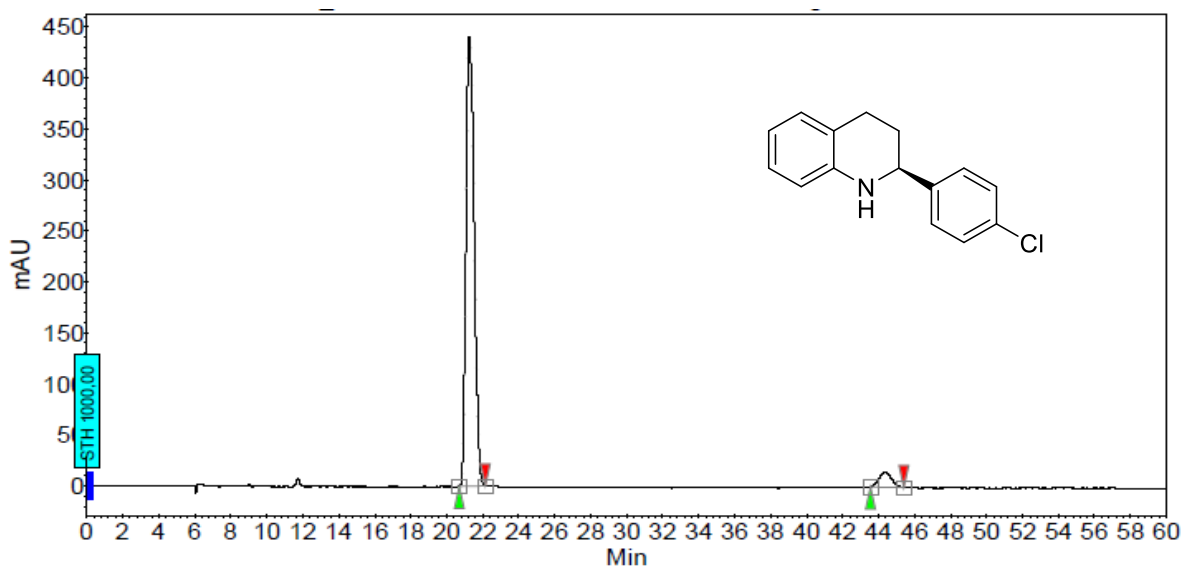
(S)-2-(4-nitrophenyl)-1,2,3,4-tetrahydroquinoline (44e)



Peak Results :

Index	Name	Time [Min]	Quantity [% Area]	Height [mAU]	Area [mAU.Min]	Area % [%]
1	UNKNOWN	29.68	95.76	613.1	627.1	95.762
2	UNKNOWN	39.57	4.24	35.3	27.8	4.238
Total			100.00	648.4	654.9	100.000

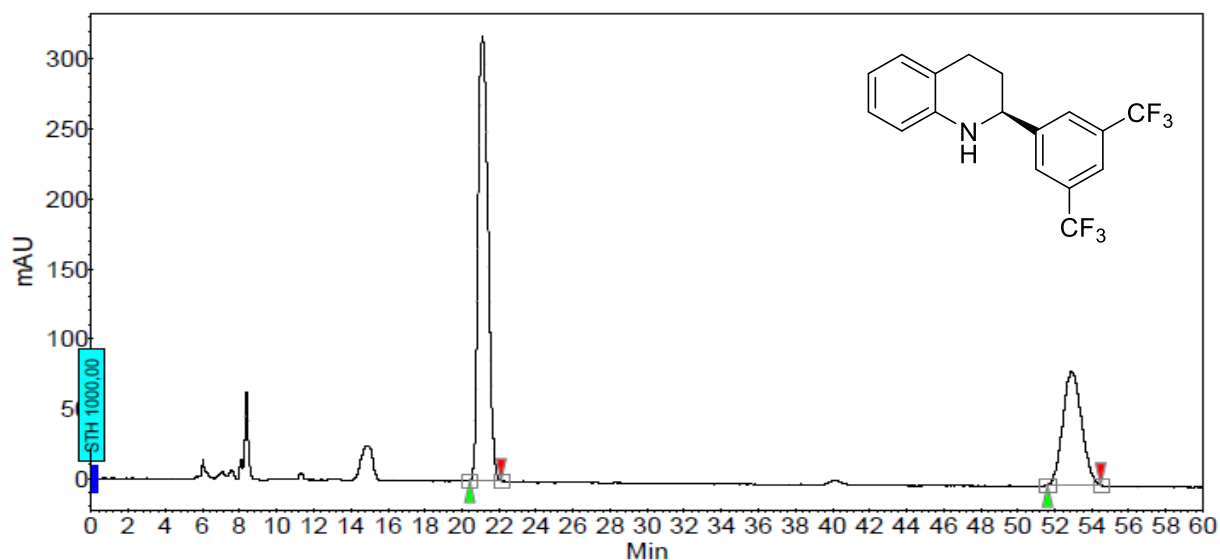
(S)-2-(4-chlorophenyl)-1,2,3,4-tetrahydroquinoline (44f)



Peak Results :

Index	Name	Time [Min]	Quantity [% Area]	Height [mAU]	Area [mAU.Min]	Area % [%]
1	UNKNOWN	21.26	95.14	440.1	232.6	95.140
2	UNKNOWN	44.32	4.86	14.7	11.9	4.860
Total			100.00	454.7	244.4	100.000

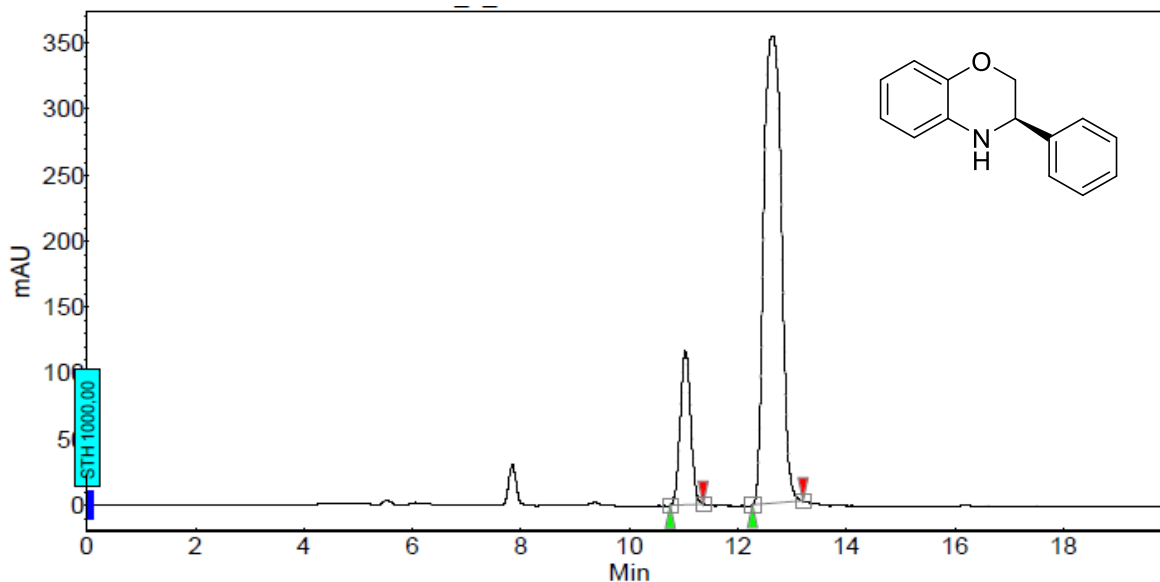
(S)-2-(3,5-bis(trifluoromethyl)phenyl)-1,2,3,4-tetrahydroquinoline (44g)



Peak Results :

Index	Name	Time [Min]	Quantity [% Area]	Height [mAU]	Area [mAU.Min]	Area % [%]
1	UNKNOWN	21.11	67.53	318.4	198.8	67.530
2	UNKNOWN	52.90	32.47	81.0	95.6	32.470
Total			100.00	399.4	294.4	100.000

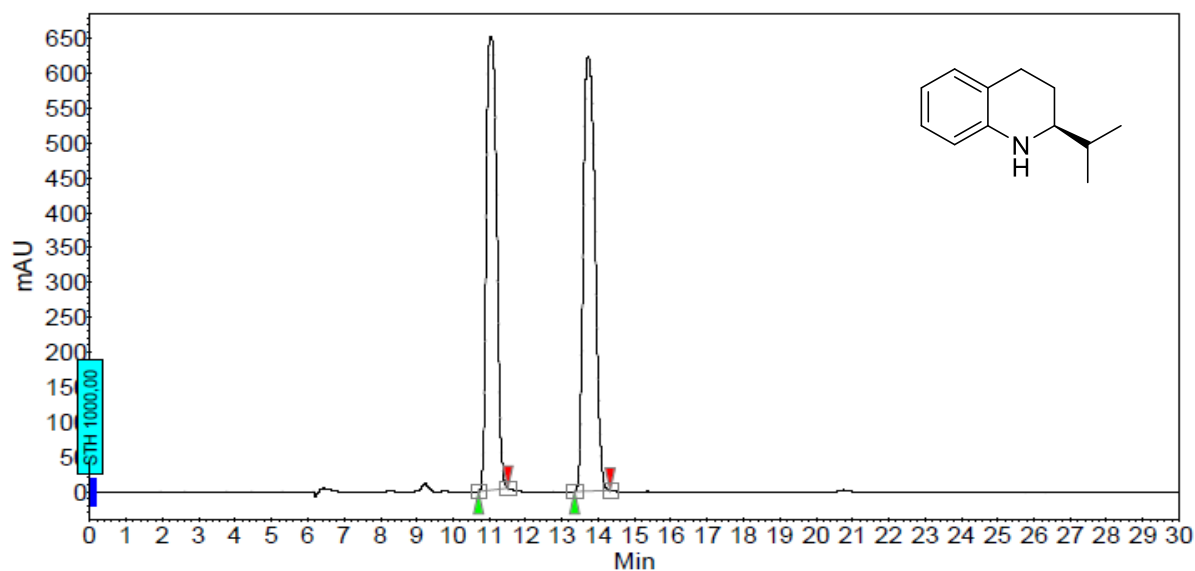
(R)-3-phenyl-3,4-dihydro-2H-benzo[b][1,4]oxazine (44h)



Peak Results :

Index	Name	Time [Min]	Quantity [% Area]	Height [mAU]	Area [mAU.Min]	Area % [%]
1	UNKNOWN	11.03	16.41	116.6	26.1	16.413
2	UNKNOWN	12.64	83.59	354.4	133.0	83.587
Total			100.00	471.1	159.1	100.000

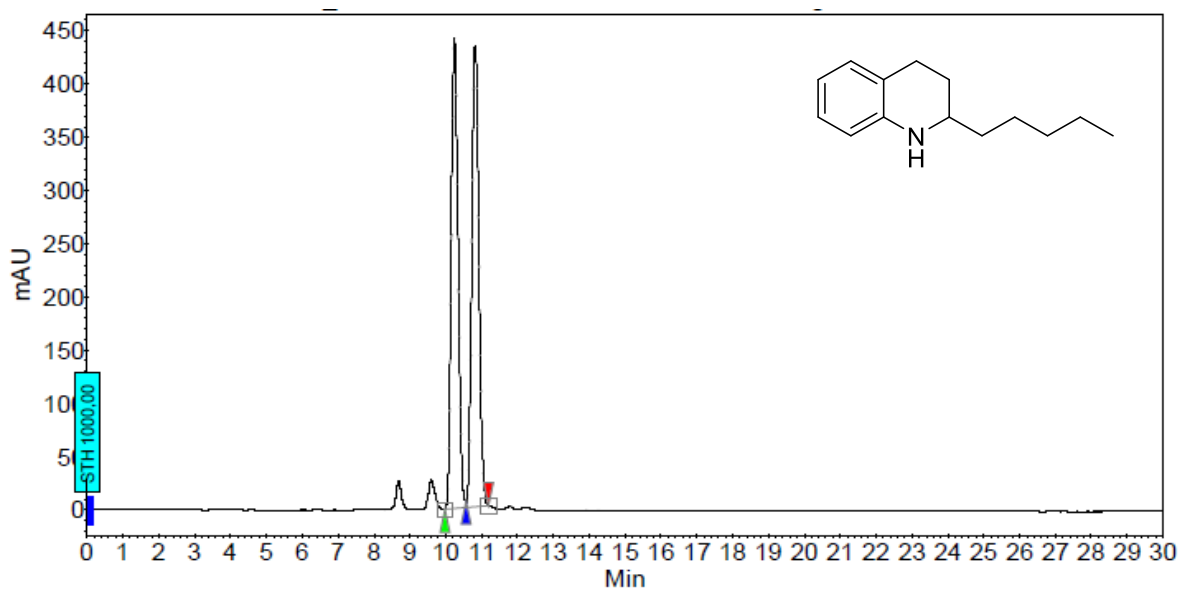
(S)-2-isopropyl-1,2,3,4-tetrahydroquinoline (44i)



Peak Results :

Index	Name	Time [Min]	Quantity [% Area]	Height [mAU]	Area [mAU.Min]	Area % [%]
1	UNKNOWN	11.04	48.12	650.2	216.2	48.124
2	UNKNOWN	13.73	51.88	622.6	233.0	51.876
Total			100.00	1272.8	449.2	100.000

2-pentyl-1,2,3,4-tetrahydroquinoline (44j)



Peak Results :

Index	Name	Time [Min]	Quantity [% Area]	Height [mAU]	Area [mAU.Min]	Area % [%]
1	UNKNOWN	10.24	49.48	442.1	96.6	49.478
2	UNKNOWN	10.82	50.52	432.9	98.6	50.522
Total			100.00	875.0	195.2	100.000

5. Curriculum Vitae

Personal data

Name	Andreas Hartl
Date of birth	December 1, 1992 in Freyung
Nationality	German
Email	andreas.hartl1@outlook.de

Education

11/2016 – current	PhD thesis in the research group of <i>Prof. Dr. O. Reiser</i> (University of Regensburg, Germany)
09/2016	Master of Science in chemistry
01/2016 – 09/2016	Master thesis in the research group of <i>Prof. Dr. O. Reiser</i> (University of Regensburg, Germany)
10/2014 – 09/2016	Advanced studies in chemistry (University of Regensburg, Germany)
11/2014	Bachelor of Science in chemistry
08/2014 – 11/2014	Bachelor thesis in the research group of <i>Prof. Dr. O. Reiser</i> (University of Regensburg, Germany)
10/2011 – 09/2014	Studies in chemistry (University of Regensburg, Germany)
09/2003 – 07/2011	Abitur (<i>A-levels</i>), Landgraf-Leuchtenberg-Gymnasium (secondary school) Grafenau, Germany.

Publications

L. Stadler, M. Homafar, **A. Hartl**, S. Najafshirvari, M. Colombo, R. Zboril, P. Martin, M.B. Gawande, J. Zhi, O. Reiser, *ACS Sustainable Chem. Eng.* **2019**, 7, 2388-2399.

“Recyclable magnetic microporous organic polymer (MOP) encapsulated with palladium nanoparticles and Co/C nanobeads for hydrogenation reactions.”

A. Levin, **A. Hartl**, O. Reiser, C. Czeslik, *Colloid Surface B* **2019**, 182, 110344.

“High-pressure study of magnetic nanoparticles with a polyelectrolyte brush as carrier particles for enzymes”

A. Hartl, O. Reiser, *Manuscript in preparation.*

“A Highly Recyclable Chiral Phosphoric Acid based Organocatalyst for Asymmetric Transfer Hydrogenations via a Straightforward Immobilization Method onto Magnetic Co/C Nanoparticles”

Conferences

26th ISHC Congress – Regensburg (Germany), August 03-08, 2017

“Microporous organic polymers embedded with magnetic Co/C nanobeads and transition metal nanoparticles as recyclable multifunctional catalysts” (poster presentation).

1st German-Russian Interdisciplinary Student Workshop – Moscow (Russia), April 25-27, 2016

“Magnetically recoverable ruthenium nanocatalysts based on microporous organic polymers for transfer hydrogenations” (oral communication, 15 min)

4th International Scientific Conference “Advances in Synthesis and Complexing” – Moscow (Russia), April 25-27, 2016

Professional References

Prof. Dr. Oliver Reiser

Institut für Organische Chemie

Universität Regensburg, Universitätsstr. 31

93053 Regensburg, Germany

Phone: 0049 941 943 4631

Email: Oliver.Reiser@chemie.uni-regensburg.de

H. Acknowledgment - Danksagung

Zunächst möchte ich mich bei Prof. Dr. Oliver Reiser für die Überlassung des interessanten Forschungsthemas und die stetige Unterstützung sowie die konstruktive Anleitung während der gesamten Arbeit herzlich bedanken.

Den Mitarbeitern der Zentralen Analytik der Universität Regensburg möchte ich für die unproblematische Annahme und zügige Messung meiner zahlreichen Proben danken, insbesondere Barbara Baumann und Helmut Schüller. Für die schnellen Termine und die Geduld während der vielen, längeren ICP-Messungen möchte ich mich auch ganz herzlich bei Vanessa Tomanek und Joachim Rewitzer bedanken.

An die beiden Mitarbeiterinnen des Sekretariats der Arbeitsgruppe, Antje Weigert und Michaela Schüle ebenfalls ein herzliches Dankeschön für die freundliche und geduldige Hilfe bei bürokratischen und organisatorischen Problemen aller Art.

Für die technische sowie synthetische Unterstützung bedanke ich mich bei den aktuellen und ehemaligen Mitarbeitern des Arbeitskreises Klaus Döring, Simone Dürmeier, Brigitte Eichenseher und insbesondere auch Helena Konkell, Johannes Floß und Roxane Harteis für die Messung meiner zahllosen HPLCs.

Für die durchweg unterstützende und freundliche Atmosphäre möchte ich mich bei allen ehemaligen und aktuellen Mitarbeitern des Arbeitskreises bedanken. Besonderer Dank gilt hierbei Tobias Babl, Simon Budde, Anurag-Nitin Chinchole, Robert Eckl, Peter Ehrnsberger, Dr. Christian Eichinger, Sebastian Engl, Dr. Thomas Ertl, Dr. Christian Faderl, Sebastian Fischer, Dr. Thomas Föll, Dr. Matthias Gnahn, Dr. Martin Hofmann, Dr. Benjamin Kastl, Tomislav Krolo, Dr. Michael Leitner, Natalijaa Moor, Dr. Saerom Park, Eva Plut, Andreas Ratzenböck, Alexander Reichle, Anna Rustler Carina Sonnleitner, Dr. Lisa Stadler, Dr. Lukas Traub, Lisa Uhlstein und Dr. Thomas Weinbender. Unsere gemütlichen Runden in der Küche mit oder ohne Karten spielen, Grillabende, Ausflüge zum See oder andere gemeinsame Unternehmungen haben mir Zeit am Arbeitskreis deutlich versüßt und ich bin unendlich dankbar für die Freundschaften die ich auf diesem Weg schließen konnte.

Meinen Laborkollegen Simon Budde, Dr. Christian Eichinger, Anurag-Nitin Chinchole und Anna Rustler möchte ich für die super Atmosphäre, lustige Musik und stetige Unterstützung in allen Bereichen sehr herzlich danken. Besonders bedanke ich mich hierbei bei Simon und Christian, ihr habt die Zeit im Labor zu etwas Unvergesslichem gemacht. Auch an die erweiterte „Stammtischlabor Crew“ Peter Ehrnsberger, Maximilian Frantah, Dr. Thomas Föll, Dr. Lisa Stadler und Dr. Lukas Traub ein herzliches Dankeschön für

die stetigen Besuche und damit einhergehenden netten Gespräche, dank euch wurde es auch im Labor nie langweilig.

Dem kleinen Kreis meiner Nanopartikel-Kollegen in der Gruppe Dr. Christian Eichinger, Dr. Benjamin Kastl und Dr. Lisa Stadler möchte ich dafür danken, dass ihr stets für meine Probleme ein offenes Ohr hattet und mir so gut wie immer mit einem wissenschaftlichen Rat zur Seite standet.

Für die personelle Unterstützung in der „Handbib“ danke ich Anna Rustler und Peter Ehrnsberger, dank euch war das Schreiben deutlich effizienter und angenehmer als im Homeoffice.

Meinen ehemaligen Bachelorstudentinnen und Forschungspraktikant(inn)en Anton Abramov, Maximilian Frantah, Kevin Grill, Lisa Merl, Anna Rustler und Kathrin Strunk danke ich ebenfalls für ihre synthetische Unterstützung und gewissenhafte Arbeit.

Für das schnelle und gewissenhafte Korrekturlesen dieser Arbeit bedanke ich mich nochmals bei Anurag-Nitin Chinchole, Dr. Christian Eichinger, Anna Rustler und Dr. Lisa Stadler.

Zu guter Letzt möchte ich auch von ganzem Herzen meiner Familie für die stetige und bedingungslose Unterstützung und Motivation danken, ohne euch wäre ich nicht so weit gekommen. Danke, dass ich immer auf euch zählen konnte.

I. Declaration

Herewith I declare that this present thesis is a presentation of my original work prepared single-handed. Wherever contributions from others are involved, all of them are marked clearly, with reference to the literature, license, and acknowledgment of a collaborative research.

Regensburg,

Andreas Hartl